TABLE OF CONTENTS

Page

LIST OF FIGURES

Page

LIST OF ABREVIATIONS

AWGN	Additive White Gaussian Noise
AF	Amplify-and-Forward
AMI	Advanced Metering Infrastructure
APP	A Posteriori Probability
BPSK	Binary Phase Shift Keying
BCJR	Bahl-Cocke-Jelinek-Raviv
BER	Bit-Error Rate
BG	Bernoulli-Gaussian
BRS	Best Relay Selection
CHG	Greenhouse Gas
CRC	Cyclic Redundancy Check
CCI	Co-Channel Interference
CSCG	Circularly Symmetric Complex Gaussian
CR	Cooperative Relaying
CF	Compress-and-Forward
DT	Direct Transmission
DF	Decode-and-Forward
EF	Estimate-and-Forward
EM	Electromagnetic

EMI	Electromagnetic Interference
EPA	Equal Power Allocation
ERC	Equal-Ratio Combining
FRC	Fixed-Ratio Combining
FC	Fusion Center
GSM	Global System for Mobile Communications
GM	Gaussian Mixture
GPS	Global Positioning System
HMM	Hidden Markov Model
HAN	Home Area Network
ICT	Information and Communication Technology
IN	Impulsive Noise
IAT	Inter Arrival Time
ISM	Scientific and Medical
IoT	Internet of Things
i.i.d.	Independent and Identically Distributed
i.n.d.	Independent and Non-identically Distributed
LLR	Log-Likelihood Ratio
LMMSE	Linear Minimum Mean Square Error
LDPC	Low-Density Parity-Check

LTE	Long-Term Evolution
ML	Maximum Likelihood
MIMO	Multiple-Input Multiple-Output
MRC	Maximum-Ratio Combining
M-PSK	M-ary Phase Shift Keying
MMSE	Minimum Mean Square Error
MAC	Multiple Access Control
MSE	Mean Square Error
MAP	Maximum-A-Posteriori
MDR	Minimum Distance Receiver
MEMs	Micro-electro-mechanical sytems
NBI	NarrowBand Interference
NAN	Neighbor Area Network
NIST	National Institute of Standards and Technology
OPA	Optimal Power Allocation
OBE	Optimal Bayesian Estimation
OFDM	Orthogonal Frequency-Division Multiplexing
PDC	Post Detection Combining
PLC	Power Line Communication
PPP	Poisson Point Process

PEP	Pairwise Error Probability
PAPD	Peak Amplitude Probability Distribution
PDF	Probability Density Function
QoS	Quality of Service
QPSK	Quadrature Phase Shift Keying
RFI	Radio Frequency Interference
SNR	Signal-to-Noise Ratio
SC	Selection Combining
SIC	Soft Information Combining
STBC	Space-Time Block Coding
SWIPT	Simultaneous Wireless Information and Power Transfer
SEP	Symbol Error Probability
SER	Symbol-Error Rate
SIM	Subscriber Identity Module
SEP	Smart Energy Profile
2G	Second Generation
TSMG	Two State Markov-Gaussian
UWB	Ultra-WideBand
VANET	Vehicular Ad hoc Network
WLAN	Wireless Local Area Network

WSN	Wireless Sensor Network
WAMR	Wireless Automatic Meter Reading
WAN	Wide Area Network
WiMAX	Worldwide Interoperability for Microwave Access
Wi-Fi	Wireless Fidelity

LISTE OF SYMBOLS AND UNITS OF MEASUREMENTS

x	Variable
$\mathbf{x}$	Vector
$E\{\cdot\}$	Expectation operator
lim	Limits
max	Maximum value
$\exp(\cdot)$	Exponential function
$Q(\cdot)$	Q function
erf	Error function
erfc	Complementary error function
$\Gamma(\cdot)$	Gamma function
$\Gamma(\cdot,\cdot)$	Upper incomplete gamma function
$\gamma(\cdot,\cdot)$	Lower incomplete gamma function
$\log_2$	Logarithm with base 2
ln	Natural logarithm
$\delta(x)$	Kronecker delta function

INTRODUCTION

Motivations

Our planet is gradually heading towards an energy famine due to growing population and industrialization. Energy consumed throughout the world was about 17 terawatts in 2008, which is expected to be doubled by 2050 Report, U. S. (2012). Hence, increasing electricity consumption and prices, diminishing fossil fuels and lack of significance in environment-friendliness due to their emission of greenhouse gasses (mostly carbon dioxide due to carbon fuel consumption), and inefficient usage of existing energy supplies have caused serious network congestion problems in many countries in recent years Gungor, V. C., Lu, B. & Hancke, G. P. (2010). In addition to this overstressed situation, nowadays, the electric power system is facing many challenges, such as high maintenance cost, aging equipment, lack of effective fault diagnostics, low power supply reliability, limitation in investment efficiency, flexibility, unidirectional telecommunications, automation, etc., which further increase the possibility of system breakdown Gungor *et al.* (2010); Tuna, G., Gungor, V. C. & Gulez, K. (2013). Furthermore, the adaptation of the new renewable energy sources (e.g, wind energy, solar energy) with existing power plants to provide an alternative way for electricity production gave rise to additional issues. To address these challenges, a new concept of next generation electric power systems, called the "smart grid", has emerged in which two-way digital communication is provided along with power flow between the consumer and the grid Farhangi, H. (2010); Gungor, V. C., Sahin, D., Kocak, T., Ergut, S., Buccella, C., Cecati, C. & Hancke, G. P. (2011). Smart metering, monitoring, and control system have also been added. Therefore, it is widely acknowledged that the legacy power grid has to be modernized to improve its performance in which the incorporation of Information and Communication Technologies (ICTs) will play a significant role Fang, X., Misra, S., Xue, G. & Yang, D. (2012). In the smart grid, through two-way communication and with a smooth integration of alternative and renewable energy sources, as shown in Fig 1.1, the electric power system becomes more reliable, efficient, safe,

secure, and environment-friendly Tuna *et al.* (2013); Yan, Y., Qian, Y., Sharif, H. & Tipper, D. (2013). Therefore, the design, development, and deployment of dedicated robust communication networks for smart grid environments that collect and analyzes data captured about power generation, transmission, distribution, and consumption is imperative Gungor *et al.* (2011). Based on the data received from the deployed communication networks, smart grid technology supports smart power management by providing information and recommendations to utilities, their suppliers, and their consumers.

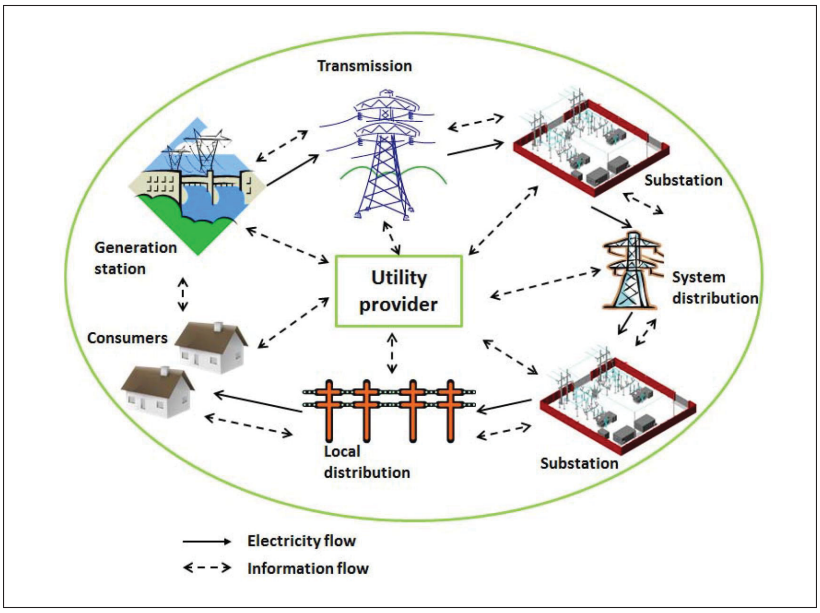

Figure 0.1 Illustration of the two-way electricity and information flows for smart grid scenario
Taken from Matta et al. (2012)

In general, smart grid communication technologies can be broadly classified into two main categories Gungor *et al.* (2010): wired communications and wireless communications. Although, traditional power grid communication systems are typically realized through wired communications (e.g., power line communication (PLC), optical fiber communication, coper conductive wire communication), it requires expensive communication cables to be installed and regularly maintained, and thus, the cost of its installation might be expensive especially for remote con-

trol and monitoring and is not widely implemented in today's systems Gungor *et al.* (2010). On the other hand, wireless communication is becoming more and more popular in smart grid applications, since they offer significant benefits over wired communications, like low-cost installations, easy user access, rapid implementation with less infrastructure, and mobility. The convenience of wireless technologies has led to the deployment of a variety of wireless communication systems such as cellular networks, wireless ad-hoc networks, wireless local area networks (WLANs), wireless sensor networks (WSNs), and wireless mesh networks in various smart grid applications Gungor *et al.* (2010,1).

In particular, the most promising method of smart grid communication explored in the literature is based on WSNs due to their inherent characteristics such as their low-cost, flexibility, wider coverage, self-organization and rapid deployment Gungor *et al.* (2010); Liu, Y. (2012); Tuna *et al.* (2013). WSNs usually consist of a large number of low power, low cost, and multifunctional sensor nodes to monitor the overall grid and to communicate with the task manager in order to decide the appropriate actions. In this way, a problem in any part of the grid can be diagnosed proactively and immediate action can be taken in order to prevent any failures that might affect the grid's performance. With these advancements, nowadays, the potential applications of WSNs in smart grids span a wide range from generation segments to the consumer premises, including remote system monitoring, equipment fault diagnostics, wireless automatic meter reading (WAMR), etc Gungor *et al.* (2010).

Problem Statement

The implementation of the WSN-based smart grid has several challenges. The major technical challenges are the reliability of wireless links between the sensor nodes, effect of impulsive noise observed in harsh smart grid environments, resource constraints of sensor nodes, security, quality of service (QoS) requirements, heterogeneous environmental conditions, etc. Gungor *et al.* (2010); Tuna *et al.* (2013). Specifically, research activities related to the reliability of

WSNs in harsh smart grid environments in the presence of impulsive noise are extremely important for the deployment of WSNs in the smart grid Agba, B. L., Sacuto, F., Au, M., Labeau, F. & Gagnon, F. (2019); Alam, M. S., Labeau, F. & Kaddoum, G. (2016); Ndo, G., Labeau, F. & Kassouf, M. (2013); Sacuto, F., Agba, B. L., Gagnon, F. & Labeau, F. (2012); Tuna *et al.* (2013). The noise characteristics in many particular smart grid environments, such as around power transmission lines, power substations, and around some home utilities are highly non-Gaussian and are inherently impulsive in nature Agba *et al.* (2019); Alam *et al.* (2016); Middleton, D. (1977); Ndo *et al.* (2013); Sacuto *et al.* (2012); Tuna *et al.* (2013). For example, in power substations, the noise emitted from power equipment, such as transformers, busbars, circuit-breakers, and switch-gears are impulsive Hikita, M., Yamashita, H., Hoshino, T., Kato, T., Hayakawa, N., Ueda, T. & Okubo, H. (1998); Portuguds, I., Moore, P. J. & Glover, I. (2003); Sacuto *et al.* (2012). Also, the interference emitted from a microwave oven is impulsive Kanemoto, H., Miyamoto, S. & Morinaga, N. (1998). Hence, the WSN-based smart grid communication system will be affected by the generated impulsive noise. Impulsive noise may degrade the communication system performance because its spectrum is powerful enough to be detected by any commercial wireless device. Therefore, numerous researchers from the wireless communication and power utility communities have begun to investigate several impulsive noise models to characterize actual smart grid environments and the reliability of smart grid communications in the presence of these impulsive interferences.

Along the years, the emergence of various impulsive noise models, such as the Middleton Class-A noise model Middleton (1977), Bernoulli-Gaussian noise model Ghosh, M. (1996), two-state Markov-Gaussian model Fertonani, D. & Colavolpe, G. (2009), Zimmermann Markov chain Zimmermann, M. & Dostert, K. (2002), Markov-Middleton model Ndo *et al.* (2013), among others, have launched new research interests. These noises can be broadly classified into two main categories: memoryless impulsive noise and bursty impulsive noise. They offer different switching rules and noise parameters to characterize the noise. Due to the uniqueness

of these noise models, novel transceiver architectures and communication protocols need to appear to meet the reliability requirements of different smart grid communication cases.

To this end, the study of reliable transmission over channels impaired by those impulsive interferences is necessary and essential.

Research Objectives

In this thesis, we will focus on laying down the fundamental basis for the development of a robust and secure WSN for smart grid communications in the presence of memoryless and bursty impulsive noise to be realized in real-world smart grid applications. To achieve this goal, we have developed application specific innovative optimal and sub-optimal detection and estimation techniques.

In this regard, previous studies have shown sufficient evidences that the impulsive noise observed in smart grid environments is time-correlated. To handle the correlation among the noise samples, we have considered Markov chain models. The very next step incorporates the design and performance analysis of WSNs by considering the RF noise model in the design process. Particular attention is given to how the time-correlation among the noise samples can be taken into account. For this, we have introduced the definition and methodology of the maximum a posteriori (MAP) detection criterion that can effectively utilize the bursty impulsive noise behavior in the detection process using the well-known Bahl-Cocke-Jelinek-Raviv (BCJR) algorithm. In addition, Bayesian minimum mean square error (MMSE) estimator is shown to be the optimal estimation technique under that scenario. On this basis, we consider modeling the WSN-based smart grid communication systems on the MATLAB platform.

To elaborate on the reliability of WSN-based smart grid communications over various impulsive channels, three steps are adopted: (i) investigation and performance analysis of impulsive noise mitigation techniques for point-to-point WSN communication systems impaired by

bursty impulsive noise; (ii) design and performance analysis of collaborative WSN for reliable smart grid communications; (iii) optimal MMSE estimation of the physical phenomenon of substations (like temperature, voltage, current etc., typically modeled by a Gaussian source) in the presence of impulsive noise.

Contributions and Outline

The dissertation is structured as shown in Fig 0.2, and detailed as follows.

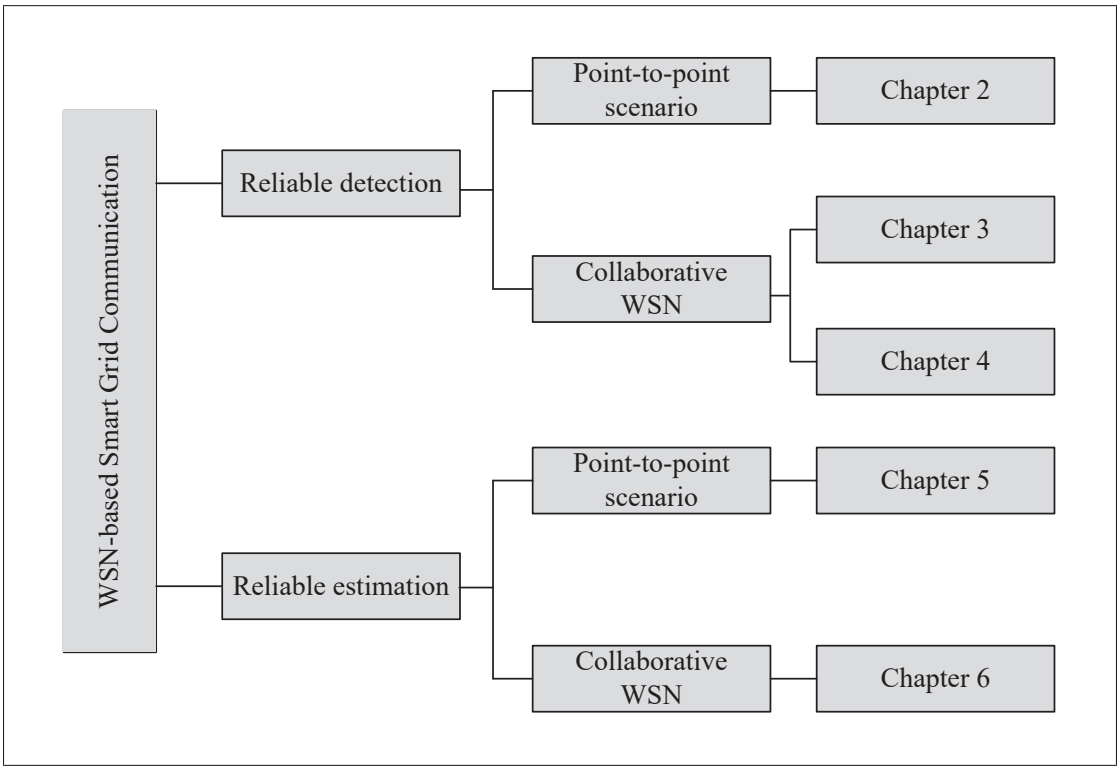

Figure 0.2 The paradigm of thesis contribution

In this Chapter, the motivations of our work has been discussed. Moreover, we have discussed the problems and our research objectives. In particular, some recent interesting applications of collaborative WSNs in smart grid environments are also presented.

Chapter 1 briefly introduces the state-of-arts of smart grid communications, WSNs for smart grid communications, impulsive noise and the common models that characterize it, the concept of collaborative WSNs for smart grid communications, and the different tools used in this thesis.

Chapter 2 investigates the widely used non-linear methods such as clipping, blanking, and combined clipping-blanking to mitigate the noxious effects of bursty impulsive noise for point-to-point single-carrier low-density parity-check coded transmission systems. This noise model is promising when being applied to the high voltage substation scenarios. Moreover, the log-likelihood ratio (LLR)-based impulsive noise mitigation using the MAP detection criterion is also derived for the considered scenario. In this context, provided simulation results highlight the superiority of the LLR-based mitigation scheme over the simple clipping/blanking schemes.

Chapter 3 considers the performance analysis of a single-relay decode-and-forward (DF) co-operative relaying scheme over channels impaired by bursty impulsive noise. For this channel, the bit error rate (BER) performances of direct transmission and a DF relaying scheme using M-PSK modulation in the presence of Rayleigh fading with a MAP receiver are derived.

On the other hand, in Chapter 4, we propose a novel relay selection protocol for a multi-relay DF collaborative WSN taking into account the bursty impulsive noise. The proposed protocol chooses the N'th best relay considering both the channel gains and the states of the impulsive noise of the source-relay and relay-destination links. To analyze the performance of the proposed protocol, we first derive closed-form expressions for the probability density function (PDF) of the received SNR. Then, these PDFs are used to derive closed-form expressions for the BER and the outage probability. Finally, we also derive the asymptotic BER and outage expressions to quantify the diversity benefits.

Unlike the aforementioned chapters, which consider the reliable detection of finite alphabets in the presence of bursty impulsive noise, Chapters 5 and 6 investigate the optimal MMSE estimation for a scalar Gaussian source impaired by impulsive noise. In Chapter 5, the MMSE optimal Bayesian estimation for a scalar Gaussian source, in the presence of bursty impulsive noise is considered. On the other hand, in Chapter 6, we investigate the distributed estimation of a scalar Gaussian source in WSNs in the presence of Middleton class-A noise.

Finally, Chapter 7 concludes this dissertation and points out several future research directions.

Practical Scenario's: Towards the Application of Collaborative WSNs in Impulsive Smart Grid Environments

The collaborative and low-cost nature of WSNs have made them ubiquitous in different parts of the smart grid, namely generation, transmission, distribution, and customer-side applications. For this, WSN is considered an ideal technology and a vital part of the next generation electric grid. Following are some possible applications of collaborative WSNs in impulsive noise environments.

Substation Equipment Condition Monitoring

A substation is a very crucial part of an electric power system. Power transmission and distribution substations are mainly comprised of many critical components such as transformers, circuit breakers, switch-gears, busbars etc. Monitoring the health of these substation equipment is of paramount importance in smart grids since these equipment are responsible for successful power transmission and any failure or breakdown in them may cause blackouts Matta, N., Ranhim-Amoud, R., Merghem-Boulahia, L. & Jrad, A. (2012); Nasipuri, A., Cox, R., Conrad, J., Van der Zel, L., Rodriguez, B. & McKosky, R. (2010).

In this context, Hydro-Quebec, one of the biggest power utility companies in North America has more than 500 substations in distinct geographical areas. Monitoring the health of these

substation equipment could be achieved through the deployment of a dedicated collaborative WSN in the substations, as shown in Fig 0.3. However, high voltage substation equipment produce significant impulsive noise as observed in a Hydro-Quebec's impulsive noise measurement campaign Sacuto *et al.* (2012). These interferences corrupt the signals transmitted from the sensor nodes and have to be taken into account to evaluate their impact on WSNs. Our objective is to propose robust collaborative WSN transceiver architectures in substations to mitigate the effect of the impulsive noise. This work may contribute to the deployment of collaborative WSN in Hydro-Quebec substations where significant improvement can be achieved.

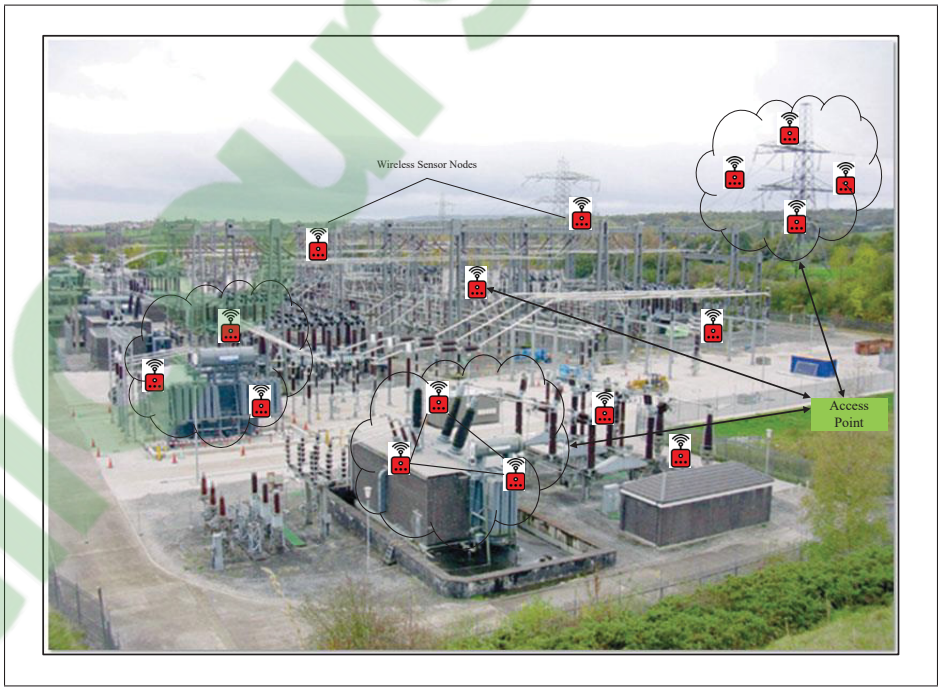

Figure 0.3 Collaborative WSN for substation monitoring systems

Home Automation

Collaborative WSN has been identified as a promising technology to enhance the performance of today's electric system in various aspects. In addition to the high voltage substation moni-

toring system, WSNs are also a promising candidate for home automation Brak, M. E., Brak, S. E., Essaaidi, M. & Benhaddou, D. (2014); Erol-Kantarci, M. & Mouftah, H. T. (2011); Liu (2012). Fig 0.4 shows a typical home automation system architecture that is connected to the smart grid through advanced metering infrastructure (AMI). As depicted in the figure, sensor nodes are connected with each of the home utilities to collect information and send their sensed information to the sink node for further control. By doing this, the customers can remotely read their electrical usage, manage load control, monitor for electrical faults, and support appliance level reporting Brak *et al.* (2014); Erol-Kantarci & Mouftah (2011); Liu (2012). Hence, the customers are benefiting through greater transparency of electrical usage. However, many home utilities like the microwave oven, heater, refrigerator create impulsive noise Kanemoto *et al.* (1998); Middleton (1977), which will degrade the reliability of the wireless links between the sensor nodes. Hence, robust collaborative WSNs must be designed to mitigate the effect of impulsive noise.

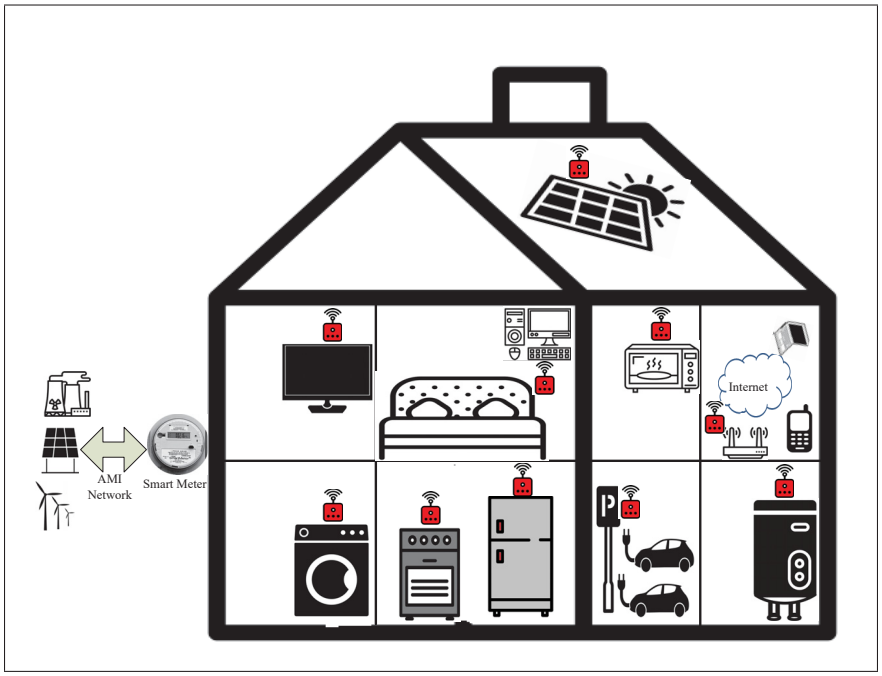

Figure 0.4 Collaborative WSN for home automation
Adopted from Brak et al. (2014)

Author's Publications

The outcomes of the author's Ph.D. research are either published or submitted to the IEEE journals and conferences, which are listed below.

Alam, M. S., Selim, B., Kaddoum, G., and Agba, B. L., "MAP receiver for bursty impulsive noise mitigation in NOMA-based systems", *IEEE Commun. Lett.*, Jul. 2019, prepared for submission.

Alam, M. S., Selim, B., Kaddoum, G., and Agba, B. L., "Mitigation techniques for impulsive noise with memory", *IEEE Systems J.*, May 2019, under review.

Alam, M. S., Kaddoum, G., and Agba, B. L., "A novel relay selection strategy of cooperative network impaired by bursty impulsive noise", *IEEE Trans. Veh. Technol.*, Vol. 68, no. 7, pp. 6622-6635, Jul. 2019.

Alam, M. S., Kaddoum, G., and Agba, B. L., "Bayesian MMSE estimation of a Gaussian source in the presence of bursty impulsive noise", *IEEE Commun. Lett.*, Vol. 22, no. 9, pp. 1846-1849, Jul. 2018.

Alam, M. S., Kaddoum, G., and Agba, B. L., "Performance analysis of distributed wireless sensor network for Gaussian source estimation in the presence of impulsive noise", *IEEE Signal Process. Lett.*, Vol. 25, no. 6, pp. 803-807, Jun. 2018.

Alam, M. S., Labeau, F., and Kaddoum, G., "Performance analysis of DF cooperative relaying over bursty impulsive noise channel", *IEEE Trans. Commun.*, Vol. 64, no. 7, pp. 2848-2859, Jul. 2016.

Apart from the afore-listed journal papers that contribute to the main body of the dissertation, the other scientific publications that the author either has been involved in or drafted as the first author not included in this dissertation, are listed as follows.

Eshteiwi, K., Kaddoum, G., and **Alam, M. S.**, "Exact and asymptotic ergodic capacity of full duplex relaying with co-channel interference in vehicular communications", *IEEE Systems J.*, Jul. 2019, under review.

Selim, B., **Alam, M. S.**, Kaddoum, G., and Agba, B. L., "Multi-stage clipping for the mitigation of impulsive noise in ODFM-NOMA systems", *IEEE Wireless Commun. Lett.*, Jul. 2019, under review.

Selim, B., **Alam, M. S.**, Kaddoum, G., and Agba, B. L., "Effect of impulsive noise on uplink NOMA systems", *IEEE Trans. Veh. Technol. (corres.)*, Jul. 2019, under review.

Selim, B., **Alam, M. S.**, Evangelista, V. C., Kaddoum, G., and Agba, B. L., "NOMA in impulsive noise environments: Performance degradation, mitigation, and Challenges", *IEEE Wireless Commun. Mag.*, May 2019, under review.

Au, M., Kaddoum, G., Gagnon, F., Bashar, E., and **Alam, M. S.**, "Joint code-frequency index modulation for IoT and multi-user communications", *IEEE J. Selected Topics Signal Process.*, Dec. 2018, accepted for publication.

Attalah, M., **Alam, M. S.**, and Kaddoum, G., "Secrecy Analysis of wireless sensor network in smart grid with destination assisted jamming", *IET Commun.*, Apr. 2019, accepted for publication.

Alam, M. S., Selim, B., Kaddoum, G., and Agba, B. L., "Analysis and comparison of several mitigation techniques for Middleton class-A noise", *Proc. IEEE Latincom*, Jul. 2019, under review.

CHAPTER 1

BACKGROUND AND LITERATURE REVIEW

In this chapter, we conduct a systematic literature review of communication technologies in smart grid applications that have been proposed in the literature by other quality researchers. In particular, we emphasized on the possibility of WSNs in harsh smart grid environments and the associated design challenges. Specially, the impact of the impulsive noise phenomenon observed in smart grid environments on the reliability of wireless networks is discussed.

This chapter is organized as follows. Section 1.1 defines the smart grid technology and outlines the potential benefits of the smart grid over the traditional grid. In Section 1.2, we discuss most of the existing communication technologies that have been considered for smart grid environments. Section 1.3 highlights the possible applications of WSNs in different parts of smart grid while the basic structure of a WSN along with its characteristics is presented in Section 1.4. Section 1.5 identifies the design challenges of WSNs in harsh and hostile smart grid environments. In Section 1.6, the definition of impulsive noise, major impulsive noise sources in smart grid environments, and the existing impulsive noise models for communication channels are presented. In Section 1.7, we discuss the conventional impulsive noise mitigation techniques. Also, the LLR computation for communication systems impaired by bursty impulsive noise using the MAP detection criterion as well as a low-complexity LLR calculation in case of communication systems impaired by memoryless impulsive noise is shown. Section 1.8 gives a flavor of the concept of cooperative communications and reviews the existing literature on the performance analysis of cooperative communication schemes over impulsive noise channels. Through the literature review, we will show that existing WSN transceiver architectures cannot handle the impulsive noise characteristics properly and asks for further investigation.

1.1 What is Smart Grid?

The definition of smart grid varies among researchers and organizations. Basically, smart grid refers to a new concept of next generation power grid in which two-way digital communica-

tion is provided along with power flow between the consumer and the grid and where smart metering, monitoring, and control system have also been added Farhangi (2010); Gungor *et al.* (2011). In order to allow such "smarter" functionalities, smart grid needs to be integrated with an ICT infrastructure that collects and analyzes data captured about power generation, transmission, distribution, and consumption Gungor *et al.* (2011). Based on these data, smart grid technology supports smart power management by providing information and recommendations to utilities, their suppliers, and their consumers.

The potential benefits of smart grids are outlined as follows Tuna *et al.* (2013); Yan *et al.* (2013):

- Enhanced customer experience in terms of service reliability and quality by providing increased energy consumption information available to customers,
- Several environmental benefits. A smart grid can potentially increase the energy efficiency that lowers carbon fuel consumption and, as a result, the greenhouse gas (GHG) emission,
- Improved reliability and safety,
- Increased productivity, easy integration of renewable energy sources and plug-in electric vehicles,
- A reduction in peak energy demand with properly optimize the energy usage that will avoid power blackout,
- Improved physical and operational security and resilience against attacks.

In the following section, we will conduct a systematic literature review that briefly provides an overview of the promising wired and wireless smart grid communication technologies.

1.2 Smart Grid Communications

For a reliable smart grid, monitoring of the power system parameters in the transmission and distribution segments as well as monitoring and control of substation devices from outside

the station is crucial Fang *et al.* (2012); Farhangi (2010). In order to allow such advanced functionalities and avoid possible disruptions in electric systems due to unexpected failures, a highly reliable, scalable, secure, cost-effective, and robust communication network must be operational within the power grid Gungor *et al.* (2011); Yan *et al.* (2013). Basically, smart grid communication networks can be divided into three segments namely: home area networks (HANs), neighbor area networks (NANs), and wide area networks (WANs) as shown in Fig 1.1.

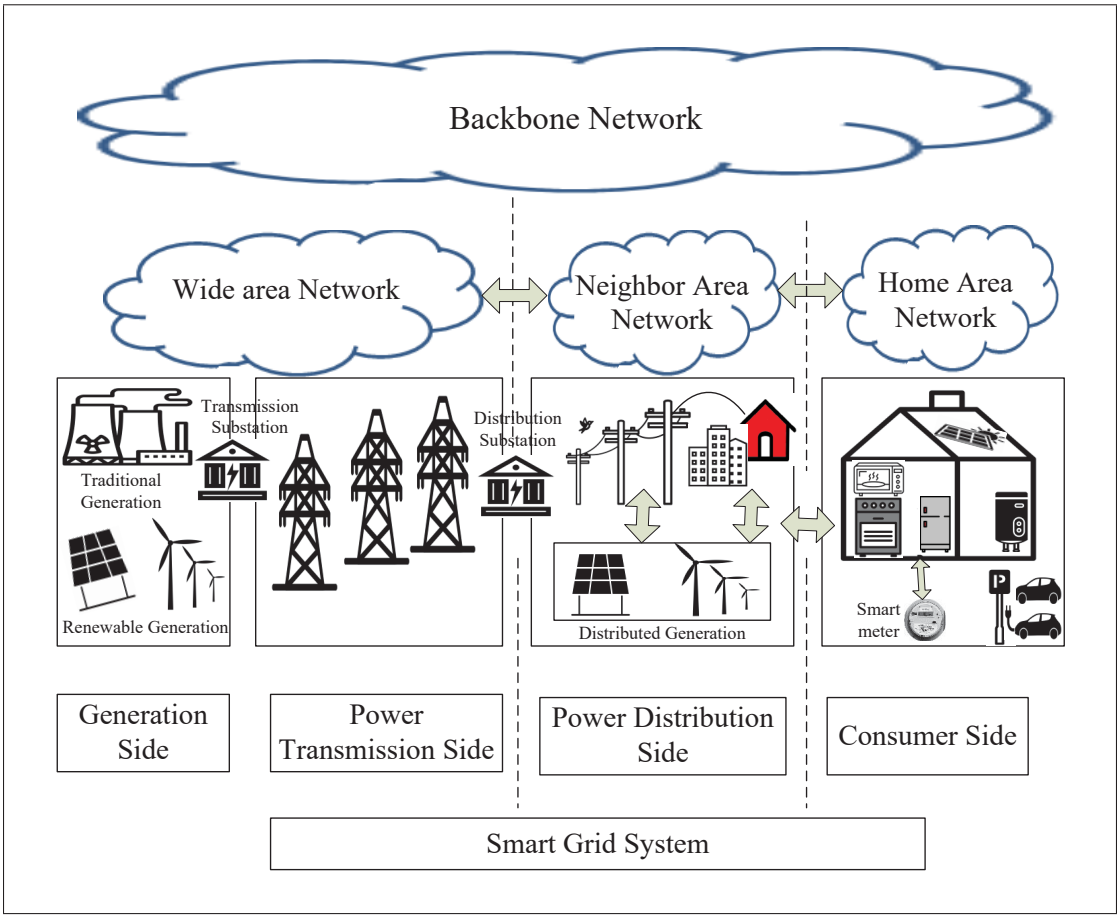

Figure 1.1 Illustration of the smart grid from generation to customer side
Adopted from Fadel et al. (2015)

- Home area network: HAN is applicable for home automation. It creates a communication path among smart meters, home appliances (e.g.: freezer, microwave oven, washing ma-

chine, dryer, water heater, TV), and plug-in electric vehicles. By doing this, utilities will be able to communicate with the consumers to monitor and inform their possible power consumption. In addition, consumers will be able to collect information about their consumption behaviors and the electricity usage costs from different utilities via in-home display panels.

- Neighbor area network: NANs establish a communication path between data collectors and smart meters in a neighborhood area such that the measured data from the smart meters can be transmitted to the data concentrators.

- Wide area network: WANs serve as the backbone for communication between the service provider's data center and data concentrators. For that, it covers long distance data transmissions for smart grid monitoring and control applications.

Many researchers and international organizations are working for the development of versatile communication technologies and standards for smart grid automation. The common communication technologies include power line communication, optical fiber communication, satellite communication, wireless communication, and so forth. Each communication technology has its own advantages and disadvantages according to the location and requirement of the application Gungor, V. C. & Lambert, F. C. (2006). In the following, we briefly discuss these communication technologies along with their advantages and disadvantages.

1.2.1 Power Line Communication

The power line communication (PLC) is one of the earliest initiatives for the automation of the electrical grid. It involves the transmission of data and electricity simultaneously over existing power lines without necessitating dedicated communication infrastructure for the two-way data communication. On the basis of the frequency bandwidth, PLC can be divided into two categories: broadband PLC and narrowband PLC. Narrowband PLC is well suited for low data rate applications such as advanced metering infrastructure (AMI) in urban areas, data communication between the smart meters and the data concentrators, and for HAN purposes

Gungor & Lambert (2006). Advantages of PLC include Gungor & Lambert (2006); Gungor *et al.* (2011): low installation cost given the existing infrastructure and extensive coverage since the power lines are already installed everywhere. The disadvantages of PLC are the following Gungor & Lambert (2006); Gungor *et al.* (2011): the power lines have several noise sources such as power supplies, electric motors, and radio interference which cause high BER during data transmission and hence degrade the performance of PLC. Also, PLC is characterized by a highly time varying nature and it is hard to model the characteristics of the channel.

1.2.2 Satellite Communication

Satellite communication can be an excellent alternative communication infrastructure for remote control and monitoring of substations in scenarios where other communication infrastructures such as telephone or cellular networks might not exist Gungor & Lambert (2006); Khan, F., ur Rehman, A., Arif, M., Aftab, M. & Jadoon, B. K. (2016). In addition, it can be used as a backup for the existing substations automation communication network. Specially, in case of equipment disaster, terrestrial link failure, network or link congestion, critical data in smart grid systems can be routed through satellite systems Gungor & Lambert (2006). Furthermore, satellite global positioning system (GPS) can be used for time synchronization in smart grid communications with accuracy in the microsecond range. Due to these reasons, the application of satellite communication for remote substation monitoring has already been considered Tisot, A. (2004). The benefits of satellite communication include wide geographical coverage and rapid installation compared to wired networks. The disadvantages are that it requires longer round-trip delay, higher cost, short life-span, sensitive to weather conditions and the effect of fading, which may heavily degrade the performance.

1.2.3 Optical Fiber Communication

Optical fiber communications system can be one of the technically attractive communication infrastructures for high voltage substation environments, providing extremely high data rate, with an immunity to electromagnetic interference (EMI) and radio frequency interference (RFI)

Gungor & Lambert (2006). Furthermore, the existing optical fiber communication might be useful for backbone communication due to its high bandwidth capacity.

Although optical fiber communication systems offer several advantages compared to other wired and wireless networks, the corresponding installation cost might be expensive for remote control and monitoring of substations. Also, the substation equipment are not usually equipped to access the fiber network. Hence, from an economic point of view, it would be too expensive to deploy optical networks only for smart grid applications.

1.2.4 Wireless Communications

There are different wireless communication technologies that can be used for smart grid communication Gungor & Lambert (2006); Gungor *et al.* (2011); Khan *et al.* (2016). Wireless communication technologies have significant advantages over wired communications, such as, rapid installation of the communication infrastructure and saving in cabling cost Gungor & Lambert (2006). On the other hand, the performance of wireless communications is limited by bandwidth efficiency, maximum distances among communication devices, EMI, and channel fading. Basically, smart grid communications can be supported either by an existing wireless communication infrastructure of a public network (e.g., public cellular network) or by installing a dedicated wireless network. In the following, we describe both of these wireless communication technologies.

1.2.4.1 Cellular Communications

The cellular network has the advantage of being the most deployed wireless communication technology and can be a good option for communication between smart meters and the utility. This avoids spending operational costs and time for building a dedicated communication infrastructure. Existing cellular communication technologies are 2G, 2.5G, 3G, WiMAX, and LTE. These technologies have found numerous applications in HAN for home monitoring and load control. For example, in such applications, subscriber identity module (SIM) card can be

embedded in the smart meters and the recorded data is relayed to the control panel of the smart grid via the cellular network. By this way, the domestic users are always in touch with their home appliances via their mobile phone. Nowadays, utility companies from different countries all over the world are using these cellular communication technologies for smart grid applications (e.g., T-mobiles GSM network is chosen for the deployment of Echelon's Networked Energy Services (NES) system; Telenor, Telecom Italia, China Mobile, Vodaphone have also agreed to put their GSM network for smart meter communications) Gungor *et al.* (2011). The feasibility of LTE is investigated in Cheng, P., Wang, L., Zhen, B. & Wang, S. (2011) to support smart metering and remote control communications in smart grid environments. On the other hand, WiMAX is the most interesting cellular technology for smart grid communications. It is more applicable as a backbone solution for smart grid applications. Also, WiMAX chip based smart meters are already deployed for smart grid environments Gungor *et al.* (2011). The potential benefits of using today's WiMAX technology are high data rates (up to 75 Mbps), lower deployment and operating costs, large coverage area, proper security protocols, smooth communications, adequate bandwidth, scalability, etc.

In conclusion, although the use of the cellular network is the simplest alternative available to utility companies compared to a dedicated network, we have to keep in mind that the cellular networks are designed for mobile voice telephony to end users and are ill prepared to handle the signaling traffic from the millions of smart meters Gungor *et al.* (2011).

1.2.4.2 ZigBee Network

ZigBee is a widely used wireless communication technology for smart grid environments Gungor *et al.* (2011); Khan *et al.* (2016); Usman, A. & Shami, S. H. (2013). ZigBee is based on the IEEE 802.15.4 standard and has a data rate of 20 to 250 Kbps. It is well suited for applications that require a low data rate, low cost, long battery life, low complexity, and high level of scalability and reliability Gungor *et al.* (2011). ZigBee is an ideal technology for applications including smart lighting, home automation, energy monitoring, automatic meter reading, and many other applications that require short-range wireless transfer of data at relatively low

rates Gungor *et al.* (2011); Khan *et al.* (2016); Usman & Shami (2013). The U.S. National Institute of Standards and Technology (NIST) has recommended ZigBee and ZigBee smart energy profile (SEP) as the most suitable communication standards for smart grid residential automation Gungor *et al.* (2011). ZigBee integrated smart meters can be used to communicate with the ZigBee embedded devices and can control them. Moreover, the consumers can view their energy consumption in real-time through the received messages provided by ZigBee SEP. The main limitation of ZigBee for practical applications is the adverse effect of interference coming from other technologies that share the same frequency band (e.g., Wi-Fi, Bluetooth, Microwave signals).

1.2.4.3 WLAN

WLAN/Wi-Fi technology (IEEE 802.11) has found numerous applications in smart grid environments specially in home area networks due to its vast deployment around the world, low cost, and plug and play devices. The Wi-Fi based mesh network can be used for NAN scenarios where different meters in the locality relay information received from HAN to the access point in their region Usman & Shami (2013). Also, backhaul communication between the access points in multiple NANs to the central database can also be implemented using Wi-Fi technology Usman & Shami (2013). The major disadvantage of WLAN technology is a high potential for interference as it is operated in the unlicensed ISM band. Security is also a major designing issue for the same reason.

Now, with the recent advances in wireless communications and digital electronics, WSN becomes a promising technology for smart grid communications due to its low-cost, flexibility, wider coverage, self-organization and rapid deployment Gungor *et al.* (2010); Liu (2012); Tuna *et al.* (2013). In the WSN, the sensor nodes may communicate via Zigbee, wireless LAN/Wi-Fi, etc Gungor *et al.* (2011). However, the selection of the most appropriate wireless communication technology depends on the specific application domain Fadel, E., Gungor, V., Nassef, L., Akkari, N., Maik, M. A., Almasri, S. & Akyildiz, I. F. (2015); Gungor *et al.* (2011). In the

following section, we will provide an overview of the applications of WSNs in different parts of the smart grid.

1.3 WSN Applications in Smart Grid Communications

Applications of WSNs in smart grids spans a wide range, from generation segments to consumer premises. WSNs can be used for accurate monitoring and control of generation, transmission, distribution, and consumption of electricity by facilitating its sensing and communication capabilities. In general, the WSN-based smart grid applications can be broadly classified into three main categories. These are generation side, transmission and distribution (T&D) side, and consumer side applications.

- Generation side applications: Generally, monitoring is the most crucial task to be performed for the generation side smart grid applications. WSNs can be used as an ideal technology for monitoring and control of the generation side functionalities in the smart grid. Some of these applications are Fadel *et al.* (2015); Tuna *et al.* (2013): remote monitoring of wind and solar farms operating in harsh environments and hostile locations, power quality monitoring, real-time generation monitoring, and distributed generation. One of the main objectives of the smart grid is to expedite the use of renewable energy sources. Since the renewable sources are situated in harsh environments, their unpredictable behavior creates more challenges during their operation and management. WSNs provide an economical solution for monitoring and controling the behavior of renewable energy resources Erol-Kantarci & Mouftah (2011).

- Transmission and distribution side applications: The transmission and distribution segment of the smart grid covers overhead power lines, underground power lines, and substations. The monitoring applications designed for this side play a vital role in smart grid since these systems are responsible for successful power transmission, where any equipment failure or breakdown of these systems may cause blackouts. Some of the T&D sides WSN-based smart grid applications include outage detection, overhead transmission line monitoring, conductor temperature and dynamic thermal rating monitoring, fault detection,

underground cable system monitoring, conductor and lattice theft identification, insulators monitoring, equipment fault diagnostics, etc. Fadel *et al.* (2015); Tuna *et al.* (2013). In addition, WSN-based substation monitoring applications include circuit breaker status monitoring, power transformer and distribution transformer monitoring, ambient temperature monitoring Nasipuri *et al.* (2010). The authors in Lin, J., Zhu, B., Zeng, P., Liang, W., Yu, H. & Xiao, Y. (2015) proposed an efficient wireless sensor network framework for transmission line monitoring. The design challenges associated with transmission line monitoring using WSNs are that most sensors are placed around the supports which makes the network dense at that place, whereas it is sparse in most of the other areas. In addition, traffic shows a large amount of variability. To handle these issues, Lin *et al.* (2015) proposed a clustering algorithm to simplify network management and a hybrid media access control (H-MAC) protocol to handle traffic variability. The design and deployment of a large-scale WSN for substation monitoring are presented in Matta *et al.* (2012); Nasipuri *et al.* (2010).

- Consumer side applications: Consumer side WSN-based smart grid applications are directly involved with the end-users' premises. Through two-way communication between the supplier and the consumer, it is possible to monitor and control the end-user power consumption without sacrificing their demand. Typical applications are AMI, automated panels management, residential energy management, building automation, equipment control and monitoring, process control monitoring, and demand side load management Fadel *et al.* (2015); Tuna *et al.* (2013). These could be accomplished by deploying a WSN where the sensor nodes are attached to the utilities to sense, monitor, and provide feedback Brak *et al.* (2014); Erol-Kantarci & Mouftah (2011); Liu (2012). Due to low bandwidth and short-range requirements of consumer side HAN applications, the WSN can utilize some cost-effective communication technologies, such as Zigbee, 6LoWPAN, Wi-Fi, and Bluetooth Brak *et al.* (2014); Fadel *et al.* (2015); Liu (2012).

1.4 Characteristics of WSN

Recent advances in hardware technologies allow more signal processing functions to be integrated into a single chip. Through the use of advanced micro-electro-mechanical systems (MEMs) technology, it will be possible to integrate a radio frequency (RF) circuit, a low power digital signal processor, analog-to-digital (A/D) and digital-to-analog (D/A) converters, a battery, and other application interfaces into one device for multiple onboard functions such as sensing, computing, and communications and also the device be as small as possible Akyildiz, I. F., Su, W., Sankarasubramaniam, Y. & Cayirci, E. (2002). Such intelligent devices called sensors, can be used as a fully-functional wireless sensor node as well as networked through wireless links, referred to as wireless sensor networks and recognized as one of the most important technologies for the 21st century Akyildiz *et al.* (2002). Due to their low cost and low complexity design requirement, individual sensors can only perform simple local computation and communicate over a short range at low data rates. But when deployed in large numbers across a spatial domain, these primitive sensors can form an intelligent network to measure aspects or identities of the physical environment on a potentially unprecedented scale and with high precision Akyildiz *et al.* (2002). Sensor networks are ideal for situation awareness applications such as environmental monitoring, healthcare monitoring, home applications, smart factory instrumentation, military surveillance, precision agriculture, space exploration, and intelligent transportation.

1.4.1 Basic Structure of WSNs

Wireless sensor networks, which normally consist of a large number of sensor nodes, each capable of sensing, processing, and transmitting environmental information, are deployed to monitor certain physical phenomena or to detect and track certain objects in an area of interest. Fig 1.2 depicts a typical application of WSNs where the sensor nodes are scattered in a sensor field. Each of these scattered sensor nodes is capable of collecting data and route it back to the sink mostly by a multi-hop, infrastructureless architecture as shown in Fig 1.2. The sink acts

as a coordinator of the network and transmits the received data from the sensor nodes to the user through a wireless link. There are two main types of networks:

- Star topology: Each sensor can transmit the observations directly to the sink.
- Mesh topology: The nodes are positioned in a large area and the farther ones don't have a radio visibility with the coordinator. In this case, each node acts both as a sensor and as a router to forward the data of the neighbor nodes toward the sink.

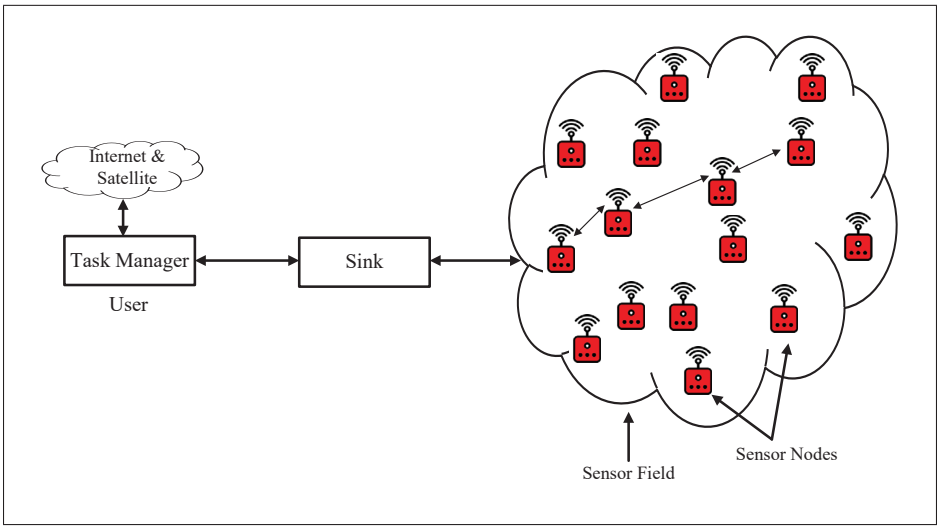

Figure 1.2 Typical sensor network scenario
Adopted from Akyildiz et al. (2002)

1.4.2 Sensor Node Components

Every sensor node is composed of four basic components Akyildiz *et al.* (2002): a sensing unit, a processing unit, a transceiver unit, and a power unit. It is also possible to include additional components such as location finding system, a power generator, and a mobilizer Akyildiz *et al.* (2002).

The function of each of these components are:

- Sensing units are usually composed of sensors and analog-to-digital converters (ADCs). The sensors respond to a physical stimulus by producing analog signals and the analog signals are converted into a digital form by the ADC, and then fed into the processing unit.

- The processing unit, which is generally associated with a small storage unit and responsible of collecting signals captured from the sensors as well as the execution of communication protocols and signal processing algorithms on the gathered sensor data. It also manages the procedures that make the sensor node collaborate with the other nodes to carry out the assigned tasks.

- A transceiver unit connects the node to the network. It contains the transmitter and receiver usually tuned on ISM frequency bands (433MHz, 800MHz and 2:4GHz) Akyildiz *et al.* (2002).

- The power unit is on of the most important components since power consumption determines the lifetime of a sensor node.

1.4.3 Benefits of WSNs for Smart Grid Automation

- Ability to cover large area: Wireless sensor networks usually consist of a large number of physically separated sensor nodes that work autonomously and are logically linked by self-organizing means. Hence, although the coverage of a single sensor node is small, the deployment of a large number of sensor nodes across a spatial domain forms an intelligent network that works collaboratively and simultaneously so that, the coverage area of the whole network is extended in a potentially unprecedented scale Akyildiz *et al.* (2002); Gungor & Lambert (2006). Therefore, the coverage limitations of traditional monitoring systems can be handled efficiently.

- Operating in harsh environmental conditions: The sensor nodes in WSNs are reliable, rugged, and comfort to severe weather conditions (e.g., ambient temperature, pressure etc.) Gungor & Lambert (2006). For this reason, WSNs can operate in remote harsh environments.

- Lower cost: Because of their small size, lower price, and ease of deployment, the installation cost of WSNs are expected to be less expensive than conventional monitoring systems Gungor & Lambert (2006).

1.5 Design Challenges of WSNs in Smart Grids

Briefly, the smart grid offers a large number of opportunities over the traditional grid. The benefits of the smart grid will be achieved by allowing two-way communication between the different entries of the grid. These communications could be accomplished by deploying WSNs. However, the implementation of WSN-based smart grid has several challenges. This section discusses the major design challenges for the realization of WSN-based smart grid communications.

- Reliability of wireless networks: Due to the wireless nature, the connectivity between the sensor nodes will be affected by multipath fading and shadowing, strong RF interference, non-uniform radio signal strength, and highly harsh environments. In such environments, the propagation of low power RF signals from the sensor nodes is often unpredictable. Although various solutions and protocols are provided for reliable WSN communications in ideal conditions, they are not well suited for harsh smart grid environments Tuna *et al.* (2013). Vulnerable link quality in WSNs is a very challenging task and this motivates the researchers to propose an efficient and effective protocol for such environments.

- Quality of service (QoS) requirements: Different WSN-based applications in smart grids ask for different QoS specifications and requirements in terms of reliability, latency, network throughput, etc. For example, for fault detection and correction in the electric power system, it is very important to receive the alarm data from the sensor nodes to the controller in a timely manner and latency is a design issue for that scenario. A summary of different QoS requirements for different smart grid applications is given in (Tuna *et al.*, 2013, Table I).

- Resource constraints of sensor nodes: In WSNs, all nodes are equipped with a battery and hence the sensor nodes applications are constrained by limited battery life. For this reason, WSN-based smart grid applications clearly ask for designing energy efficient protocols to operate for a sufficiently long time without having to replace the batteries. This is particularly important for substation and high voltage transmission line monitoring applications due to the relative inaccessibility of the regions for safety and regulatory purposes. The design and implementation of WSNs are also constrained by the memory and processing power of the sensor nodes.

  For solving the issue of limited battery life of sensor nodes, many energy efficient protocols have been investigated in the literature where various energy-efficient medium access and routing protocols and duty-cycling have been considered. However, these techniques are able to provide only limited lifetime Erol-Kantarci, M. & Mouftah, H. T. (2012). On the other hand, energy harvesting methods play an important role in the lifetime of WSNs. By harvesting the energy from the ambient resources it is possible to extend the lifetime of the sensor nodes Shaikh, F. K. & Zeadally, S. (2016); Tuna *et al.* (2013). Major energy harvesting techniques that can be used in smart grid applications are solar energy harvesting, thermal energy harvesting, vibration-based energy harvesting, air flow energy harvesting, electromagnetic wave energy harvesting, modulated backscattering, magnetic field energy harvesting, biochemical energy harvesting, etc Tuna *et al.* (2013). Finally, a combination of both energy harvesting technique and efficient energy consumption can be implemented to achieve an energy-autonomous WSN Matta *et al.* (2012).

- Effect of impulsive noise: In smart grid applications, the links between the sensor nodes may be subject to different noise and interference effects. The noise characteristics in many smart grid environments, such as around power transmission lines, power substations, and around some home utilities are highly non-Gaussian and are inherently impulsive in nature Agba *et al.* (2019); Hikita *et al.* (1998); Kanemoto *et al.* (1998); Middleton (1977); Sacuto *et al.* (2012). For example, in power substations, the noise emitted from power equipments, such as transformers, busbars, circuit-breakers, and switch-gears are impulsive Agba *et al.*

(2019); Hikita *et al.* (1998); Sacuto *et al.* (2012). Also, the interference emitted from a microwave oven is impulsive Kanemoto *et al.* (1998). Hence, WSN-based smart grid communication systems will be affected by the generated impulsive noise for substation and home monitoring applications. Although there exists a large number of publications on WSN-based smart grid applications in various aspects, most of them are restricted to the AWGN assumption. In practice, AWGN is a common assumption to bundle together a lot of sources of noise, beyond thermal. Hence, conventional communication schemes designed for WSN-based monitoring systems under the AWGN assumption show worse performance in the presence of impulsive noise Alam *et al.* (2016). Thus, it is imperative to consider the impulsive noise characteristics in the design of WSN-based smart grid communication systems which ask for further investigation.

- Security: The wireless nature of WSNs also makes WSN-based smart grid applications vulnerable to various external attacks, i.e. physical and cyber threats. Hence, security is an essential issue in the design of WSN-based smart grid communications in order to securely transmit the data from the end-users to the data collection centers. In addition to cyber security issues that have been widely investigated in the literature since the beginning of smart grid projects, one may also analyze the physical layer security aspects that have been hardly investigated in the smart grid scenario Lee, E.-K., Gerla, M. & Oh, S. Y. (2012). How the performance of the later scheme can be improved by designing new advanced algorithms to satisfy smart grid scenarios needs further investigation.

- Heterogeneous environment conditions: Due to the complex and dynamic nature of WSN-based smart grid applications, single communication technique is not sufficient to provide flexible, secure, resilient, cost-effective, and reliable communication Fadel *et al.* (2015). Hence, a combination or mixed topology may be incorporated over the smart grid for better interpretability.

- Packet errors and variable link capacity: In WSNs, the capacity of the link depends on the signal level, interference, and bit error rate. In addition, wireless links exhibit varying characteristics over time and space due to obstructions in electric power systems. Hence,

the bandwidth and communication latency at each wireless link is location dependent and can vary intermittently. This makes it challenging to meet the QoS requirements Gungor *et al.* (2010).

In particular, research activities related to the reliability of WSNs in harsh smart grid environments in the presence of impulsive noise are extremely important for the deployment of WSNs in the smart grid Agba *et al.* (2019); Alam *et al.* (2016); Ndo *et al.* (2013); Sacuto *et al.* (2012). Impulsive noise may degrade the system performance for communications because its spectrum is powerful enough to be detected by any commercial wireless device. Hence, one should understand the impact of impulsive noise and modify the wireless communication technologies to adapt them to the impulsive channel such that better performance could be achieved. In the following section, the impulsive noise phenomena in substations and the existing impulsive noise models are discussed.

1.6 Impulsive Noise

Impulsive noise is defined by a process that switches from a background Gaussian noise to another noise for a short duration and as a result, the whole noise process is non-Gaussian Vaseghi, S. V. (2008). The noise characteristics in many wireless environments are highly non-Gaussian and are inherently impulsive in nature. Some of these include:

- Noise in power substations: Noise measurement campaigns in power substations Agba *et al.* (2019); Hikita *et al.* (1998); Portuguds *et al.* (2003); Sacuto *et al.* (2012) observed that the most powerful noise that is emitted from power equipment in a power substation such as from circuit-breakers, transformers, switch-gears, and busbars are impulsive in nature. In this context, the observed noise is composed of AWGN background noise with short oscillations occurring randomly which confirms that impulsive noise mainly characterizes the high voltage power substation RF environments. This noise is created mainly due to some electrical phenomenon like partial discharges, corona effects, etc. that occur within high voltage equipment in power substations. The observations revealed that the nature

of the noise depends on the feeding voltage of the equipment, the weather, and the nature of the insulators. Also, the measurements in time domain show the bursty nature of the impulsive noise Agba *et al.* (2019); Portuguds *et al.* (2003); Sacuto *et al.* (2012).

- Noise in powerline communication: The noise observed in powerline is the sum of noise waveforms produced and emitted to the lines from appliances connected to the power line network Ferreira, H., Lampe, L., Newbury, J. & Swart, T. (2010). The resultant noise is distributed with high amplitudes and short durations and is classified as impulsive noise Ferreira *et al.* (2010). In addition to the AWGN noise, power line communication systems are often encountered by the following types of impulsive noise Ferreira *et al.* (2010): (1)- Cyclic impulsive noise synchronous to AC mains, this class of noise is created by silicon-controlled rectifiers or thyristor-based light dimmers and appliances with a brush motor which involve a switching operation and impulsive noise are created synchronously to the mains voltage. (2)- Cyclic impulsive noise asynchronous to AC mains, which include the noise coming from a switching regulator. (3)- Isolated impulsive noise, this noise is created when a wall switch or a thermostat in heaters/foot-warmers makes/breaks the AC current.

- Microwave oven interference: The interference emitted from the microwave oven were measured in Kanemoto *et al.* (1998); Miyamoto, S. & Morinaga, N. (1997). From the measurement it was verified that the statistical characteristics of microwave oven interference are much different from those of Gaussian noise and the first order statistic is characterized by the Middleton Class-A impulsive noise model. Also, the interference is basically a periodic burst interference.

- Noise in indoor wireless communication: For possible indoor wireless communications, the authors in Blackard, K. L., Rappaport, T. S. & Bostian, C. W. (1993) developed statistical physical models for the generated indoor noises based on the results of their extensive measurement campaign. The measurements are done in three different bands at 918 MHz, 2.44 GHz, and 4 GHz in different places like inside a large grocery store, in an open-plan soft-partitioned office building and in a closed-plan hard-partitioned office building. Statistical analyses of the measurements are presented in the form of peak amplitude probability

distributions (PAPD), pulse duration distributions, and interarrival time distributions. The analysis indicates that the noise generated from photocopiers, printers (both line printers and cash register receipt printers), elevator door switches, microwave ovens, gas-powered engines with spark-gap ignition systems, and refrigeration compression motors that affect the indoor communication in office and retail environments are impulsive in nature. Also, in most cases, the impulses occur in short bursts.

- Man-made and natural noise: While in the above parts we discuss about particular impulsive noise environments, Middleton in his work in Middleton (1977) and the references therein showed that most man-made and natural electromagnetic interference or noise are highly non-Gaussian random processes whose distributions are impulsive in nature. In his measurement campaign, he considered interference effect from many man-made and natural interference sources like: interference from ore-crushing machinery in mines, interference from power lines radiations, interference from sun radiations, interference from fluorescent lights in mines and shops, automotive ignition noise from moving vehicles, atmospheric noise, etc. which shows excellent agreement with the statistical canonical models he proposed for different impulsive noise environments. These models classify noise environments into three general classes, Class-A, Class-B, and Class-C.

A theoretical impulsive noise is composed of short duration pulses with random occurrence times and amplitudes, different durations, and rise and fall times. Depending on the situation, to provide realistic, analytically tractable representations of the impulsive nature, many statistical-physical models have been developed in the literature. These are: Middleton Class-A noise model Middleton (1977), Bernoulli-Gaussian noise model Ghosh (1996), two-state Markov-Gaussian model Fertonani & Colavolpe (2009), Zimmermann Markov chain Zimmermann & Dostert (2002), and Markov-Middleton model Ndo *et al.* (2013). They offer different switching rules and noise parameters to characterize the noise. In the following, we will provide an overview of each model and explain the physical significance of each parameter of that model.

1.6.1 Middleton Class-A Model

David Middleton in his pioneer work Middleton (1977) classified the man-made and natural electromagnetic (EM) interference or noise into three broad categories, namely, Class-A, Class-B, and Class-C, according to the duration (T_I) of the typical interfering input waves compared to the receiver bandwidth ($\triangle f_R$) for communications using narrow-band receiver.

The necessary and sufficient condition for each class are described as follows Middleton (1977):

- The Class-A model considers that the noise consists of interferences that are mainly spectrally narrower than the receiver bandwidth. Here the transient decay period is negligible compared to the emission duration of the input noise and is stated as:

$$T_I \triangle f_R \gg 1. \tag{1.1}$$

  This model is more appropriate than the others for interference coming from other communications, EM emission from machinery, powerline radiations, and other EM clutter Middleton (1977).

- The Class-B model, on the other hand, corresponds to the category of noise whose spectral occupation is greater than the receiver bandwidth. Here the transient decay period is dominant compared to the emission duration and

$$T_I \triangle f_R \ll 1. \tag{1.2}$$

  This model is suitable for impulsive noise coming from other communications, EM clutter, and automobile ignition Middleton (1977).

- The Class-C model considers the more general case and assume that the noise is generated as additive mixtures of Class-A and Class-B noise and follows the same criterion as for the Class-B model.

$$T_I \triangle f_R \ll 1. \tag{1.3}$$

The main advantage of these models is that they are canonical Middleton (1977), that is, their analytical forms are invariant for particular noise source and its quantifying parameter values Middleton (1977); Middleton, D. (1999). However, these models are restricted to the following assumptions Middleton (1999):

- the noise events are independent,
- at any given instant any number of noise sources can emit, that is, the number of available noise sources is mathematically infinite, and
- the models represent the noise for the narrowband receiver case.

Out of the three noise models, the Class-A model is considered as the most suitable model for impulsive noise modeling in the literature because it requires the lowest number of parameters to represent and exhibits the most tractable PDF. In addition, it is applicable to a wide variety of electromagnetic environments where the model is well matched with the measured impulsive distributions Middleton (1999).

The Middleton Class-A model can be seen as a superposition of statistically independent impulsive source emissions where the sources are Poisson distributed and the amplitude of the sources follow the Gaussian distribution. The PDF of a real-valued Class-A noise sample n_k, where k represents the discrete-time index, is given by Middleton (1977)

$$f(n_k) = \sum_{m=0}^{\infty} \frac{p_m}{\sqrt{2\pi}\sigma_m} \exp\left(-\frac{n_k^2}{2\sigma_m^2}\right), \tag{1.4}$$

with

$$p_m = \frac{\exp^{-A} A^m}{m!}, \qquad \text{and} \qquad \sigma_m^2 = \sigma^2 \frac{m/A + \Gamma}{1+\Gamma}. \tag{1.5}$$

where p_m is the steady state probability of the m^{th} impulsive source and σ_m^2 is the variance of that impulsive source. For $m = 0$, the model generates the traditional AWGN component.

The parameters A, Γ, and σ^2 are called global parameters Middleton (1977) as these characterize the PDF. The physical significance of these parameters are Middleton (1977):

- A is called the impulsive index. This is defined as the average number of impulses per unit time (λ) impinging on the receiver times the impulse mean duration ($\bar{T}$)

$$A = \lambda \bar{T}. \tag{1.6}$$

  The smaller A, the fewer the number of impulsive events and/or their duration. In such case, the impulses are not dominant compared to the AWGN in the time domain Middleton (1977). Higher A implies that the impulse is more dominant compared to AWGN and by increasing it more, the impulsive noise becomes closer to the Gaussian noise.

- Γ is called the Gaussian to impulsive noise power ratio. It gives information on how strong the impulsive noise is compared to the independent AWGN noise and is defined as

$$\Gamma = \sigma_G^2/\sigma_I^2. \tag{1.7}$$

  The lower the Γ is, the stronger the impulsive noise compared to the background AWGN noise.

- σ^2 represents the total power of the noise n_k and is given by

$$\sigma^2 = \sigma_G^2 + \sigma_I^2. \tag{1.8}$$

In conclusion, although this model is popular due its canonical property, tractable PDF and good results to generate the amplitudes of impulsive noise as stated earlier, it does not provide any information on noise time-correlation.

1.6.2 Bernoulli-Gaussian Model

The Bernoulli-Gaussian model is the simplest form of impulsive noise modeling. Here, the occurrence of the impulses is modelled by a binary Bernoulli distribution and the amplitude of the impulses is modelled by a Gaussian distribution Ghosh (1996); Vaseghi (2008). Therefore, the

impulsive noise is represented as a product of Bernoulli distribution and Gaussian distribution as follows:

$$i_k = b_k g_k, \tag{1.9}$$

where b_k is the Bernoulli process, that is, an i.i.d. sequence of zeros and ones that takes a value of 1 with the probability of $p(b_k = 1) = \lambda$ and a value of 0 with a probability of $p(b_k = 0) = 1 - \lambda$, and g_k is the Gaussian process. Here, $b_k = 1$ indicates the presence of an impulse and $b_k = 0$ means the absence of an impulse. Therefore, the combined noise seen at the receiver is Ghosh (1996)

$$n_k = w_k + b_k g_k, \tag{1.10}$$

where w_k is the background AWGN noise. The PDF of n_k is given by Vaseghi (2008)

$$f(n_k) = \frac{1-\lambda}{\sqrt{2\pi\sigma_0^2}} \exp\left(-\frac{n_k^2}{2\sigma_0^2}\right) + \frac{\lambda}{\sqrt{2\pi\sigma_1^2}} \exp\left(-\frac{n_k^2}{2\sigma_1^2}\right). \tag{1.11}$$

where σ_0^2 is the variance of the background Gaussian noise and σ_1^2 is the variance of the impulsive noise. The whole model is therefore represented by only three parameters σ_0^2, σ_1^2, and λ. This model can be considered as an approximation of the Middleton Class-A model considering $m = 0$ and 1 only Vaseghi (2008). The concept of this model is thus simple because it assumes that there is only one sources of impulsive noise that generates i.i.d. impulses for a one-sample duration.

This model can also be represented by a binary-state Markov chain Vaseghi (2008) as shown in Figure 1.3. In this figure, *G* corresponds to the impulse off condition when only background Gaussian noise is present and *I* corresponds to the impulsive condition. As seen in the figure, this model is memoryless Vaseghi (2008) meaning that the probability of a transition to a next state is independent of the current state of the model and is given by

$$p(s_{k+1} = G \mid s_k = G) = p(s_{k+1} = G \mid s_k = I) = 1 - \lambda, \tag{1.12}$$

where s_{k+1} and s_k denotes the states at time $k+1$ and k. Similarly

$$p(s_{k+1} = I \mid s_k = I) = p(s_{k+1} = I \mid s_k = G) = \lambda. \tag{1.13}$$

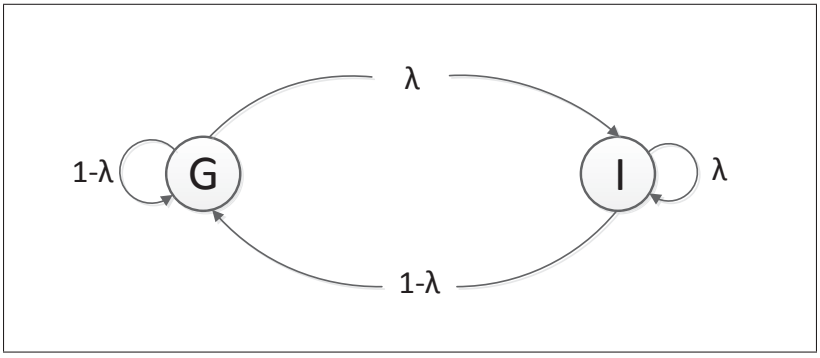

Figure 1.3 Markov chain representation of Bernoulli-Gaussian noise model

In conclusion, like the Middleton Class-A model, the Bernoulli-Gaussian model is also memoryless. However, these memoryless models which assume i.i.d. realizations of impulse emissions can not properly describe the bursty nature of the impulses Agba *et al.* (2019); Fertonani & Colavolpe (2009); Mitra, J. & Lampe, L. (2010); Ndo *et al.* (2013); Sacuto *et al.* (2012); Zimmermann & Dostert (2002) observed in many practical channels. Bursty nature refers to the time-correlation behavior of impulses that each impulse spans over several consecutive noise samples and may lead to severe performance degradation during data transmission Fertonani & Colavolpe (2009). In order to handle this time-correlation among consecutive samples, Markov chains have been investigated in the literature Agba *et al.* (2019); Fertonani & Colavolpe (2009); Mitra & Lampe (2010); Ndo *et al.* (2013); Sacuto *et al.* (2012); Zimmermann & Dostert (2002) which characterize the actual channel by a significant amount of memory. In the following, we will provide an overview of the Markovian impulsive noise models.

1.6.3 Two-state Markov-Gaussian Model

The two-state Markov-Gaussian model was introduced by Fertonani Fertonani & Colavolpe (2009) to characterize the correlated impulsive channel, different from the i.i.d. impulsive channel. For this model, at each time epoch k, the statistical properties of the noise sample n_k are completely defined by the channel state s_k, $s_k \in \{G,B\}$ where G stands for good channel (when the transmitted signal is only impaired by the background Gaussian noise) and B for bad channel (transmitted signals are impaired by impulsive interferers also). Conditioned on s_k, the PDFs of n_k are represented by Gaussian distributions whose variance is usually very high for the bad state compared to the good state, and expressed as Fertonani & Colavolpe (2009)

$$p(n_k = y_k - x_k | s_k = G) = \frac{1}{\sqrt{2\pi\sigma_G^2}} \exp\left(-\frac{n_k^2}{2\sigma_G^2}\right). \tag{1.14}$$

$$p(n_k = y_k - x_k | s_k = B) = \frac{1}{\sqrt{2\pi R\sigma_G^2}} \exp\left(-\frac{n_k^2}{2R\sigma_G^2}\right). \tag{1.15}$$

where $R \geq 1$ is the ratio between the average noise power in the bad channel and that in the good channel and σ_G^2 is the noise power of the good channel. The statistical description of the state process $s^K = \{s_0, s_1, \ldots, s_{K-1}\}$ completely characterizes the channel and for this model s^K is expressed as a stationary first-order Markov process Fertonani & Colavolpe (2009) with

$$p(s^{K+1}) = p(s_0) \prod_{k=0}^{K-1} p(s_{k+1}|s_k). \tag{1.16}$$

for each realization of the process. Therefore, the state process is described by the state transition probabilities $p_{s_k s_{k+1}} = p(s_{k+1}|s_k)$, $s_k, s_{k+1} \in \{G,B\}$. The state process underlying the channel is the same as the Gillbert-Elliott model Mushkin, M. & Bar-David, I. (1989) and provides a simple and effective way for describing a bursty evolution of the channel state Fertonani & Colavolpe (2009); Mushkin & Bar-David (1989). From the state transition probabilities, the stationary probabilities p_G and p_B of being in G and B state are respectively given

by Fertonani & Colavolpe (2009),

$$p_G = p(s_k = G) = \frac{p_{BG}}{p_{GB} + p_{BG}}. \tag{1.17}$$

$$p_B = p(s_k = B) = \frac{p_{GB}}{p_{GB} + p_{BG}}. \tag{1.18}$$

where P_{BG} denotes the transition probability from state B to state G and similarly p_{GB} is the transition probability from G to B. Therefore, the couple (p_{GB}, p_{BG}) completely describes the channel. Also, according to the notation in Fertonani & Colavolpe (2009), the parameter $\gamma = \frac{1}{p_{GB}+p_{BG}}$ quantifies the channel memory and there is a one-to-one correspondence between the pair (p_{GB}, p_{BG}) and (p_B, γ), with $\gamma = 1$ meaning that the channel is memoryless and $\gamma > 1$ indicating that the channel has persistent memory.

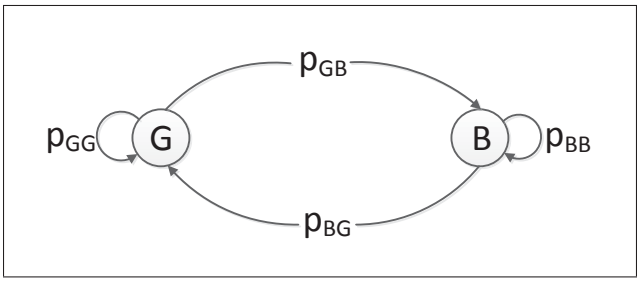

Figure 1.4 Markov chain representation of two-state Markov-Gaussian noise model

In conclusion, the two-state Markov-Gaussian model is a modification of the Bernoulli-Gaussian model that handles the noise memory with an extra parameter γ Fertonani & Colavolpe (2009). For the Bernoulli-Gaussian model, the state process S^K is represented by a stationary Bernoulli process, for this reason, it is called Bernoulli-Gaussian model whereas for the Markov-Gaussian model S^K is represented by the first-order Markov process and hence referred as Markov-Gaussian model. The latter model reduces to the former when $\gamma = 1$ Fertonani & Colavolpe (2009), that is, when the transition probabilities depend on the arrival state only. Therefore, the Markov-Gaussian model can be represented by the Markov chain by selecting different transition probabilities Vaseghi (2008) as shown in Figure 1.4.

1.6.4 Zimmermann Model

Zimmermann in his impulsive measurement campaign Zimmermann & Dostert (2002) showed that impulsive noise can cause burst errors in powerline communication systems. Although Gilbert-Elliot model Mushkin & Bar-David (1989) is a simple method of modeling random burst events which model the inter-arrival time (IAT) and the width of the impulsive events by an exponential distribution, Zimmermann measurements at powerline networks revealed that IATs as well as impulsive widths correspond to superpositions of several exponential distributions. To model such a scenario, he generalized the Gilbert-Elloit model by considering that the noise is composed of v background noise states and w impulsive states with a total number of $n = v + w$ states as shown in Figure 1.5. By setting $n = 2$, this proposed model reduces to the Gilbert-Elloit model.

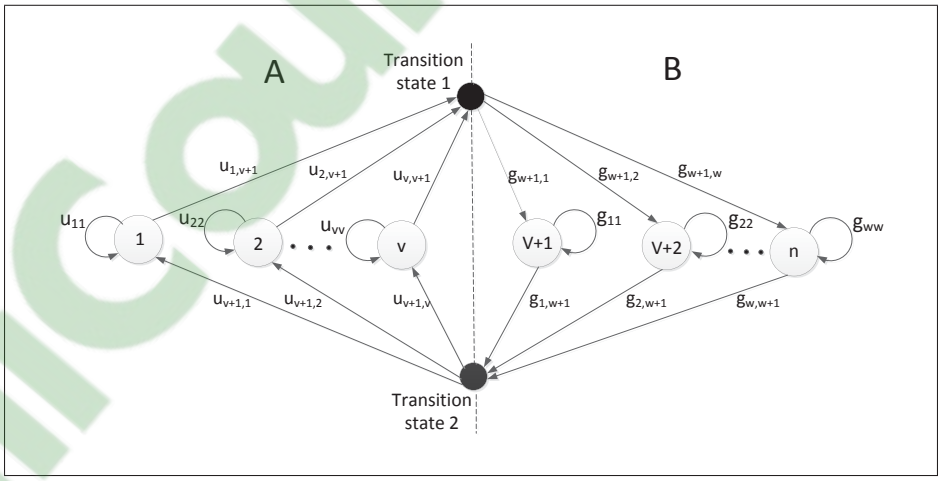

Figure 1.5 The Zimmermann noise model
Adopted from Zimmermann et al. (2002)

From Figure 1.5, it is seen that the states are partitioned into two groups A $(i = 1, 2, \ldots, v)$ and B $(i = v+1, v+2, \ldots, n)$. The states in A represent the impulse-free events and the states in B represent the occurrence of an impulsive event. In addition, in contrast to the Gilbert-Elloit model, two transition states are introduced that organize the transition from the impulse-free state to the impulsive state and vice versa. By doing so, the states in A and B can be described

by the independent transition probability matrices U and G as follows:

$$U = \begin{bmatrix} u_{1,1} & 0 & \dots & 0 & u_{1,v+1} \\ 0 & u_{2,2} & \ddots & \vdots & u_{2,v+1} \\ \vdots & \ddots & \ddots & 0 & \vdots \\ 0 & \dots & 0 & u_{v,v} & u_{v,v+1} \\ u_{v+1,1} & u_{v+1,2} & \dots & u_{v+1,v} & 0 \end{bmatrix}, G = \begin{bmatrix} g_{1,1} & 0 & \dots & 0 & g_{1,w+1} \\ 0 & g_{2,2} & \ddots & \vdots & g_{2,w+1} \\ \vdots & \ddots & \ddots & 0 & \vdots \\ 0 & \dots & 0 & g_{w,w} & g_{w,w+1} \\ g_{w+1,1} & g_{w+1,2} & \dots & g_{w+1,w} & 0 \end{bmatrix}$$

where the elements of the matrices U and G are determined from measured distributions by curve-fitting techniques Zimmermann & Dostert (2002).

In conclusion, the Zimmermann model gives good results in time domain since the model fits well with the measured data. Also, the model generates impulsive noise samples with a time correlation.

1.6.5 Markov-Middleton Model

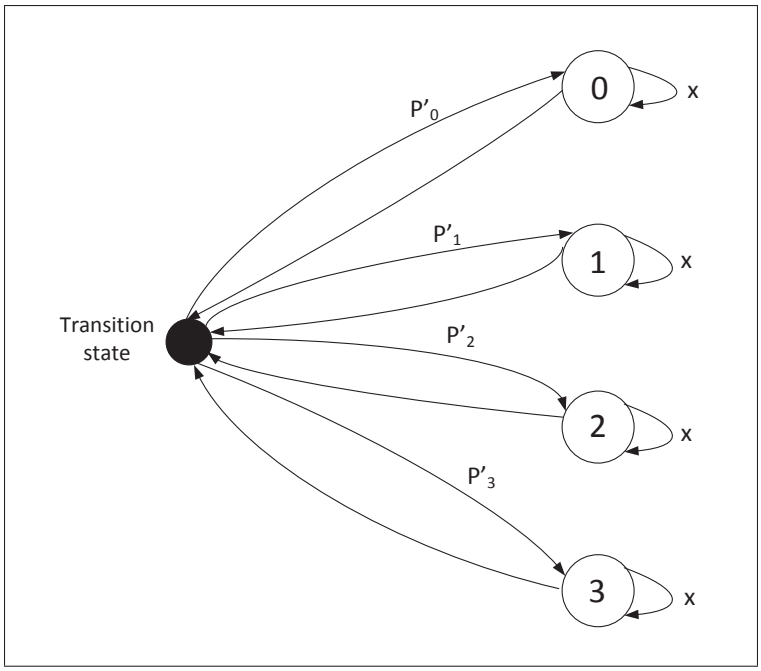

Figure 1.6 The Markov-Middleton noise model
Adopted from Ndo et al. (2002)

The Markov-Middleton model Ndo *et al.* (2013) consists of a Hidden Markov Model (HMM) Vaseghi (2008), and whose parameters are similar to the Middleton Class-A model. The main advantage of this model is that it follows the same PDF as the widely accepted and physically justified Middleton Class-A model. For this reason, this model also has better tractability and canonical property as the Middleton Class-A model and the existing methods in the literature that are successfully applied to estimate the parameters of the former model can be equally used to the later Ndo *et al.* (2013).

The truncated version with the first four terms of the PDF of a Markov-Middleton model is given by Ndo *et al.* (2013)

$$f(n_k) = \sum_{m=0}^{3} \frac{p'_m}{\sqrt{2\pi}\sigma_m} \exp\left(-\frac{n_k^2}{2\sigma_m^2}\right). \tag{1.19}$$

with

$$p'_m = \frac{p_m}{\sum_{m=0}^{3} p_m}. \tag{1.20}$$

where p'_m is the probability of entering state m from the transition state as shown in Figure 1.6 and σ_m^2 is the variance of the noise sample at that state as defined in (1.5). Also, the parameter x defines the probability of correlation between the noise samples which is independent of the Middleton Class-A parameters A, Γ and σ^2. The transition matrix of this model is given by Ndo *et al.* (2013)

$$P = \begin{bmatrix} x+(1-x)p'_0 & (1-x)p'_1 & (1-x)p'_2 & (1-x)p'_3 \\ (1-x)p'_0 & x+(1-x)p'_1 & (1-x)p'_2 & (1-x)p'_3 \\ (1-x)p'_0 & (1-x)p'_1 & x+(1-x)p'_2 & (1-x)p'_3 \\ (1-x)p'_0 & (1-x)p'_1 & (1-x)p'_2 & x+(1-x)p'_3 \end{bmatrix}$$

It is seen that for $x = 0$, the above model reduces to the i.i.d. Middleton Class-A model because under this consideration $p_{ij} = p'_j$ for all i, j, which means that the transition to state j is independent of the state i. In conclusion, the Markov-Middleton model is a modification of the Middleton Class-A model with an extra parameter that allows the control of the noise memory.

Now, to improve the reliability of wireless communications in the presence of impulsive noise, several impulsive noise mitigation techniques have been investigated in the literature. In the following sections, we will discuss the basic concepts of these mitigation techniques.

1.7 Impulsive Noise Mitigation Techniques

1.7.1 Conventional Impulsive Noise Mitigation Techniques

A common and rather simple approach for mitigation of impulsive interference is to detect high peak amplitudes in the time domain and reduce them which is the idea behind non-linear preprocessors that can be applied at the receiver. This non-linearity reduces the effect of large received signal amplitudes which are assumed to be the result of impulsive interference.

1.7.1.1 Clipping

For clipping, the received signal samples are compared to a clipping threshold T_c. If the absolute value of the signal sample exceeds T_c, it is clipped as follows Ndo, G., Siohan, P. & Hamon, M.-H. (2010):

$$r_k = \begin{cases} y_k & \text{if } |y_k| \leq T_c \\ T_c \; sgn(y_k) & \text{otherwise,} \end{cases} \tag{1.21}$$

where r_k is the clipped output of y_k.

1.7.1.2 Blanking

For blanking, the received signal samples whose absolute value is greater than a given blanking threshold T_b are replaced by zero, which can be formulated as Zhidkov, S. V. (2006)

$$r_k = \begin{cases} y_k & \text{if } |y_k| \leq T_b \\ 0 & \text{otherwise,} \end{cases} \tag{1.22}$$

where r_k is the blanked output of y_k.

1.7.1.3 Combined Clipping-Blanking

For combined clipping-blanking, two threshold values T_b and T_c are needed. The definition of this operation is recalled as

$$r_k = \begin{cases} y_k & \text{if } |y_k| \leq T_c \\ T_c \; sgn(y_k) & \text{if } T_c < |y_k| \leq T_b \\ 0 & \text{if } |y_k| > T_b, \end{cases} \tag{1.23}$$

Hence, for this scheme, the medium amplitude signals are clipped while the large amplitude signals are blanked.

From the above non-linear operations it can be inferred that the optimal values of T_c and T_b play a vital role in obtaining the best mitigation performance.

In general, derivatives of the aforementioned nonlinear methods have been widely investigated in case of OFDM transmission impaired by memoryless impulsive noise Ndo *et al.* (2010); Zhidkov (2006). Although OFDM systems were shown to be more resilient to non-Gaussian impulsive interference compared to single-carrier systems due to the random distribution of their noise energy over multiple sub-carriers Ndo *et al.* (2010); Zhidkov (2006), we note that OFDM is outperformed by its single-carrier counterpart when the impulses are very strong and/or they occur frequently Ghosh (1996), which likely exists in contemporary communication systems including smart grid communications, power line communications, industrial wireless sensor network communications, etc. Also, there are certain circumstances, for example, in the low SNR region, where, under impulsive noise, single-carrier modulation performs better than multi-carrier modulation Shongwe, T., Han Vinck, A. & Ferreira, H. C. (2015). Moreover, the IFFT and FFT complexities are eliminated through single-carrier communication. This is essential for internet of things (IoT) applications in industry, smart grid, smart home, etc., which require tiny sensors with low complexity and small batteries; thus, operating in the low SNR regime. Likewise, the assumption of memoryless noise model is not valid for many communication scenarios, for example, see Agba *et al.* (2019); Asiyo, M. O. & Afullo,

T. J. (2017); Bai, T., Zhang, H., Zhang, R., Yang, L.-L., Al Rawi, A. F., Zhang, J. & Hanzo, L. (2017); Blackard *et al.* (1993); Ndo *et al.* (2013); Sacuto, F., Labeau, F. & Agba, B. L. (2014); Shongwe *et al.* (2015); Zimmermann & Dostert (2002) and the references therein. The memoryless noise models might be able to generate noise samples by ensuring a good trade-off between mathematical simplicity and accurate characterization of the physical phenomenon, but they cannot take into account one of the main features of the actual noise, i.e., the time-correlation among the impulsive noise samples. To improve the reliability in the presence of bursty impulsive noise modeled by a Markov-Gaussian process, convolutional error correcting coding Mitra & Lampe (2010) and LDPC coding Alam *et al.* (2016); Fertonani & Colavolpe (2009) have been considered in the literature. It was shown that considerable performance gains can be achieved when the impulsive noise memory is utilized in the detection process. The author in Lampe, L. (2011) has considered sparse Bayesian learning methods to estimate the presence of bursty impulsive noise.

Despite the practical relevance of impulsive noise with memory, to the best of our knowledge, there are no existing results on the performance analysis of impulsive noise mitigation techniques for point-to-point single-carrier communication systems impaired by bursty impulsive noise. Moreover, although widely acknowledged for their simplicity, ease of implementation, and fairly good performance, nonlinear preprocessing techniques have not been considered in the context of this scenario.

1.7.2 LLR-based Mitigation

LLR receivers are known to improve the performance of conventional receivers. Therefore, they have been proposed for the mitigation of impulsive noise where the receiver performs the computation of the LLR for each symbol considering the exact statistics of the impulsive noise. Two algorithms are commonly employed for the calculation of LLR values. The first scheme which is suitable for memoryless noise models performs the LLR computation on a symbol-by-symbol basis, whereas in the second scheme, referred to as the BCJR or the MAP algorithm Bahl, L., Cocke, J., Jelinek, F. & Raviv, J. (1974), the LLR values are calculated

after receiving an information block sequence. The later algorithm is quite suitable for noise models with memory and is generally more complex to be implemented than the previous one.

1.7.2.1 LLR Calculation for Memoryless Impulsive Noise:

The derivation of the LLR expression for BPSK modulated signals over Middleton class-A noise has been detailed in Nakagawa, H., Umehara, D., Denno, S. & Morihiro, Y. (2005); Umehara, D., Yamaguchi, H. & Morihiro, Y. (2004) and can be expressed as

$$\begin{aligned} L_A(y_k) &= \ln \frac{p(y_k|x_k=+1)}{p(y_k|x_k=-1)} = \ln \frac{p_A(y_k-1)}{p_A(y_k+1)} \\ &= \ln \sum_{m=0}^{\infty} \frac{p_m}{\sqrt{2\pi\sigma_m^2}} \exp\left(-\frac{(y_k-1)^2}{2\sigma_m^2}\right) - \ln \sum_{m=0}^{\infty} \frac{p_m}{\sqrt{2\pi\sigma_m^2}} \exp\left(-\frac{(y_k+1)^2}{2\sigma_m^2}\right), \end{aligned} \tag{1.24}$$

where p_A is the Middleton class-A PDF. It is easily seen that the LLR calculation in the above expression cannot be easily simplified due to the logarithm and the exponential functions. As in (1.24), the LLR expression for the Bernoulli-Gaussian noise assuming BPSK modulation can be written as

$$\begin{aligned} L_{BG}(y_k) &= \ln \frac{p(y_k|x_k=+1)}{p(y_k|x_k=-1)} = \ln \frac{p_{BG}(y_k-1)}{p_{BG}(y_k+1)} \\ &= \ln \sum_{m=0}^{1} \frac{p_m}{\sqrt{2\pi\sigma_m^2}} \exp\left(-\frac{(y_k-1)^2}{2\sigma_m^2}\right) - \ln \sum_{m=0}^{1} \frac{p_m}{\sqrt{2\pi\sigma_m^2}} \exp\left(-\frac{(y_k+1)^2}{2\sigma_m^2}\right) \end{aligned} \tag{1.25}$$

1.7.2.2 LLR Calculation for Impulsive Noise with memory

Here, we introduce the LLR computation in case of impulsive noise with memory by utilizing the well-known BCJR or MAP algorithm. The MAP decoding algorithm is a recursive technique that computes the LLR of each bit, based on the entire observed data block of length K. For BPSK modulation, the LLR value at time k, $k = 1, 2, \ldots, K$ is defined as

$$L_k = \ln \left\{ \frac{p(x_k=1|y^K)}{p(x_k=-1|y^K)} \right\}, \tag{1.26}$$

where $y^K = \{y_0, y_1, \ldots, y_{K-1}\}$ is the whole sequence to be detected, and K is the size of the sequence. Thus, at each k, the optimal MAP detector at the receiver evaluates the a posteriori probability (APP) $p(x_k|y^K)$ for each symbol x_k belonging to the binary modulation alphabet {1,-1}. By defining the probabilities

$$\begin{aligned} \alpha_k(s_k) &= p(y_0, y_1, \ldots, y_{k-1}, s_k) && (1.27) \\ \beta_k(s_k) &= p(y_k, y_{k+1}, \ldots, y_{K-1}|s_k) && (1.28) \\ \delta_k(x_k, s_k, s_{k+1}) &= p(s_{k+1}|s_k)p(n_k = y_k - x_k|s_k) && (1.29) \end{aligned}$$

it is shown in Alam *et al.* (2016) that the APP can be rewritten as

$$p(x_k = b, y^K) = p(x_k = b) \sum_{s_k, s_{k+1}} \alpha_k(s_k)\beta_{k+1}(s_{k+1})\delta_k(x_k = b, s_k, s_{k+1}), \quad (1.30)$$

where s_k and s_{k+1} denote the noise states at time k and $k+1$ respectively, where $\alpha_k(s_k)$ and $\beta_k(s_k)$ are referred to as the forward and backward filters, and $\delta_k(x_k, s_k, s_{k+1})$ represents the branch metrics of the trellis diagram used for decoding the Markov-Gaussian model. The forward and backward filters can be recursively computed as

$$\begin{aligned} \alpha_{k+1}(s_{k+1}) &= \sum_{s_k, x_k} \alpha_k(s_k)p(x_k)\delta_k(x_k, s_k, s_{k+1}), && (1.31) \\ \beta_k(s_k) &= \sum_{s_{k+1}, x_k} \beta_{k+1}(s_{k+1})p(x_k)\delta_k(x_k, s_k, s_{k+1}), && (1.32) \end{aligned}$$

where the forward and backward filters are initialized with

$$\alpha_0(s_0 = S) = p_S, \text{ and } \beta_K(s_K = S) = 1. S \in (G, B) \quad (1.33)$$

Hence, the MAP decoding algorithm consists of the following steps:

- Initialize forward and backward recursions $\alpha_0(s_0)$ and $\beta_K(s_K)$
- Compute branch metrics δ_k

- Carry out forward recursion $\alpha_{k+1}(s_{k+1})$ based on $\alpha_k(s_k)$
- Carry out backward recursion $\beta_k(s_k)$ based on $\beta_{k+1}(s_{k+1})$
- Compute APP and LLR values

On the other hand, in case of AWGN channel, the LLRs are given by Nakagawa *et al.* (2005)

$$L(y_k) = \frac{2}{\sigma_G^2} y_k. \tag{1.34}$$

From (1.34), it is observed that the LLRs linearly depend on the observation y_k in case of AWGN channel.

In addition to these techniques, other forms of impulsive noise mitigation techniques include: (i)- iterative techniques Zhidkov, S. V. (2003), where the idea is to estimate the impulsive noise as accurately as possible at the receiver side through iteration and to subtract the estimation from the received vector, (ii)- error correction coding employing convolutional coding Li, T., Mow, W. H. & Siu, M. (2008), turbo coding Umehara *et al.* (2004), low density parity check coding Nakagawa *et al.* (2005), polar coding Hadi, A., Rabie, K. M. & Alsusa, E. (2016), etc., and (iii)- compressed sensing Al-Naffouri, T. Y., Quadeer, A. A. & Caire, G. (2014); Lin, J., Nassar, M. & Evans, B. L. (2013).

On the othe hand, collaborative WSNs where the sensor nodes cooperate among themselves can be one of the promising candidates for transmission in smart grid environments due to their reliability over fading and interference channels Laneman, J. N., Tse, D. N. & Wornell, G. W. (2004); Nosratinia, A., Hunter, T. E. & Hedayat, A. (2004). In the following sections, we will discuss the basic concepts of cooperative communication and its opportunities to overcome the adverse effect of impulsive noise in high voltage smart grid environments.

1.8 Cooperative Communication

The basic idea behind cooperative communication relies on the fact that the signal transmitted or broadcast by the source node is not received by the destination node only but also by the other nodes in the transmission range of the source node. These nodes are referred to as relays. The destination then combines the signal coming from the source as well as the relays to form a global decision, thereby creating spatial diversity. Thus, the overall system acts as a virtual MIMO communication system, although each node is equipped with a single antenna, and achieves the potentials of space diversity such as improved performance, extended coverage, lower transmission power, increased system capacity, etc. Laneman *et al.* (2004); Nosratinia *et al.* (2004).

The concept of cooperative diversity was originally introduced in Van Der Meulen, E. C. (1971) by Vander Meulen's earlier work on relay channel model and its performances are investigated extensively by Cover and EI Gamal in Cover, T. & Gamal, A. E. (1979). Later, more detail are analyzed in Laneman, J. N. & Wornell, G. W. (2003); Laneman *et al.* (2004); Sendonaris, A., Erkip, E. & Aazhang, B. (2003a,0). The classical relay channel model is comprised of three terminals Laneman *et al.* (2004); Sendonaris *et al.* (2003a); Van Der Meulen (1971): a source that transmits information, a destination that receives information, and a relay that both receives and transmits information in order to enhance communication between the source and destination. Models with multiple relays have been examined in Kramer, G., Gastpar, M. & Gupta, P. (2005); Laneman & Wornell (2003); Sadek, A. K., Su, W. & Liu, K. R. (2007) and others.

In cooperative communication, the key aspects are related to the processing of the signal received at the relay transmitted from the source and the ability of the receiver at the destination to coherently and optimally combine the incoming signals. The former is categorized by the cooperative communication protocol and the later is dependent on the types of combining at the destination. In the following, we will provide a flavor of these techniques.

1.8.1 Cooperative Communication Protocols

There are different cooperative communication protocols proposed in the literature based on different types of processing at the relay terminals. The cooperative communication takes place in two phases Laneman *et al.* (2004): in the first phase, the source transmits its signal $x_{s,k}, k = 1, 2, \ldots, K$. The relay then processes its corresponding received signal $y_{r,k}$ and forwards it to the destination in the second phase. The basic relaying protocols are:

- Amplify-and-forward relaying: In amplify-and-forward (AF) relaying Laneman *et al.* (2004), each relay receives a noisy and faded version of the signal transmitted by the source and as the name implies, the relay then just amplifies the received signal subject to a total power constraint without decoding it and forwards it to the destination. The destination then combines the signal received from the source and the relay by using any of a variety of combining techniques detailed later to make a final decision about the transmitted signal. For AF relaying,

$$x_{r,k} = \beta_r y_{r,k}. \tag{1.35}$$

  where $x_{r,k}$ is the transmitted signal from the relay and β_r is the amplification factor at the relay given by

$$\beta_r = \sqrt{\frac{\mathrm{P}_r}{|\, h_{sr}\,|^2\, \mathrm{P}_s + \sigma_r^2}}. \tag{1.36}$$

  where P_s is the transmitted power from the source, P_r is the transmitted power from the relay, h_{sr} is the fading coefficient between the source and the relay, and σ_r^2 is the variance of the AWGN noise that corrupts the received signal at the relay. It is shown that this method achieves full spatial diversity in the number of cooperative terminals Laneman & Wornell (2003); Laneman *et al.* (2004). Although this method is simple and achieves the full spatial diversity, its downside is that the noise accumulated in the received signal at the relay is also amplified and forwarded to the destination.

- Decode-and-forward relaying: In decode-and-forward (DF) relaying, the relay decodes the received signal, re-encodes it, and then forwards it to the destination Laneman *et al.* (2004);

Sendonaris *et al.* (2003a). For this scheme, the relay forms an estimate $\hat{x}_{s,k}$ by decoding its corresponding received signal $y_{r,k}$ and relays a re-encoded version of $\hat{x}_{s,k}$ to the destination. The destination then combines the signal received from the source and the relay to make the final decision. So, DF relaying is prone to error propagation due to the probability of decoding errors at the relay.

Besides these two most common basic relaying techniques, a few other proposed relaying protocols are:

- Compress-and-forward relaying: In compress-and-forward (CF) relaying, the relay transmits a quantized and compressed version of the received signal to the destination, without decoding the source message at all Cover & Gamal (1979); Kramer *et al.* (2005); Lai, L., Liu, K. & El Gamal, H. (2006). Some authors also prefer the names estimate-and-forward, observe-and-forward, and quantize-and-forward.

- Coded cooperation: Coded cooperation is a method that integrates the cooperation into channel coding Hunter, T. E. & Nosratinia, A. (2006). Although the relay repeats the bits sent by the source in the above relaying, in coded cooperation, the relay sends incremental redundancy, which then combined at the receiver with the codeword sent by the source, results in a codeword with a larger redundancy.

However, all of the above fixed relaying techniques suffer from low spectral efficiency Laneman *et al.* (2004). This problem can be overcomed through adaptive relaying such as selective relaying and incremental relaying.

- Selective relaying: In selective relaying , if the SNR of a signal received at the relay exceeds a certain threshold, the relay decodes the received signal and forwards the decoded information to the destination Laneman *et al.* (2004). On the other hand, if the SNR falls below the threshold, the relay remains idle.

- Incremental relaying: For incremental relaying, a feedback channel from the destination to the source and the relay is necessary Laneman *et al.* (2004). The destination sends an

acknowledgment to the relay if it is able to receive the source message correctly in the first transmission phase. So the relay does not need to transmit and the source transmits new information in the next time slot. On the other hand, if the source transmission was not successful in the first phase, the relay forwards the received signal from the source through any of the fixed relaying protocols by exploiting the limited feedback from the destination. This protocol has the best spectral efficiency among the previously described fixed and selection relaying protocols since the relay does not always need to transmit.

1.8.2 Types of Combining

The effectiveness of cooperative relaying is also dependent on the ability of the receiver to coherently and optimally combine the incoming signals Goldsmith, A. (2005). Various combining strategies have been proposed in the literature based on the complexity and the availability of channel knowledge at the receiver. A combining strategy defines how the receiver deals with multiple signals that are assumed to arrive through independently fading paths. Combining strategies are categorized based on the weights that are associated with the individual branches. These are Goldsmith (2005):

- Equal-ratio combining: In equal-ratio combining (ERC), after co-phasing, the signals coming from individual branches are combined with equal weights. It is the easiest method of combining. Co-phasing is the process where the phase associated with the incoming signals arrived over independent paths are removed prior to the combining Goldsmith (2005).

- Fixed-ratio combining: In fixed-ratio combining (FRC), each individual signal is assigned a fixed weight that does not change for the entire communication where the weight associated with each branch is an estimate of the perceived average channel quality.

- Selection combining (SC): In this method, the signal from the path that has the highest average SNR is selected and the remaining signals are discarded.

- Maximum-ratio combining (MRC): In this, the signal received from all the individual branches are optimally combined (optimally in the sense that the output SNR is maximized

at the decision device). MRC is based on the assumption that the receiver knows the channel gain h_k corresponding to the individual branches.

- Soft information combining: In soft information combining (SIC) Changcai, H. & Weiling, W. (2008), the soft information generated from different branches are properly weighted and combined to make the final decision about the information bits.

1.8.3 Cooperative Communications over Impulsive Noise Channels

There exists a large number of publications on cooperative diversity schemes in various aspects such as cooperation protocols, information theoretic analysis, relay selection schemes, diversity-multiplexing trade-offs, optimal power allocation, cross-layer design, etc. However, most of these are restricted to the conventional assumption that the noise samples at the relays and the destination are AWGN which basically represents the thermal noise at the receiver. As mentioned earlier, many practical wireless communication systems are not only impaired by the AWGN noise but also by the impulsive noise which may degrade the system performance for communications because its spectrum is powerful enough to be detected by any commercial wireless device.

The performance of cooperative communications in impulsive noise channels has only recently been considered in the literature. The error rate performance of the AF cooperative relaying (CR) scheme with M relays over flat fading channels in the presence of impulsive noise modeled by Middleton Class-A noise has been investigated in Al-Dharrab, S. & Uysal, M. (2009a). It is assumed that the relays employ either space-time block coding (STBC) or repetition-based coding to forward their observation to the destination. Through the derivations of pairwise error probability (PEP) assuming minimum distance receiver (MDR), they provided the bounds on the error rate performance for both spatially dependent and independent impulsive noise environments. Simulation results demonstrated that the performance of cooperative systems highly depends on the impulsive nature of the noise and different diversity orders are achieved in different SNR regions. Also, for different relays locations, the same diversity order is obtained irrespective of the location of the relays. In addition, for smaller SNR values, in highly

impulsive environments, the performance in spatially dependent noise is better than that over the spatially independent case and this flips for the higher SNR region. On the other hand, in near-Gaussian noise, both cases show a similar performance. They have further investigated the optimal power allocation (OPA) among cooperating nodes based on the minimization of the union bound on the BER. It is shown that better performance gain could be obtained in a highly impulsive environment through optimal power allocation using numerical search.

A similar performance analysis has been carried out in Savoia, R. & Verde, F. (2011) for both centralized (STBCs are designed in a centralized fashion) and decentralized (STBCs are designed in a decentralized manner) space-time block coded cooperative diversity schemes with multi-relay DF relaying in case of fading and Middleton Class-A impulsive disturbance. By employing cyclic redundancy check (CRC) at the relays, it is assumed that, out of all the available relays, the ones that successfully decode the source symbol will serve as potential relays for cooperation. For detection, the maximum likelihood (ML) criterion is employed at the destination. To show the effect of impulsiveness, both the diversity order and coding gain are evaluated at the output of the ML detector by deriving the PEP and symbol error probability (SEP) expressions. Numerical results show that the system achieves full diversity order and coding gain asymptotically as seen for the case of Gaussian noise, however at finite SNR, due to the effect of impulsive disturbance the diversity order fluctuates and does not increase monotonically with the SNR.

Meanwhile Al-Dharrab & Uysal (2009a); Savoia & Verde (2011) considered the impact of Class-A impulsive disturbance on the performance of different CR schemes, the authors in Nasri, A. & Schober, R. (2010) generalize the performance analysis of CR schemes which is valid for any non-Gaussian noise and interference. Examples of such non-Gaussian noise and interference include: narrow-band interference (NBI), co-channel interference (CCI), and ultra-wideband (UWB) interference Nasri & Schober (2010). The only restriction imposed on the noise is that all its moments are finite. Closed-form asymptotic symbol-error rate (SER) and BER expressions have been derived for an AF cooperative relaying scheme with multiple relays transmitting over independent Rayleigh faded channels in the presence of any non-Gaussian

noise and interference and employing MRC combining at the destination. The framework is valid for arbitrary linear modulation formats and an arbitrary number of relays. The simulation results reveal that, at high SNR, full diversity order is obtained by this system that is equal to the number of paths between the source and the destination and is independent of the type of noise. In addition, a new relay selection technique is proposed for non-Gaussian environments based on the developed asymptotic expressions which take into account the possibly non-Gaussian behavior of the noise. The obtained results showed that the new relay selection criterion yields significant performance improvement over the conventional relay selection scheme developed for Gaussian cases.

The authors in Tepedelenlioglu, C. & Gao, P. (2005) investigate the performance of different diversity combining techniques over fading channels with impulsive noise modeled by Middleton Class-A through the derivation of average BER. The combining techniques are MRC, ERC, SC, and post detection combining (PDC) which have been proposed in the literature for AWGN channels depending on the complexity and the degree of knowledge available at the receiver. For the analysis two noise models are considered. In model *I*, it is assumed that different diversity branches are influenced by the same physical process creating the impulses, thereby the noise samples in different branches will be statistically dependent whereas under model *II*, it is assumed that the noise samples in different branches are independent and identically distributed. From the simulation results it is seen that while, for both model *I* and *II*, the MRC combining is the best choice out of all the combining techniques in most cases, PDC performs better than EGC, MRC, and SC when the number of branches is more than four under model *II*. In other situations, PDC shows the worse performance among all the combining techniques. Also, there exists a trade-off between diversity gain and coding gain and this become more adverse when the noise is more impulsive.

The authors in Van Khuong, H. & Le-Ngoc, T. (2010) studied the performance of direct transmission and DF CR scheme with single relay over independent frequency-flat Rayleigh fading and Bernoulli-Gaussian impulsive noise through the derivation of the SEP expression. For cooperation, it is assumed that the relay forwards its decoded information to the destination

only if it successfully recovers the source information, otherwise, it will stay in silent mode. Different combining schemes are assumed at the destination based on the level of available knowledge of the impulsive noise at the destination. Both the analytical and simulation results showed that using MRC at the destination, CR performs significantly better than direct transmission under the same bandwidth efficiency and power consumption for low impulse power and impulse rate. On the other hand, an additional 3 dB gain could be achieved by considering the optimal Bayes receiver Tepedelenlioglu & Gao (2005) at the destination in place of MRC. This is because MRC is optimal over AWGN channels in the sense of minimizing the BER and does not take into account the impulsive effect in the detection process, the Bayes receiver shows optimal performance over the impulsive channel by using the knowledge of the impulsive noise's stochastic properties in the detection process. However, the diversity order obtained for both receiver cases are the same. Optimal power allocation for the source and relay of this scheme is also studied using exhaustive search and it is shown that OPA brings a negligible performance improvement compared to the equal power allocation (EPA) scheme. In Van Khuong, H. & Le-Ngoc, T. (2011), the same authors have further investigated the performance with source retransmission in the second phase when the relay fails to detect the source signal and showed that CR with source retransmission brings negligible performance improvement.

However, all of the above performance analysis for CR schemes have been carried out over impulsive channels modeled by either Middleton Class-A or simple Bernoulli-Gaussian which usually generate the impulses with i.i.d. realizations. The i.i.d. behavior does not provide any information on the bursty nature of the impulsive noise which was observed in practice on measured impulses in many impulsive noise measurement campaigns, for example, in power substations Sacuto *et al.* (2012); Shan, Q., Glover, I. A. & et.al. (2011); Zimmermann & Dostert (2002) or near a microwave oven Kanemoto *et al.* (1998); Nassar, M., Lin, X. E. & Evans, B. L. (2011). In this context, Fertonani & Colavolpe (2009) provided a transceiver architecture for the correlated impulsive noise channel. A two-state Markov-Gaussian model is adopted to describe the typical bursty nature of the impulsive noise. The achievable information rate as well

as the BER of this channel are computed by exploiting LDPC codes and iterative receivers based on MAP detection. It is shown that exploiting the memory of the noise process at the receiver improves the obtained performance which is significantly better than the case of conventional receivers that neglect the channel memory. Also, the performance gain provided by the presence of memory quantitatively depends on different noise environments characterized by the different noise parameter values.

Assuming the two-state Markov-Gaussian noise model as considered in Fertonani & Colavolpe (2009) to characterize the channel, the authors in Mitra & Lampe (2010) studied the performance of various optimum and sub-optimum decoding metrices using convolutional coding at the transmitter and Viterbi decoding at the receiver. The analytical expressions for the cutoff rate and BER performances are derived for the proposed metrics. From the simulation and analytical results, it is confirmed that compared to the conventional Euclidean distance metric which is optimal for the AWGN channel, better performance could be achieved by incorporating the proposed improved decoding metrics based on the amount of information about the noise process available at the receiver. In addition, the effect of interleaving depth on the performance is also analyzed and it is shown that an interleaver depth of about twice the average time spent in the bad noise state is required to successfully disperse the noise bursts. On the other hand, a significant performance degradation is observed with imperfect interleaving.

To the best of our knowledge, no research results have been published on the performance analysis of collaborative WSN schemes over bursty impulsive noise channels . It is therefore important to develop cooperative relaying schemes over such channel that take into account the memory of the impulsive noise for detection.

On the other hand, although the impacts of memoryless impulsive noise have been widely investigated on the detection of finite alphabets in point-to-point and collaborative WSN communications, the performance of estimation techniques in the presence of impulsive noise is not widely acknowledged. Recently, the authors in Banelli, P. (2013) considered the MMSE OBE for a Gaussian source impaired by Middleton class-A impulsive noise. It is shown that

the performance of the proposed MMSE OBE strictly depends on the statistical characteristics of the received signal. The authors in Flam, J. T., Chatterjee, S., Kansanen, K. & Ekman, T. (2012) derived the MMSE OBE and its mean square error (MSE) performance bounds in closed form when both the noise and the source signals are Gaussian mixture (GM) distributed. The obtained results showed that the performance improvement of the optimal MMSE estimator over the Linear MMSE (LMMSE) estimator under this condition is substantial. However, the analyses in Banelli (2013); Flam *et al.* (2012) are restricted to the point-to-point scenario impaired by memoryless impulsive noise. To the best of my knowledge, no results exist for the collaborative estimation of Gaussian sources in the presence of impulsive noise.

The above results motivate us to consider the performance analysis of collaborative WSN for reliable transmission over impulsive noise channels.

CHAPTER 2

MITIGATION TECHNIQUES FOR IMPULSIVE NOISE WITH MEMORY

Md Sahabul Alam [1], Bassant Selim[1], Georges Kaddoum[1], Basile L. Agba [2]

[1] Département de Génie Electrique, École de Technologie Supérieure,
1100 Notre-Dame Ouest, Montréal, Québec, Canada H3C 1K3
[2] Hydro-Quebec Research Institute (IREQ), Varennes, QC, Canada, J3X 1S1

Article submitted in IEEE Systems Journal, May, 2019.

2.1 Abstract

Impulsive noise, a common impediment preventing the system from achieving error-free transmission, is significant in many wireless and power line communication environments. Although the performance of several mitigation techniques for orthogonal frequency division multiplexing (OFDM)-based multi-carrier communication systems impaired by memoryless impulsive noise are widely acknowledged, we note that OFDM is outperformed by its single-carrier counterpart when the impulses are very strong and/or they occur frequently, which is likely to exist in contemporary communication systems including smart grid communications. On the other hand, many communication technologies used in the smart grid do not employ OFDM and likewise, the assumption of memoryless noise is not valid for such communication scenarios. Memoryless noise models cannot take into account one of the main features of the actual noise, i.e., the time-correlation among the noise samples. The aim of this paper is to compare and analyze several mitigation techniques such as clipping, blanking, and combined clipping-blanking to mitigate the noxious effects of bursty impulsive noise for low-density parity-check coded single-carrier communication systems. Moreover, we propose a log-likelihood ratio (LLR)-based impulsive noise mitigation for the considered scenario. In this context, provided simulation results highlight the superiority of the LLR-based mitigation scheme over the clipping/blanking schemes.

2.2 Introduction

Interference and noise characterized by a non-Gaussian impulsive behavior are common impediments in many practical communication systems. Several studies show sufficient evidence that many communication environments, such as, smart grid communications Agba *et al.* (2019); Sacuto *et al.* (2014), power line communications (PLCs) Asiyo & Afullo (2017); Zimmermann & Dostert (2002), indoor wireless communications Blackard *et al.* (1993), industrial wireless sensor network communications Cheffena, M. (2012), digital subscriber loop (DSL) communications Bai *et al.* (2017), etc. are impaired by impulsive man-made electromagnetic interference or atmospheric noise Middleton (1977). For example, in power grids, due to partial discharge and switching effects, the noise emitted from various power equipment, such as transformers, busbars, circuit-breakers, and switchgears are impulsive. Due to the adverse effects of such interference on the system's performance, over the last few decades, several statistical models and their canonical parameters were suggested to model different impulsive behaviour Fertonani & Colavolpe (2009); Ghosh (1996); Middleton (1977); Ndo *et al.* (2013). They offer different switching rules and noise parameters to characterize the noise and are mainly classified into two categories: impulsive noise without memory (Middleton Class-A noise model Middleton (1977), Bernoulli-Gaussian noise model Ghosh (1996), etc.), and impulsive noise with memory (two-state Markov-Gaussian model Fertonani & Colavolpe (2009), Zimmermann Markov chain model Zimmermann & Dostert (2002), Markov-Middleton model Ndo *et al.* (2013), etc.). Memoryless impulsive noise models assume that the impulsive noise samples are independent and identically distributed (i.i.d.), which simplifies the impulsive noise generation and parameter estimation. On the other hand, for noise models with memory, impulsive samples appear in bursts which implies that there is a time correlation among the noise samples.

The installation of wireless technologies requires the exact characteristics of the surrounding noise. In this context, it is widely acknowledged that communication systems designed under the additive white Gaussian noise (AWGN) assumption typically suffer from sever performance degradation and their reliability is significantly affected when exposed to impulsive noise Alam *et al.* (2016); Alam, M. S., Kaddoum, G. & Agba, B. (2018a); Alam, M. S., Kad-

doum, G. & Agba, B. L. (2018b); Spaulding, A. & Middleton, D. (1977) . This elevates the need for the performance analysis of communication systems, which are not only disturbed by background Gaussian noise, but also by impulsive noise, in order to provide pragmatic information for the system designer. A typical stringent requirement towards realizing such systems is the high reliability in the presence of impulsive noise.

Several methods have been investigated to improve the reliability of wireless communications in the presence of impulsive noise. A simple and efficient approach is to precede the receiver with a non-linear preprocessor such as clipping, blanking, or combined clipping-blanking. Gaetan *et al.* Ndo *et al.* (2010) considered an adaptive clipping-based impulsive noise mitigation technique to overcome the noxious effects of impulsive noise in OFDM-based PLC channels. They determined an optimized clipping threshold based on the well-known false alarm and good detection trade-off. It was shown that the optimized threshold relies on the signal-to-noise ratio (SNR) variations and leads to significant improvements over other kinds of empirical clipping. Unlike Ndo *et al.* (2010), the authors in Tseng, D.-F., Han, Y. S., Mow, W. H., Chang, L.-C. & Vinck, A. H. (2012) have proposed a robust clipping scheme that does not require a priori knowledge of the probability density function (PDF) of the impulsive noise to derive the clipping threshold. Through computer simulations, it was shown that the proposed scheme performs better than Ndo *et al.* (2010) under certain circumstances without relying on the exact PDF of the impulsive noise. The authors in Zhidkov (2006) derived a closed-form optimal blanking threshold for OFDM receivers employing blanking non-linearity to cancel the effect of impulsive noise. Their results show that the optimized threshold maximizes the SNR at the output of the blanking non-linearity.

The analysis of Ndo *et al.* (2010); Tseng *et al.* (2012); Zhidkov (2006) were based on the fact that OFDM signals with large number of subcarriers can be modeled by a complex Gaussian process with Rayleigh envelope distribution. In Zhidkov, S. V. (2008), Zhidkov carried out a comprehensive study of the threshold optimization for OFDM receivers with three types of non-linearity: clipping, blanking, and combined clipping-blanking, where the multi-component Gaussian mixture impulsive noise model was considered. The Bernoulli-Gaussian

(BG) model and the Middleton Class-A model are special cases of this noise model when the number of components are equal to two and infinity, respectively. Here, similar to Zhidkov (2006), the threshold optimization criterion was to maximize the SNR at the output of the non-linearity. It was shown that, while the clipping and the blanking schemes can individually perform significantly better than one another in different SNR regions, the combined clipping-blanking scheme, combining the benefits of both schemes, provides the best solution. Recently, more comparisons of the performance of clipping and blanking methods for the mitigation of the performance degradation in impulsive noise environments were considered in Oh, H. & Nam, H. (2017). The authors in Rožić, N., Banelli, P., Begušić, D. & Radić, J. (2018) proposed a set of novel multiple-threshold based impulsive noise suppression techniques for multi-carrier communication systems impaired by frequency selective fading channels. It was shown that the suppressors perform better than the traditional clipping, clamping, combined clipping-blanking processors and approaches the performance of optimal Bayesian estimation (OBE), as the number of threshold increases. In addition to the threshold based preprocessors, other forms of impulsive noise mitigation techniques include: (i)- iterative techniques Zhidkov (2003), where the idea is to estimate the impulsive noise as accurately as possible at the receiver side through iteration and to subtract the estimation from the received vector, (ii)- error correction coding employing convolutional coding Li *et al.* (2008), turbo coding Umehara *et al.* (2004), LDPC coding Nakagawa *et al.* (2005), polar coding Hadi *et al.* (2016), etc., and (iii)- compressed sensing Al-Naffouri *et al.* (2014); Lin *et al.* (2013).

However, all of the above mentioned performance analysis for impulsive noise mitigation techniques have been carried out on OFDM-based multi-carrier communication systems impaired by memoryless impulsive noise. Although OFDM systems were shown to be more resilient to non-Gaussian impulsive interference compared to single-carrier systems due to the random distribution of their noise energy over multiple sub-carriers Ndo *et al.* (2010); Zhidkov (2006), we note that OFDM is outperformed by its single-carrier counterpart when the impulses are very strong and/or they occur frequently Ghosh (1996), which likely exists in contemporary communication systems including smart grid communications, power line communications,

industrial wireless sensor network communications, etc. Also, there are certain circumstances, for example, in the low SNR region, where, under impulsive noise, single-carrier modulation performs better than multi-carrier modulation Shongwe *et al.* (2015). Moreover, the IFFT and FFT complexities are eliminated through single-carrier communication. This is essential for internet of things (IoT) applications in industry, smart grid, smart home, etc., which require tiny sensors with low complexity and small batteries; thus, operating in the low SNR regime. Likewise, the assumption of memoryless noise model is not valid for many communication scenarios, for example, see Agba *et al.* (2019); Asiyo & Afullo (2017); Bai *et al.* (2017); Blackard *et al.* (1993); Ndo *et al.* (2013); Sacuto *et al.* (2014); Shongwe *et al.* (2015); Zimmermann & Dostert (2002) and the references therein. The memoryless noise models might be able to generate noise samples by ensuring a good trade-off between mathematical simplicity and accurate characterization of the physical phenomenon, but they cannot take into account one of the main features of the actual noise, i.e., the time-correlation among the impulsive noise samples. To improve the reliability in the presence of bursty impulsive noise modeled by a Markov-Gaussian process, convolutional error correcting coding Mitra & Lampe (2010) and LDPC coding Alam *et al.* (2016); Fertonani & Colavolpe (2009) have been considered in the literature. It was shown that considerable performance gains can be achieved when the impulsive noise memory is utilized in the detection process. The author in Lampe (2011) has considered sparse Bayesian learning methods to estimate the presence of bursty impulsive noise.

Despite the practical relevance of impulsive noise with memory, to the best of our knowledge, there are no existing results on the performance analysis of impulsive noise mitigation techniques for single-carrier communication systems impaired by bursty impulsive noise. Moreover, although widely acknowledged for their simplicity, ease of implementation, and fairly good performance, nonlinear preprocessing technoques have not been considered in the context of this scenario. The aim of this paper is to provide further investigation on several conventional non-linear methods that can potentially mitigate the effects of impulsive noise with memory. To address the memory of impulsive noise, we consider a two-state Markov-Gaussian

(TSMG) process. A TSMG process is a simple and effective way to model the time-correlation among the noise samples. The contributions of this work are summarized as follows:

- We propose and analyze the widely used non-linear methods such as clipping, blanking, and combined clipping-blanking to mitigate the noxious effects of the TSMG impulsive noise. Precisely, we derive a closed-form solution for the optimal threshold of the non-linear operations based on the probability of good detection and false alarm trade-off and provide performance comparisons in terms of bit error rate (BER) to reflect which mitigation technique shows superior performance in which impulsive scenario.

- In addition, an optimal impulsive noise mitigation technique using log-likelihood ratio (LLR) computation based on MAP detection criterion is proposed. It is shown that for single-carrier communication systems, an effective way of impulsive noise mitigation is to utilize the exact LLR of each symbol in the detection process by taking into account the exact impulsive noise statistics.

- We further investigate the LLR combined with clipping and blanking operations. Interestingly, it is shown that the exact LLR computation after the clipping, blanking non-linearity does not provide any improvement compared to the case when the exact LLR of the received signal is computed without any pre-treatment.

The rest of the paper is organized as follows. In Section 2.3, the system model is introduced and an overview of the TSMG noise model is presented. In Section 2.4, we discuss the conventional impulsive noise mitigation techniques and provide the optimal threshold determination to declare the presence and absence of impulsive noise. Also, the LLR computation for single carrier communication systems impaired by bursty impulsive noise using the MAP detection criterion as well as a low-complexity LLR calculation in case of communication systems impaired by memoryless impulsive noise is shown. Section 2.5 provides the BER performance of these mitigation techniques and Section 2.6 further investigates the LLR optimality along with clipping and blanking operations. Finally, some conclusions are drawn in Section 2.7.

2.3 System Model

A basic block diagram of the system considered in this work is shown in Fig. 2.1. We consider a LDPC coded transmission over a flat fading channel in the presence of bursty impulsive noise modeled by a two-state Markov-Gaussian process.

2.3.1 Signal Model

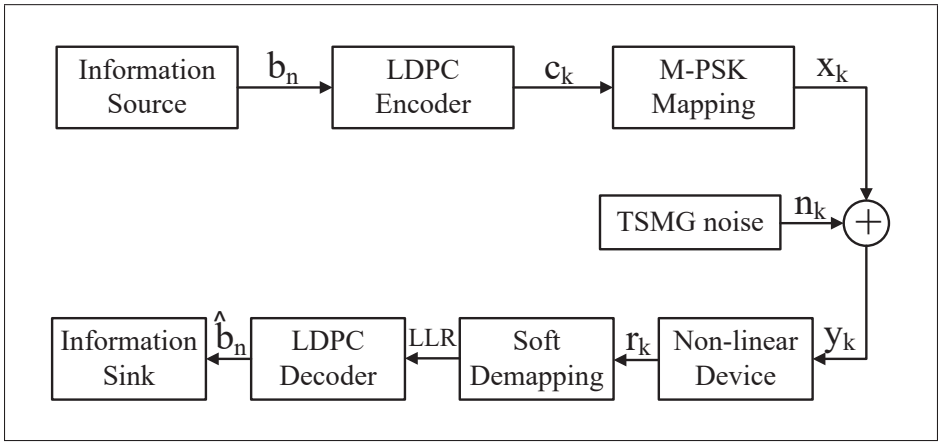

Figure 2.1 Block diagram for the evaluation of LDPC coded single-carrier communication system over TSMG noise with non-linear impulsive mitigation device

In this context, the source generates a block of information bits of size N $(b_0, b_1, \ldots, b_{N-1})$, which is passed through a LDPC encoder block to produce $\mathbf{c^K} = c_0, c_1, \ldots, c_{K-1}$, before being mapped into an M-ary PSK modulated sequence $(x_0, x_1, \ldots, x_{K-1})$. The received signal at each time epoch k, $k = 0, 1, \ldots, K-1$ is therefore given by

$$y_k = x_k + n_k, \tag{2.1}$$

where x_k is the transmitted symbol from the source and n_k represents the TSMG noise. An overview of this model is provided in the following section.

2.3.2 The Two-state Markov-Gaussian Model

The TSMG model was introduced by Fertonani Fertonani & Colavolpe (2009) to characterize the correlated impulsive channel which is different from the i.i.d. impulsive channel. For this model, at each time epoch k, the statistical properties of the noise sample n_k are completely defined by the channel state s_k, $s_k \in \{G,B\}$ where G stands for good channel (when the transmitted signal is impaired only by background Gaussian noise) and B for bad channel (transmitted signals are additionally impaired by impulsive interferers). Conditioned on s_k, the PDFs of n_k are represented by Gaussian distributions, whose variance is usually much higher for the bad state than for the good state, expressed as Fertonani & Colavolpe (2009)

$$p(n_k = y_k - x_k | s_k = G) = \frac{1}{\sqrt{2\pi\sigma_G^2}} \exp\left(-\frac{n_k^2}{2\sigma_G^2}\right), \tag{2.2}$$

$$p(n_k = y_k - x_k | s_k = B) = \frac{1}{\sqrt{2\pi\sigma_B^2}} \exp\left(-\frac{n_k^2}{2\sigma_B^2}\right), \tag{2.3}$$

where σ_G^2 is the average noise power of the good channel, σ_B^2 is the average noise power of the bad channel, and the parameter $R = \frac{\sigma_B^2}{\sigma_G^2} \geq 1$ is the impulsive to Gaussian noise power ratio. The statistical description of the state process $s^K = \{s_0, s_1, \ldots, s_{K-1}\}$ completely characterizes the channel and for this model, s^K for each realization of the process, is expressed as a stationary first-order Markov process Fertonani & Colavolpe (2009) with

$$p(s^{K+1}) = p(s_0) \prod_{k=0}^{K-1} p(s_{k+1}|s_k). \tag{2.4}$$

Therefore, the state process is described by the state transition probabilities $p_{s_k s_{k+1}} = p(s_{k+1}|s_k)$, $s_k, s_{k+1} \in \{G,B\}$. The state process underlying the channel is the same as for the Gillbert-Elliott model Mushkin & Bar-David (1989) which provides a simple and effective way for describing the bursty evolution of the channel state Fertonani & Colavolpe (2009); Mushkin & Bar-David (1989). From the state transition probabilities, the stationary probabilities p_G and p_B of being

in the G and B state are respectively obtained as Fertonani & Colavolpe (2009),

$$p_G = p(s_k = G) = \frac{p_{BG}}{p_{GB} + p_{BG}}. \tag{2.5}$$

$$p_B = p(s_k = B) = \frac{p_{GB}}{p_{GB} + p_{BG}}. \tag{2.6}$$

where P_{BG} denotes the transition probability from state B to state G and similarly, p_{GB} is the transition probability from G to B. Therefore, the couple (p_{GB}, p_{BG}) completely describes the channel. Also, according to the notation in Fertonani & Colavolpe (2009), the parameter $\gamma = \frac{1}{p_{GB}+p_{BG}}$ quantifies the channel memory and there is a *one-to-one correspondence* between the pair (p_{GB}, p_{BG}) and (p_B, γ), with $\gamma = 1$ meaning that the channel is memoryless, while $\gamma > 1$ indicates that the channel has persistent memory.

Therefore, the TSMG model is a modification of the Bernoulli-Gaussian model that handles the noise memory with an extra parameter γ. For the Bernoulli-Gaussian model, the state process S^K is represented by, as the name suggests, a stationary Bernoulli process, whereas for the Markov-Gaussian model S^K is represented by a first-order Markov process. The latter model reduces to the former when $\gamma = 1$ Fertonani & Colavolpe (2009), that is, when the transition probabilities depend on the arrival state only. Therefore, the Markov-Gaussian model can be represented by a Markov chain Vaseghi (2008), as shown in Figure 2.2.

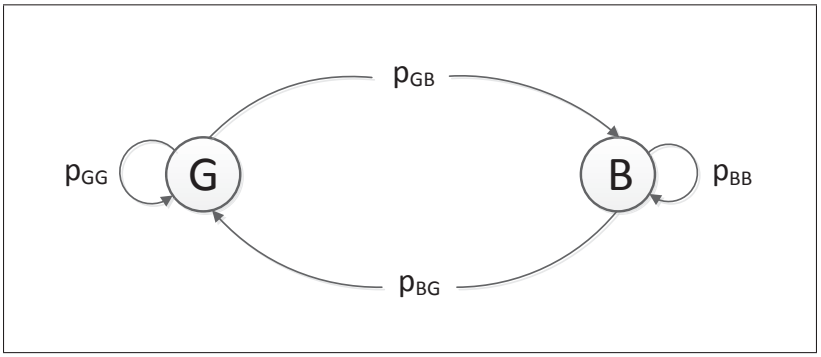

Figure 2.2 Markov chain representation of two-state Markov-Gaussian noise model

2.4 Impulsive Noise Mitigation Techniques

2.4.1 Conventional Impulsive Noise Mitigation Techniques

A common and rather simple approach for mitigation of impulsive interference is to detect high peak amplitudes in the time domain and reduce them which is the idea behind non-linear preprocessors that can be applied at the receiver. This non-linearity reduces the effect of large received signal amplitudes which are assumed to be the result of impulsive interference. In general, derivatives of different nonlinear methods such as, clipping, blanking, and combined clipping-blanking have been widely investigated in case of OFDM transmission impaired by memoryless impulsive noise.

In this section, we further investigate these non-linear impulsive noise mitigation techniques in light of single-carrier modulation impaired by TSMG noise.

2.4.1.1 Clipping

For clipping, the received signal samples are compared to a clipping threshold T_c. If the absolute value of the signal sample exceeds T_c, it is clipped as follows Ndo *et al.* (2010):

$$r_k = \begin{cases} y_k & \text{if } |y_k| \leq T_c \\ T_c \; sgn(y_k) & \text{otherwise,} \end{cases} \tag{2.7}$$

where r_k is the clipped output of y_k.

2.4.1.2 Blanking

For blanking, the received signal samples whose absolute value is greater than a given blanking threshold T_b are replaced by zero, which can be formulated as Zhidkov (2006)

$$r_k = \begin{cases} y_k & \text{if } |y_k| \leq T_b \\ 0 & \text{otherwise,} \end{cases} \tag{2.8}$$

where r_k is the blanked output of y_k.

2.4.1.3 Combined Clipping-Blanking

For combined clipping-blanking, two threshold values T_b and T_c are needed. The definition of this operation is recalled as

$$r_k = \begin{cases} y_k & \text{if } |y_k| \leq T_c \\ T_c \; sgn(y_k) & \text{if } T_c < |y_k| \leq T_b \\ 0 & \text{if } |y_k| > T_b, \end{cases} \tag{2.9}$$

Hence, for this scheme, the medium amplitude signals are clipped while the large amplitude signals are blanked.

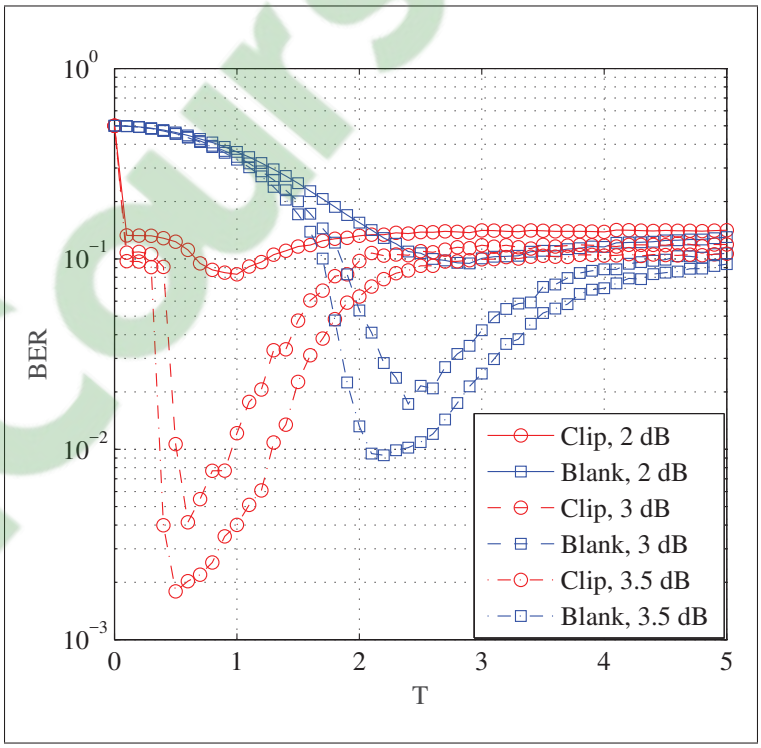

Figure 2.3 BER variations with respect to the clipping/blanking threshold over TSMG noise. In the simulations it is assumed that $p_B = 0.1$, $\gamma = 100$, and $R = 20$

From the above non-linear operations it can be inferred that the optimal values of T_c and T_b play a vital role in obtaining the best mitigation performance. Fig. 2.3 shows the BER with respect

to the clipping/blanking threshold T for different SNR values. In what follows, the SNR is defined as SNR $= \mathrm{P}/\sigma_G^2$, where P is the average source transmission power for each symbol and σ_G^2 is the background Gaussian noise power. From Fig. 2.3, it is clearly shown that an optimal clipping, blanking threshold, which minimizes the BER at the receiver, always exists and that the optimal threshold changes with the SNR variations for both clipping and blanking non-linearities. It is therefore interesting to determine the optimal threshold as a function of the SNR to get the best performance driven by these non-linearities.

2.4.1.4 Optimal Threshold Determination for the Non-Linearity

Here, we seek to determine the optimal threshold to declare the presence and absence of impulsive noise to be used in the clipping/blanking non-linearity. In order to approximately detect the optimal threshold, we consider the probability of good detection and false alarm trade-off Ndo *et al.* (2010). Considering BPSK modulation in the system model of Fig. 2.1, the PDF of the received signal y_k conditioned on s_k is given by

$$p(y_k|s_k) = \frac{1}{2}\frac{1}{\sqrt{2\pi\sigma_{s_k}^2}}\exp\left(-\frac{(y_k-1)^2}{2\sigma_{s_k}^2}\right) + \frac{1}{2}\frac{1}{\sqrt{2\pi\sigma_{s_k}^2}}\exp\left(-\frac{(y_k+1)^2}{2\sigma_{s_k}^2}\right). \tag{2.10}$$

Hence, for a given threshold T, the conditional probability of good detection for a real-valued BPSK modulated transmission scheme impaired by TSMG noise is given by

$$\begin{aligned} P_D &= \int_T^{\infty} p(y_k|s_k = B), \\ &= \frac{1}{2}\int_T^{\infty} \frac{1}{\sqrt{2\pi\sigma_B^2}}\left\{ e^{-\frac{(y_k-1)^2}{2\sigma_B^2}} + e^{-\frac{(y_k+1)^2}{2\sigma_B^2}} \right\}, \\ &= \frac{1}{4}\mathrm{erfc}\left(\frac{T-1}{\sqrt{2}\sigma_B}\right) + \frac{1}{4}\mathrm{erfc}\left(\frac{T+1}{\sqrt{2}\sigma_B}\right). \end{aligned} \tag{2.11}$$

where $\mathrm{erfc}(x) = \frac{2}{\sqrt{\pi}}\int_x^{\infty} e^{-t^2}dt$ is the complementary error function Goldsmith (2005).

On the other hand, the probability of false alarm becomes

$$\begin{aligned} P_F &= \int_T^{\infty} p(y_k|s_k = G), \\ &= \frac{1}{2}\int_T^{\infty} \frac{1}{\sqrt{2\pi\sigma_G^2}} \left\{ e^{-\frac{(y_k-1)^2}{2\sigma_G^2}} + e^{-\frac{(y_k+1)^2}{2\sigma_G^2}} \right\}, \\ &= \frac{1}{4}\text{erfc}\left(\frac{T-1}{\sqrt{2}\sigma_G}\right) + \frac{1}{4}\text{erfc}\left(\frac{T+1}{\sqrt{2}\sigma_G}\right). \end{aligned} \tag{2.12}$$

Numerous criteria can be utilized to derive the corresponding optimal threshold. In this regards, we consider the weighted combination criterion and the siegert criterion which require less parameters compared to the other available criteria Ndo *et al.* (2010).

2.4.1.4.1 Weighted Combination Criterion

Using the weighted combination criterion Ndo *et al.* (2010), the optimal threshold T_w^{opt} is obtained as

$$\begin{aligned} T_w^{opt} &= \arg\max_{T>0} \{P_D - P_F\}, \\ &= \arg\max_{T>0} \left\{ \frac{1}{4}\text{erf}\left(\frac{T-1}{\sqrt{2}\sigma_G}\right) + \frac{1}{4}\text{erf}\left(\frac{T+1}{\sqrt{2}\sigma_G}\right) - \frac{1}{4}\text{erf}\left(\frac{T-1}{\sqrt{2}\sigma_B}\right) - \frac{1}{4}\text{erf}\left(\frac{T+1}{\sqrt{2}\sigma_B}\right) \right\}. \end{aligned}$$

The variations of the optimization function $\eta = (P_D - P_F)$ with respect to the threshold T is shown in Fig. 2.4 for different SNRs. From Fig. 2.4, it is observed that there is a single optimal threshold T^{opt} which is dependent on the SNR. Hence, the optimal threshold is obtained by taking $\frac{d\eta}{dT} = 0$, which yields

$$\frac{1}{\sigma_G}\left\{ e^{-\frac{(y_k-1)^2}{2\sigma_G^2}} + e^{-\frac{(y_k+1)^2}{2\sigma_G^2}} \right\} = \frac{1}{\sigma_B}\left\{ e^{-\frac{(y_k-1)^2}{2\sigma_B^2}} + e^{-\frac{(y_k+1)^2}{2\sigma_B^2}} \right\}, \tag{2.13}$$

Given that

$$\log_b(A+C) = \log_b A + \log_b(1+C/A), \tag{2.14}$$

and

$$\log(1+e^{-x}) = \log 2 - x/2, \tag{2.15}$$

and after some mathematical manipulations, the optimum threshold is obtained as

$$T_w^{opt} = \sqrt{\frac{2\sigma_B^2\sigma_G^2}{\sigma_B^2-\sigma_G^2}\ln\left(\frac{\sigma_B}{\sigma_G}\right)-1}. \tag{2.16}$$

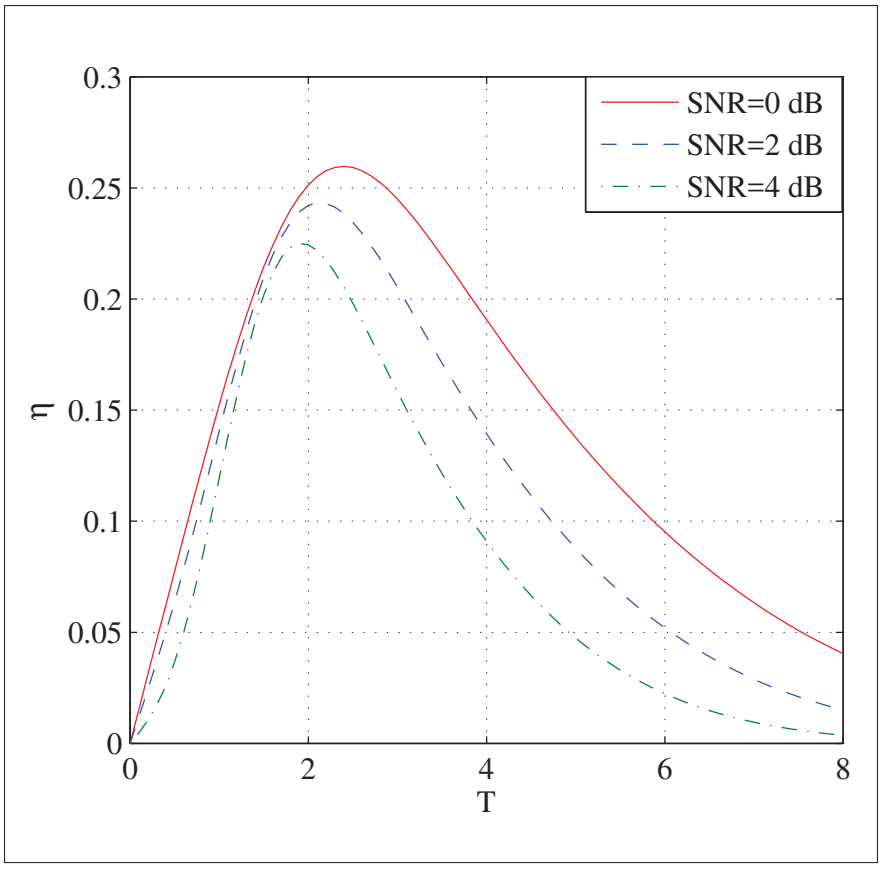

Figure 2.4 The variations of $\eta = (P_D - P_F)$ with respect to the clipping/blanking threshold T for different SNR values. In the simulations it is assumed that the TSMG noise is characterized by $p_B = 0.1$, $\gamma = 100$, and $R = 20$

2.4.1.4.2 Siegert Criterion

For the siegert criterion Ndo *et al.* (2010), the probability of occurrence of the impulses is required. According to this criterion, the optimal threshold T_s^{opt} should satisfy

$$T_s^{opt} = \arg\max_{T>0} \{p_B P_D + p_G(1-P_F)\}, \tag{2.17}$$

Following a similar approach as in Section 2.4.1.4.1, we get

$$T_s^{opt} = \sqrt{\frac{2\sigma_B^2\sigma_G^2}{\sigma_B^2-\sigma_G^2}\ln\left(\frac{p_G\sigma_B}{p_B\sigma_G}\right)-1}. \tag{2.18}$$

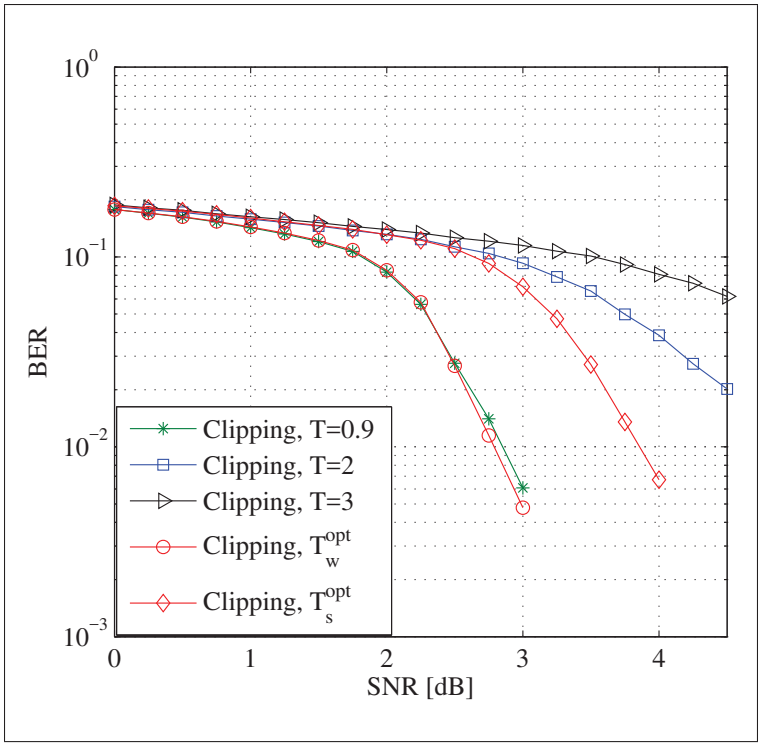

Figure 2.5 Clipping BER performances over TSMG noise. In the simulations it is assumed that $p_B = 0.1$, $\gamma = 100$, and $R = 20$

The robustness of the derived thresholds T_w^{opt} and T_s^{opt} for the clipping operation is shown in Fig. 2.5 where a LDPC coded and BPSK modulated transmission is considered. From Fig. 2.5,

it is observed that, for the clipping scheme, the optimal clipping threshold using the weighted combination criterion shows better BER performance than the siegert criterion. It achieves an SNR gain of around 1 dB for a targeted BER of 10^{-3} which illustrates the importance of determining the optimal threshold for the non-linear operation. In addition, it is revealed that for the considered scheme the clipping performance obtained with a fixed threshold $T = 0.9$ approaches the performance obtained in case of weighted combination criterion, whereas for different values of the threshold, the performance deteriorates. Therefore, it can be concluded that the threshold optimized according to the weighted combination criterion is the best choice for the clipping operation in the context of TSMG noise mitigation. In addition, for a given set of noise parameters, we do not need an optimization for each SNR, a fixed optimum works.

On the other hand, it is verified that the performances of the blanking scheme is significantly worse for the optimum threshold assuming the two aforementioned criteria. Nevertheless, the optimal threshold can be determined numerically. Hence, to check the robustness of the clipping and blanking operations in comparison to other bursty impulsive noise mitigation techniques in Section 2.5, we consider the clipping with T_w^{opt} and blanking with T_{num}^{opt} where T_{num}^{opt} is the optimal threshold determined numerically.

2.4.2 LLR-based Mitigation

LLR receivers are known to improve the performance of conventional receivers. Therefore, they have been proposed for the mitigation of impulsive noise where the receiver performs the computation of the LLR for each symbol considering the exact statistics of the impulsive noise. Two algorithms are commonly employed for the calculation of LLR values. The first scheme which is suitable for memoryless noise models performs the LLR computation on a symbol-by-symbol basis, whereas in the second scheme, referred to as the Bahl-Cocke-Jelinek-Raviv (BCJR) or the maximum a posteriori (MAP) algorithm Bahl *et al.* (1974), the LLR values are calculated after receiving an information block sequence. The later algorithm is quite suitable for noise models with memory and is generally more complex to be implemented than the previous one.

2.4.2.1 LLR Calculation for Memoryless Impulsive Noise:

The derivation of the LLR expression for BPSK modulated signals over Middleton class-A noise has been detailed in Nakagawa *et al.* (2005); Umehara *et al.* (2004) and can be expressed as

$$\begin{aligned} L_A(y_k) &= \ln \frac{p(y_k|x_k=+1)}{p(y_k|x_k=-1)} = \ln \frac{p_A(y_k-1)}{p_A(y_k+1)} \\ &= \ln \sum_{m=0}^{\infty} \frac{p_m}{\sqrt{2\pi\sigma_m^2}} \exp\left(-\frac{(y_k-1)^2}{2\sigma_m^2}\right) - \ln \sum_{m=0}^{\infty} \frac{p_m}{\sqrt{2\pi\sigma_m^2}} \exp\left(-\frac{(y_k+1)^2}{2\sigma_m^2}\right), \end{aligned} \tag{2.19}$$

where p_A is the Middleton class-A PDF. It is easily seen that the LLR calculation in the above expression cannot be easily simplified due to the logarithm and the exponential functions. As in (2.19), the LLR expression for the Bernoulli-Gaussian noise assuming BPSK modulation can be written as

$$\begin{aligned} L_{BG}(y_k) &= \ln \frac{p(y_k|x_k=+1)}{p(y_k|x_k=-1)} = \ln \frac{p_{BG}(y_k-1)}{p_{BG}(y_k+1)} \\ &= \ln \sum_{m=0}^{1} \frac{p_m}{\sqrt{2\pi\sigma_m^2}} \exp\left(-\frac{(y_k-1)^2}{2\sigma_m^2}\right) - \ln \sum_{m=0}^{1} \frac{p_m}{\sqrt{2\pi\sigma_m^2}} \exp\left(-\frac{(y_k+1)^2}{2\sigma_m^2}\right) \end{aligned} \tag{2.20}$$

2.4.2.2 LLR Calculation for Impulsive Noise with memory

Here, we introduce the LLR computation in case of impulsive noise with memory by utilizing the well-known BCJR or MAP algorithm. The MAP decoding algorithm is a recursive technique that computes the LLR of each bit, based on the entire observed data block of length K. For BPSK modulation, the LLR value at time k, $k = 1,2,\ldots,K$ is defined as

$$L_k = \ln \left\{ \frac{p(x_k=1|y^K)}{p(x_k=-1|y^K)} \right\}, \tag{2.21}$$

where $y^K = \{y_0, y_1, \ldots, y_{K-1}\}$ is the whole sequence to be detected, and K is the size of the sequence. Thus, at each k, the optimal MAP detector at the receiver evaluates the a posteriori

probability (APP) $p(x_k|y^K)$ for each symbol x_k belonging to the binary modulation alphabet {1,-1}. By defining the probabilities

$$\alpha_k(s_k) = p(y_0, y_1, \ldots, y_{k-1}, s_k) \tag{2.22}$$

$$\beta_k(s_k) = p(y_k, y_{k+1}, \ldots, y_{K-1}|s_k) \tag{2.23}$$

$$\delta_k(x_k,s_k,s_{k+1}) = p(s_{k+1}|s_k)p(n_k = y_k - x_k|s_k) \tag{2.24}$$

it is shown in Alam *et al.* (2016) that the APP can be rewritten as

$$p(x_k = b, y^K) = p(x_k = b) \sum_{s_k, s_{k+1}} \alpha_k(s_k)\beta_{k+1}(s_{k+1})\delta_k(x_k = b, s_k, s_{k+1}), \tag{2.25}$$

where s_k, s_{k+1} denote the noise states at time k and $k+1$ respectively, where $\alpha_k(s_k)$ and $\beta_k(s_k)$ are referred to as the forward and backward filters, and $\delta_k(x_k, s_k, s_{k+1})$ represents the branch metrics of the trellis diagram, as shown in Fig. 2.6, used for decoding the Markov-Gaussian model. The forward and backward filters can be recursively computed as

$$\alpha_{k+1}(s_{k+1}) = \sum_{s_k, x_k} \alpha_k(s_k)p(x_k)\delta_k(x_k, s_k, s_{k+1}), \tag{2.26}$$

$$\beta_k(s_k) = \sum_{s_{k+1}, x_k} \beta_{k+1}(s_{k+1})p(x_k)\delta_k(x_k, s_k, s_{k+1}), \tag{2.27}$$

where the forward and backward filters are initialized with

$$\alpha_0(s_0 = S) = p_S, \text{ and } \beta_K(s_K = S) = 1. S \in (G, B) \tag{2.28}$$

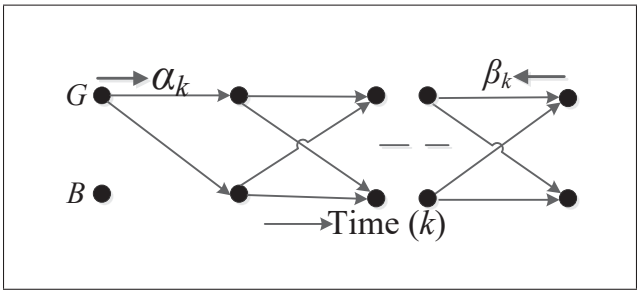

Figure 2.6 Trellis representation of the two-state Markov-Gaussian noise model

Hence, the MAP decoding algorithm consists of the following steps:

- Initialize forward and backward recursions $\alpha_0(s_0)$ and $\beta_K(s_K)$
- Compute branch metrics δ_k
- Carry out forward recursion $\alpha_{k+1}(s_{k+1})$ based on $\alpha_k(s_k)$
- Carry out backward recursion $\beta_k(s_k)$ based on $\beta_{k+1}(s_{k+1})$
- Compute APP and LLR values

On the other hand, in case of AWGN channel, the LLRs are given by Nakagawa *et al.* (2005)

$$L(y_k) = \frac{2}{\sigma_G^2} y_k. \tag{2.29}$$

From (2.29), it is observed that the LLRs linearly depend on the observation y_k in case of AWGN channel.

Conversely, Fig. 2.7 shows the LLR variations with respect to y_k in the presence of TSMG. From Fig. 2.7, it is verified that $L(y_k)$ exhibits a non-linear behaviour against y_k. It has been reported in Nakagawa *et al.* (2005) that the exact LLR calculation according to (2.19) provides significant performance improvement compared to the case where the impulsive noise is not taken into account. Indeed, the BER improvement comes from the non-linearity. However, the analysis in Nakagawa *et al.* (2005) is restricted to the memoryless impulsive noise only and the authors have not mentioned what will happen when the noise memory is taken into account and how the conventional clipping/blanking non-linearity behaves in comparison to LLR based schemes under both memoryless and with memory impulsive noise.

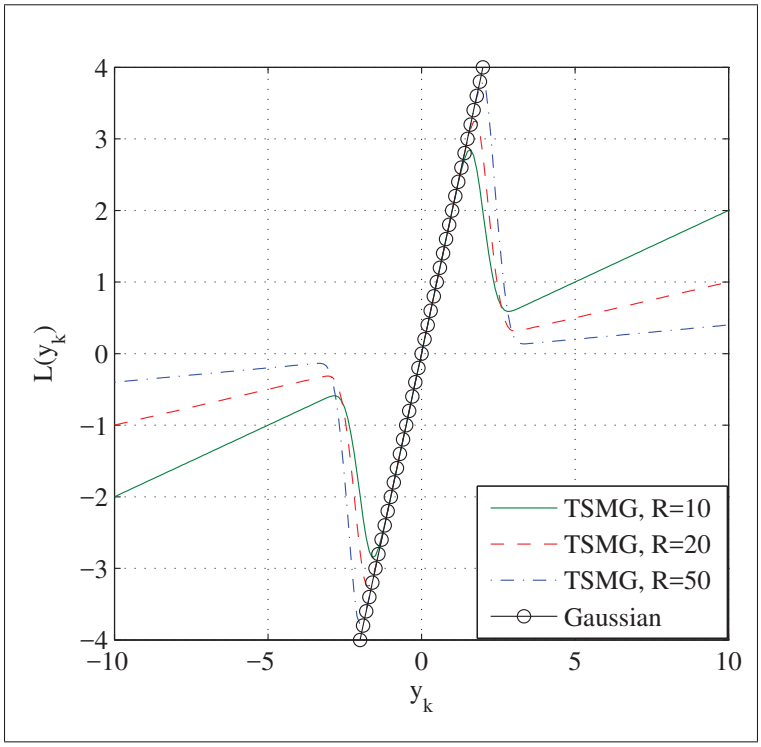

Figure 2.7 Variations of the LLR $L(y_k)$ for TSMG noise with BPSK mapping. It is assumed that SNR $= 0$ dB and the TSMG noise is characterized by $p_B = 0.1$, $\gamma = 100$, and $R = 10, 20, 50$

2.5 Performances Evaluation

In this section, the performance of the non-linear impulsive noise mitigation techniques discussed earlier is examined against TSMG noise. The noise is generated based on the parameters: $p_B = 0.1$, $\gamma = 100$, and $R = 20$. Moreover, in what follows, it is assumed that a sequence of equally likely information bits of length $32,400$ is encoded using LDPC channel coding based on the DVB-S2 standard Mackay, D. J. C. (2009) with a code rate of $1/2$. The coded sequence is then mapped into a BPSK modulation sequence. For LDPC decoding, the number of iterations is set to 50.

Fig. 2.8 depicts the BER performance against the SNR of various non-linear mitigation schemes for communication systems impaired by TSMG noise. The BER performances are obtained by averaging the error rate over 300 frames with $64,800$ samples for every LDPC coded frame.

To calculate the BER for clipping, blanking, and combined clipping-blanking based schemes, we assume that the received signal at the output of these non-linearities are Gaussian and hence the LLR values are calculated according to (2.29). As benchmarks, we also include the performance of direct transmission over AWGN channels and the performance of the system without any treatment at the receiver side. For the later case, we assume that the receiver does not have any knowledge about the impulsive noise and it calculate the LLR values according to (2.29) based on the received signal. From Fig. 2.8, we observe that, the MAP-based LLR scheme provides a significant performance gain over the sample-by-sample (i.i.d.) based LLR computation and the other non-linear schemes, obviously at the expense of a higher complexity. It achieves an SNR gain of around 1.5 dB over the i.i.d.-based LLR computation scheme and around 2.0 over the blanking scheme which are significant for powerful channel codes like LDPC coded scenarios.

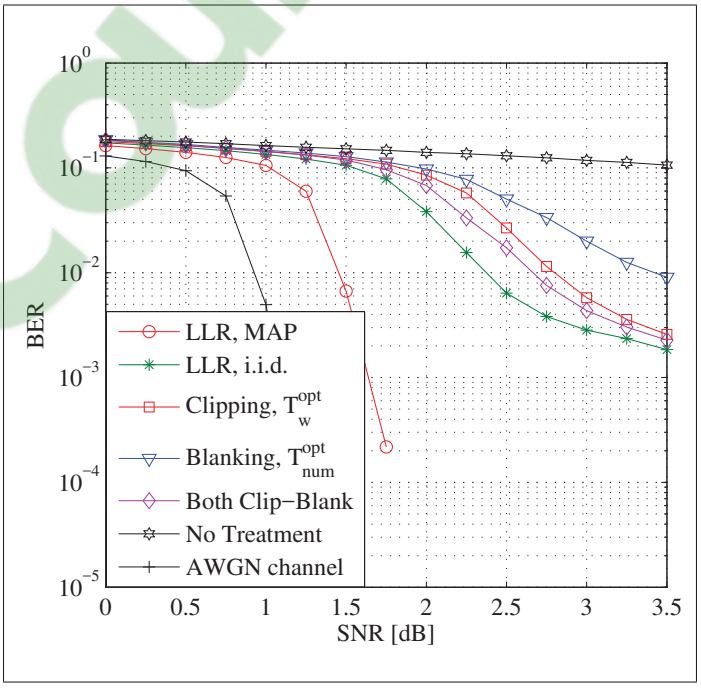

Figure 2.8 BER performance of various mitigation schemes for a LDPC coded communication system impaired by TSMG impulsive noise. A system employing BPSK modulation is considered and the TSMG noise is characterized by $p_B = 0.1$, $\gamma = 100$, and $R = 20$

Fig. 2.9 also shows the performance improvement brought by the LLR computation in case of when we consider $\gamma = 1$ in the TSMG noise process which corresponds to the Bernoulli-Gaussian noise. Precisely, when the exact impulsive noise statistics is exploited in the LLR computation, we achieve a significant performance gain irrespective of the noise process. Interestingly, from Fig. 2.9, we also remark that while the LLR computation using MAP algorithm shows better performance than the sample-by-sample LLR calculation for TSMG noise, the later shows the same performance in case of Bernoulli-Gaussian noise. This confirms that, for Bernoulli-Gaussian noise, the optimal LLR computation using MAP algorithm simplifies to memoryless sample-by-sample algorithm. In addition, as in TSMG noise, the clipping scheme shows better performance than the blanking scheme, whereas the combined clipping-blanking scheme outperforms the clipping scheme in the higher SNR regions by taking the advantages of both clipping and blanking schemes.

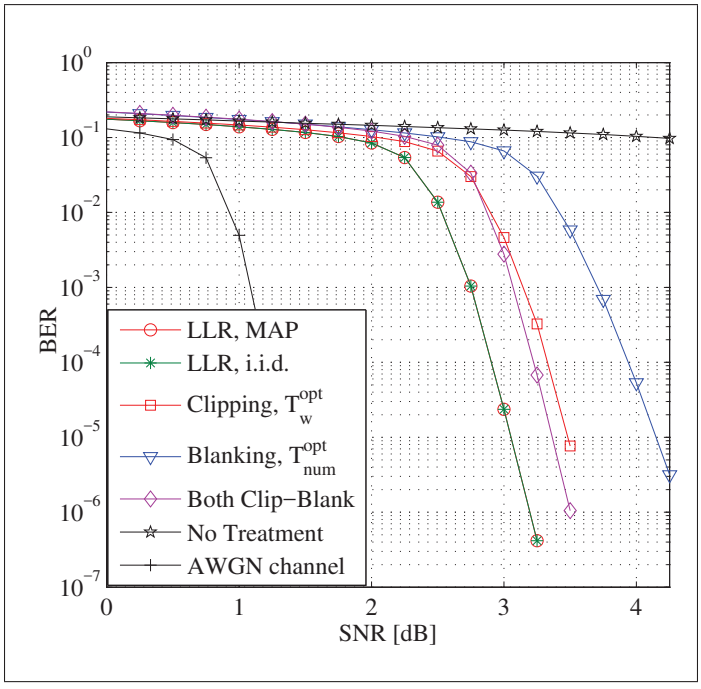

Figure 2.9 BER performance of various mitigation schemes for a LDPC coded communication system impaired by Bernoulli-Gaussian impulsive noise. A system employing BPSK modulation is considered and the Bernoulli-Gaussian noise is characterized by $p_B = 0.1$ and $R = 20$

Furthermore, we also investigate the performance of the considered schemes when we set the TSMG noise parameter $R = 100$ instead of $R = 20$. The resulting BER performance is shown in Fig. 2.10. As portrayed in the figure, when the value of R increases, i.e, when the impulsive noise component becomes more powerful compared to the Gaussian noise component, the performance of the blanking scheme outperforms the clipping scheme and the performance of the combined clipping-blanking scheme approaches the sample-by-sample LLR scheme. Hence, it can be concluded that the choice of the most suitable non-linear preprocessing technique depends on the application noise environment.

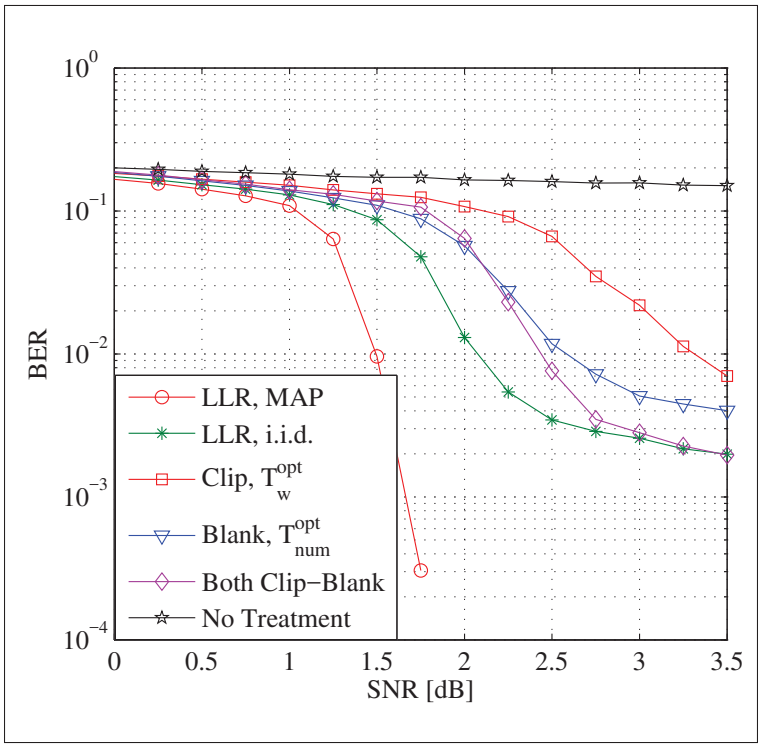

Figure 2.10 BER performance of various mitigation schemes for a LDPC coded communication system impaired by TSMG impulsive noise. A system employing BPSK modulation is considered and the TSMG noise is characterized by $p_B = 0.1$, $\gamma = 100$, and $R = 100$

2.6 Exact LLR Derivation when using a Non-linearity

Here, we consider the exact LLR calculation when the clipping and blanking operations are realized. The LLR of the clipped or blanked signal r_k is defined as

$$L(r_k) = \ln \frac{P_R(r_k|x_k = 1)}{P_R(r_k|x_k = -1)} \tag{2.30}$$

where P_R is the PDF of the non-linearity output r_k. The conditional PDFs $P_R(r_k|x_k)$ after the clipping and blanking operations are respectively given by Ndo, G. (2010)

$$P_R^{(c)}(r_k|x_k) = P_Y(r_k|x_k) + \delta(r_k+T)P_Y(y_k < -T|x_k) + \delta(r_k-T)P_Y(y_k > T|x_k) \tag{2.31}$$

$$P_R^{(b)}(r_k|x_k) = P_Y(r_k|x_k) + \delta(r_k)\left[P_Y(y_k < -T|x_k) + P_Y(y_k > T|x_k)\right] \tag{2.32}$$

where $P_Y(r_k|x_k)$ can be obtained according to (2.25) and

$$P_Y(y_k > T|x_k) = p_G Q\left(\frac{T-1}{\sigma_G}\right) + p_B Q\left(\frac{T-1}{\sigma_B}\right) \tag{2.33}$$

$$P_Y(y_k < -T|x_k) = p_G Q\left(\frac{T+1}{\sigma_G}\right) + p_B Q\left(\frac{T+1}{\sigma_B}\right) \tag{2.34}$$

where $Q(x)$ denotes the Q-function and $\delta(x)$ is the Kronecker symbol given by

$$\delta(x) = \begin{cases} 1 & \text{if } x = 0 \\ 0 & \text{if } x \neq 0 \end{cases} \tag{2.35}$$

On the other hand, for the blanking scheme, the LLR before and after the non-linearity is the same, i.e,

$$L^{(b)}(r_k) = L(y_k). \tag{2.36}$$

Fig. 2.11 shows the BER performances obtained for a LDPC coded BPSK modulated transmission over TSMG noise where the clipping operation is performed and the exact LLR is computed at the output of the clipped signal. From Fig. 2.11, we observe that the performance of the considered scheme improves with the increase of the clipping threshold T and con-

verges to the LLR performance obtained without clipping. This result confirms that the exact LLR computation after the clipping, blanking non-linearity does not provide any improvement compared to the case when the exact LLR of the received signal is computed without any pre-treatment.

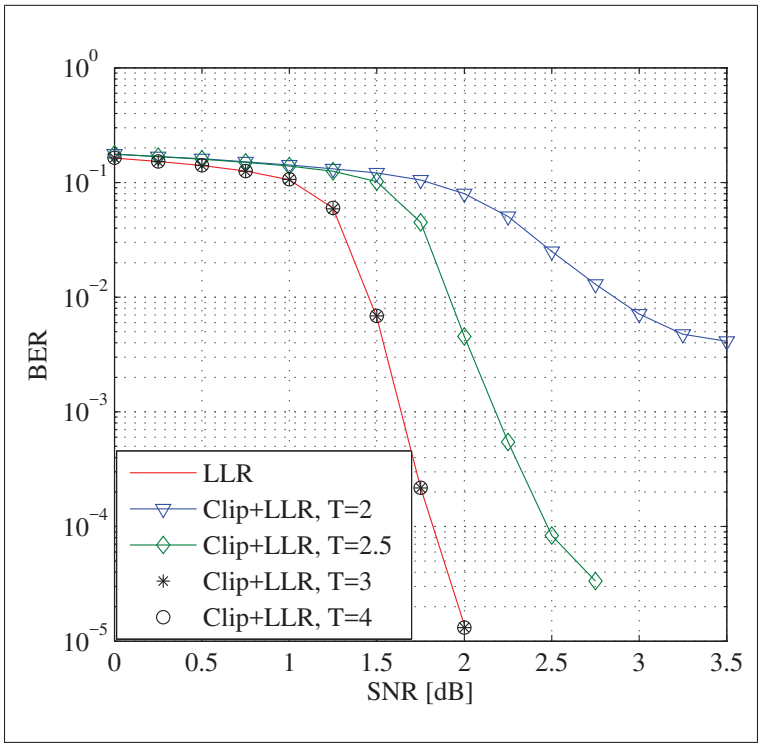

Figure 2.11 BER variations of the combined clipping and LLR operations over TSMG noise. In the simulations it is assumed that $p_B = 0.1$, $\gamma = 100$, and $R = 20$

2.7 Conclusion

In this paper, we evaluated some practical impulsive noise mitigation techniques for LDPC coded single-carrier systems subject to bursty impulsive noise modelled by a Markov-Gaussian process. The provided simulation results showed that the LLR-based impulsive noise mitigation technique with the MAP detection criterion outperforms the simple but more popular clipping, blanking, and combined clipping/blanking schemes at the expense of higher compu-

tational complexity. This is caused by the imperfect level of clipping and blanking of signal samples affected by impulsive noise due to the lack of noise memory information in the mitigation process. It is also shown that there always exists an optimal clipping, blanking threshold that minimizes the BER and that this optimal threshold value changes with the SNR variations. In this paper, an optimal threshold determination based on good detection and false alarm trade-off has been investigated considering two optimization criterion namely: weighted combination criterion and seigert criterion. We further showed that the optimal LLR computation with clipping, blanking pretreatment does not provide any improvement in the mitigation performance. This finding proves that the LLR-based mitigation scheme can be considered as the most promising method for the mitigation of the harmful effects of bursty impulsive noise.

In this paper, we have only discussed the mitigation techniques for TSMG noise where the number of states are restricted to two. The mitigation techniques for Markov Middleton noise will be investigated in our future research.

CHAPTER 3

PERFORMANCE ANALYSIS OF DF COOPERATIVE RELAYING OVER BURSTY IMPULSIVE NOISE CHANNEL

Md Sahabul Alam [1], Fabice Labeau [2], Georges Kaddoum[1]

[1] Département de Génie Electrique, École de Technologie Supérieure,
1100 Notre-Dame Ouest, Montréal, Québec, Canada H3C 1K3
[2] Department of Electrical Engineering, McGill University,
845 Sherbrooke St. Ouest, Montréal, Québec, Canada H3A 0G4

Article published in IEEE Transactions on Communications, July, 2016.

3.1 Abstract

In this article, we consider the performance analysis of a decode-and-forward (DF) cooperative relaying (CR) scheme over channels impaired by bursty impulsive noise. Although, Middleton class-A model and Bernoulli-Gaussian model give good results to generate a sample distribution of impulsive noise, they fail in replicating the bursty behavior of impulsive noise, as encountered for instance within power substations. To deal with that, we adopt a two-state Markov-Gaussian process for the noise distribution. For this channel, we evaluate the bit error rate (BER) performance of direct transmission (DT) and a DF relaying scheme using M-ary phase shift keying (M-PSK) modulation in the presence of Rayleigh fading with a maximum a posteriori (MAP) receiver. From the obtained results, it is seen that the DF CR scheme in bursty impulsive noise channel still achieves the space diversity and performs significantly better than DT under the same power consumption. Moreover, the proposed MAP receiver attains the lower bound derived for DF CR scheme, and leads to large performance gains compared to the conventional receiving criteria which were optimized for additive white Gaussian noise (AWGN) channel and memoryless impulsive noise channel.

3.2 Introduction

The noise characteristics in many environments, such as around power transmission lines, power substations, and in some mobile radio scenarios are highly non-Gaussian and are inherently impulsive in nature Middleton (1977). For example, in power substations the noise emitted from power equipments, such as transformers, busbars, circuit-breakers, and switchgears are impulsive Hikita *et al.* (1998); Portuguds *et al.* (2003); Sacuto *et al.* (2012). For smart grid technology Hossain, E., Han, Z. & Poor, H. V. (2012), in order to assist the electricity transportation via control, interaction with, and monitoring of power equipment from outside the station, a communication network must be operational within the substation. This could be accomplished by deploying a wireless sensor network (WSN) Gungor *et al.* (2010); Tuna *et al.* (2013) where the deployed sensor nodes collect information from the pieces of equipment, and send their sensed information to the remote smart grid monitoring center for further process. In such applications, the generated impulsive noise from the substation equipment that affects the wireless links between the sensor nodes displays a bursty behaviour as observed in experimental measurements Sacuto *et al.* (2012). The models commonly used in the literature to represent impulsive noise are either Middleton class-A Middleton (1977) or Bernoulli-Gaussian Ghosh (1996). Although these models give good results to generate a sample distribution of impulsive noise, they cannot describe the bursty nature of the impulses, i.e., the correlation among the noise samples in the time domain. To handle this, Markov chain models have been investigated in the literature Fertonani & Colavolpe (2009); Mitra & Lampe (2010); Mushkin & Bar-David (1989); Ndo *et al.* (2013), representing the impulsive noise characteristics by including a significant amount of memory.

One of the designing challenges for WSN-based smart grid monitoring applications is how reliably the sensor nodes send their sensed data to the substation monitoring center Gungor *et al.* (2010); Tuna *et al.* (2013). Cooperative WSNs where the sensor nodes cooperate among each other can be one of the promising candidates for transmission in impulsive channels due to its reliability over fading and interference channels Laneman *et al.* (2004); Nosratinia *et al.* (2004). It is based on the broadcast nature of the wireless medium and achieves the potentials

of spatial diversity in wireless networks without necessitating the placement of multiple antennas at each node. It is very attractive for WSN since the sensor nodes cannot afford multiple antennas due to their size and cost constraints. The two most popular relaying strategies are DF relaying and amplify-and-forward (AF) relaying. Although there exists a large number of publications on these relaying schemes in various aspects, many of them are restricted to the AWGN assumption. In practice, AWGN is a common assumption to bundle together a lot of sources of noise, beyond thermal. The performance of CR in impulsive channel has only been considered in the literature recently. The pairwise error probability (PEP) of AF CR scheme over flat fading channel in the presence of impulsive noise modeled by Middleton class-A has been investigated in Al-Dharrab & Uysal (2009a); Al-Dharrab, S. & Uysal, M. (2009b). Upper bounds on PEP expressions are derived for both space time block coded scheme and repetition-based coded scheme. Simulation results demonstrated that the performance of cooperative systems highly depends on the impulsive nature of the noise and different diversity orders are achieved in different signal-to-noise ratio (SNR) regions. Similar performance analysis is carried out in Savoia & Verde (2011) for DF CR schemes. It is shown that similar to the Gaussian noise case, the system achieves full diversity order asymptotically with SNR in impulsive noise scenario. The authors in Siamack, G., Jamil, H., Tarlochan, S. S. & Serguei, P. (2012) studied the impact of impulsive noise modeled by a Bernoulli-Gaussian process on the performance of cooperative relaying system in a smart grid scenario. It is shown that as the impulse occurs, probability increases, the performance of the system is getting worse. In Nasri & Schober (2010), closed-form asymptotic symbol-error rate (SER) and BER expressions were derived for an AF CR scheme with multiple relays which is valid for arbitrary non-Gaussian noise and interference with finite moments. The simulation results reveal that, at high SNR, full diversity order is obtained and is independent of the type of noise. While the above papers quantify the diversity advantages in the presence of impulsive noise, the authors in Van Khuong & Le-Ngoc (2010,1) studied the performance of DT and DF CR schemes over flat Rayleigh fading and Bernoulli-Gaussian impulsive noise assuming different receiving structures at the destination. The obtained results showed that DF CR performs significantly better than DT under the same bandwidth efficiency and power consumption. It is also shown

that while the optimal Bayes receiver Tepedelenlioglu & Gao (2005) and the maximum ratio combining (MRC) have the same diversity order as expected, the optimal Bayes receiver obtains an additional 3dB SNR gain over the MRC combiner by considering impulsive noise in the detection process. The above results motivate us to consider the performance analysis of CR over correlated impulsive noise channel. While the complexity of DF relaying is higher than AF relaying duo to its digital processing, we consider DF relaying in our analysis since it reduces the effects of additive noise at the relay Fareed, M. M. & Uysal, M. (2009).

However, all of the above performance analyses for CR schemes have been carried out over independent and identically distributed (i.i.d.) impulsive channels[1], which cannot include any information on noise time-correlation. To address this issue, we consider a two-state Markov-Gaussian process Fertonani & Colavolpe (2009) for noise modeling. A two-state Markov-Gaussian process is a simple and effective way to model a bursty impulsive noise channel Fertonani & Colavolpe (2009); Mitra & Lampe (2010). In this context, the authors in Mushkin & Bar-David (1989) calculate the capacity of a Gilbert-Elliott channel which is a varying binary symmetric channel with memory. It is shown that the capacity of the channel increases monotonically with increasing the utilization of memory information at the receiver side and converges to a maximum value which is the capacity of the same channel when perfect state information is available at the receiver. It is also shown that, even if the memory of the channel is ignored through proper interleaving, the capacity of the interleaved channel is lower than the capacity of the original channel. The authors in Fertonani & Colavolpe (2009) compute the achievable information rate of a two-state Markov-Gaussian channel through an information-theoretic analysis. We would like to point out that, while the state process of a two-state Markov-Gaussian noise model is the same as in a Gilbert-Elliott model, the same analytical arguments do not lead to a closed-form expression for this model since the channel output alphabet is non-binary Fertonani & Colavolpe (2009); Mitra & Lampe (2010). Hence, Fertonani & Colavolpe (2009) evaluates the information rate of this channel by means of the simulation-based method described in Arnold, D. M., Loeliger, H.-A., Vontobel, P. O., Kavčić,

[1] Throughout the article, the terms ‘impulsive noise’ and ‘impulsive channel’ are used interchangeably.

A. & Zeng, W. (2006). It is shown that the ultimate performance limit of such channels improves as the channel memory becomes more significant. Aims at approaching the ultimate performance limit as close as possible, Fertonani & Colavolpe (2009) provides a transceiver architecture for DT-based on powerful codes and iterative detection. It is shown that the proposed MAP-based iterative receiver with LDPC channel coding is able to exploit the memory of the noise process at the receiver and perform fairly close to the ultimate limit. To the best of our knowledge, no research results have been published on CR schemes impaired by such bursty impulsive channels. Here, we provide a mathematical framework for the performance analysis of DF CR schemes over bursty impulsive noise channel. Our work is an extension of Fertonani & Colavolpe (2009) to the CR scenario. While we do not attempt to modify the MAP detector proposed in Fertonani & Colavolpe (2009) to exploit the channel memory, our analysis also includes uncoded scenario and derive analytical error rate expressions for the proposed system, thus providing a framework to validate the simulation results. We expect to gain more compared to the optimal memoryless receiver Tepedelenlioglu & Gao (2005); Van Khuong & Le-Ngoc (2010) proposed for CR scheme over impulsive noise channel by considering noise memory in the detection process. Two different relaying strategies are considered depending on the processing performed by the relay: simple DF relaying (SR) and selective DF relaying (SDFR). In simple DF relaying, the relay transmits all the symbols it receives, whereas, in selective DF relaying, it is assumed that the relay forwards its decoded signal only if the received SNR at the relay is greater than a certain threshold, otherwise the relay remains silent and the destination decodes based on the direct transmission from the source only.

The contributions of this work are as follows. First, we derive a SER formula for DT using M-PSK modulation in the presence of Rayleigh frequency flat fading and two-state Markov-Gaussian impulsive noise. To validate the derived SER formula for DT, we considered the optimal MAP detection criterion that has been used in Fertonani & Colavolpe (2009) for symbol detection in a two-state Markov-Gaussian noise, and adapt the Bahl-Cocke-Jelinek-Raviv (BCJR) algorithm Bahl *et al.* (1974) to be implemented in the detector for this case. Then, we

extend the derived SER formula for DT to the case of DF CR schemes and provide a lower bound under the hypothetical assumption that the receivers have the knowledge of the state of the noise process. Finally, we propose an optimal MAP receiver for the considered DF CR schemes that utilize the MAP detection criterion for each link.

It is shown that the proposed optimal MAP receiver achieves the lower bound derived for DF CR scheme and performs significantly better than the conventional schemes developed for AWGN channel and memoryless impulsive noise channel. Indeed, the BER obtained with the memoryless receiver can be divided by almost 10^3 to get the BER with optimal MAP receiver under coded transmission. Also, DF CR schemes perform significantly better than DT under the same power consumption. In addition, for simple relaying, using the BER of the relay at the destination, the proposed optimal MAP receiver performs significantly better than the case where the MAP receiver does not have any knowledge about the error at the relay and achieves similar performance as that obtained through selective DF relaying.

The rest of the paper is organized as follows. In Section 3.3, the system model is introduced and Section 3.4 provides an overview of two-state Markov-Gaussian process. In Section 3.5, we provide the mathematical framework for the proposed scenario. Section 3.6 provides the performances in terms of BER and finally, some conclusions are drawn in Section 3.7.

3.3 System model

Here, we consider a DF cooperative relaying scheme with single relay (m), as shown in Fig 3.1, where the data transmission between the source-destination (sd) pair is assisted by m. We assume that all nodes are equipped with a single antenna and share the same bandwidth for data transmission. We also assume that each node operates in half-duplex mode and hence cannot transmit and receive simultaneously. Both s and m terminals use time division multiplexing for channel access. The cooperative communication takes place in two time slots, with normalized time intervals t_0 and $t_1 = 1 - t_0$. In the first time slot, s transmits the data to d, and due to the broadcast nature of the wireless channel, m also receives it. The relay then demodulates and

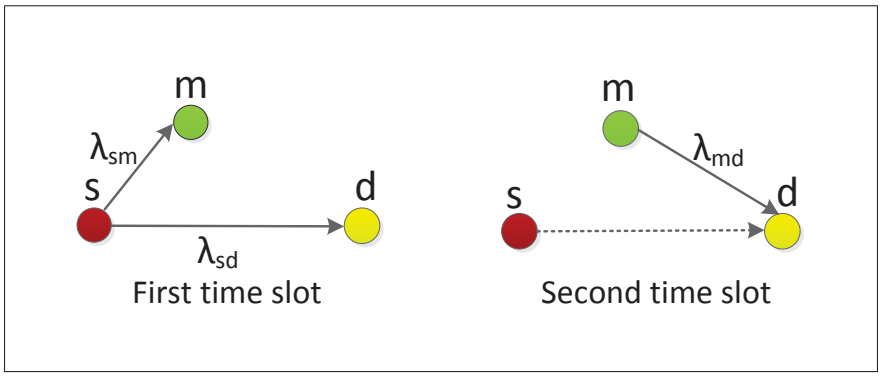

Figure 3.1 Cooperative communication with half-duplex relaying

decodes the received signal to recover the source information and based on the relaying strategy, it either retransmits in the second time slot of duration t_1, or declares that it will remain silent. During this period, s remains in the silent mode as indicated by the dotted line in Fig 3.1. For simple DF relaying, the relay always retransmits the decoded data to the destination in the second time slot. The destination then receives the noisy observation sequences from s in the first time slot as well as from m in the second time slot. The overall operation is shown in Fig 3.1. Hence, the decoded data with possible errors are forwarded from the relay to the destination. It is different from most papers on single-relay DF CR schemes where it is typically assumed that if the relay decodes the source message perfectly it will forward its decoded information to the destination, otherwise it will stay in silent mode, i.e., what we call *selective DF relaying* Laneman *et al.* (2004), which is decided by comparing the received SNR at the relay to a given threshold. However, in practical relaying systems an arbitrary chosen threshold does not guarantee error-free detection and hence decoding errors may occur at the relay Lee, K. & Hanzo, L. (2009); Liang, D., Ng, S. X. & Hanzo, L. (2010); Sneessens, H. H., Louveaux, J. & Vandendorpe, L. (2008) even if the received SNR at the relay is greater than a predetermined threshold value. Therefore, though the destination assumes that perfect decoded data were transmitted from the relay, actually the forwarded data may contain hard decision errors. So, there will be a performance degradation if the relay can not be guaranteed to be error-free. Specially, this problem becomes more crucial when the relay moves away from the source

and becomes closer to the destination. Although this problem could be solved by considering cyclic redundancy check (CRC) checking at the relays, it is bandwidth-consuming Wang, T., Cano, A., Giannakis, G. B. & Laneman, J. N. (2007) and induces extensive overhead since CRC checking usually takes place at the MAC layer. The authors in Jayakody, D. N. & Flanagan, M. F. (2015); Jayakody, D. N., Li, J. & Flanagan, M. F. (2015) and the references therein consider soft information relaying to mitigate the effect of decoding error propagation from the relay to the destination. It is shown that soft relaying performs better than hard information relaying under poor source-relay link conditions. However, these schemes require complex offline computation of soft noise parameters which increases the complexity of decoding at the destination for real-time transmission. To avoid these, our analysis remains more general and considers that decoding error might be propagated by the relay.

Consider that the source s generates a frame of binary information of length L bits $(b_0,\ldots,b_{L-1})$, mapped into a M-PSK modulated sequence $(x_{s,0},x_{s,1},\ldots,x_{s,K-1})$, and transmitted to both m and d in the first time slot. The signals received at m and d at each time epoch k, $k=0,1,\ldots,K-1$ can be respectively expressed as

$$y_{sm,k}=\sqrt{\mathrm{P}_s}h_{sm,k}x_{s,k}+n_{sm,k}, \tag{3.1}$$

$$y_{sd,k}=\sqrt{\mathrm{P}_s}h_{sd,k}x_{s,k}+n_{sd,k}, \tag{3.2}$$

where P_s is the average source transmission power for each symbol, $x_{s,k}$ is the transmitted symbol from s, $h_{ij,k}$ is the channel coefficient for the ij link, $i\in(s,m)$ and $j\in(m,d)$, and $n_{ij,k}$ is the noise term for the ij link that captures the combined effects of AWGN and the impulsive interferers. We assume independent Rayleigh fading in all links, i.e., for each ij link, $h_{ij}\equiv a_{ij}e^{j\theta_{ij}}$ is modeled as a zero-mean, independent, circularly symmetric complex Gaussian random variable with variance $\Omega_{ij}\equiv\varepsilon\{|h_{ij}|^2\}=1/\lambda_{ij}^{\eta}$, where $\varepsilon\{\cdot\}$ denotes expectation operator, λ_{ij} is the relative distance of i from j, and η is the path loss exponent. Hence, the channel amplitudes, a_{ij} are Rayleigh distributed, whereas the channel phases, θ_{ij} are uniformly distributed in $[-\pi,\pi)$. It is assumed that the channel coefficients are known by the receiver side, but not

by the transmitter side. The noise sample $n_{ij,k}$ is modeled as a two-state Markov-Gaussian process, which is in fact a Markov process in with the marginal distribution in each state are Gaussian. In the following section we will provide an overview of the model and explain the physical significance of each parameter. We assume that the noise samples for each link are mutually independent of the other links.

In the second time slot, at m, the received signal y_{sm} is passed through a demodulator to recover the source information. The relay then decodes the source information, potentially making an error. After recovering the source information, the relay modulates it using the same modulation format as in s and forwards it to the destination with average transmission power P_m. The signal received at the destination in this case is given by

$$y_{md,k} = \sqrt{\mathrm{P}_m} h_{md,k} x_{m,k} + n_{md,k}, \tag{3.3}$$

where $x_{m,k}$ is the transmitted signal from m. For fair comparison between DT and CR schemes, in our discussion we assume that the total source transmission power for direct transmission P_T is equal to the sum of source and relay transmission power in cooperative communication and hence the total transmission power is constrained as follows:

$$\mathrm{P}_s + \mathrm{P}_m = \mathrm{P}_T. \tag{3.4}$$

3.4 An overview of two-state Markov-Gaussian model

A two-state Markov-Gaussian model is introduced by Fertonani Fertonani & Colavolpe (2009) to characterize the correlated impulsive noise. At each time epoch k, the statistical properties of the noise sample $n_{ij,k}$ are completely defined by the channel state $s_k \in \{G,B\}$. In our noise modeling, G stands for the good channel that is impaired by the background Gaussian noise only and B for the bad channel which is impaired by impulsive interferers also. For each ij link, we model $n_{ij,k}$ as a zero-mean, circularly symmetric complex Gaussian random variable with variances depending on s_k, so that conditioned on s_k, the probability density functions

(PDFs) of $n_{ij,k}$ can be expressed as

$$p(n_{ij,k}|s_k = G) = \frac{1}{\pi\sigma_G^2}\exp\left(-\frac{|y_{ij,k} - \sqrt{\mathrm{P}_i}h_{ij,k}x_{i,k}|^2}{\sigma_G^2}\right), \tag{3.5}$$

$$p(n_{ij,k}|s_k = B) = \frac{1}{\pi\sigma_B^2}\exp\left(-\frac{|y_{ij,k} - \sqrt{\mathrm{P}_i}h_{ij,k}x_{i,k}|^2}{\sigma_B^2}\right), \tag{3.6}$$

where σ_G^2 and σ_B^2 are the average noise power of the good channel and bad channel respectively. The parameter $R = \sigma_B^2/\sigma_G^2$ quantifies the relative power of the impulsive noise compared to Gaussian noise. The statistical description of the state process $s^K = \{s_0, s_1, \ldots, s_{K-1}\}$ completely characterizes the channel and, for Markov-Gaussian model, s^K is expressed as a stationary first-order Markov-process with

$$p(s^K) = p(s_0)\prod_{k=0}^{K-1} p(s_{k+1}|s_k), \tag{3.7}$$

for each realization of the process. Therefore, the state process is described by the state transition probabilities $p_{s_k s_{k+1}} = p(s_{k+1}|s_k)$, $s_k, s_{k+1} \in \{G, B\}$. From the state transition probabilities, the stationary probabilities p_G and p_B of being in G and B state are respectively given by Fertonani & Colavolpe (2009),

$$p_G = p(s_k = G) = \frac{p_{BG}}{p_{GB} + p_{BG}}, \tag{3.8}$$

$$p_B = p(s_k = B) = \frac{p_{GB}}{p_{GB} + p_{BG}}, \tag{3.9}$$

where p_{BG} denotes the transition probability from state B to state G and similarly p_{GB} is the transition probability from G to B. Also, according to the notation in Fertonani & Colavolpe (2009), the parameter $\gamma = \frac{1}{p_{GB}+p_{BG}}$ quantifies the noise memory, with $\gamma = 1$ meaning that the noise is memoryless and $\gamma > 1$ indicating that the noise has persistent memory. Finally, the time evolution of the noise state sequence can be represented by means of a trellis diagram displayed in Fig. 3.2, where all the possible paths given the initial state G are shown. This trellis

representation is important for MAP symbol detection and will be discussed in the following section.

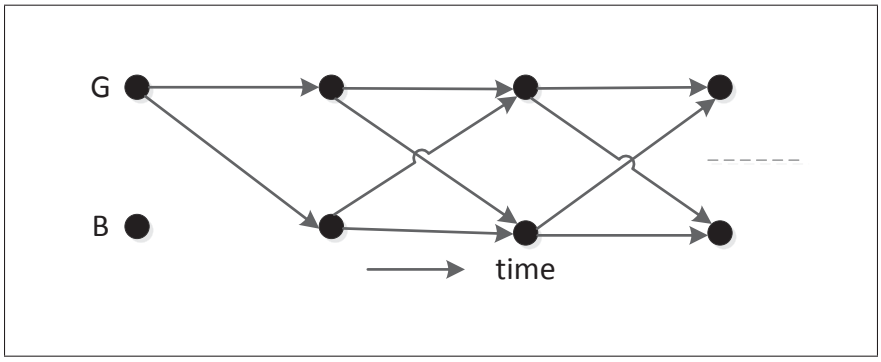

Figure 3.2 Trellis representation of the two-state Markov-Gaussian noise model

3.5 Performance analysis

3.5.1 Maximum a Posteriori (MAP) Detection

For a two-state Markov-Gaussian noise channel, the optimum receiver for DT is designed in Fertonani & Colavolpe (2009) that exploits the MAP detection criterion for symbol detection. The algorithm derived for MAP symbol detection is based on the factor graphs and the sum-product algorithm assuming no fading. Here, we consider the same detection criterion and summarize the straightforward BCJR algorithm to be implemented into the MAP detector in the presence of Rayleigh fading. The BCJR algorithm is based on the probabilistic arguments and works on a trellis diagram depicted in Fig. 3.2 for MAP decoding of two-state Markov-Gaussian noise channel. However instead of a trellis, when it is exported into a Tanner graph, it becomes the sum-product algorithm.

For M-PSK modulation scheme with $M = 2$, the MAP decoding rule at the destination is given by

$$\hat{x}_{s,k} = \begin{cases} 1 & \text{if } L_k \geq 0 \\ -1 & \text{if } L_k < 0 \end{cases} \tag{3.10}$$

where, $\hat{x}_{s,k}$ is the estimate of the source's transmitted sequence $x_{s,k}$ generated at d and L_k is the log-likelihood ratio (LLR). For direct transmission, L_k at the destination is defined by

$$L_{sd,k} = \ln \left\{ \frac{p(x_{s,k} = 1|y_{sd}^K)}{p(x_{s,k} = -1|y_{sd}^K)} \right\}, \tag{3.11}$$

where $y_{sd}^K = \{y_{sd,0}, y_{sd,1}, \ldots, y_{sd,K-1}\}$ is the whole sequence to be detected and K is the size of the sequence. For computation, at each k, the optimal MAP detector at the destination evaluates the a posteriori probability $p(x_{s,k}|y_{sd}^K)$ for each symbol $x_{s,k}$ belonging to the binary modulation alphabet {1,-1}. The a posteriori probability $p(x_{s,k} = b \mid y_{sd}^K)$, $b \in \{1, -1\}$ can be computed from

$$p(x_{s,k} = b|y_{sd}^K) \propto p(x_{s,k} = b, y_{sd}^K) = \sum_{s_k, s_{k+1}} p(x_{s,k} = b, y_{sd}^K, s_k, s_{k+1}) \tag{3.12}$$

where s_k, s_{k+1} denote the noise states at time k and $k+1$ respectively and the proportionality indicates that the two sides may differ with a positive multiplicative factor that does not have any effect on the detection process Fertonani & Colavolpe (2009). Let us define the following quantities

$$\alpha_k(s_k) = p(y_{sd,0}, y_{sd,1}, \ldots, y_{sd,k-1}, s_k), \tag{3.13}$$

$$\beta_k(s_k) = p(y_{sd,k}, y_{sd,k+1}, \ldots, y_{sd,K-1}|s_k), \tag{3.14}$$

$$\delta_k(x_{s,k}, s_k, s_{k+1}) = p(s_{k+1}|s_k) p(n_{sd,k} = y_{sd,k} - \sqrt{\mathrm{P}_s} h_{sd,k} x_{s,k}|s_k) \tag{3.15}$$

where $\alpha_k(s_k)$ and $\beta_k(s_k)$ are referred to as the forward and backward filters and $\delta_k(x_{s,k}, s_k, s_{k+1})$ represents the branch metrics of the trellis diagram shown in Fig. 3.2. For a two-state Markov-Gaussian model, the quantity $p(n_{sd,k} = y_{sd,k} - \sqrt{\mathrm{P}_s} h_{sd,k} x_{s,k}|s_k)$ is given by (3.5) and (3.6) respectively. Assuming independent transmitted symbols $x_{s,k}$, using (3.13), (3.14), and (3.15),

the probability term $p(x_{s,k}=b, y_{sd}^{K}, s_k, s_{k+1})$ in (3.12) can be represented as

$$p(x_{s,k}=b, y_{sd}^{K}, s_k, s_{k+1}) = p(x_{s,k}=b)\alpha_k(s_k)\beta_{k+1}(s_{k+1})\delta_k(x_{s,k}=b, s_k, s_{k+1}), \tag{3.16}$$

Thus, from (3.12)

$$p(x_{s,k}=b, y_{sd}^{K}) = p(x_{s,k}=b)\sum_{s_k, s_{k+1}} \alpha_k(s_k)\beta_{k+1}(s_{k+1})\delta_k(x_{s,k}=b, s_k, s_{k+1}), \tag{3.17}$$

Then, the LLR values at the destination are obtained by

$$\begin{aligned} L_{sd,k} &= \ln\left\{\frac{p(x_{s,k}=1, y_{sd}^{K})}{p(x_{s,k}=-1, y_{sd}^{K})}\right\} \\ &= \ln\left\{\frac{p(x_{s,k}=1)\sum_{s_k, s_{k+1}} \alpha_k(s_k)\beta_{k+1}(s_{k+1})\delta_k(x_{s,k}=1, s_k, s_{k+1})}{p(x_{s,k}=-1)\sum_{s_k, s_{k+1}} \alpha_k(s_k)\beta_{k+1}(s_{k+1})\delta_k(x_{s,k}=-1, s_k, s_{k+1})}\right\}. \end{aligned} \tag{3.18}$$

The forward and backward filters can be computed recursively as

$$\alpha_{k+1}(s_{k+1}) = \sum_{s_k, x_{s,k}} \alpha_k(s_k)p(x_{s,k})\delta_k(x_{s,k}, s_k, s_{k+1}), \tag{3.19}$$

$$\beta_k(s_k) = \sum_{s_{k+1}, x_{s,k}} \beta_{k+1}(s_{k+1})p(x_{s,k})\delta_k(x_{s,k}, s_k, s_{k+1}), \tag{3.20}$$

where the forward and backward filters are initialized with

$$\alpha_0(s_0 = S) = p_S, \text{ and } \beta_K(s_K = S) = 1.\ S \in (G, B) \tag{3.21}$$

However, for M-PSK modulation scheme with $M > 2$, the first step is to compute the a posteriori probability $p(x_{i,k}|y_{ij,k})$ for each symbol $x_{i,k}$ belonging to the M-PSK modulation alphabet using the MAP symbol detector explained above. The next step is to consider a standard soft demapper Tosato, F. & Bisaglia, P. (2002) which performs reliable metric computation at the bit level, given the input probability $p(x_{i,k}|y_{ij,k})$. Note that, this block is not needed in case of BPSK since the generated LLR values for the BPSK symbols are the same as the bits. The

demapper extracts the quantity $p(b_{l,k} = b|y_{ij,k})$ through the input-output relationship given by

$$p(b_{l,k} = b|y_{ij,k}) \propto \sum_{x_{i,k} \in \chi(l,b)} p(x_{i,k}|y_{ij,k}), \tag{3.22}$$

where $b_{l,k}$ is the lth bit of symbol $x_{i,k}$ and $\chi(l,b)$ denote the set of $x_{i,k}$ symbols having their lth bit equal to b. For example, the LLR values for the first and second bit in Q-PSK modulation scheme can be obtained by

$$L^{(1)}_{ij,k} = \ln\left\{\frac{b_{1,k}=0|y_{ij,k}}{b_{1,k}=1|y_{ij,k}}\right\} = \ln\left\{\frac{(x_{i,k}=00|y_{ij,k})+(x_{i,k}=01|y_{ij,k})}{(x_{i,k}=10|y_{ij,k})+(x_{i,k}=11|y_{ij,k})}\right\}. \tag{3.23}$$

$$L^{(2)}_{ij,k} = \ln\left\{\frac{b_{2,k}=0|y_{ij,k}}{b_{2,k}=1|y_{ij,k}}\right\} = \ln\left\{\frac{(x_{i,k}=00|y_{ij,k})+(x_{i,k}=10|y_{ij,k})}{(x_{i,k}=01|y_{ij,k})+(x_{i,k}=11|y_{ij,k})}\right\}. \tag{3.24}$$

It should be mentioned that in order to evaluate the LLR values required for the evaluation of the BER, the receivers need the knowledge of the noise parameters $(p_B, \gamma, R, \sigma_G^2)$ and the amplitude of the channel coefficients h_{ij}. Similar to Fertonani & Colavolpe (2009), it is assumed that these parameters are perfectly known at the receiver side. This assumption is made since we are mainly interested to focus on the BER performance comparison of different receivers, and to evaluate the impact of noise memory. How the receiver side gets these knowledge is beyond the scope of this paper.

3.5.2 BER of Direct Transmission

In order to derive the analytical SER formula for direct transmission, we assume that the destination receiver has the knowledge of the variance of each state. Then, for the considered two-state Markov-Gaussian noise, the conditional probability of symbol error for M-PSK modulated signal when the channel is in good state is given by the integral expression(Simon, M. K. & Alouini, M.-S., 2005, Eq. (8.23))

$$P^G_{e,DT} = \frac{1}{\pi}\int_0^{(M-1)\pi/M} \exp\left(-\frac{\mathrm{P_T}}{\sigma_G^2}\frac{g_{PSK}}{\sin^2\theta}\right), \tag{3.25}$$

where $g_{PSK} = \sin^2(\pi/M)$. Similarly, the conditional SER when the channel is in bad state is given by

$$P_{e,DT}^{B} = \frac{1}{\pi}\int_{0}^{(M-1)\pi/M} \exp\left(-\frac{\mathrm{P_T}}{\sigma_B^2}\frac{g_{PSK}}{\sin^2\theta}\right), \tag{3.26}$$

Assuming that the receiver has knowledge of the state s_k, a lower bound on the average SER for the direct transmission is expressed as

$$P_{e,DT} = p_G^{sd} P_{e,DT}^{G} + p_B^{sd} P_{e,DT}^{B}, \tag{3.27}$$

where $p_G^{sd} = p_{BG}^{sd}/p_{GB}^{sd} + p_{BG}^{sd}$ and $p_B^{sd} = p_{GB}^{sd}/p_{GB}^{sd} + p_{BG}^{sd}$ are the steady-state probabilities of having in good state and bad state respectively for the *sd* link. When fading is present, the conditional SER for a given channel realization h_{sd} is expressed as

$$P_{e,DT}(h_{sd}) = \frac{p_G^{sd}}{\pi}\int_{0}^{(M-1)\pi/M} \exp\left(-\gamma_G^{sd}\frac{g_{PSK}}{\sin^2\theta}\right) + \frac{p_B^{sd}}{\pi}\int_{0}^{(M-1)\pi/M} \exp\left(-\gamma_B^{sd}\frac{g_{PSK}}{\sin^2\theta}\right), \tag{3.28}$$

where, $\gamma_G^{sd} = \frac{\mathrm{P_T}|h_{sd}|^2}{\sigma_G^2}$ and $\gamma_B^{sd} = \frac{\mathrm{P_T}|h_{sd}|^2}{\sigma_B^2}$ are the instantaneous link SNRs for the *sd* link in good and bad state respectively. Since $h_{sd} \sim CN(0,\Omega_{sd})$, i.e., the link experience Rayleigh fading, γ_u^{sd} is exponentially distributed with the probability density function

$$f_{\gamma_u^{sd}}(\gamma) = \frac{1}{\bar{\gamma}_u^{sd}} e^{-\frac{\gamma}{\bar{\gamma}_u^{sd}}}, \tag{3.29}$$

where, $\bar{\gamma}_u^{sd} = \varepsilon\{\gamma_u^{sd}\} = \frac{\mathrm{P_T}\Omega_{sd}}{\sigma_{u,sd}^2}$ incorporates the average SNR of *sd* link, $u \in (0,1) \equiv (G,B)$ and $\sigma_{u,sd}^2 = R_{sd}^{u}\sigma_G^2$ is the variance of n_{sd} with R_{sd} is the impulsive to Gaussian noise power ratio for the *sd* link. By averaging (3.28) with respect to the random variable γ_u^{sd} and making use of (Simon & Alouini, 2005, Eq. (8.113)), the average SER is given by

$$P_{e,DT} = \sum_{u=0}^{1}\left(\frac{M-1}{M}\right)\left\{1 - \sqrt{\frac{g_{PSK}\bar{\gamma}_u^{sd}}{1+g_{PSK}\bar{\gamma}_u^{sd}}}\left(\frac{M}{(M-1)\pi}\right)\left[\frac{\pi}{2} + \tan^{-1}\left(\sqrt{\frac{g_{PSK}\bar{\gamma}_u^{sd}}{1+g_{PSK}\bar{\gamma}_u^{sd}}}\cot\frac{\pi}{M}\right)\right]\right\}. \tag{3.30}$$

For BPSK $(M=2)$, (3.30) becomes the BER of direct transmission

$$P_{b,DT} = \frac{p_G^{sd}}{2}\left(1-\sqrt{\frac{\bar{\gamma}_G^{sd}}{1+\bar{\gamma}_G^{sd}}}\right)+\frac{p_B^{sd}}{2}\left(1-\sqrt{\frac{\bar{\gamma}_B^{sd}}{1+\bar{\gamma}_B^{sd}}}\right). \tag{3.31}$$

3.5.3 BER of DF Cooperative Relaying

In case of DF cooperative relaying, the SER at the relay follows the same form as in (3.30), i.e.,

$$P_{e,m} = \sum_{u=0}^{1}\left(\frac{M-1}{M}\right)\left\{1-\sqrt{\frac{g_{PSK}\bar{\gamma}_u^{sm}}{1+g_{PSK}\bar{\gamma}_u^{sm}}}\left(\frac{M}{(M-1)\pi}\right)\left[\frac{\pi}{2}+\tan^{-1}\left(\sqrt{\frac{g_{PSK}\bar{\gamma}_u^{sm}}{1+g_{PSK}\bar{\gamma}_u^{sm}}}\cot\frac{\pi}{M}\right)\right]\right\}. \tag{3.32}$$

where, $\bar{\gamma}_u^{sm} = \frac{\mathrm{P_T}\Omega_{sm}}{R_{sm}^u\sigma_G^2}$, $u \in \{G,B\}$ is the average received SNR of *sm* link. The end-to-end SER performance of DF cooperative relaying scheme depends on different relaying strategies such as SR in which the relay always transmits in the second phase. The end-to-end SER under this condition is equal to

$$P_{e,coop}^{SR} = P_{e,m}\cdot P_{e,smd}^{er} + (1-P_{e,m})\cdot P_{e,smd}^{ner}, \tag{3.33}$$

where $P_{e,smd}^{er}$ is the probability of error at the destination after combining the two signals coming from the source and the relay when the error is propagated from the relay. Also, $P_{e,smd}^{ner}$ is the probability of error at the destination when there is no error propagation from the relay and hence the source and the relay will transmit the same data. On the other hand, in SDFR it is assumed that the relay forwards its decoded signal only if the source-relay SNR is larger than a certain threshold, otherwise the relay remains silent and the destination decodes based on the direct transmission from the source only. A lower bound of this protocol is obtained if it is assumed that the relay is able to decode the source symbol successfully when the received SNR at the relay is greater than a certain threshold and retransmits on the second phase only if it is successfully decoded. The average SER at the destination under this scheme can be computed as

$$P_{e,coop}^{SDFR} = P_{e,m}\cdot P_{e,DT} + (1-P_{e,m})\cdot P_{e,smd}^{ner}, \tag{3.34}$$

However, in practical relaying systems, an arbitrary chosen threshold does not guarantee error-free detection, and hence decoding errors may occur at the relay even if the received SNR at the relay is greater than a predetermined threshold value. The actual average SER at the destination for this scheme for a given threshold γ_t can be expressed as

$$P_{e,coop}^{SDFR} = p\{\gamma_u^{sm} > \gamma_t\}\left[P_{e,m}|\gamma_u^{sm} > \gamma_t \cdot P_{e,smd}^{er} + (1 - P_{e,m}|\gamma_u^{sm} > \gamma_t) \cdot P_{e,smd}^{ner}\right] + p\{\gamma_u^{sm} \leq \gamma_t\} \cdot P_{e,DT}, \tag{3.35}$$

Since γ_u^{sm} is an exponential random variable with mean $\bar{\gamma}_u^{sm}$, we have

$$p\{\gamma_u^{sm} \leq \gamma_t\} = 1 - \exp\left(-\gamma_t/\bar{\gamma}_u^{sm}\right), \tag{3.36}$$

When $\gamma_u^{sm} > \gamma_t$, the SER at the relay decreases, but it remains nonzero regardless of the value of γ_t Onat, F. A., Adinoyi, A., Fan, Y., Yanikomeroglu, H., Thompson, J. S. & Marsland, I. D. (2008). Following the same procedure in Onat *et al.* (2008), for BPSK/Q-PSK modulation scheme the BER at the relay given that $\gamma_u^{sm} > \gamma_t$ is equal to

$$P_{b,m}|\gamma_u^{sm} > \gamma_t = \frac{1}{2}\sum_{u=0}^{1}(p_B^{sm})^u (p_G^{sm})^{1-u}\left[erfc(\sqrt{\gamma_t}) - e^{\gamma_t/\bar{\gamma}_u^{sm}}\sqrt{\frac{\bar{\gamma}_u^{sm}}{1+\bar{\gamma}_u^{sm}}}erfc\left(\sqrt{\gamma_t\left(1+\frac{1}{\bar{\gamma}_u^{sm}}\right)}\right)\right]. \tag{3.37}$$

In order to compute $P_{e,smd}^{er}$ and $P_{e,smd}^{ner}$ we have to know which combiner is used for combining the signals coming from the source and the relay. For AWGN channel, i.e., when impulsive noise is absent, the maximum ratio combining is optimal in the sense of minimizing the SER. The MRC combining is

$$y_d = \sqrt{\mathrm{P_s}}h_{sd}^* y_{sd} + \sqrt{\mathrm{P_m}}h_{md}^* y_{md}. \tag{3.38}$$

When impulsive noise is present, the optimal MAP combining is

$$\begin{aligned} L_{coop,k} &= \ln\left\{\frac{p(x_{s,k} = x_0|y_{sd}^K, y_{md}^K)}{p(x_{s,k} = x_z|y_{sd}^K, y_{md}^K)}\right\} \\ &= \ln\left\{\frac{\sum_{x_{m,k}\in\{x_0,\ldots,x_z,\ldots,x_{M-1}\}} p(x_{s,k} = x_0, x_{m,k}|y_{sd}^K, y_{md}^K)}{\sum_{x_{m,k}\in\{x_0,\ldots,x_z,\ldots,x_{M-1}\}} p(x_{s,k} = x_z, x_{m,k}|y_{sd}^K, y_{md}^K)}\right\}, \end{aligned} \tag{3.39}$$

where $L_{coop,k}$ is the symbol LLR value at the destination in case of cooperative communication. Without loss of generality, it is assumed that the source transmits x_0. Using the Bayes rule, the following probability term is given by

$$p(x_{s,k}, x_{m,k}|y_{sd}^K, y_{md}^K) = \frac{p(y_{sd}^K, y_{md}^K|x_{s,k}, x_{m,k})p(x_{s,k}, x_{m,k})}{p(y_{sd}^K, y_{md}^K)}, \tag{3.40}$$

We assume that for the given transmitted signals, y_{sd}^K and y_{md}^K are independent from each other. Under this consideration, we have

$$p(y_{sd}^K, y_{md}^K|x_{s,k}, x_{m,k}) = p(y_{sd}^K|x_{s,k}) \cdot p(y_{md}^K|x_{m,k}), \tag{3.41}$$

where the equality is due to the conditional independence of y_{sd}^K and y_{md}^K and using the facts that $p(y_{sd}^K|x_{s,k}, x_{m,k}) = p(y_{sd}^K|x_{s,k})$ and $p(y_{md}^K|x_{s,k}, x_{m,k}) = p(y_{md}^K|x_{m,k})$. Substituting (3.41) in (3.39), results in

$$L_{coop,k} = \ln\left\{\frac{p(x_{s,k} = x_0, y_{sd}^K)}{p(x_{s,k} = x_z, y_{sd}^K)}\right\} + \ln\left\{\frac{p(x_{m,k} = x_0, y_{md}^K)}{p(x_{m,k} = x_z, y_{md}^K)}\right\} + \ln\left\{\frac{1 + \frac{q_m}{1-q_m}\left(\frac{p(x_{m,k}=x_z, y_{md}^K)}{p(x_{m,k}=x_0, y_{md}^K)}\right)}{1 + \frac{q_m}{1-q_m}\left(\frac{p(x_{m,k}=x_0, y_{md}^K)}{p(x_{m,k}=x_z, y_{md}^K)}\right)}\right\}. \tag{3.42}$$

where $q_m = \sum_{z=1}^{M-1} p(x_{m,k} = x_z|x_{s,k} = x_0)$ is the SER at the relay. With M-PSK modulation, there are $M-1$ ways of making an incorrect decision at the relay and their impacts on the detection process at the destination should be different. For BPSK modulation scheme, (3.42) reduces to

$$L_{coop,k} = \ln\left\{\frac{p(x_{s,k} = 1, y_{sd}^K)}{p(x_{s,k} = -1, y_{sd}^K)}\right\} + \ln\left\{\frac{p(x_{m,k} = 1, y_{md}^K)}{p(x_{m,k} = -1, y_{md}^K)}\right\} + \ln\left\{\frac{1 + \frac{\theta_m}{1-\theta_m}\left(\frac{p(x_{m,k}=-1, y_{md}^K)}{p(x_{m,k}=1, y_{md}^K)}\right)}{1 + \frac{\theta_m}{1-\theta_m}\left(\frac{p(x_{m,k}=1, y_{md}^K)}{p(x_{m,k}=-1, y_{md}^K)}\right)}\right\}. \tag{3.43}$$

where θ_m be the average probability of bit error in detecting the source information at m.[2] The second term in (3.43) can be computed as (3.18) with the computation of α, β, and δ for the *md* link. The receiver at the destination is then composed of two MAP detectors, one for detecting the source transmission and the other for the relay's transmission. The third term can

[2] There is of course an underlying assumption here that the average on probability is the same as the total average.

be estimated by knowing the average error probability at the relay (θ_m) and the output of the MAP detector for the *md* link. The soft information are then combined using a soft combiner and input to the MAP decoder to regenerate the information bits. The whole operation is shown in Fig. 3.3. We assume that in addition to the decoded bits, the relay also transmits to the destination some side information, for example, the relay may transmit the value of the channel state information Sneessens *et al.* (2008), so that the decoder at the destination can determine the corresponding error probabilities in the relayed signal.

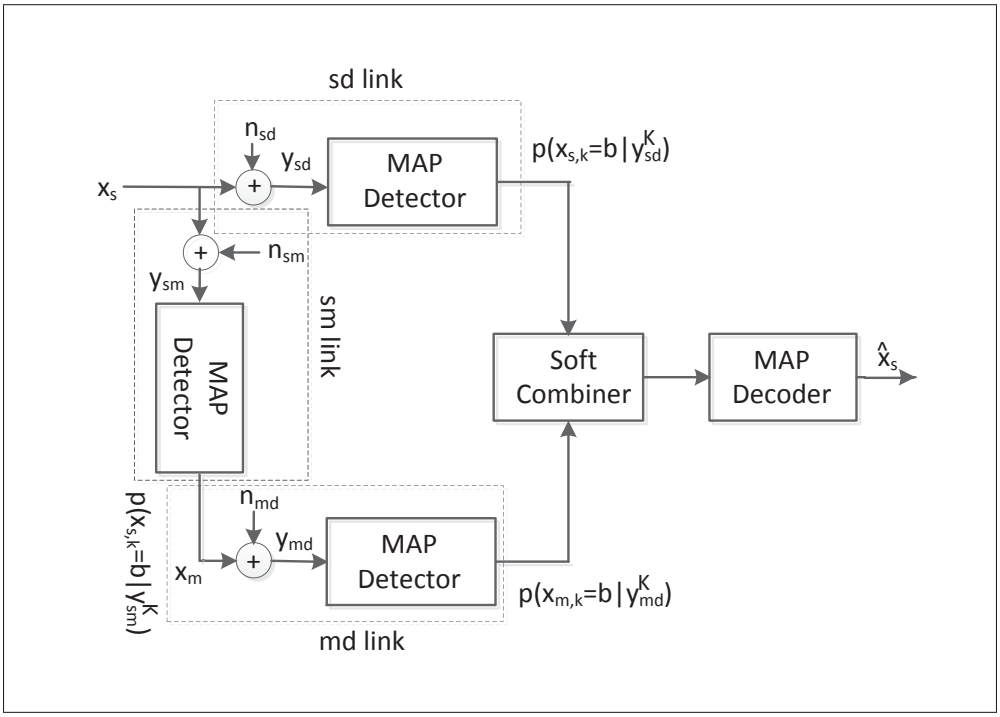

Figure 3.3 MAP receiver for DF cooperative relaying over correlated impulsive noise channel. The system is composed of three MAP detectors, one for each link

In order to derive the SER, it is assumed that the destination receiver has the knowledge of the states of n_{sd} and n_{md}, and variances of each state. This makes the problem tractable and constitutes a lower bound on the actual SER. Under this consideration, the optimal combiner is based on MRC Van Khuong & Le-Ngoc (2010). For MRC, the SNR after combining the two signals is the sum of the SNRs of the *sd* and *md* links and conditioned on $\sigma^2 = [\sigma^2_{u,sd} \quad \sigma^2_{v,md}]$,

$P_{e,smd}^{ner}$ is the SER of a two-branch MRC receiver in Rayleigh fading channel which is given in (Simon & Alouini, 2005, Eq. (9.14)). For BPSK modulation with independent and non-identically distributed (i.n.d.) Rayleigh channels, this is given as (Proakis, J. G., 2001, Eq. (14.5-28))

$$P_{b,smd}^{ner}(\sigma_{u,sd}^2,\sigma_{v,md}^2)=\frac{1}{2}\left(\frac{\psi(\bar{\gamma}_u^{sd})}{1-\bar{\gamma}_v^{md}/\bar{\gamma}_u^{sd}}+\frac{\psi(\bar{\gamma}_v^{md})}{1-\bar{\gamma}_u^{sd}/\bar{\gamma}_v^{md}}\right), \tag{3.44}$$

where $\psi(\bar{\gamma})=1-\sqrt{\frac{\bar{\gamma}}{1+\bar{\gamma}}}$ and $\sigma_{u,sd}^2=R_{sd}^u\sigma_G^2$ and $\sigma_{v,md}^2=R_{md}^v\sigma_G^2$ are the variances of n_{sd} and n_{md}, respectively. By averaging $P_{b-smd}^{ner}(\sigma_{u,sd}^2,\sigma_{v,md}^2)$ with respect to $\sigma_{u,sd}^2$ and $\sigma_{v,md}^2$, we obtain the average BER for the *smd* link as

$$P_{b,smd}^{ner}=\frac{1}{2}\sum_{u=0}^{1}\sum_{v=0}^{1}(p_B^{sd})^u(p_G^{sd})^{1-u}(p_B^{md})^v(p_G^{md})^{1-v}\left(\frac{\psi(\bar{\gamma}_u^{sd})}{1-\bar{\gamma}_v^{md}/\bar{\gamma}_u^{sd}}+\frac{\psi(\bar{\gamma}_v^{md})}{1-\bar{\gamma}_u^{sd}/\bar{\gamma}_v^{md}}\right). \tag{3.45}$$

To calculate $P_{e,smd}^{er}$, similar to Onat *et al.* (2008), it is assumed that the dominant cause of detection errors at the destination is due to the incorrectly detected symbol error sent by the relay. For Rayleigh faded channel, in the absence of impulsive noise the error probability under this condition can be approximated by Onat *et al.* (2008)

$$P_{e,smd}^{er}(\sigma_{u,sd}^2,\sigma_{v,md}^2)=\frac{\bar{\gamma}_v^{md}C_{z,M}}{\bar{\gamma}_v^{md}C_{z,M}+\bar{\gamma}_u^{sd}}, \tag{3.46}$$

where $C_{z,M}$ depends on the particular value of M and is defined in Onat *et al.* (2008). In the special case of $M=2$, $C_{z,M}=1$. Then, for impulsive noise channel the average BER for the *smd* link becomes

$$P_{b,smd}^{er}=\sum_{u=0}^{1}\sum_{v=0}^{1}(p_B^{sd})^u(p_G^{sd})^{1-u}(p_B^{md})^v(p_G^{md})^{1-v}\left(\frac{\bar{\gamma}_v^{md}}{\bar{\gamma}_v^{md}+\bar{\gamma}_u^{sd}}\right). \tag{3.47}$$

3.6 Numerical results

Here, first we present the BER performances of DT and DF CR schemes where a sequence of equally likely information bits of length $64,800$ is mapped onto BPSK modulation sequence

and transmitted over two state Markov-Gaussian channels characterized by the identical parameters of bad state occurring rate $p_B = 0.1$, channel memory $\gamma = 100$, and impulsive to Gaussian noise power ratio $R = 100$. In our simulations, it is assumed that the distance between the source and the destination is normalized to unity, i.e., $\lambda_{sd} = 1$ and $\lambda_{sr} = 0.4$, $\lambda_{rd} = 0.6$. Also, slot durations $t_0 = t_1 = 1/2$, both the source and the relay transmit power $\mathrm{P}_s = \mathrm{P}_m = \mathrm{P}_T/2$, and the path loss exponent $\eta = 2$.

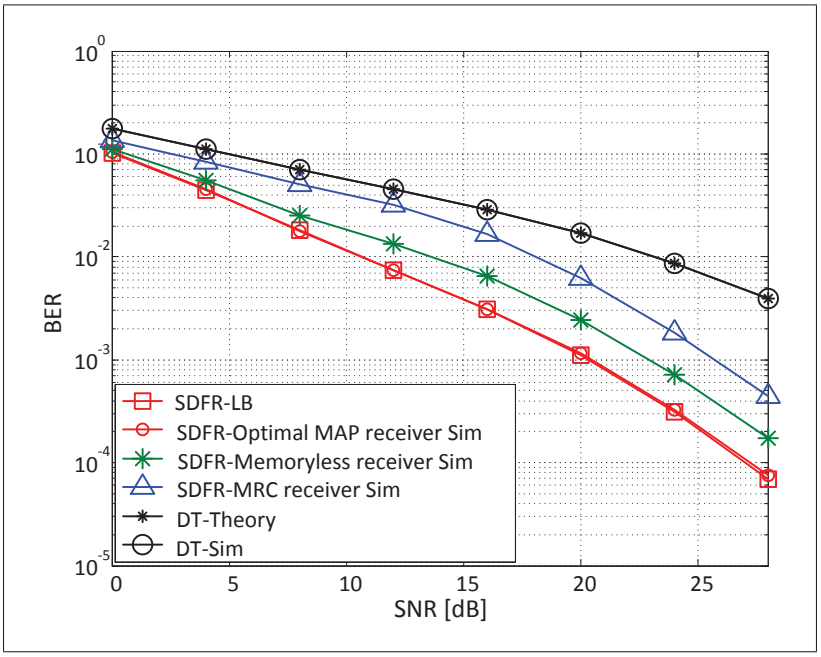

Figure 3.4 Analytical and simulated BER performances of direct transmission (DT) and selection decode-and-forward relaying (SDFR) schemes against SNR. A system employing a BPSK modulation is considered and the performance of various decoding schemes over two-state Markov-Gaussian channels, each characterized by $p_B = 0.1$, $\gamma = 100$, $R = 100$ is shown

Fig. 3.4 shows the analytical and simulated BER performances of both DT and SDFR schemes assuming different receiver structures. The proposed optimal MAP receiver uses the MAP detection criterion, the memoryless receiver Tepedelenlioglu & Gao (2005) is optimal for i.i.d. Bernoulli-Gaussian noise, and the MRC combiner Proakis (2001) is optimal for AWGN channel. Similar to Proakis (2001); Van Khuong & Le-Ngoc (2010), it is assumed that the relay

is able to detect whether the source symbol is correctly detected or not, and that it forwards to the destination only if it is correctly decoded. The exact BER expression in (3.31) and the lower bound of BER expression in (3.34) are used to obtain the analytical results for DT and SDFR, respectively. For the simulation results, it is assumed that the noise samples n_{sm}, n_{sd}, and n_{md} are mutually independent, with each characterized by the noise parameter values listed above. The BER performances are calculated for 2000 frames of $64,800$ information bits each against *SNR*. The *SNR* is defined as, $SNR = \varepsilon\{|x_{s,k}|^2\}/\sigma_G^2$, where σ_G^2 is the background Gaussian noise power. For the considered BPSK modulated signal, $\varepsilon\{|x_{s,k}|^2\}$ is equal to one and the Gaussian noise power σ_G^2 is adjusted to achieve a given SNR. Also, the SNR is equal to the SNR of the *sd* link, because the distance between *s* and *d* is normalized to unity. To obtain the simulated BER, the LLR values for the direct transmission from source-to-relay and source-to-destination links are obtained using the formula in (3.18), and the LLR values for the cooperative *smd* link are obtained using (3.43) with the assumption that $x_{s,k} = x_{m,k}$ and hence $\theta_m = 0$. From Fig. 3.4, it is seen that the analytical result perfectly matches with the simulation result for DT and SDFR schemes. Also, SDFR performs significantly better than DT under the same power consumption which confirms the benefit of utilizing CR over bursty impulsive noise channel. Moreover, our proposed MAP receiver achieves the lower bound derived for SDFR. It obtains a minimum SNR gain of around 5 dB over the MRC combiner in (3.38) and around 2 dB over the optimal memoryless receiver at the expense of higher complexity due to the MAP detection. This confirms the benefits of utilizing the noise memory in the detection process.

Although similar conclusions hold for all values of p_B, γ, and R, the performance gain provided by the utilization of memory in the detection process depends on those values. This is shown in Fig. 3.5 for different realizations of p_B, γ, and R. From the figure it is seen that for a given value of p_B, as the value of R increases, the BER performance degrades. Interestingly, from the figure it is also seen that with increasing R, the gain provided by the memory increases. This implies that the larger the value of the impulsive interferers are, the better the performance gain provided by the memory. Also, the optimal MAP receiver shows the same performance as the

memoryless receiver when we consider $\gamma = 1$ in the noise process, which corresponds to the i.i.d. case of Markov-Gaussian noise commonly known as Bernoulli-Gaussian noise in the literature. This is expected since the memoryless receiver is optimal for i.i.d. Bernoulli-Gaussian noise. These results confirm that the optimal MAP receiver reduces to the memoryless receiver when there is no time correlation among the noise samples. Again, the AWGN receiver achieves the worst performances in these impulsive environments. Finally, we also reported the corresponding curves for an AWGN channel. From the obtained results it is obvious that the three receivers show the same performance over AWGN channel.

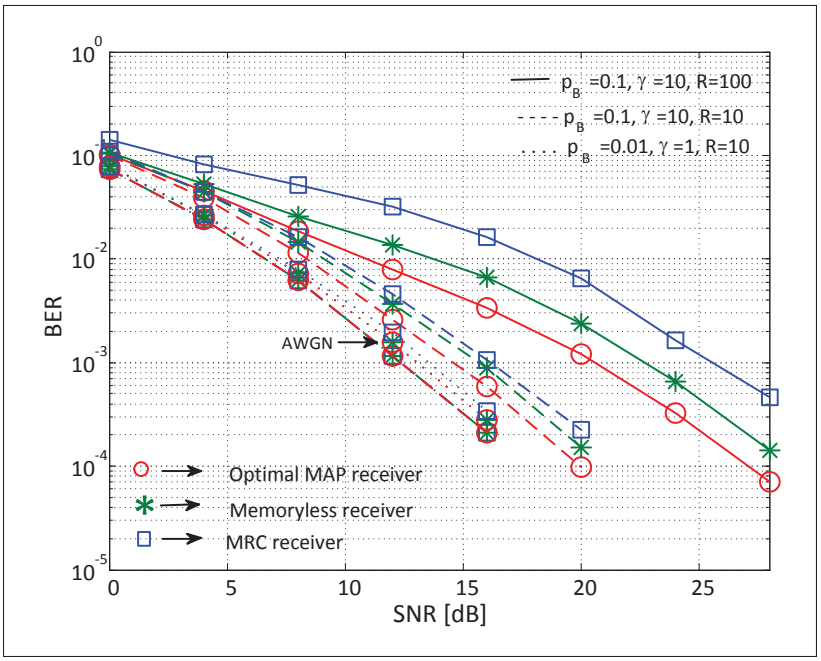

Figure 3.5 BER performances of selection decode-and-forward relaying (SDFR) scheme. A BPSK modulation is adopted and the effect of various noise parameters are considered

Fig. 3.6 compares the BER performances of DT with SR scheme. The analytical BER for SR scheme is obtained using the formula in (3.33). For the simulation results, the following cases are considered: (i)- the destination has perfect knowledge about θ_m, which is utilized in the detection process using (3.43) and (ii)- when θ_m is not utilized by the destination, the LLR values are obtained using the first two terms of (3.43). From Fig. 3.6 it is seen that the

simulation result obtained in case (ii) perfectly matches the analytical result. In addition, our proposed optimal MAP decoder in case (i) showed better performance than in case (ii). It achieves a SNR gain of around 8 dB by exploiting θ_m at the destination. Also, SR scheme performs significantly better than DT under both cases. From Fig. 3.6 it is further verified that similar to SDFR, in case of SR, the optimal MAP receiver performs significantly better than the optimal memoryless receiver Huynh, K. Q. & Aulin, T. (2012) when both utilizes θ_m at the destination.

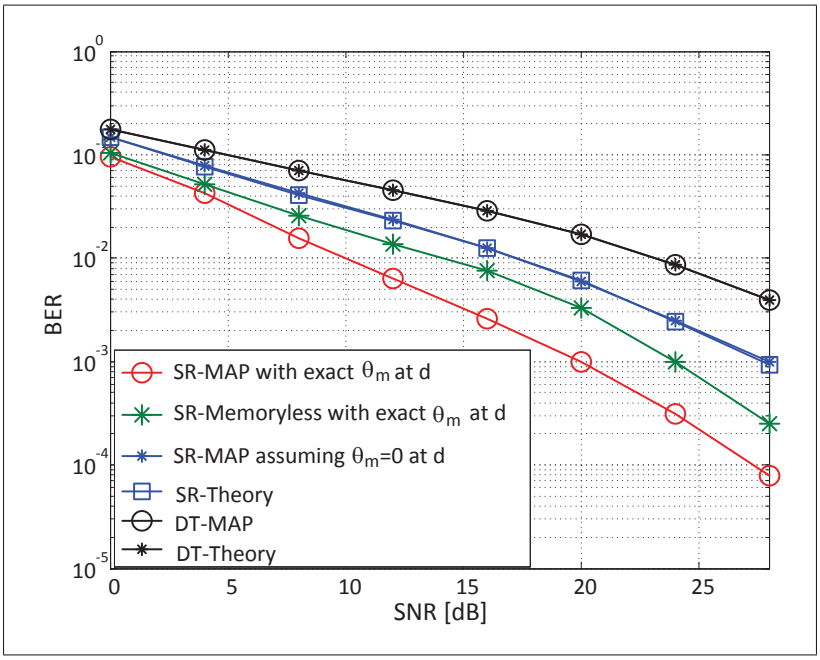

Figure 3.6 Analytical and simulated BER performances of direct transmission (DT) and simple relaying (SR) schemes against SNR with different realizations of θ_m at the destination. A BPSK modulation is adopted and each channel is characterized by $p_B = 0.1$, $\gamma = 100$, $R = 100$

Fig. 3.7 evaluates the analytical BER performances of selective DF cooperative communication system using (3.35) for different levels of threshold at the relay. As a performance benchmark, the performance of SR with optimal MAP receiver is also shown. From the numerical results, we observe that although in general SNR threshold-based selection relaying improves the BER

performance compared to the simple relaying, but by utilizing the BER of the relay at the destination, the proposed MAP receiver-based simple relaying performs better than the SNR-based selection relaying regardless of the value of threshold at the relay. This again confirms the benefit of exploiting θ_m at the destination.

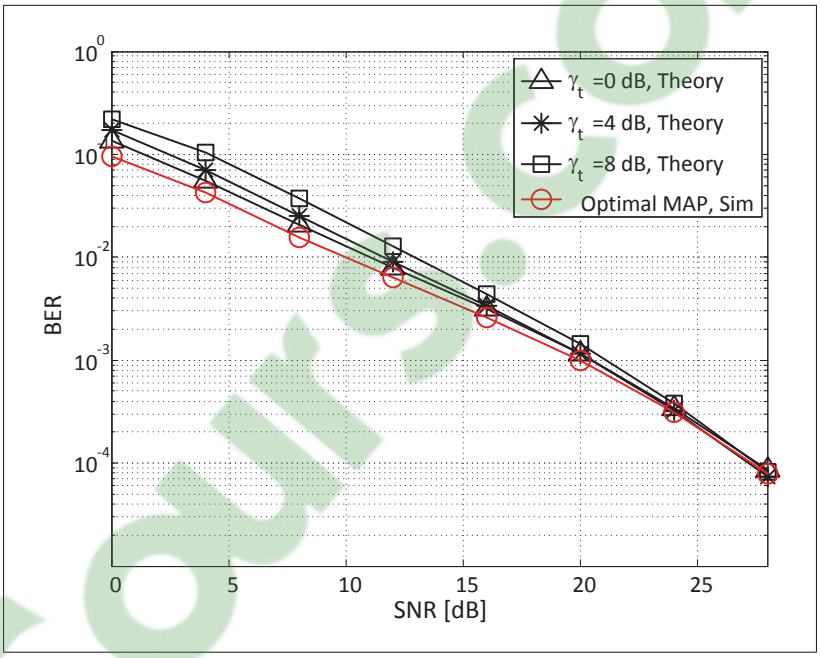

Figure 3.7 BER performances of threshold-based selection decode-and-forward relaying (SDFR) scheme with different values of threshold γ_t. A BPSK modulation is adopted and each channel is characterized by $p_B = 0.1$, $\gamma = 10$, $R = 10$

We also considered systems employing powerful channel codes such as low-density parity check (LDPC) codes. Fig. 3.8 shows the simulated BER performances of SDFR scheme for LDPC coded transmission assuming three different detectors at the receiver side. It is assumed that a sequence of equally likely information bits of length $32,400$ is first encoded using LDPC channel coding based on the DVB-S2 standard with the code rate of $1/2$. The coded sequence is then interleaved using a random interleaver and mapped onto BPSK modulation sequence, and then transmitted over two state Markov-Gaussian channels each of which is characterized by $p_B = 0.1$, $\gamma = 100$, and $R = 100$. For LDPC decoding at the relay as well as the destination,

the number of iterations is set to 50. As described earlier, the optimal MAP detector uses the MAP detection criterion, the memoryless detector is optimal for i.i.d. Bernoulli-Gaussian noise, and the AWGN detector is optimal for AWGN channel. As expected, from Fig. 3.8, it is observed that similar to uncoded transmission, significant performance gains are achieved when the noise memory is taken into account in the detection process. Indeed, in the BER range of 10^{-5}, the BER obtained with the memoryless receiver can be divided by almost 10^3 to get the BER with optimal MAP receiver.

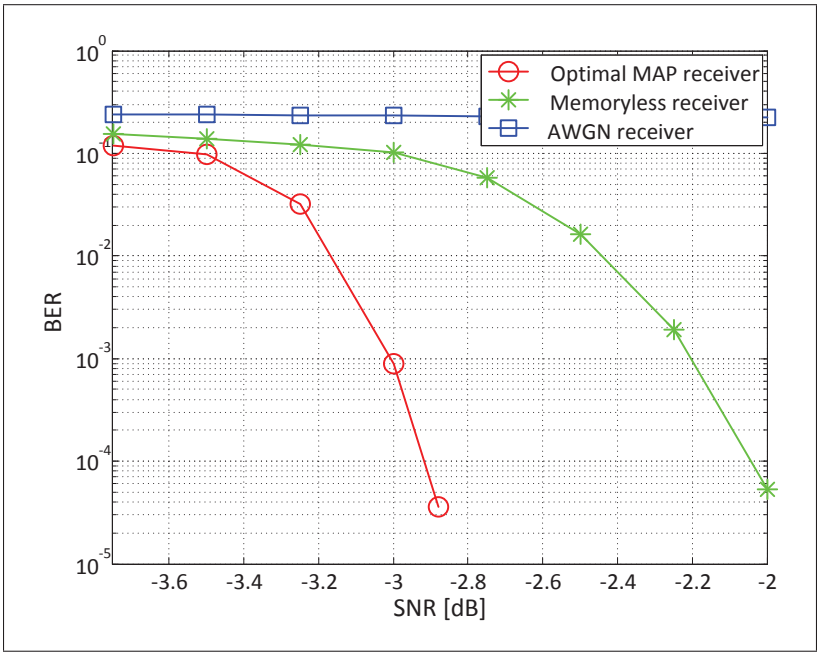

Figure 3.8 BER performances of coded selection decode-and-forward relaying (SDFR) scheme. A BPSK modulation is adopted and each channel is characterized by $p_B = 0.1$, $\gamma = 100$, $R = 100$

Fig. 3.9 also shows the performance of SR scheme with MAP receiver using the following two different realizations of θ_m at the destination in case of coded transmission: (i)- the destination has perfect knowledge about θ_m and is utilized in the detection process and, (ii)- θ_m is estimated at the destination with 10 percent estimation error for utilization. It is obvious from Fig. 3.9 that similar to SDFR, significant performance gains are achieved in SR scheme, when the noise

memory is taken into account in the detection process. Interestingly, the performance gain is practically the same, even if the destination does not have perfect knowledge about θ_m.

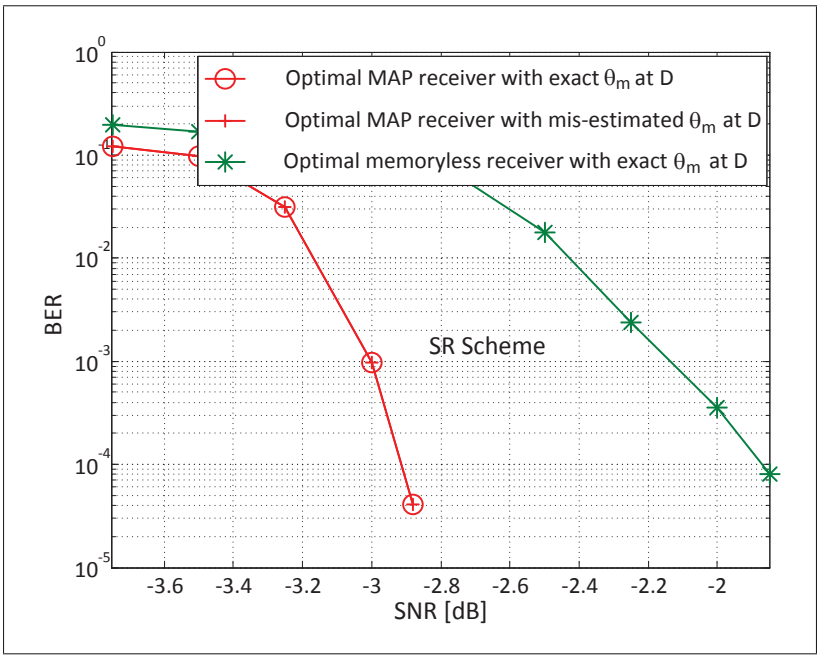

Figure 3.9 BER performances of coded simple relaying (SR) scheme assuming different realizations of θ_m at the destination. A BPSK modulation is adopted and each channel is characterized by $p_B = 0.1$, $\gamma = 100$, $R = 100$

So far, we have assumed BPSK modulation. Finally, we study the performances of DT and DF cooperative relaying schemes using Gray-coded Q-PSK modulation under both uncoded and coded scenario. We assume the same SNR for both BPSK and Q-PSK modulation schemes. The obtained results are shown in the figures from Fig. 3.10 - Fig. 3.12. From the obtained results it is seen that as in BPSK, the same arguments are hold for Q-PSK modulation scheme also, i.e., the analytical result matches well the simulation result. Also, the proposed MAP receiver attains the lower bound derived for DF CR scheme, and leads to large performance gains compared to the conventional receiving criteria which were optimized for additive white Gaussian noise (AWGN) channel and memoryless impulsive noise channel.

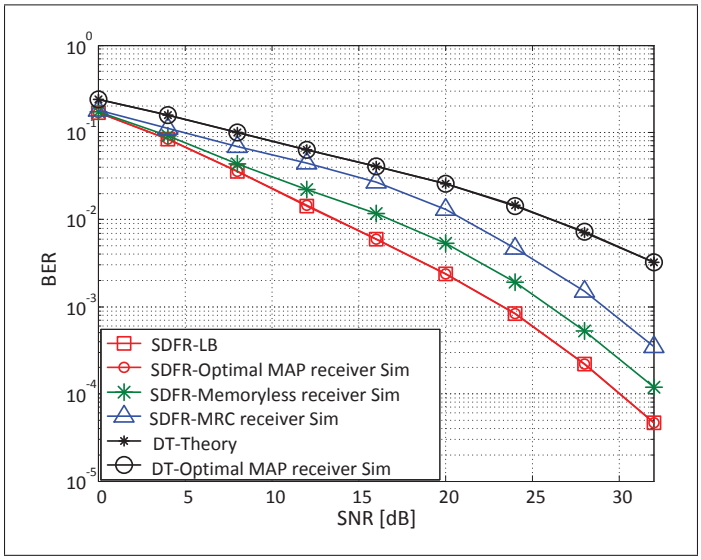

Figure 3.10 Analytical and simulated BER performances of direct transmission (DT) and selection decode-and-forward relaying (SDFR) schemes against SNR. A system employing a Q-PSK modulation is considered and the performance of various decoding schemes over two-state Markov-Gaussian channels, each characterized by $p_B = 0.1$, $\gamma = 100$, $R = 100$ is shown

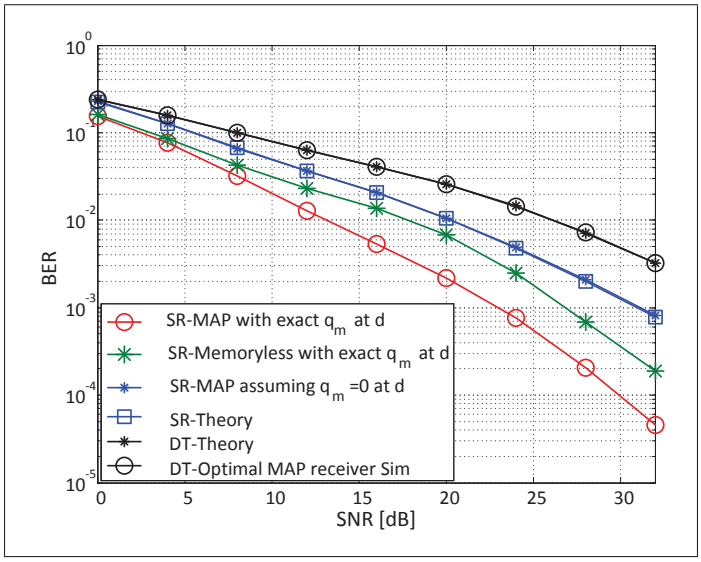

Figure 3.11 Analytical and simulated BER performances of direct transmission (DT) and simple relaying (SR) scheme against SNR with different realizations of q_m at the destination. A Q-PSK modulation is adopted and each channel is characterized by $p_B = 0.1$, $\gamma = 100$, $R = 100$

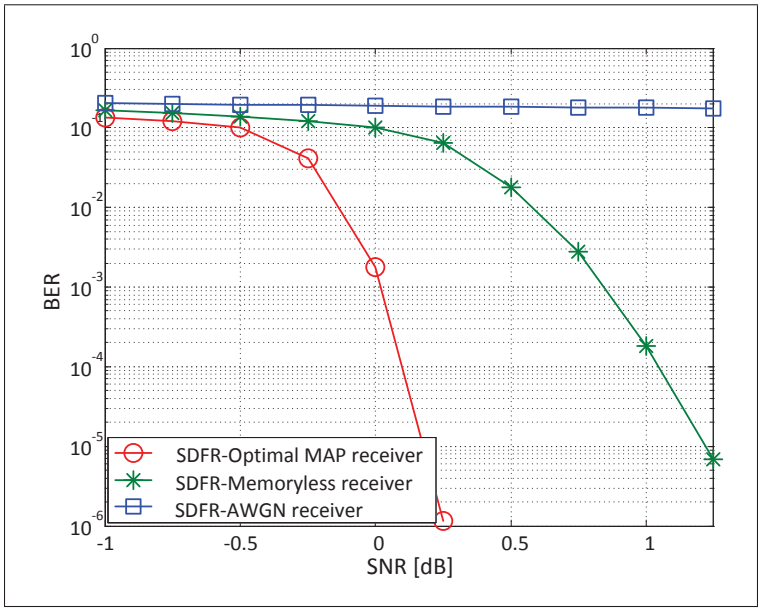

Figure 3.12 BER performances of coded selection decode-and-forward relaying (SDFR) scheme. A Q-PSK modulation is adopted and each channel is characterized by $p_B = 0.1$, $\gamma = 100$, $R = 100$

3.7 Conclusion

Cooperative relaying has been identified as a promising technology since last decade due to its reliability over fading and interference channels. In this article, we have presented the mathematical model to verify the analytical and simulated performances for DF CR schemes over time-correlated impulsive noise channel in the presence of Rayleigh fading. We also investigated the receiver structure at the destination for the proposed model. From the obtained results, it is observed that the analytical results agree with the simulations and our proposed MAP receiver achieves the lower bound derived for DF CR scheme, and performs significantly better than the conventional schemes developed for additive white Gaussian noise channel and memoryless impulsive noise channel. Also, DF CR scheme performs significantly better than DT under the same power consumption. Additionally, for simple relaying, the proposed MAP receiver achieves an SNR gain of around 8 dB by utilizing the relay-induced BER at the destination and attains similar performance as obtained through selective DF relaying.

CHAPTER 4

A NOVEL RELAY SELECTION STRATEGY OF COOPERATIVE NETWORK IMPAIRED BY BURSTY IMPULSIVE NOISE

Md Sahabul Alam [1], Georges Kaddoum[1], Basile L. Agba [2]

[1] Département de Génie Electrique, École de Technologie Supérieure,
1100 Notre-Dame Ouest, Montréal, Québec, Canada H3C 1K3
[2] Hydro-Quebec Research Institute (IREQ), Varennes, QC, Canada, J3X 1S1

Article published in IEEE Transactions on Vehicular Technology, May, 2019.

4.1 Abstract

Best relay selection (BRS) is crucial in enhancing the performance of cooperative networks. In contrast to most previous works, where the guidelines for BRS are limited to Gaussian noise, in this article, we propose a novel relay selection protocol for a decode-and-forward cooperative network taking into account the bursty impulsive noise (IN). The proposed protocol chooses the N'th best relay considering both the channel gains and the states of the IN of the source-relay and relay-destination links. For this scheme, to obtain the state of IN, we propose a state detection algorithm using maximum a posteriori (MAP) detection. To analyze the performance of the proposed protocol, we first derive closed-form expressions for the probability density function (PDF) of the received signal-to-noise ratio assuming all the relays know the state of IN perfectly (genie-condition). Then, these PDFs are used to derive closed-form expressions for the bit error rate (BER) and the outage probability. Finally, we also derive the asymptotic BER and outage expressions to quantify the diversity benefits. We show that the proposed MAP-based N'th BRS protocol attains the derived genie-aided analytical results and outperforms the conventional relay selection protocol, optimized for the Gaussian case, and which does not take into account the IN memory.

4.2 Introduction

For over a decade, cooperative relaying (CR) has been deemed efficient for reliable transmission over fading and interference channels Laneman & Wornell (2003); Laneman *et al.* (2004); Nosratinia *et al.* (2004). In addition to many other wireless applications, it is specially attractive for wireless sensor network applications, where the sensor nodes may not be able to afford multiple antennas, because of many constraints including their size, cost, power, etc. In particular, opportunistic relaying, where the BRS is performed between the available relays, is an efficient approach to improve the performance of CR as it makes efficient use of the system resources Bletsas, A., Khisti, A., Reed, D. P. & Lippman, A. (2006); Ibrahim, A. S., Sadek, A. K., Su, W. & Liu, K. R. (2008). Also, the system complexity and the synchronization requirements are relaxed through opportunistic relaying, compared to other CR schemes where all relays transmit simultaneously or sequentially over orthogonal channels Bletsas *et al.* (2006); Fareed & Uysal (2009); Ibrahim *et al.* (2008); Tourki, K., Yang, H.-C., Alouini, M.-S. & Qaraqe, K. A. (2013). Therefore, the techniques and analysis of BRS have received considerable attention in the literature.

In this regard, the authors in Bletsas *et al.* (2006) have proposed a BRS technique, where out of all the available relays, a subset of M relays, possessing error-free detection of the source transmission, are first selected. The best relay is then picked from the subset based on the minimum or the harmonic mean of the source-relay (SR) and relay-destination (RD) channel gains. It is shown that the proposed scheme exhibits the same performance as obtained in the case where all the relays transmit simultaneously through space-time coding Laneman & Wornell (2003). Ibrahim *et al.* Ibrahim *et al.* (2008) have introduced another BRS criterion where the best relay is the one that has the maximum value of the instantaneous scaled harmonic mean function of its SR and RD channel gains. The novelty of this protocol relies on the fact that the relay is not required to forward the source information if the direct link from the source to the destination is of high quality. Since a cooperation is not always taking place, this new scheme achieves higher bandwidth efficiency while the full diversity is guaranteed. Fareed *et al.* Fareed & Uysal (2009) have presented another BRS method, with a low implementation

complexity, requiring neither error detection methods at the relay nodes Bletsas *et al.* (2006) nor feedback information at the source Ibrahim *et al.* (2008). For this scheme, based on the minimum of the *SR* and *RD* links' signal-to-noise ratios (SNRs), the best relay is chosen at the destination node and it is permitted to transmit only if the minimum of its *SR* and *RD* links' SNRs is higher than the direct link SNR. Their obtained results demonstrate that the proposed error-prone BRS method is able to extract the full diversity. The authors in Tourki *et al.* (2013) have investigated an opportunistic regenerative relaying scheme, where similar to Fareed & Uysal (2009), it is assumed that there might be a possible error propagation. To determine the effect of erroneously detected data at the best relay, in their work, they have derived the exact statistics of each hop. Finally, their analyses have been validated through simulations. The authors in Ikki, S. S. & Ahmed, M. H. (2010) have considered the performance analysis of the N'th BRS scheme for both decode-and-forward (DF) and amplify-and-forward (AF) CR systems. Their obtained results show that for the special case where $N = 1$, the performance of this scheme coincides with the results available in the literature for the BRS under similar circumstances. The authors in Al-Badarneh, Y. H., Georghiades, C. N. & Alouini, M.-S. (2018) have generalized the asymptotic analysis of an N'th BRS problem using extreme value theory for various fading models commonly used to characterize wireless channels. Also, the selection of N'th best relay for cognitive DF relay networks and cooperative energy harvesting DF relay networks have been considered in Al-Badarneh, Y. H., Georghiades, C. N. & Alouini, M.-S. (2019); Zhang, X., Zhang, Y., Yan, Z., Xing, J. & Wang, W. (2015) and Zhang, J., Pan, G. & Xie, Y. (2018), respectively. The theory of order statistics David, H. A. & Nagaraja, H. N. (2003) has been considered as a powerful tool to analyze these performances.

Although instructive, all of the above performance analyses for BRS protocols have been carried out under the assumption of additive white Gaussian noise (AWGN) only. In practice, the noise characteristics usually observed in many environments are inherently impulsive Agba *et al.* (2019); Asiyo & Afullo (2017); Bai *et al.* (2017); Blackard *et al.* (1993); Cheffena (2012); Middleton (1977); Ndo *et al.* (2013); Sacuto *et al.* (2014); Shongwe *et al.* (2015); Zimmermann & Dostert (2002). For instance, in power substations, due to partial discharge

and switching effects, IN with a bursty behavior is generated from the substation equipment Agba *et al.* (2019); Ndo *et al.* (2013); Sacuto *et al.* (2014); Shongwe *et al.* (2015). In addition to substation environments, bursty impulsive noise is also observed in indoor wireless networks Blackard *et al.* (1993), industrial wireless sensor networks Cheffena (2012), power line communication (PLC) networks Asiyo & Afullo (2017); Zimmermann & Dostert (2002), and digital subscriber loop (DSL) networks Bai *et al.* (2017). This article is mainly motivated by this kind of situation where the noise exhibits significant bursty impulsive behavior. The performance of BRS protocols in IN and interference limited environments has barely been considered in the literature. The authors in Qian, Y., Li, J., Zhang, Y. & Jayakody, D. N. K. (2018) have considered the performance analysis of BRS for DF relay-based PLC systems. Although, Bernoulli-Gaussian model is considered to take into account the combined effects of background Gaussian noise and impulsive noise for deriving the cumulative distribution function (CDF) of the received SNR, the BRS is performed based on the standard *max-min* criterion optimized for AWGN channel and the effect of impulsive noise is not considered in the relay selection process. The extension of conventional optimal *max-min* BRS criterion for interference limited environments, in case of AF relaying strategy, has been investigated in Krikidis, I., Thompson, J. S., McLaughlin, S. & Goertz, N. (2009). It is shown that the conventional BRS criterion becomes inefficient under this scenario since the presence of interference modifies the *max-min* BRS statistics. While Krikidis *et al.* (2009) have considered various BRS protocols for CR in the presence of Gaussian interference, the authors in Ahmed, I., Nasri, A., Michalopoulos, D. S., Schober, R. & Mallik, R. K. (2012) have investigated the performance of the BRS and partial BRS protocols impaired by generic noise and interference. Through the derived asymptotic error rate expressions, it is apparent that in contrast to the Gaussian case, the performance of BRS in generic noise depends on the noise moments.

However, the analysis of Krikidis *et al.* (2009) and Ahmed *et al.* (2012) assume that the interfering signals are manifested throughout the transmission and lack the flexibility to deal with the presence or absence of IN and its bursty behavior. In this vein, the authors in Alam *et al.* (2016) have considered the performance analysis of a single-relay DF CR scheme over

Rayleigh faded bursty IN channels and have proposed an optimal receiver structure that utilizes the MAP detection criterion. It is shown that the performance of such channels improve with the utilization of noise memory at the receiver side through MAP detection, and converges to the derived lower bound: the ultimate performance limit of the same channel obtained under the assumption that perfect noise state information is available at the receiver. In Alam, M. S. & Labeau, F. (2016a), the performance of the single-relay scheme is extended to the multi-relay scenario where all the relays transmit sequentially over orthogonal channels Laneman *et al.* (2004). It is shown that as in Alam *et al.* (2016), the MAP receiver also achieves the lower bound drawn for the multi-relay DF CR scheme, and performs significantly better than the conventional schemes. The performance of BRS protocols in bursty IN environments have been investigated in Alam, M. S. & Labeau, F. (2016b). It is assumed that out of all the available M relays, a subset of N relays, not affected by IN are selected first and the best relay is chosen among them based on the optimal *max-min* criterion. Although, the scheme has shown to offer considerable performance improvement in comparison to the BRS strategy optimized for AWGN channels, we note that the achievable potential gain of that scheme is rather limited since the best relay is selected among a subset. In addition to that the analysis in Alam & Labeau (2016b) is limited to the BER performance only for the finite SNR and, since it is assumed that the selected relay is never affected by the IN, the paper used the available SNR PDFs for AWGN to derive the BER.

In this article, we investigate the performance of BRS protocols for a DF CR scheme over Rayleigh fading channels subject to bursty IN where BRS is performed among all the available relays. This work is an extension of Alam & Labeau (2016b). Here, in addition to BER, the analysis also includes outage probability and derive closed-form and asymptotic performances for the proposed scenario. To address the bursty behavior of IN samples, we consider a two-state Markov-Gaussian (TSMG) process Fertonani & Colavolpe (2009). A TSMG process is a simple and effective way to model the time-correlation among the noise samples Fertonani & Colavolpe (2009); Mitra & Lampe (2010). Also, we consider the realistic scenario of a *fixed DF CR* Fareed & Uysal (2009); Tourki *et al.* (2013), which does not require any error de-

tection and correction at the relay nodes and hence decoding errors might be propagated from the selected relay.

The contributions of this work are summarized as follows.

- We propose a novel relay selection protocol called *N*'th BRS, based on both the channel gains of the *SR* and *RD* links, and the states of IN affecting these links. To obtain the IN state, we propose a MAP-based state detection algorithm Bahl *et al.* (1974). The objective of considering MAP is to exploit the noise memory in the state detection process.

- To validate the performance of the proposed protocol, we derive novel closed-form expressions for the PDF of the received SNR at the selected relay and at the destination assuming all the relays know the state of IN perfectly (genie-condition). These PDFs are used to derive closed-form expressions for the BER using BPSK modulation and the outage probability.

- We further derive the asymptotic BER and outage expressions as these are useful for quick evaluation of the performance and quantify the achievable diversity order.

We show that the proposed MAP-based *N*'th BRS attains the derived analytical results for genie-condition and significantly outperforms the conventional relay selection protocol, optimized for AWGN environments, and which does not take into account the noise memory. In addition, it is revealed that, in the different SNR regions, the different relay selection protocols present different diversity orders under similar circumstances and the proposed MAP-based *N*'th BRS protocol achieves the full diversity order in high SNR regions.

The rest of the chapter is organized as follows: Section 4.3 introduces the system model. In Section 4.4, we provide an overview of the relay selection protocols. In Section 4.5 and 4.6, we provide the performance analysis of the proposed relay selection protocol in terms of BER and outage probability, respectively, and Section 4.7 derives the same performances for high SNR scenarios. Section 4.8 shows the numerical results and finally, Section 4.9 concludes this work.

4.3 System Model

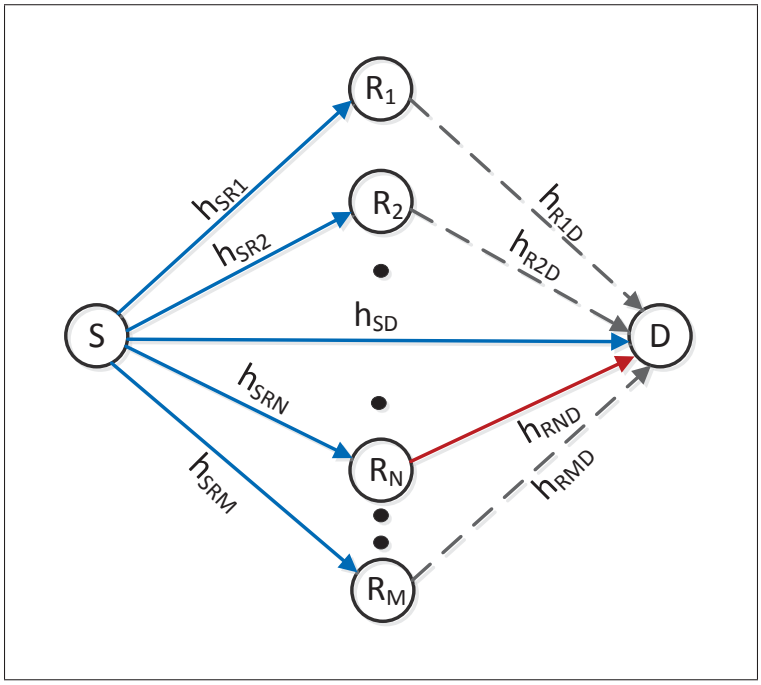

Figure 4.1 Illustration of the considered DF CR with the N'th best relay selection

We consider a DF cooperative network where M relays assist the data transmission between the source-destination (SD) pair, as shown in Fig 4.1. We assume that all node terminals have single transmit/receive antennas and share a single communication channel. Also, all nodes are assumed to operate in half-duplex mode. For CR, the transmission is organized in two-time slots. In the first-time slot, the source transmits the data to the destination and the relays. In the second-time slot, the relays form a competition (detailed in Section 4.4) and only the selected relay decodes the message received from the source and forwards it to the destination including possible errors. In our study, during this time, the source remains silent. The destination then combines the noisy sequences received from the source and the selected relay to recover the source information. Although the error propagation problem in this protocol could be resolved by incorporating cyclic redundancy check (CRC) at the relays, we note that this is bandwidth-consuming Wang *et al.* (2007) and, since CRC checking is usually performed at the MAC layer,

it induces excessive signaling overhead. To avoid this, we consider a more general case where there might be a decoding error propagation from the selected relay.

4.3.1 Signal Model

In the first-time slot of the considered CR system, the source S generates a binary information frame of size K $(b_0, b_1, \ldots, b_{K-1})$, mapped into a BPSK modulated sequence $(x_{S,0}, \ldots, x_{S,K-1})$, and broadcasted to the destination and M relay nodes. The signals received at relay R_m, $R_m \in \{R_1, R_2, \ldots, R_M\}$ and D at each time epoch k, $k = 0, 1, \ldots, K-1$ can be written, respectively, as

$$y_{SR_m,k} = \sqrt{P_S} h_{SR_m,k} x_{S,k} + n_{SR_m,k}, \tag{4.1}$$

$$y_{SD,k} = \sqrt{P_S} h_{SD,k} x_{S,k} + n_{SD,k}, \tag{4.2}$$

where P_S is the average source transmission power per symbol, $x_{S,k}$ is the transmitted symbol from S, $h_{ij,k}$ is the ij link channel coefficient, $i \in (S, R_m)$ and $j \in (R_m, D)$, and $n_{ij,k}$ is the associated noise term. In this article, the destination is assumed to be affected by AWGN only, while the relays are subject to impulsive interference. This refers to the scenario where the sensor nodes acting as relays are located in the field of application generating the IN while the destination is the remote monitoring centre located in the far field. We assume that the channel coefficients of each ij link follow a Rayleigh distribution and are static for one symbol duration, while they vary from one symbol to another. Therefore, $h_{ij,k}$ is modeled as a zero-mean, independent, circularly symmetric complex Gaussian (CSCG) random variable with variance $\Omega_{ij} \equiv \mathrm{E}\{|h_{ij}|^2\} = 1/\lambda_{ij}^{\eta}$, where $\mathrm{E}\{\cdot\}$ denotes expectation operator, λ_{ij} is the relative distance from i to j, and η is the path loss exponent Laneman *et al.* (2004). It is also assumed that the noise sample $n_{SR_m,k}$ follows the TSMG process that we will detail in the following subsection. We further assume that both the noise samples and the channel coefficients for each link are statistically independent. Unless otherwise explicitly mentioned, the instantaneous SNR of the ij link is given by $\gamma_{ij} = P_i |h_{ij}|^2 / \sigma_G^2$, where σ_G^2 represents the variance of the background Gaussian noise. The corresponding average SNR is given by $\overline{\gamma}_{ij} = P_i \Omega_{ij} / \sigma_G^2$.

In the second time slot, the N'th best relay R_N demodulates the received signal y_{SR_N} to recover the source information. Then, R_N modulates the recovered signal using BPSK modulation and forwards it to the destination. The signal received at the destination node is therefore given by

$$y_{R_ND,k} = \sqrt{P_N} h_{R_ND,k} x_{R_N,k} + n_{R_ND,k}, \tag{4.3}$$

where P_N is the average relay transmission power and $x_{R_N,k}$ is the forwarded symbol from R_N which may be different from $x_{S,k}$ due to the possibility of decoding errors at the relay.

4.3.2 Noise Model

For a TSMG model, at each k, the statistical behavior of $n_{SR_m,k}$ is fully described by the noise state $s_{m,k} \in \{G,B\}$. In the context of our noise modeling, G is referred to as the good state and B as the bad state. The motivation of considering such a noise model stems from the fact that the good state happens when the channel is impaired by AWGN only, while the bad state takes place when this latter is subject to impulsive interference. For each SR_m link, we model $n_{SR_m,k}$ as a zero-mean, independent, CSCG random variable, so that conditioned on $s_{m,k}$, the PDF of $n_{SR_m,k}$ can be expressed as

$$f(n_{SR_m,k}|s_{m,k} = t) = \frac{1}{\pi\sigma_t^2} \exp\left(-\frac{|n_{SR_m,k}|^2}{\sigma_t^2}\right), \quad t \in (G,B). \tag{4.4}$$

Moreover, the parameter $\rho = \sigma_B^2/\sigma_G^2$ specifies the impulsive to Gaussian noise power ratio. The statistical description of the state process $\mathbf{s}_m^K = \{s_{m,0}, s_{m,1}, \ldots, s_{m,K-1}\}$ completely describes the channel and can be evaluated by the state transition probabilities $p_{s_{m,k}s_{m,k+1}} = p(s_{m,k+1}|s_{m,k})$, $s_{m,k}, s_{m,k+1} \in \{G,B\}$. Given these transition probabilities, the stationary probability p_G of being in the good state and p_B of being in the bad state are respectively given by Fertonani & Colavolpe (2009),

$$p_G = \frac{p_{BG}}{p_{GB} + p_{BG}} \quad \text{and} \quad p_B = \frac{p_{GB}}{p_{GB} + p_{BG}}. \tag{4.5}$$

It is worth mentioning that the parameter $\mu = \frac{1}{p_{GB}+p_{BG}}$ characterizes the noise memory and $\mu > 1$ represents a channel that has a persistent memory.

4.4 Relay Selection Protocols

4.4.1 Conventional Best Relay Selection Protocol

As customary in the literature, for conventional BRS protocol, the best relay R_b from the available M relays is selected according to the following rule

$$R_b = \arg \max_{m \in \{1,2,\ldots,M\}} \left\{ \min \left\{ |h_{SR_m}|^2, |h_{R_m D}|^2 \right\} \right\}. \tag{4.6}$$

This *max-min* BRS criterion establishes a tight upper bound in terms of end-to-end SNR Bletsas *et al.* (2006). Although this strategy exhibits the optimal performance for Gaussian environments, it may become inefficient in the presence of bursty IN since this *max-min* BRS criterion relies on the channel statistics only and does not take into account the IN behavior when selecting the relay. Therefore, in the following section, we will propose a relay selection protocol for opportunistic relaying in the presence of bursty IN. The proposed protocol can be regarded as an extension of the conventional BRS protocol.

4.4.2 Proposed Relay Selection Protocol in the Presence of Bursty Impulsive Noise

In this section, we focus on investigating the BRS in the presence of bursty IN. Since the conventional optimal BRS criterion cannot exploit the IN behavior, it may incur large performance degradation in the presence of strong interference at the relays. Hence, definite changes are required to the *max-min* criterion to adapt to IN environments. On the other hand, if there is any way for each relay to know the state of the IN, the relay selection could be performed, based on the combined effect of the channel quality and the impulsive behavior. Given the IN state information, the conventional *max-min* relay selection criterion can be extended to achieve the optimal performance. In this vein, from the implementation perspective, we assume that each

relay has the ability to locally perform a noise state detection test at each time slot to determine whether it is affected by Gaussian noise or by impulsive state. When this state information is available at all the relays, a rational selection strategy would be as follows. First, rank ($r_{m,k}$) each relay (R_m) at time epoch k according to the conventional *max-min* criterion with the channel gain ordered in a non-increasing fashion. The relay R_m in the first position of the ordered vector will be the best relay ($r_{m,k} = M$, full rank), the relay in the second position will be the second-best relay and so on. Then, the very next step is to check the state of the noise that affects the best relay. If the best relay is affected by impulsive state, try the second-best relay and so on. We termed this N**'th best relay selection** strategy for the proposed scenario. Finally, when all the relays are affected by impulsive state, choose the best relay that is in the impulsive state and has the bottleneck channel quality confirmed by (4.6). The received SNR at each relay under this condition becomes $\gamma^B_{SR_m} = \gamma_{SR_m}/\rho$. Hence, the conventional *max-min* BRS criterion in (4.6) gives us

$$R_b^B = \arg \max_{m \in \{1,2,\ldots,M\}} \left\{ \min \left\{ \gamma_{SR_m}/\rho, \gamma_{R_m D} \right\} \right\}. \tag{4.7}$$

This new BRS criterion is very much dependent on the value of ρ and for $\rho >> 1$, it is highly likely that $\min\{\gamma_{SR_m}/\rho, \gamma_{R_m D}\}$ yields γ_{SR_m}/ρ. Thus, the BRS criterion in (4.7) can be modified as

$$R_b^B | \rho >> 1 = \arg \max_{m \in \{1,2,\ldots,M\}} \left(\gamma_{SR_m}/\rho \right). \tag{4.8}$$

The selection criterion in (4.8) is known as the partial BRS protocol Krikidis *et al.* (2009). This is because this latter is dependent on the channel quality for the *SR* link only and not on the end-to-end channel gains. It is shown in Krikidis *et al.* (2009) that this partial relay selection criterion poses the best performance from an asymptotic point of view.

The end-to-end steps of the proposed N'th BRS protocol are shown in Fig 4.2. As a consequence, in the following subsections, we detail different state detection algorithms to study the impact of the noise state information explicitly in the relay selection process.

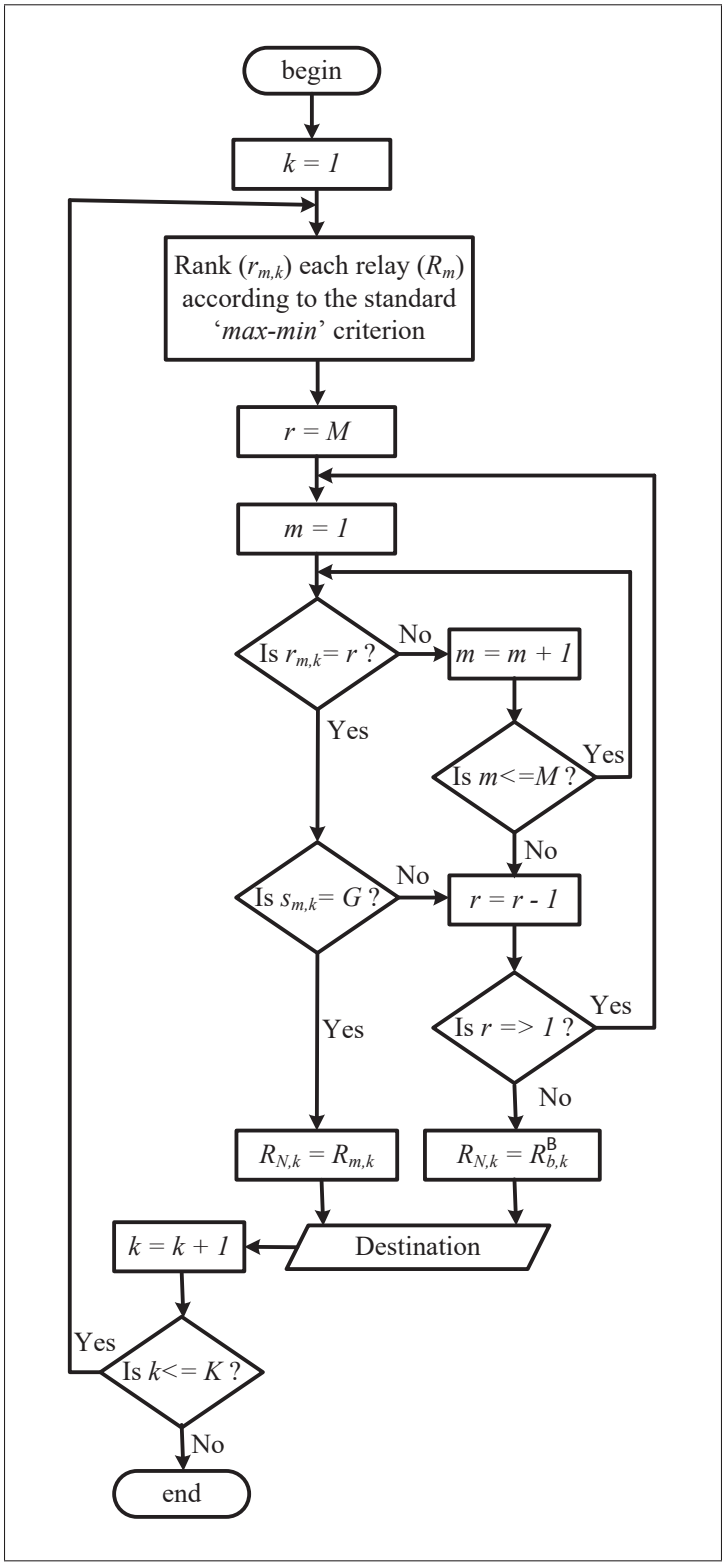

Figure 4.2 Flow diagram of the proposed *N*'th BRS protocol in the presence of bursty impulsive noise

4.4.2.1 Genie detection

Genie detection assumes that all the available relays have exact knowledge of the noise state. Although, this approach allows us to provide a tight limit of the best achievable performance, we observe that it is only conceptually valuable and the implementation of this detector is a very challenging task, if not impractical. In what follows, to reach the achievable performance, we propose some algorithms to obtain the states of IN.

4.4.2.2 Proposed MAP based state detection algorithm

To know the state of IN, in this scheme, at each k, each relay evaluates the a posteriori probability $p(s_{m,k}|y_{SR_m}^K)$ that the state $s_{m,k}$ is the actual channel state of relay R_m at k, given the received sequence $y_{SR_m}^K = \{y_{SR_m,0}, y_{SR_m,1}, \ldots, y_{SR_m,K-1}\}$. This can be evaluated as

$$p\left(s_{m,k}|y_{SR_m}^K\right) \propto p\left(s_{m,k}, y_{SR_m}^K\right). \tag{4.9}$$

Let us define the following quantities

$$\begin{aligned}
\alpha_k(s_{m,k}) &= p\left(y_{SR_m,0}, y_{SR_m,1}, \ldots, y_{SR_m,k-1}, s_{m,k}\right), && (4.10)\\
\beta_k(s_{m,k}) &= p\left(y_{SR_m,k}, y_{SR_m,k+1}, \ldots, y_{SR_m,K-1}|s_{m,k}\right), && (4.11)\\
\delta_k(x_{S,k}, s_{m,k}, s_{m,k+1}) &= p\left(s_{m,k+1}|s_{m,k}\right)p\left(n_{SR_m,k}|s_{m,k}\right), && (4.12)
\end{aligned}$$

where $\alpha_k(s_{m,k})$, $\beta_k(s_{m,k})$, and $\delta_k(x_{S,k}, s_{m,k}, s_{m,k+1})$ represent the forward filter, backward filter, and branch metrics of the trellis diagram, respectively, as shown in Fig. 4.3. For the TSMG model, $p(n_{SR_m,k}|s_{m,k})$ in (4.12) can be evaluated using (4.4). Then, from (4.10) and (4.11), $p(s_{m,k}, y_{SR_m}^K)$ in (4.9) can be expressed as

$$p(s_{m,k}, y_{SR_m}^K) = \alpha_k(s_{m,k})\beta_k(s_{m,k}). \tag{4.13}$$

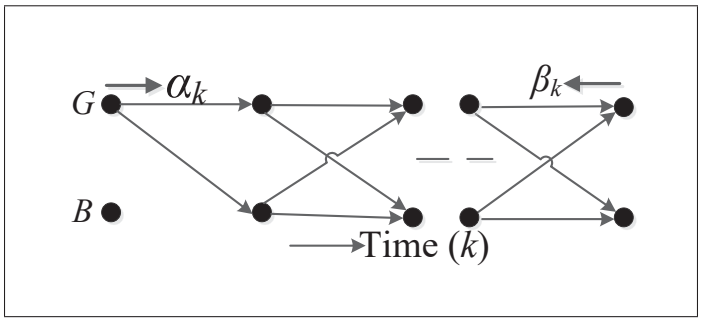

Figure 4.3 Trellis diagram for the representation of the TSMG noise model

Therefore, the state of the IN can be obtained as

$$\hat{s}_{m,k} = \begin{cases} G & \text{if } L_{s_{m,k}} \geq 0 \\ B & \text{if } L_{s_{m,k}} < 0 \end{cases} \tag{4.14}$$

where, $\hat{s}_{m,k}$ represents the estimate of $s_{m,k}$ (hard decision) and $L_{s_{m,k}}$ is the log-likelihood ratio (LLR). For this, the LLR values at the relays can be computed by

$$L_{s_{m,k}} = \ln \left\{ \frac{\alpha_k(s_{m,k} = G)\beta_k(s_{m,k} = G)}{\alpha_k(s_{m,k} = B)\beta_k(s_{m,k} = B)} \right\}. \tag{4.15}$$

Accordingly, the algorithm computes the forward and backward filters recursively as

$$\alpha_{k+1}(s_{m,k+1}) = \sum_{s_{m,k}, x_{S,k}} \alpha_k(s_{m,k}) p(x_{S,k}) \delta_k(x_{S,k}, s_{m,k}, s_{m,k+1}), \tag{4.16}$$

$$\beta_k(s_{m,k}) = \sum_{s_{m,k+1}, x_{S,k}} \beta_{k+1}(s_{m,k+1}) p(x_{S,k}) \delta_k(x_{S,k}, s_{m,k}, s_{m,k+1}), \tag{4.17}$$

where we initialize the forward and backward filters as $\alpha_0(s_{m,0} = s) = p_s$ and $\beta_K(s_{m,K} = s) = 1$, $s \in \{G, B\}$.

4.4.2.3 Memoryless state detection

Here, we consider a state detection algorithm known as memoryless state detection. Even though, this scheme is aware of the IN state, it cannot take into account the inherent noise

memory. In this case, it is assumed that $\mu = 1$ in the noise state detection process, which reflects the Bernoulli-Gaussian noise Ghosh (1996) instead of TSMG noise. In this scenario, the previous MAP-based state detection algorithm is simplified to a sample-by-sample algorithm and the probability of being in a state will depend on $p(s_{m,k}|y_{SR_m,k})$, given by

$$p(s_{m,k}|y_{SR_m,k}) \propto p(s_{m,k}, y_{SR_m,k}), \tag{4.18}$$

$$= p(s_{m,k}) \sum_{x_{S,k}} p(n_{SR_m,k}|s_{m,k}) p(x_{S,k}). \tag{4.19}$$

Then, the LLR values at each relay can be obtained from

$$L_{s_{m,k}} = \ln \left\{ \frac{p_G \sum_{x_{S,k}} p(n_{SR_m,k}|s_{m,k} = G) p(x_{S,k})}{p_B \sum_{x_{S,k}} p(n_{SR_m,k}|s_{m,k} = B) p(x_{S,k})} \right\}. \tag{4.20}$$

From the LLR values, every relay then determines the noise states using (4.14).

Although implementation related details are not our primary concern, in our scheme, the best relay can be selected either at the destination node in a centralized manner, or this selection can be performed distributively amongst the relays. For the first scheme, the channel state information (CSIs) of each SR and RD links, and the state of the impulsive noise of each SR links are required at the destination node. Similar to Fareed & Uysal (2009), it can be assumed that the destination node has the knowledge of h_{SR_m} and h_{R_mD} at the end of the first time slot. However, it is worth mentioning that the proposed scheme also needs to transmit the noise state information from the relays to the destination. The destination then prepares a ranking table of all the relays based on this information and chooses the best relay depending on the ranking information. Hence, an increase of signalling overhead is unavoidable for relay selection in impulsive environments.

For the implementation of a distributed scheme, similar to Bletsas *et al.* (2006), it is assumed that the relay nodes monitor the instantaneous channel conditions toward the source and the destination, and decide in a distributed fashion which one has the strongest path for information relaying. The best relay then checks its noise state information. When the best relay determines

that it is in the impulsive state, it sends a beacon signal and the second best relay will check its impulsive state. The process continues until an interference free best relay is selected or to the point where all the relays are affected by impulsive state.

4.4.3 Random Relay Selection Protocol

In contrast to the previous relay selection protocols, for this protocol, one relay is picked randomly from all the available relays. This is suitable for simple scenario since its implementation neither requires the channel statistics nor the IN states and will probably show the worst performance.

4.4.4 Complexity Discussion

It is worth pointing out that, despite the performance increase, the complexity of the proposed MAP-based relay selection scheme grows exponentially with the frame length, due to the execution of the forward-backward algorithm, while it grows linearly in case of symbol-by-symbol selection schemes Fertonani, D., Barbieri, A. & Colavolpe, G. (2007). For example, the complexity of MAP selection for an M-ary modulation system is $O(M^K)$, where K is the frame length. On the other hand, the complexity of the symbol-by-symbol selection schemes are $O(K)$. However, in Section 4.8 we show that the complexity of the MAP-based relay selection scheme is justified by its potential performance gain, making it a potential candidate for reliable communication scenarios. Hence, the proposed relay selection algorithm exhibits a performance/complexity trade-off.

4.5 BER Performance Analysis

In this section, we derive the BER expression of the proposed relay selection scheme under independent and identically distributed (i.i.d.) Rayleigh fading and bursty IN assuming that all the relays have perfect knowledge of IN state (genie-condition). We first consider the scenario where the selected relay is in good state. Since we assume that error can be propagated from

the selected relay, the end-to-end error probability under this consideration can be expressed as

$$P_{e,D}(N) = P_{e,R_N} \cdot P^{er}_{e,SR_ND} + (1 - P_{e,R_N}) \cdot P^{ner}_{e,SR_ND}, \tag{4.21}$$

where P_{e,R_N} is the error probability at the N'th best relay, P^{er}_{e,SR_ND} is the destination error probability when an error is propagated from the N'th best relay, and P^{ner}_{e,SR_ND} is the error probability at the destination when there is no error propagation from the N'th best relay.

Meanwhile, when all the relays are considered to be affected by IN, the system is forced to choose a best relay (R^B_b) that is in the impulsive state and has the bottleneck channel quality confirmed by (4.8). The overall BER performance will therefore be governed by the probability for which each of the selected relays transmits in either the good state or the bad state. For example, the first best relay will transmit in the good state with probability $(1 - p_B)$ and the second best relay will transmit with probability $p_B(1 - p_B)$ and so on. Finally, the probability of having all the available relays in bad state is p^M_B. The overall error probability at the destination is therefore given by

$$P_{e,D} = \sum_{N=1}^{M} (1 - p_B) p_B^{N-1} P_{e,D}(N) + p_B^M P^B_{e,D}. \tag{4.22}$$

where $P^B_{e,D}$ is the destination error probability when all the relays are in bad state. As discussed, the first and second terms in (4.22) represent respectively the overall probability of error at the destination when the selected relay is either in good state or in bad state.

4.5.1 Calculation of $P_{e,D}(N)$

4.5.1.1 BER analysis at the N'th best relay

The PDF of the received SNR from the source to the N'th best relay γ_{SR_N} can be obtained by

$$\begin{aligned} f_{\gamma_{SR_N}}(x) &= \frac{C_M}{\overline{\gamma}_{R_mD}} \sum_{k=0}^{M-N} \binom{M-N}{k} (-1)^k \frac{\overline{\gamma}_a}{(k+N)\overline{\gamma}_{SR_m} - \overline{\gamma}_a} \left(e^{-x/\overline{\gamma}_{SR_m}} - e^{-x(k+N)/\overline{\gamma}_a} \right) \\ &\quad + \frac{C_M}{\overline{\gamma}_{SR_m}} \sum_{k=0}^{M-N} \binom{M-N}{k} (-1)^k e^{-x(k+N)/\overline{\gamma}_a}, \end{aligned} \tag{4.23}$$

where $C_M = M\binom{M-1}{N-1}$ and $\overline{\gamma}_a = \frac{\overline{\gamma}_{SR_m}\overline{\gamma}_{R_mD}}{\overline{\gamma}_{SR_m}+\overline{\gamma}_{R_mD}}$.

Proof: The joint PDF of the N'th order statistics, $X_{(N)} = f_{\gamma_{SR_N}\gamma_{R_ND}}$ can be written as David & Nagaraja (2003); Papoulis, A. & Pillai, S. U. (2002)

$$f_{\gamma_{SR_N}\gamma_{R_ND}}(x,z) = \begin{cases} M\binom{M-1}{N-1} f_{\gamma_{SR_m}}(x) f_{\gamma_{R_mD}}(z) \left[F_{\gamma_a}(x)\right]^{M-N} \left[1-F_{\gamma_a}(x)\right]^{N-1}; & \text{if } x < z \\ M\binom{M-1}{N-1} f_{\gamma_{SR_m}}(x) f_{\gamma_{R_mD}}(z) \left[F_{\gamma_a}(z)\right]^{M-N} \left[1-F_{\gamma_a}(z)\right]^{N-1}; & \text{if } x > z \end{cases} \tag{4.24}$$

where $F(x)$ is the CDF of $f(x)$. For Rayleigh fading channel, (4.24) can be rewritten as

$$f_{\gamma_{SR_N}\gamma_{R_ND}}(x,z) = \begin{cases} M\binom{M-1}{N-1} \frac{1}{\overline{\gamma}_{SR_m}} e^{-\frac{x}{\overline{\gamma}_{SR_m}}} \frac{1}{\overline{\gamma}_{R_mD}} e^{-\frac{z}{\overline{\gamma}_{R_mD}}} \left[1-e^{-\frac{x}{\overline{\gamma}_a}}\right]^{M-N} \left[e^{-\frac{x}{\overline{\gamma}_a}}\right]^{N-1}; & \text{if } x < z; \\ M\binom{M-1}{N-1} \frac{1}{\overline{\gamma}_{SR_m}} e^{-\frac{x}{\overline{\gamma}_{SR_m}}} \frac{1}{\overline{\gamma}_{R_mD}} e^{-\frac{z}{\overline{\gamma}_{R_mD}}} \left[1-e^{-\frac{z}{\overline{\gamma}_a}}\right]^{M-N} \left[e^{-\frac{z}{\overline{\gamma}_a}}\right]^{N-1}; & \text{if } x > z \end{cases} \tag{4.25}$$

Now, from the joint distribution, the marginal distribution of γ_{SR_N} can be obtained as

$$f_{\gamma_{SR_N}}(x) = \int_{z=0}^{\infty} f_{\gamma_{SR_N}\gamma_{R_ND}}(x,z)dz, \tag{4.26}$$

Substituting (4.25) in (4.26), we get

$$\begin{aligned} f_{\gamma_{SR_N}}(x) &= \int_{z=0}^{x} M\binom{M-1}{N-1} \frac{1}{\overline{\gamma}_{SR_m}} e^{-\frac{x}{\overline{\gamma}_{SR_m}}} \frac{1}{\overline{\gamma}_{R_mD}} e^{-\frac{z}{\overline{\gamma}_{R_mD}}} \left[1-e^{-\frac{z}{\overline{\gamma}_a}}\right]^{M-N} \left[e^{-\frac{z}{\overline{\gamma}_a}}\right]^{N-1} dz \\ &+ \int_{z=x}^{\infty} M\binom{M-1}{N-1} \frac{1}{\overline{\gamma}_{SR_m}} e^{-\frac{x}{\overline{\gamma}_{SR_m}}} \frac{1}{\overline{\gamma}_{R_mD}} e^{-\frac{z}{\overline{\gamma}_{R_mD}}} \left[1-e^{-\frac{x}{\overline{\gamma}_a}}\right]^{M-N} \left[e^{-\frac{x}{\overline{\gamma}_a}}\right]^{N-1} dz, \\ &= I_1 + I_2. \end{aligned} \tag{4.27}$$

Then, using the binomial expansion, I_1 in (4.27) can be written as

$$I_1 = \frac{M\binom{M-1}{N-1}}{\overline{\gamma}_{SR_m}\overline{\gamma}_{R_mD}} e^{-\frac{x}{\overline{\gamma}_{SR_m}}} \int_{z=0}^{x} e^{-\frac{z}{\overline{\gamma}_{R_mD}}} \sum_{k=0}^{M-N} \binom{M-N}{k} (-1)^k e^{-\frac{(k+N-1)z}{\overline{\gamma}_a}} dz, \tag{4.28}$$

Solving the integration and after some mathematical manipulations, (4.28) can be written as

$$I_1 = \frac{M\binom{M-1}{N-1}}{\overline{\gamma}_{R_mD}} \sum_{k=0}^{M-N} \binom{M-N}{k} (-1)^k \frac{\overline{\gamma}_a}{(k+N)\overline{\gamma}_{SR_m} - \overline{\gamma}_a} \left(e^{-x/\overline{\gamma}_{SR_m}} - e^{-x(k+N)/\overline{\gamma}_a}\right). \tag{4.29}$$

In a similar way, I_2 can be written as

$$\begin{aligned} I_2 &= \frac{M\binom{M-1}{N-1}}{\overline{\gamma}_{SR_m}\overline{\gamma}_{R_mD}} e^{-\frac{x}{\overline{\gamma}_{SR_m}}} \sum_{k=0}^{M-N} \binom{M-N}{k} (-1)^k e^{-\frac{x(k+(N-1))}{\overline{\gamma}_a}} \int_{z=x}^{\infty} e^{-\frac{z}{\overline{\gamma}_{R_mD}}} dz, \\ &= \frac{M\binom{M-1}{N-1}}{\overline{\gamma}_{SR_m}} \sum_{k=0}^{M-N} \binom{M-N}{k} (-1)^k e^{-\frac{x(k+N)}{\overline{\gamma}_a}}. \end{aligned} \tag{4.30}$$

Substituting the value of (4.29) and (4.30) in (4.27), (4.23) is obtained. Therefore, the error probability of the source to the selected relay link can be obtained by Proakis (2001)

$$P_{e,R_N} = \frac{1}{2}\int_0^{\infty} \text{erfc}(\sqrt{x}) f_{\gamma_{SR_N}}(x) dx, \tag{4.31}$$

where $f_{\gamma_{SR_N}}$ is provided in (4.23) and $\text{erfc}(\cdot)$ is the complementary error function. Solving the integral in (4.31) yields

$$\begin{aligned} P_{e,R_N} &= \frac{C_M}{\overline{\gamma}_{R_mD}} \sum_{k=0}^{M-N} \binom{M-N}{k} (-1)^k \frac{\overline{\gamma}_a}{(k+N)\overline{\gamma}_{SR_m} - \overline{\gamma}_a} \left[\omega\left(\frac{1}{\overline{\gamma}_{SR_m}}\right) - \omega\left(\frac{k+N}{\overline{\gamma}_a}\right) \right] \\ &\quad + \frac{C_M}{\overline{\gamma}_{SR_m}} \sum_{k=0}^{M-N} \binom{M-N}{k} (-1)^k \omega\left(\frac{k+N}{\overline{\gamma}_a}\right). \end{aligned} \tag{4.32}$$

To get (4.32), we use the identity $\omega(\theta) = \frac{1}{2\theta}\left[1 - \frac{1}{\sqrt{1+\theta}}\right]$.

4.5.1.2 BER analysis at the destination

In order to compute P^{er}_{e,SR_ND} and P^{ner}_{e,SR_ND}, we need the knowledge of the combining technique considered at the destination. For Gaussian channel, the maximum ratio combining (MRC) is optimal with regard to minimizing the BER Proakis (2001). At this stage, since the selected N'th best relay is not affected by IN, we can perform MRC at the destination. The combined SNR at the destination, γ_{SR_ND}, is then the sum of two independent SNRs γ_{SD} and γ_{R_ND} with

corresponding PDFs $f_{\gamma_{SD}}$ and $f_{\gamma_{R_ND}}$. Similar to (4.23), the PDF of γ_{R_ND} is given by

$$\begin{aligned} f_{\gamma_{R_ND}}(x) &= \frac{C_M}{\overline{\gamma}_{SR_m}} \sum_{k=0}^{M-N} \binom{M-N}{k} (-1)^k \frac{\overline{\gamma}_a}{(k+N)\overline{\gamma}_{R_mD} - \overline{\gamma}_a} \left(e^{-x/\overline{\gamma}_{R_mD}} - e^{-x(k+N)/\overline{\gamma}_a} \right) \\ &\quad + \frac{C_M}{\overline{\gamma}_{R_mD}} \sum_{k=0}^{M-N} \binom{M-N}{k} (-1)^k e^{-x(k+N)/\overline{\gamma}_a}, \end{aligned} \tag{4.33}$$

Also, the PDF of $f_{\gamma_{SD}}$ is

$$f_{\gamma_{SD}}(y) = \frac{1}{\overline{\gamma}_{SD}} e^{-y/\overline{\gamma}_{SD}}, \tag{4.34}$$

Therefore, the PDF of $\gamma_{SR_ND} = \gamma_{SD} + \gamma_{R_ND}$ can be obtained by the well-known convolution theorem as

$$f_{\gamma_{SR_ND}}(\theta) = \int_0^\theta f_{\gamma_{R_ND}}(z) f_{\gamma_{SD}}(\theta - z) dz, \tag{4.35}$$

which is expressed as

$$\begin{aligned} f_{\gamma_{SR_ND}}(\theta) &= \frac{C_M}{\overline{\gamma}_{SR_m}} \sum_{k=0}^{M-N} \binom{M-N}{k} (-1)^k \frac{\overline{\gamma}_a}{(k+N)\overline{\gamma}_{R_mD} - \overline{\gamma}_a} \\ &\quad \times \left[\frac{\overline{\gamma}_{R_mD}}{\overline{\gamma}_{SD} - \overline{\gamma}_{R_mD}} \left(e^{-\theta/\overline{\gamma}_{SD}} - e^{-\theta/\overline{\gamma}_{R_mD}} \right) - \frac{\overline{\gamma}_a}{(k+N)\overline{\gamma}_{SD} - \overline{\gamma}_a} \left(e^{-\theta/\overline{\gamma}_{SD}} - e^{-(k+N)\theta/\overline{\gamma}_a} \right) \right] \\ &\quad + \frac{C_M}{\overline{\gamma}_{R_mD}} \sum_{k=0}^{M-N} \binom{M-N}{k} (-1)^k \frac{\overline{\gamma}_a}{(k+N)\overline{\gamma}_{SD} - \overline{\gamma}_a} \left(e^{-\theta/\overline{\gamma}_{SD}} - e^{-(k+N)\theta/\overline{\gamma}_a} \right). \end{aligned} \tag{4.36}$$

Then, the error probability of the combined path assuming there is no error propagated from the selected relay is obtained by

$$P_{e,SR_ND}^{ner} = \frac{1}{2} \int_0^\infty \operatorname{erfc}(\sqrt{\theta}) f_{\gamma_{SR_ND}}(\theta) d\theta, \tag{4.37}$$

which is obtained as

$$\begin{aligned} P_{e,SR_ND}^{ner} &= \frac{C_M}{\overline{\gamma}_{SR_m}} \sum_{k=0}^{M-N} \binom{M-N}{k} (-1)^k \frac{\overline{\gamma}_a}{(k+N)\overline{\gamma}_{R_mD} - \overline{\gamma}_a} \\ &\quad \times \left[\frac{\overline{\gamma}_{R_mD}}{\overline{\gamma}_{SD} - \overline{\gamma}_{R_mD}} \left(\omega\left(\frac{1}{\overline{\gamma}_{SD}}\right) - \omega\left(\frac{1}{\overline{\gamma}_{R_mD}}\right) \right) - \frac{\overline{\gamma}_a}{(k+N)\overline{\gamma}_{SD} - \overline{\gamma}_a} \left(\omega\left(\frac{1}{\overline{\gamma}_{SD}}\right) - \omega\left(\frac{k+N}{\overline{\gamma}_a}\right) \right) \right] \\ &\quad + \frac{C_M}{\overline{\gamma}_{R_mD}} \sum_{k=0}^{M-N} \binom{M-N}{k} (-1)^k \frac{\overline{\gamma}_a}{(k+N)\overline{\gamma}_{SD} - \overline{\gamma}_a} \left(\omega\left(\frac{1}{\overline{\gamma}_{SD}}\right) - \omega\left(\frac{k+N}{\overline{\gamma}_a}\right) \right). \end{aligned} \tag{4.38}$$

From (4.21), it is seen that we also need the expression of P^{er}_{e,SR_ND}, which can be tightly approximated for the considered BPSK modulated system as Tourki *et al.* (2013)

$$P^{er}_{e,SR_ND} \approx \frac{\overline{\gamma}_{R_ND}}{\overline{\gamma}_{R_ND} + \overline{\gamma}_{SD}}, \tag{4.39}$$

where $\overline{\gamma}_{R_ND}$ is the expected value of γ_{R_ND} and is given by

$$\overline{\gamma}_{R_ND} = \int_0^\infty \gamma_{R_ND}(z) f_{\gamma_{R_ND}}(z) dz, \tag{4.40}$$

So, from (4.40) and (4.33), $\overline{\gamma}_{R_ND}$ is obtained as

$$\begin{aligned} \overline{\gamma}_{R_ND} &= \frac{C_M}{\overline{\gamma}_{SR_m}} \sum_{k=0}^{M-N} \binom{M-N}{k} (-1)^k \frac{\overline{\gamma}_a}{(k+N)\overline{\gamma}_{R_mD} - \overline{\gamma}_a} \left[\overline{\gamma}^2_{R_mD} - \left(\frac{\overline{\gamma}_a}{k+N} \right)^2 \right] \\ &+ \frac{C_M}{\overline{\gamma}_{R_mD}} \sum_{k=0}^{M-N} \binom{M-N}{k} (-1)^k \left(\frac{\overline{\gamma}_a}{k+N} \right)^2. \end{aligned} \tag{4.41}$$

Therefore, the end-to-end error probability under the N'th BRS strategy when the selected relay is in good state can be evaluated by substituting (4.32), (4.38), and (4.39) in (4.21).

4.5.2 Calculation of $P^B_{e,D}$

Similar to (4.21), the end-to-end probability of error when the selected relay is in bad state can be expressed as

$$P^B_{e,D} = P_{e,R^B_b} \cdot P^{er}_{e,SR^B_bD} + (1 - P_{e,R^B_b}) \cdot P^{ner}_{e,SR^B_bD}, \tag{4.42}$$

Now, the PDF of the received SNR from the source to the best relay $\gamma^B_{SR^B_b}$ under this condition can be expressed as Papoulis & Pillai (2002)

$$\begin{aligned} f_{\gamma^B_{SR^B_b}}(y) &= M F^{M-1}_x(y) f_x(y), \\ &= M \left(1 - e^{-y/\overline{\gamma}^B_{SR_m}} \right)^{M-1} \frac{1}{\overline{\gamma}^B_{SR_m}} e^{-y/\overline{\gamma}^B_{SR_m}}, \end{aligned} \tag{4.43}$$

Using the Binomial expansion, (4.43) can be expressed as

$$f_{\gamma^B_{SR^B_b}}(y) = \frac{M}{\bar{\gamma}^B_{SR_m}} \sum_{k=0}^{M-1} \binom{M-1}{k} (-1)^k e^{-ky/\bar{\gamma}^B_{SR_m}}. \tag{4.44}$$

Therefore, the error probability at the selected relay can be obtained as

$$P_{e,R^B_b} = \frac{M}{\bar{\gamma}^B_{SR_m}} \sum_{k=0}^{M-1} \binom{M-1}{k} (-1)^k \omega\left(\frac{k}{\bar{\gamma}^B_{SR_m}}\right). \tag{4.45}$$

Now, the BER at the destination can be obtained according to (4.42). It is assumed that the combining at the destination is based on MRC. Hence, P^{ner}_{e,SR^B_bD} is the BER of a two-branch MRC receiver. For i.i.d. Rayleigh channels, this is given as Proakis (2001)

$$P^{ner}_{e,SR^B_bD} = \frac{1}{2}\left(\frac{\tau(\bar{\gamma}_{SD})}{1-\bar{\gamma}_{R^B_bD}/\bar{\gamma}_{SD}} + \frac{\tau(\bar{\gamma}_{R^B_bD})}{1-\bar{\gamma}_{SD}/\bar{\gamma}_{R^B_bD}}\right), \tag{4.46}$$

where $\tau(\bar{\gamma}) = 1 - \sqrt{\frac{\bar{\gamma}}{1+\bar{\gamma}}}$ and $\bar{\gamma}_{R^B_bD} = \bar{\gamma}_{R_mD}$, since the second phase is independent of the relay selection process. In addition, similar to (4.39), the error probability P^{er}_{e,SR^B_bD}, under this condition can be approximated by

$$P^{er}_{e,SR^B_bD} \approx \frac{\overline{\gamma}_{R_mD}}{\overline{\gamma}_{R_mD} + \overline{\gamma}_{SD}}. \tag{4.47}$$

Finally, substituting (4.45), (4.46), and (4.47) in (4.42) $P^B_{e,D}$ can be obtained.

4.6 Outage analysis

The end-to-end outage probability of the proposed scheme for a data rate R when the selected relay in good state is given by Tourki *et al.* (2013)

$$P_{out}(N) = p\{\gamma_{SR_N} > \phi, \gamma_{R_ND} + \gamma_{SD} < \phi\} + p\{\gamma_{SR_N} < \phi\}\, p\{\gamma_{SD} < \phi\}, \tag{4.48}$$

where $\phi = 2^{2R} - 1$. Therefore, the overall outage probability at the destination is given by

$$P_{out} = \sum_{N=1}^{M} (1-p_B) p_B^{N-1} P_{out}(N) + p_B^M P^B_{out}. \tag{4.49}$$

where P_{out}^{B} is the outage probability at the destination when all the M relays are in bad state and therefore the selected relay is in bad state as well.

4.6.1 Calculation of $P_{out}(N)$

Now, the outage probability at the N'th best relay is obtained by

$$\begin{aligned} P_{out,SR_N} &= \int_0^{\phi} f_{\gamma_{SR_N}}(x)dx \equiv F_{\gamma_{SR_N}}(\phi), \\ &= \frac{C_M}{\overline{\gamma}_{R_mD}} \sum_{k=0}^{M-N} \binom{M-N}{k} (-1)^k \frac{\overline{\gamma}_a}{(k+N)\overline{\gamma}_{SR_m} - \overline{\gamma}_a} \left[\chi_{\overline{\gamma}_{SR_m}}(\phi) - \chi_{\frac{\overline{\gamma}_a}{k+N}}(\phi) \right] \\ &\quad + \frac{C_M}{\overline{\gamma}_{SR_m}} \sum_{k=0}^{M-N} \binom{M-N}{k} (-1)^k \chi_{\frac{\overline{\gamma}_a}{k+N}}(\phi), \end{aligned} \tag{4.50}$$

where $F_{\gamma_{SR_N}}(x)$ is the CDF of $\gamma_{SR_N}(x)$ shown in (4.23) and $\chi_a(x) = a\left(1 - e^{-x/a}\right)$. Similarly, the outage probability for the SD link becomes

$$P_{out,SD} = F_{\gamma_{SD}}(\phi) = \frac{\chi_{\overline{\gamma}_{SD}}(\phi)}{\overline{\gamma}_{SD}}, \tag{4.51}$$

On the other hand, the first term in (4.48) can be approximated as Tourki *et al.* (2013)

$$p\{\gamma_{SR_N} > \phi, \gamma_{R_ND} + \gamma_{SD} < \phi\} \approx \left(1 - F_{\gamma_{SR_N}}(\phi)\right) F_{\gamma_{SR_ND}}(\phi), \tag{4.52}$$

where $F_{\gamma_{SR_N}}(\phi)$ can be derived according to (4.50). Also, the outage probability for the SR_ND link can be obtained by taking the CDF of (4.36) yielding

$$\begin{aligned} P_{out,SR_ND} &= \frac{C_M}{\overline{\gamma}_{SR_m}} \sum_{k=0}^{M-N} \binom{M-N}{k} (-1)^k \frac{\overline{\gamma}_a}{(k+N)\overline{\gamma}_{R_mD} - \overline{\gamma}_a} \\ &\quad \times \left[\frac{\overline{\gamma}_{R_mD}}{\overline{\gamma}_{SD} - \overline{\gamma}_{R_mD}} \left(\chi_{\overline{\gamma}_{SD}}(\phi) - \chi_{\overline{\gamma}_{R_mD}}(\phi) \right) - \frac{\overline{\gamma}_a}{(k+N)\overline{\gamma}_{SD} - \overline{\gamma}_a} \left(\chi_{\overline{\gamma}_{SD}}(\phi) - \chi_{\frac{\overline{\gamma}_a}{k+N}}(\phi) \right) \right] \\ &\quad + \frac{C_M}{\overline{\gamma}_{R_mD}} \sum_{k=0}^{M-N} \binom{M-N}{k} (-1)^k \frac{\overline{\gamma}_a}{(k+N)\overline{\gamma}_{SD} - \overline{\gamma}_a} \left(\chi_{\overline{\gamma}_{SD}}(\phi) - \chi_{\frac{\overline{\gamma}_a}{k+N}}(\phi) \right). \end{aligned} \tag{4.53}$$

Hence, the end-to-end outage probability when the selected relay is in good state can be evaluated by substituting (4.50), (4.51), and (4.53) in (4.48).

4.6.2 Calculation of P_{out}^{B}

Similar to (4.48), the end-to-end outage probability when the selected relay is in bad state can be obtained by

$$P_{out}^{B} = P_{out,SR_b^B} \cdot P_{out,SD} + (1 - P_{out,SR_b^B}) \cdot P_{out,SR_b^B D}, \tag{4.54}$$

where P_{out,SR_b^B} can be obtained by taking the CDF of (4.44) yielding

$$P_{out,SR_b^B} = \frac{M}{\overline{\gamma}_{SR_m}^{B}} \sum_{k=0}^{M-1} \binom{M-1}{k} (-1)^k \chi_{\overline{\gamma}_{SR_m}^{B}}(k\phi). \tag{4.55}$$

Moreover, the outage probability $P_{out,SR_b^B D}$ at the destination under this condition can be obtained as Goldsmith (2005)

$$P_{out,SR_b^B D} = \frac{1}{2} \frac{\chi_{\overline{\gamma}_{SD}}(\phi)\, \chi_{\overline{\gamma}_{R_m D}}(\phi)}{\overline{\gamma}_{SD}\overline{\gamma}_{R_m D}}. \tag{4.56}$$

Finally, substituting (4.55), (4.56), and (4.51) in (4.54), P_{out}^{B} can be evaluated.

4.7 Asymptotic analysis

To provide more insights on the system behavior, we here reformulate the asymptotic BER and outage analysis for the proposed relay selection scheme. This allows us to validate the simulation results in high SNR regions.

4.7.1 Asymptotic BER analysis

4.7.1.1 Asymptotic equivalence of P_{e,R_N}

We show in Appendix I that the asymptotic PDF of γ_{SR_N} can be expressed as

$$f_{\gamma_{SR_N}}(x) \doteq M \binom{M-1}{N-1} \frac{1}{\overline{\gamma}_{SR_m}} \left(\frac{1}{\overline{\gamma}_a}\right)^{M-N} x^{M-N}, \tag{4.57}$$

where $\doteq$ denotes the asymptotic equality.

Then, the probability of error for the source to the selected relay link can be derived according to (4.31) and becomes

$$P_{e,R_N} \doteq M\binom{M-1}{N-1}\frac{1}{\overline{\gamma}_{SR_m}}\left(\frac{1}{\overline{\gamma}_a}\right)^{M-N}\frac{\Gamma(M-N+3/2)}{2\sqrt{\pi}(M-N+1)}, \tag{4.58}$$

where $\Gamma(\cdot)$ is the complete Gamma function. To get the closed-form expression in (4.58), we use the following identities

$$\text{erfc}(z) = \frac{\Gamma(1/2,z^2)}{\sqrt{\pi}}, \text{ and } \int_0^\infty x^{a-1}\Gamma(b,x)dx = \frac{\Gamma(a+b)}{a}. \tag{4.59}$$

4.7.1.2 Asymptotic equivalence of P^{ner}_{e,SR_ND} and P^{er}_{e,SR_ND}

To obtain the asymptotic end-to-end BER at the destination according to (4.21), we also need the asymptotic equivalence of P^{er}_{e,SR_ND} and P^{ner}_{e,SR_ND} which further requires the asymptotic PDF of γ_{R_ND} and γ_{SR_ND}. Similar to (4.57), the PDF of γ_{R_ND} is given by

$$f_{\gamma_{R_ND}}(z) \doteq M\binom{M-1}{N-1}\frac{1}{\overline{\gamma}_{R_mD}}\left(\frac{1}{\overline{\gamma}_a}\right)^{M-N} z^{M-N}. \tag{4.60}$$

Therefore, the PDF of γ_{SR_ND} can be obtained according to the convolution theorem depicted in (4.35) as

$$f_{\gamma_{SR_ND}}(\theta) \doteq M\binom{M-1}{N-1}\frac{1}{\overline{\gamma}_{R_mD}}\left(\frac{1}{\overline{\gamma}_a}\right)^{M-N}\frac{1}{\overline{\gamma}_{SD}}e^{-\theta/\overline{\gamma}_{SD}}\int_0^\theta z^{M-N}e^{z/\overline{\gamma}_{SD}}dz, \tag{4.61}$$

Integrating by parts and following some mathematical manipulations, (4.61) can be approximated as

$$f_{\gamma_{SR_ND}}(\theta) \approx \frac{M\binom{M-1}{N-1}}{(M-N+1)}\frac{1}{\overline{\gamma}_{R_mD}}\left(\frac{1}{\overline{\gamma}_a}\right)^{M-N}\frac{\theta^{M-N+1}}{\overline{\gamma}_{SD}}. \tag{4.62}$$

Then, the error probability of the combined path when there is no error propagation from the selected relay is obtained by

$$\begin{aligned} P^{ner}_{e,SR_ND} &= \frac{1}{2}\int_0^\infty \text{erfc}(\sqrt{\theta})f_{\gamma_{SR_ND}}(\theta)d\theta, & (4.63)\\ &\doteq \frac{M\binom{M-1}{N-1}}{2\sqrt{\pi}(M-N+1)}\frac{1}{\overline{\gamma}_{R_mD}}\left(\frac{1}{\overline{\gamma}_a}\right)^{M-N}\frac{1}{\overline{\gamma}_{SD}}\frac{\Gamma(M-N+5/2)}{M-N+2}. & (4.64)\end{aligned}$$

On the other hand, P^{er}_{e,SR_ND} can be derived according to (4.39), where $\overline{\gamma}_{R_ND}$ can be obtained as

$$\overline{\gamma}_{R_ND} = \int_0^\infty \gamma_{R_ND}(z) f_{\gamma_{R_ND}}(z) dz, \tag{4.65}$$

So, from (4.65) and (4.60), we have

$$\begin{aligned} \overline{\gamma}_{R_ND} &\doteq M\binom{M-1}{N-1}\frac{1}{\overline{\gamma}_{R_mD}}\left(\frac{1}{\overline{\gamma}_a}\right)^{M-N}\int_0^\infty z^{M-N+1}e^{-z/\overline{\gamma}_a}dz, \\ &= M\binom{M-1}{N-1}\frac{1}{\overline{\gamma}_{R_mD}}\overline{\gamma}_a^2\Gamma(M-N+2). \end{aligned} \tag{4.66}$$

Therefore, the asymptotic end-to-end error probability under the assumption that the N'th best relay is in good state can be evaluated by substituting (4.58), (4.64), and (4.39) in (4.21).

4.7.1.3 Asymptotic equivalence of $P^B_{e,D}$

From (4.43), the asymptotic PDF of $\gamma^B_{SR^B_b}$ can be expressed as

$$f_{\gamma^B_{SR^B_b}}(y) \doteq M\left(\frac{1}{\overline{\gamma}^B_{SR_m}}\right)^M y^{M-1}. \tag{4.67}$$

Therefore, the probability of error at the selected relay under this condition can be obtained by

$$P_{e,SR^B_b} \doteq \frac{1}{2\sqrt{\pi}}\left(\frac{1}{\overline{\gamma}^B_{SR_m}}\right)^M \Gamma(M+1/2). \tag{4.68}$$

On the other hand, the values of P^{ner}_{e,SR^B_bD} and P^{er}_{e,SR^B_bD} can be obtained according to (4.46) and (4.47), respectively. Finally, substituting the value of (4.68), (4.46), and (4.47) in (4.42) the asymptotic expression of $P^B_{e,D}$ can be obtained.

4.7.2 Asymptotic Outage Analysis

4.7.2.1 Asymptotic equivalence of $P_{out}(N)$

The asymptotic outage probability at the N'th best relay is obtained by

$$\begin{aligned} P_{out,SR_N} &= \int_0^{\phi} f_{\gamma_{SR_N}}(x)dx \equiv F_{\gamma_{SR_N}}(\phi), \\ &\doteq M\binom{M-1}{N-1}\frac{1}{\overline{\gamma}_{SR_m}}\left(\frac{1}{\overline{\gamma}_a}\right)^{M-N}\frac{\phi^{M-N+1}}{M-N+1}. \end{aligned} \tag{4.69}$$

Similarly, the outage probability for the SD link becomes

$$P_{out,SD} = F_{\gamma_{SD}}(\phi) \doteq \frac{\phi}{\overline{\gamma}_{SD}}. \tag{4.70}$$

Also, the outage probability for the SR_ND link can be obtained from the joint distribution derived in (4.62) as

$$P_{out,SR_ND} \doteq \frac{M\binom{M-1}{N-1}}{M-N+1}\frac{1}{\overline{\gamma}_{R_mD}}\left(\frac{1}{\overline{\gamma}_a}\right)^{M-N}\frac{1}{\overline{\gamma}_{SD}}\frac{\phi^{M-N+2}}{M-N+2}. \tag{4.71}$$

Hence, the end-to-end outage probability can be evaluated by substituting (4.69), (4.70), and (4.71) in (4.48) and becomes

$$P_{out}(N) \doteq \frac{M\binom{M-1}{N-1}}{M-N+1}\frac{1}{\overline{\gamma}_{SD}}\left(\frac{1}{\overline{\gamma}_a}\right)^{M-N}\phi^{M-N+2}\left[\frac{1}{M-N+2}\frac{1}{\overline{\gamma}_{R_mD}}+\frac{1}{\overline{\gamma}_{SR_m}}\right]. \tag{4.72}$$

4.7.2.2 Asymptotic equivalence of P_{out}^B

The asymptotic equivalence of P_{out}^B can be obtained according to (4.54), where the outage probability at the selected relay can be achieved by taking the CDF of (4.67) and is equal to

$$P_{out,SR_b^B} \doteq \left(\frac{\phi}{\overline{\gamma}^B_{SR_m}}\right)^M. \tag{4.73}$$

Moreover, the outage probability P_{out,SR_b^BD} at the destination under this condition can be approximated as Goldsmith (2005)

$$P_{out,SR_b^BD} \doteq \frac{1}{\overline{\gamma}_{SD}} \frac{1}{\overline{\gamma}_{R_mD}} \left(\frac{\phi^2}{2} \right). \tag{4.74}$$

From (4.72), we observe that the maximum achievable diversity order converges to $M-N+2$. Hence, the proposed N'th BRS scheme will achieve the full diversity order of $M+1$ when $N=1$, i.e., the proposed protocol chooses the first best relay for cooperation.

4.8 Numerical results

In this section, we simulate the BER and the outage performances of the proposed DF relay selection schemes to validate the theoretical results presented in Section 4.5, 4.6, and 4.7. In our simulations, it is assumed that a frame of $10,000$ bits is mapped to a BPSK modulation sequence. It is then transmitted over Rayleigh quasi-static flat fading channels where the received sequence at the relays are impaired by TSMG noise characterized by $p_B = 0.01$, $\mu = 100$, and $\rho = 100$ for each link. In this model, the N'th BRS is performed among a total number of $M = 5$ relays and equal transmission power is considered at both the source and the selected relay. Moreover, we assume that $\lambda_{SD} = 1$ and $\lambda_{SR_m} = 0.4, \forall m$, where the relays are uniformly distributed between the SD pair. The BER and the outage performances are calculated as a function of SNR which is defined as, $SNR = E\{|x_{S,k}|^2 |h_{ij}|^2\}/\sigma_G^2$. Furthermore, we assume that the the noise parameters $(p_B, \mu, \rho, \sigma_G^2)$ and the channel coefficients h_{ij} are perfectly known at the receiver. Finally, we set the path loss exponent to $\eta = 2$.

Fig. 4.4 depicts both the analytical and simulated BER performance at the selected relay, assuming different relay selection protocols. The derived BER expression in (4.32) is used to evaluate the exact analytical result and its asymptotic performance is evaluated using (4.58). The simulated BER performances are obtained by averaging the error rate over 10^5 frames with 10^4 samples for every frame. Fig. 4.4 shows that the simulation results for the genie-aided selection perfectly match the analytical results. Also, the derived asymptotic error rate

expression accurately predicts the performance for sufficiently high SNR. However, the genie detection is practically infeasible. Interestingly, we also remark that the performance of the proposed N'th BRS scheme, employing MAP-detection, almost approaches the genie-aided case and provides a significant performance gain over the other schemes. Obviously, this comes at the cost of higher complexity required for the implementation of the forward-backward algorithm. Hence, when the noise memory is exploited in the relay selection process through MAP detection, we achieve a significant performance gain. Finally, the proposed simpler memoryless algorithm still exhibits a better performance than conventional BRS schemes, by taking into account the partial IN statistics in the selection process.

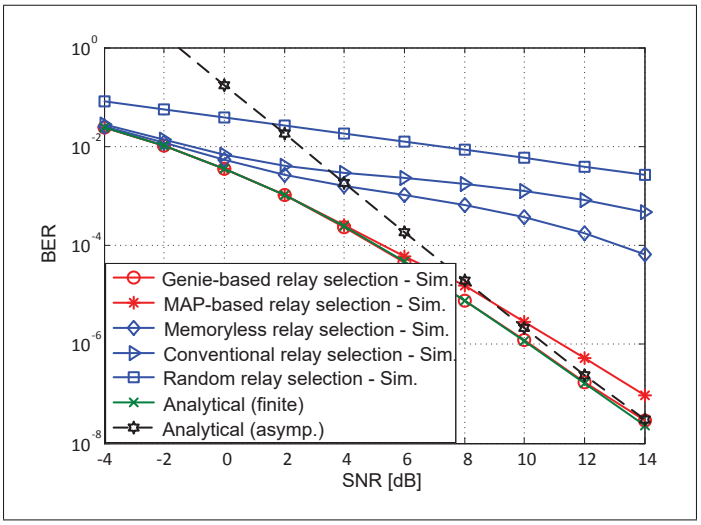

Figure 4.4 BER performances at the N'th best relay for various relay selection schemes with $M = 5$ relays over Rayleigh faded TSMG channels. A system involving an uncoded transmission and a BPSK modulation is considered

Fig. 4.5 shows the end-to-end analytical and simulated BER performances for the proposed scenario. The analytical BERs are evaluated using (4.21) and (4.42), respectively for both cases of when the selected relay is in good state or in bad state. As a benchmark, we also include the performance of direct transmission (DT) over Rayleigh faded AWGN channel. From Fig. 4.5, we observe that, the end-to-end analytical BER corresponds to the simulation

results for genie selection and its asymptotic performance reflects the exact performance for sufficiently high SNR. This further confirms that the proposed MAP-based N'th BRS scheme efficiently decreases the effects of IN which significantly improves the system performance compared to conventional schemes. Moreover, even when subjected to IN, CR outperforms DT irrespective of the relay selection process, however, the amount of improvement depends on the process.

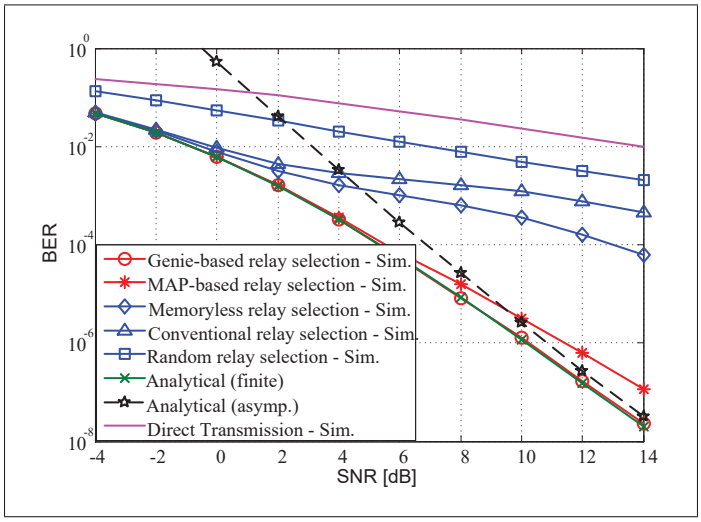

Figure 4.5 End-to-end BER performances of various N'th BRS schemes with $M = 5$ relays over Rayleigh faded TSMG channels. A system involving an uncoded transmission and a BPSK modulation is considered

To circumvent the burden of obtaining the time-consuming simulation results in the BER range of $10^{-8} - 10^{-10}$, Fig. 4.6 illustrates the analytical BER performances only. From Fig. 4.6, it is obvious that the asymptotic performance truly reflects the finite SNR BER performance for sufficiently high SNR. Therefore, we can check the diversity order of each relay selection scheme by taking the slope of BER performances shown in Fig. 4.5 Al-Dharrab & Uysal (2009a). It is verified that the obtained diversity orders of MAP-based, memoryless, conventional, and random relay selection schemes are respectively, 5.9, 3.85, 3.3, and 2.9. Hence, the proposed MAP-based N'th BRS scheme achieves the full diversity order.

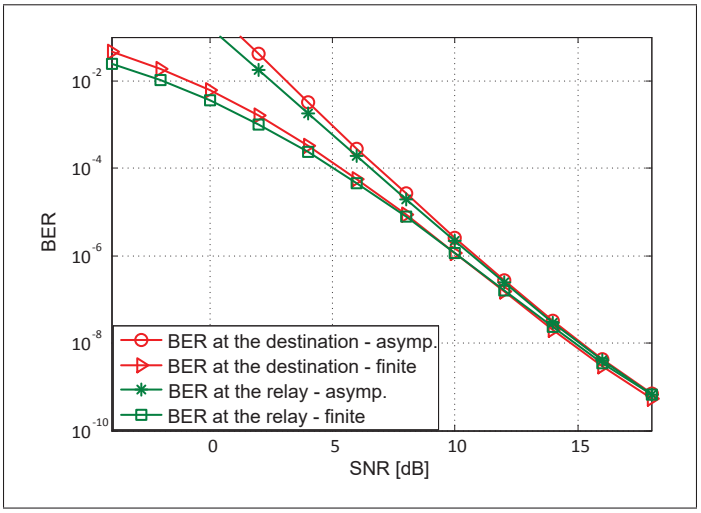

Figure 4.6 Analytical asymptotic and finite BER performances at the N'th best relay and at the destination with $M = 5$ relays over Rayleigh faded TSMG channels

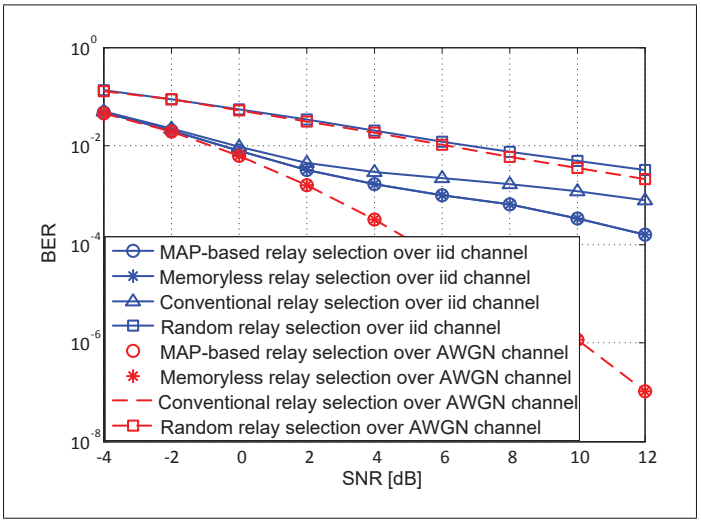

Figure 4.7 End-to-end BER performances of various N'th BRS schemes with $M = 5$ relays. A system involving an uncoded transmission and BPSK modulation is considered. It is assumed that $p_B = 0.01$ with $\mu = 1$, $\rho = 100$ for the i.i.d. channel, and $\mu = 1$, $\rho = 1$ for the AWGN channel

Fig. 4.7 presents the simulated end-to-end BER performances of the proposed relay selection protocols in case of memoryless impulsive and AWGN noise scenario. From Fig. 4.7, it is

observed that the MAP-based and memoryless relay selection schemes show the same performance, when the noise memory is reduced from $\mu = 100$ in Fig. 4.5 to $\mu = 1$, i.e., in case of memoryless impulsive noise. This confirms that, for memoryless IN, the optimal MAP detector simplifies to the sample-by-sample detector. Again, the conventional relay selection achieves the worst performance in these impulsive scenarios. We further show the corresponding results in case of Gaussian channel. Obviously, the three relay selection schemes provide the same performance in this case.

In order to illustrate the effect of best relay location, we demonstrate in Fig. 4.8 the performance of the considered relay selection schemes for asymmetric network scenarios with $\lambda_{SR_m} = 0.2$ and $\lambda_{SR_m} = 0.8$. We observe from Fig. 4.8 that the performance of opportunistic relaying degrades if the best relay is moved from the source to the destination irrespective of the relay selection process. It turns out that the best relay being closer to the source is more rewarding than closer to the destination.

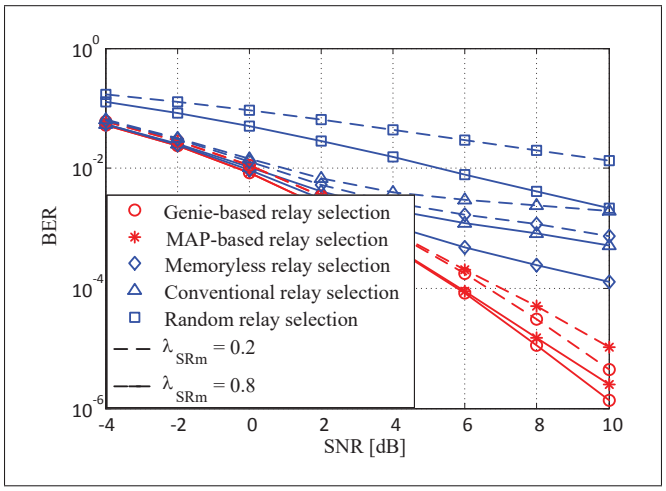

Figure 4.8 End-to-end BER performances of various N'th BRS schemes for various best relay positions. A system involving an uncoded transmission with $M = 5$ relays over Rayleigh faded TSMG channels and a BPSK modulation is considered

Furthermore, we also investigate the performance of the proposed relay selection schemes under coded transmission. It is interesting to evaluate how much gain does the proposed MAP-

based relay selection scheme provide over the other schemes for systems employing powerful channel codes such as low-density parity check (LDPC) codes. In Fig. 4.9, we show the simulated BERs at the selected relay for various relay selection schemes under LDPC coded transmission. At the transmitter, a frame of equally likely $32,400$ information bits is first encoded with the code rate of $1/2$ and then mapped to a BPSK modulation sequence. For LDPC decoding, we set the number of iterations to 50. As expected, from Fig. 4.9, we remark that similar to uncoded transmission, the proposed MAP-based N'th BRS scheme provides a significant performance gain over the other schemes.

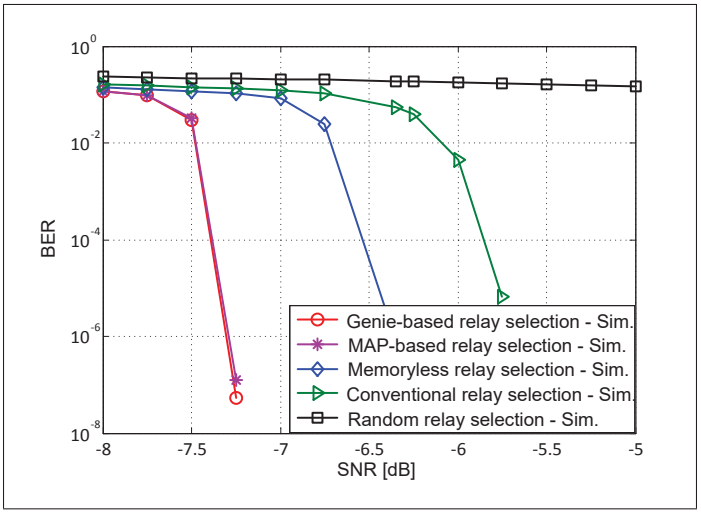

Figure 4.9 BER performances at the N'th best relay of various BRS schemes with $M = 5$ relays over Rayleigh faded TSMG channels. A system involving an LDPC coded transmission and BPSK modulation is considered

Figures 4.10 and 4.11 depict the outage probability and the corresponding asymptotic curves at the selected relay as well as the destination for a targeted data rate $R = 1$ bits/s/Hz. It is observed from figures 4.10 and 4.11 that the derived analytical outage performances provide an exact match to the simulation results for the genie-aided scheme. It also observed that the MAP-based BRS scheme performs exactly as the genie-aided scheme. Therefore, the MAP-based relay selection criterion is the most suitable one for bursty IN environments as it has

been designed according to the statistical behavior of the noise. In addition, it achieves the full diversity order of $M+1$ as shown in Fig. 4.11.

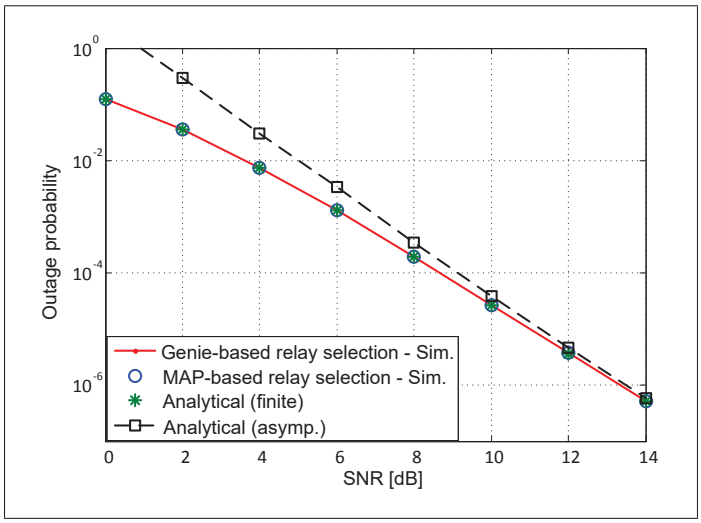

Figure 4.10 Outage performances at the N'th best relay of various relay selection schemes with $M=5$ relays over Rayleigh faded TSMG channels. A system involving an uncoded transmission and a BPSK modulation is considered

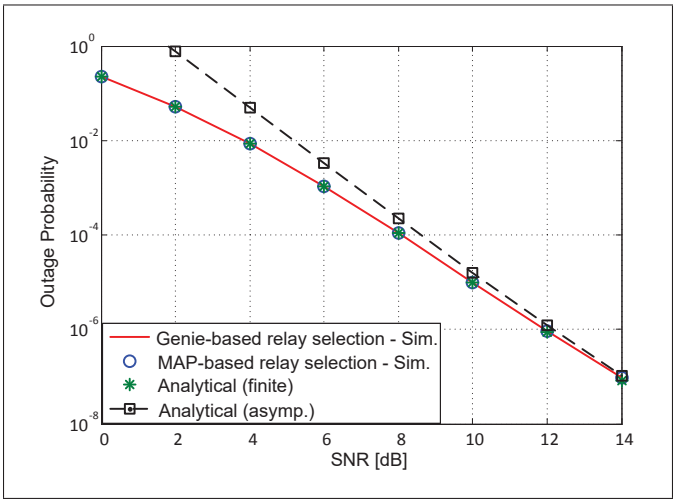

Figure 4.11 End-to-end outage performances of various N'th BRS schemes with $M=5$ relays over Rayleigh faded TSMG channels. A system involving an uncoded transmission and a BPSK modulation is considered

4.9 Conclusion

In this article, we have investigated the performance of some conventional relay selection protocols for DF CR over Rayleigh faded bursty IN channels and have proposed an improved approach for relay selection. The proposed method avoids the use of error detection methods at the relay nodes and is based on both the channel state information of source-relay and relay-destination links, and the state of the IN that affect those links. We provided closed-form expressions for the PDF of the received SNR at the N'th best relay as well as at the destination under both cases of finite SNR and asymptotic analysis. As a consequence, these PDFs are used to derive closed-form expressions for the end-to-end BER, as well as the outage probability, facilitating the achievement of the diversity order of the scheme. Simulation results confirmed the accuracy of the proposed asymptotic and finite SNR analysis. From the obtained results, it is verified that our proposed MAP-based N'th BRS scheme outperforms the conventional schemes optimized for the Gaussian case, and which cannot take into account the IN memory.

CHAPTER 5

BAYESIAN MMSE ESTIMATION OF A GAUSSIAN SOURCE IN THE PRESENCE OF BURSTY IMPULSIVE NOISE

Md Sahabul Alam [1], Georges Kaddoum[1], Basile L. Agba [2]

[1] Département de Génie Electrique, École de Technologie Supérieure,
1100 Notre-Dame Ouest, Montréal, Québec, Canada H3C 1K3
[2] Hydro-Quebec Research Institute (IREQ), Varennes, QC, Canada, J3X 1S1

Article published in IEEE Communications Letter, September, 2018.

5.1 Abstract

In this letter, we derive the minimum mean square error (MMSE) optimal Bayesian estimation (OBE) for a Gaussian source, in the presence of bursty impulsive noise, as essentially encountered within power substations. Clearly, it is observed that the presence of bursty impulsive noise makes the input-output characteristics of MMSE OBE non-linear. To handle the non-linearity, we propose a novel MMSE estimator, based on the detection of the unobservable states of the noise process, using the maximum a posteriori (MAP) detector. Resultantly, the proposed MAP-based MMSE estimator is shown to achieve the lower bound derived for the proposed scenario and outperform the various MMSE estimators that neglect the noise memory.

5.2 Introduction

The difficulty of estimating a Gaussian source from its available noisy measurements is prevalent in numerous signal processing contexts. In particular, a great deal of prior research is available in the literature, regarding the Gaussian source estimation in the presence of Gaussian noise, in various aspects. In such a scenario Kay, S. M. (1993), the linear MMSE (LMMSE) estimator is proved to be the optimal estimation technique. However, the noise that usually occurs in many environments are highly non-Gaussian and display a significant impulsive nature

Middleton (1977). For example, in power substations, the noise emitted from various power equipment is impulsive Middleton (1977); Portuguds *et al.* (2003); Sacuto *et al.* (2012). The impulsive noise measurement campaign in power substation environments also shows that the impulses occur in bursts Portuguds *et al.* (2003); Sacuto *et al.* (2012).

On the other hand, the performance of the estimation techniques, in the presence of an impulsive noise, is not widely acknowledged. Banelli considered the MMSE OBE for a Gaussian source impaired by Middleton class-A impulsive noise in Banelli (2013). In his work, he showed that the performance of the MMSE OBE strictly depends on the input-output characteristics of the received signal, which becomes non-linear for impulsive noise environments. To tackle this challenge, several MMSE estimators were introduced. The authors in Flam *et al.* (2012) derived the MMSE OBE and its mean-square error (MSE) performance bounds in closed form, assuming that both the noise and the source signals are Gaussian mixture distributed. The obtained results show that the MMSE estimator, under this condition, outperforms the LMMSE estimator. These approaches, however, have a major shortcoming; they ignore the inherent memory in the noise process. To address this, Markov chain models have been proposed Alam *et al.* (2016); Fertonani & Colavolpe (2009); in order to better represent the impulsive noise characteristics. Hence, the impact on the performance gain, observed when the memory is exploited in the estimation process, must be evaluated.

To address this issue, the present letter provides a framework for the performance analysis of Bayesian MMSE estimation of a Gaussian source, in the presence of a bursty impulsive noise source. This necessitates a two-step operation: the estimator should be optimal in minimizing the resulting MSE and can detect the state of the noise process simultaneously, thanks to the BCJR algorithm Bahl *et al.* (1974) that was found as an effective tool to detect the states of a finite state hidden Markov process. In this letter, we redesign a robust estimator combining these two techniques - MMSE estimation and the BCJR algorithm. As shown in Fig. 5.1, the MAP detector executes the BCJR algorithm and provides the hard decision of the noise state information to the MMSE estimator. Given the state, the LMMSE estimator is optimal in minimizing the MSE sense.

The contribution of this work is depicted as follows: we derived the MMSE OBE for a scalar Gaussian source estimation in the presence of bursty impulsive noise, modeled by a two-state Markov-Gaussian (TSMG) process Fertonani & Colavolpe (2009). It is shown that similarly to uncorrelated Middleton class-A noise Banelli (2013), the presence of TSMG noise also makes the input-output characteristics of MMSE OBE non-linear, especially when the environment is more impulsive. To combat the adverse effect of non-linearity, we propose a novel MMSE estimator, based on detecting the unobservable states of the noise process using the MAP state detection. Through the simulation results, the proposed MAP-based MMSE estimator achieves the MSE lower bound derived for the proposed scenario and performs significantly better than the conventional LMMSE estimator, optimized for AWGN environment, and the MMSE estimator that neglects the noise memory.

5.3 System model

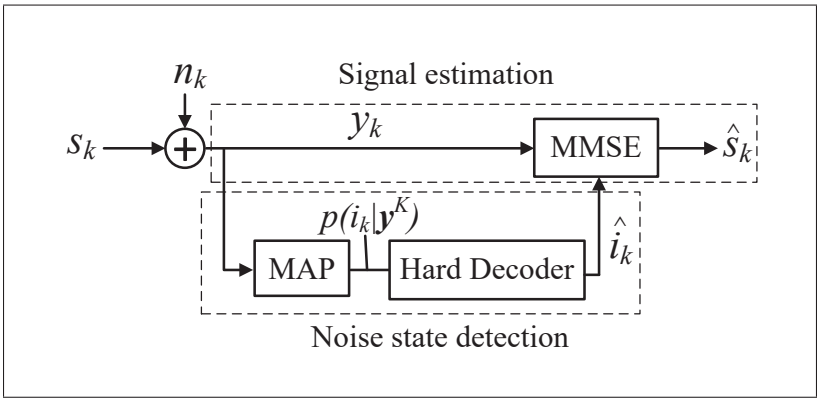

Figure 5.1 MAP-based Bayesian MMSE estimation of a Gaussian source in the presence of bursty impulsive noise

In this paper, we consider a point-to-point communication system, as shown in Fig. 5.1. We assume s_k is the parameter to be estimated, modeled by a zero-mean Gaussian random variable with variance σ_s^2. The received signal at the destination at each time epoch k can be expressed as

$$y_k = s_k + n_k, \quad k = 0, 1, \ldots, K-1 \tag{5.1}$$

where n_k is the additive noise, statistically independent of s_k, and K is the length of the whole received sequence. It is assumed that the noise sample n_k follows the TSMG process. The statistical properties of n_k are completely defined by the noise state indicator $i_k \in \{G,B\}$. In the context of our noise modeling, G and B represent respectively the good and the bad state. The channel is impaired by the Gaussian noise only in the good state, and the bad state occurs when this latter is impaired by impulsive interferers. We model n_k as a zero-mean Gaussian random variable, so that the probability density function (PDF) of n_k conditioned on i_k is represented by

$$f(n_k|i_k = m) = \frac{1}{\sqrt{2\pi\sigma_m^2}} \exp\left(-\frac{n_k^2}{2\sigma_m^2}\right), m \in (G,B), \tag{5.2}$$

For this model, the parameter $R = \sigma_B^2/\sigma_G^2$ quantifies the impulsive to Gaussian noise power ratio. The statistical description of the state process $\mathbf{i}^K = \{i_0, i_1, \ldots, i_{K-1}\}$ specifies the channel completely and is evaluated by the state transition probabilities $p_{i_k i_{k+1}} = p(i_{k+1}|i_k)$, $i_k, i_{k+1} \in \{G,B\}$. Using these transition probabilities, the stationary probabilities of being in either the good or the bad state are respectively given by Fertonani & Colavolpe (2009),

$$\pi_G = \frac{p_{BG}}{p_{GB} + p_{BG}} \quad \text{and} \quad \pi_B = \frac{p_{GB}}{p_{GB} + p_{BG}}. \tag{5.3}$$

Also, the parameter $\gamma = \frac{1}{p_{GB}+p_{BG}}$ determines the noise memory and $\gamma > 1$ indicates that the channel has a persistent memory.

5.4 Bayesian MMSE Estimation

In this section, we consider the MMSE OBE of s_k, given the observation y_k. The MMSE OBE corresponds to the posteriori mean Kay (1993) and is given by

$$\begin{aligned} \hat{s}_k(y_k) &= \mathrm{E}(s_k|y_k) = \mathrm{E}[\mathrm{E}(s_k|y_k, i_k = m)], \\ &= \sum_{m\in(G,B)} p(i_k = m|y_k)\hat{s}_{m,k}(y_k), \end{aligned} \tag{5.4}$$

where E is the expectation operator and $\hat{s}_{m,k}(y_k) = \mathrm{E}(s_k|y_k, i_k = m)$. It should be noted that given $i_k = m$, s_k and y_k are jointly Gaussian. Hence, LMMSE estimator $(\hat{s}_{m,k}(y_k))$ is the optimal estimator of s_k and we have Kay (1993)

$$\hat{s}_{m,k}(y_k) = \frac{\sigma_s^2}{\sigma_s^2 + \sigma_m^2} y_k, \tag{5.5}$$

where $\sigma_s^2 + \sigma_m^2$ is the variance of y_k, given that $i_k = m$. Since, s_k is independent of n_k, from the convolution property, the PDF of y_k can be represented by

$$f(y_k) = f(s_k) * f(n_k) = \sum_{m \in (G,B)} \pi_m f_G(y_k; 0, \sigma_s^2 + \sigma_m^2), \tag{5.6}$$

where $\pi_m = p(i_k = m)$ and $f_G(y_k; 0, \sigma_s^2 + \sigma_m^2)$ represents a zero-mean Gaussian PDF with variance $\sigma_s^2 + \sigma_m^2$. Now, from (5.4), we can deduce that the posteriori probability $p(i_k = m|y_k)$ is also required to derive the MMSE estimator. Using the Bayes rule, this can be obtained as

$$p(i_k = m|y_k) = \frac{\pi_m f_G(y_k; 0, \sigma_s^2 + \sigma_m^2)}{\sum_{j \in (G,B)} \pi_j f_G(y_k; 0, \sigma_s^2 + \sigma_j^2)}, \tag{5.7}$$

Hence, substituting equation (5.5) and (5.7) into (5.4), the MMSE OBE of s_k given y_k is obtained by

$$\hat{s}_k(y_k) = \sum_{m \in (G,B)} \frac{\pi_m f_G(y_k; 0, \sigma_s^2 + \sigma_m^2)\sigma_s^2}{\sum_{j \in (G,B)} \pi_j f_G(y_k; 0, \sigma_s^2 + \sigma_j^2)(\sigma_s^2 + \sigma_m^2)} y_k. \tag{5.8}$$

Fig. 5.2 shows the input-output characteristics of MMSE OBE, using equation (5.8) for different values of the impulsive probability π_B. As observed in Fig. 5.2, when the value of π_B increases, the impulsive noise becomes closer to the Gaussian noise and the input-output characteristics of MMSE OBE tend to the well-known LMMSE estimation. On the other hand, when the value of π_B decreases, the environment becomes more impulsive, as indicated by rare impulsive events, and the input-output characteristic becomes more non-linear. Thus, the presence of bursty impulsive noise introduces non-linearity in the measurement y_k. This necessitates the designing of a MMSE estimator, in order to achieve a better MSE performance over the conventional LMMSE estimator.

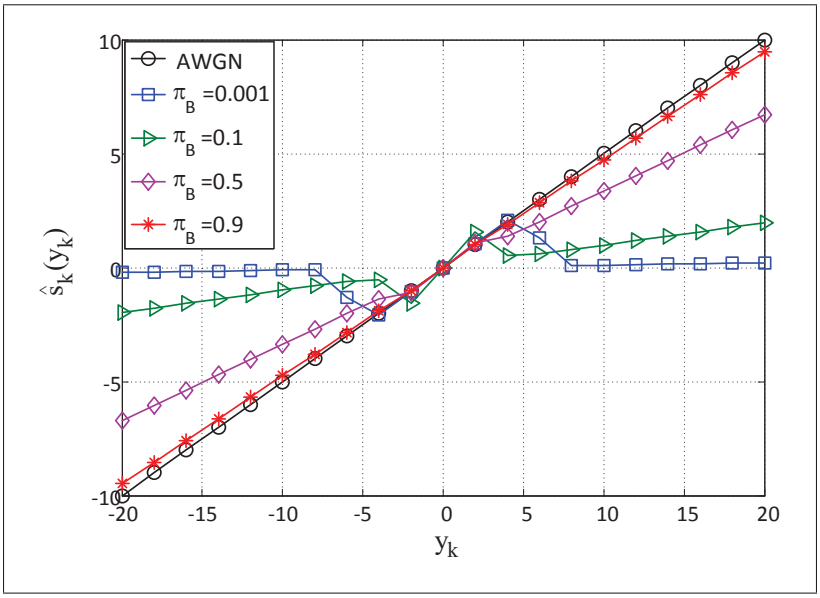

Figure 5.2 Impact of the impulsive probability π_B on the input-output characteristics of MMSE optimal Bayesian estimation. It is assumed that $\sigma_s^2 = 1$, $\sigma_n^2 = 1$, $R = 100$, and $\gamma = 100$

In addition, as well as having to estimate the source signal, if the estimator can detect the states of the impulsive process simultaneously, the conventional LMMSE estimator can be considered as the optimal choice in minimizing the MSE sense Kay (1993). In this vein, in the following section, we will discuss three state detection algorithms. To achieve the best performance, the optimal detector must detect the states of the impulsive noise as accurately as possible.

5.5 Exploiting State Information

In this section, we will discuss three state detection algorithms to pursue the explicit use of the noise state information in the MMSE estimation process. Hence, in other words, when the receiver knows whether the impulsive noise is affecting the signal samples or not, the MMSE OBE can be confirmed, according to equation (5.5). Revisiting equation (5.5), it can be illustrated by the fact that σ_m^2 can be substituted by σ_B^2, in case of the presence of an impulsive noise and with σ_G^2 otherwise.

5.5.1 Genie Detection

For genie detection, it is assumed that the receiver is deemed to have perfect noise state information. While such an approach is conceptually valuable to provide us a good indication of the best achievable performance, the realization of such a detector is very hard, if not impossible. In the context of achievable performance, the following sections provide some algorithms to obtain the states of the noise.

5.5.2 MAP-based State Detection using the BCJR Algorithm

For this scheme, at each k, the receiver evaluates the a posteriori probability $p(i_k|\mathbf{y}^K)$ that the actual channel state is i_k, given the received sequence $\mathbf{y}^K = \{y_0, y_1, \ldots, y_{K-1}\}$. This can be obtained as

$$p(i_k|\mathbf{y}^K) = \frac{p(i_k, \mathbf{y}^K)}{p(\mathbf{y}^K)} \propto p(i_k, \mathbf{y}^K), \tag{5.9}$$

We now define the following

$$\begin{aligned} \alpha_k(i_k) &= p(y_0, y_1, \ldots, y_{k-1}, i_k), & (5.10)\\ \beta_k(i_k) &= p(y_k, y_{k+1}, \ldots, y_{K-1}|i_k), & (5.11)\\ \delta_k(y_k, i_k, i_{k+1}) &= p(i_{k+1}, y_k|i_k) = p(i_{k+1}|i_k) f(y_k|i_k), & (5.12) \end{aligned}$$

where $\alpha_k(i_k)$ and $\beta_k(i_k)$ are termed as the forward and backward filters, and $\delta_k(y_k, i_k, i_{k+1})$ represents the branch metric of the trellis diagram, as shown in Fig. 5.3. Using (5.10) and (5.11), the probability $p(i_k, \mathbf{y}^K)$ in (5.9) can be written as

$$p(i_k, \mathbf{y}^K) = p(y_0, y_1, \ldots, y_{k-1}, i_k) p(y_k, y_{k+1}, \ldots, y_{K-1}|i_k) = \alpha_k(i_k)\beta_k(i_k). \tag{5.13}$$

where the first equality comes from the Markov property. Then, the noise state can be expressed as

$$\hat{i}_k = \begin{cases} G & \text{if } L_{i_k} \geq 0 \\ B & \text{if } L_{i_k} < 0 \end{cases} \tag{5.14}$$

where L_{i_k} is the log-likelihood ratio (LLR) and $\hat{i}_k$ represents the hard decision of the impulsive noise state at time epoch k. For this, the LLR values at the receiver can be computed by

$$L_{i_k} = \ln\left\{\frac{\alpha_k(i_k = G)\beta_k(i_k = G)}{\alpha_k(i_k = B)\beta_k(i_k = B)}\right\}. \tag{5.15}$$

Accordingly, the forward and backward filters can be computed recursively as

$$\begin{aligned} \alpha_{k+1}(i_{k+1}) &= \sum_{i_k} \alpha_k(i_k)\delta_k(y_k, i_k, i_{k+1}), \\ \beta_k(i_k) &= \sum_{i_{k+1}} \beta_{k+1}(i_{k+1})\delta_k(y_k, i_k, i_{k+1}), \end{aligned} \tag{5.16}$$

where the filters recursions are initialized with $\alpha_0(i_0 = m) = \pi_m$, and $\beta_K(i_K = m) = 1$.

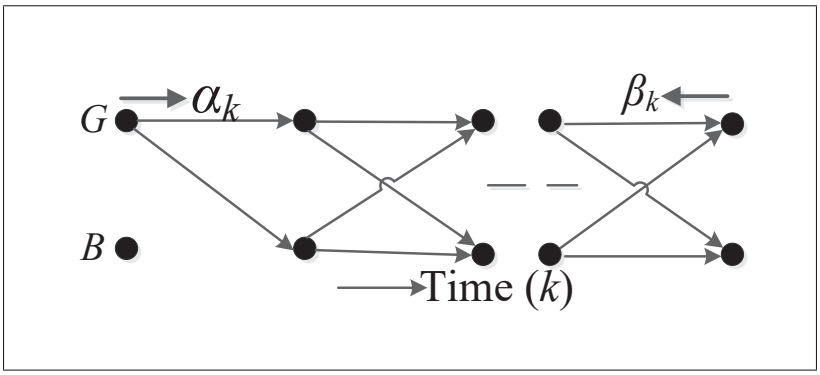

Figure 5.3 Trellis representation of the two-state Markov-Gaussian noise model

5.5.3 Sample-by-Sample State Detection

We next consider a state detection algorithm called sample-by-sample state detection scheme. Although aware of the impulsive noise state, it neglects the inherent noise memory. For such a scenario, it is assumed that $\gamma = 1$ in the state detection process, which corresponds to the Bernoulli-Gaussian noise Ghosh (1996) instead of TSMG noise. Under this approximation, the above recursive MAP-based noise state detector simplifies to a memoryless detector and the probability of having a state can be computed from the probability, $p(i_k|y_k) = p(i_k)f(y_k|i_k)$.

Using this, the LLR values are obtained as

$$L_{i_k} = \ln \left\{ \frac{\pi_G f(y_k|i_k = G)}{\pi_B f(y_k|i_k = B)} \right\}. \tag{5.17}$$

Where $f(y_k|i_k = m) = f_G(y_k; 0, \sigma_s^2 + \sigma_m^2)$. From the LLR values, the receiver then determines the noise states according to (5.14).

5.5.4 AWGN Scenario

This is the simplest estimation technique since it is blind to the noise states for the estimation process. Under this consideration, the OBE $\hat{s}_k(y_k)$ of s_k given y_k can be obtained as

$$\hat{s}_k(y_k) = \frac{\sigma_s^2}{\sigma_s^2 + \sigma_n^2} y_k. \tag{5.18}$$

where $\sigma_n^2 = \sum_{m \in (G,B)} \pi_m \sigma_m^2$ denotes the variance of n.

5.5.5 Complexity Discussion

It is worth to point out that, despite having a better performance, the complexity of the proposed MAP-based MMSE estimation scheme grows exponentially with the frame length, due to the implementation of the BCJR algorithm, while it grows linearly in case of symbol-by-symbol estimation schemes Fertonani *et al.* (2007). However, in Section 5.7 we show that the potential performance gain of this scheme justifies the increase in complexity, which makes this receiver suitable for reliable communication scenarios. On the other hand, if we only consider the forward recursions of the BCJR algorithm, then the complexity problem will probably be reduced with a compromise in its performance. Hence, this scheme exhibits a performance/complexity trade-off.

5.6 Performance Analysis

The performance of this scheme is evaluated in terms of distortion or MSE and it can be obtained by

$$D \equiv \mathrm{E}\left\{(s_k - \hat{s}_k)^2\right\} = \int_s \int_y (s_k - \hat{s}_k(y_k))^2 f(s,y) ds dy, \tag{5.19}$$

However, the closed form expression of the integrals in (5.19) is mathematically intractable which makes it difficult to analytically investigate the MSE. As a result, approximating its bounds remain an alternative solution to evaluate the performance of our proposed scheme. In this vein, a lower bound (LB) is obtained under the hypothetical assumption that there is no uncertainty about the state i_k, i.e., the genie condition. The LB (D_{LB}) under this consideration can be obtained as

$$D_{LB} = \sum_{m \in (G,B)} \pi_m \left(\sigma_s^2 - \frac{\sigma_s^4}{\sigma_s^2 + \sigma_m^2} \right). \tag{5.20}$$

To derive the upper bound (D_{UB}), we invoke the LMMSE estimator since this latter obtains the smallest MSE among all the estimators which are linear in the observations Kay (1993). The MSE of the LMMSE estimator for this scheme is

$$D_{UB} = \sigma_s^2 - \frac{\sigma_s^4}{\sigma_s^2 + \sigma_n^2}. \tag{5.21}$$

5.7 Numerical Results

In this section, we simulate the MSE performances of the proposed scenario to confirm the analytical results. It is required to estimate the source parameter s_k, which is modeled as a Gaussian random variable, with variance $\sigma_s^2 = 1$. Also, the impulsive noise that corrupts the source signal is characterized by the parameters $\pi_B = 0.1$, $\gamma = 100$, and $R = 100$ Fertonani & Colavolpe (2009). The MSE performances are calculated against average SNR. Here, the average SNR is defined as SNR$= \sigma_s^2/\sigma_n^2$.

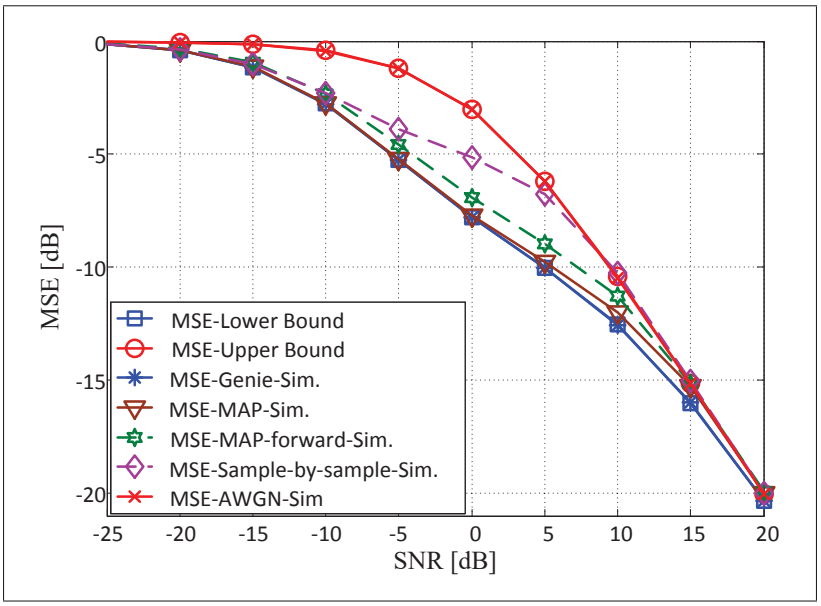

Figure 5.4 Analytical and simulated MSE performances of different estimation techniques against the SNR. It is assumed that $\pi_B = 0.1$, $R = 100$, and $\gamma = 100$

Fig. 5.4 shows the simulated MSE performances of different estimation techniques. The simulated MSE performances are obtained by calculating the sample means of $(s_k - \hat{s}_k(y_k))^2$ using 2×10^5 frames with $K{=}10^3$ samples of each frame. In Fig. 5.4, the simulation result attained under genie aided estimation perfectly matches the lower bound is well displayed. However, the genie detection is practically infeasible. Interestingly, from the figure, it is also observed that the proposed MAP-based MMSE estimator almost approaches the performance of genie aided scheme and performs significantly better than the conventional schemes. It obtains a minimum SNR gain of around 8 dB over the LMMSE estimator and around 5 dB over the sample-by-sample estimator, at the expense of a higher complexity, due to the BCJR algorithm. Moreover, by considering the forward recursions of the BCJR algorithm, a tight performance gap with the original scheme is observed, while the complexity problem is reduced. This confirms that significant performance gains can be obtained when the noise memory is utilized in the estimation process. In addition, simpler sample-by-sample-based estimator still exhibits better performance than the LMMSE scheme, by utilizing the impulsive noise statistics in the estimation process. Finally, the LMMSE leads to the worst performances.

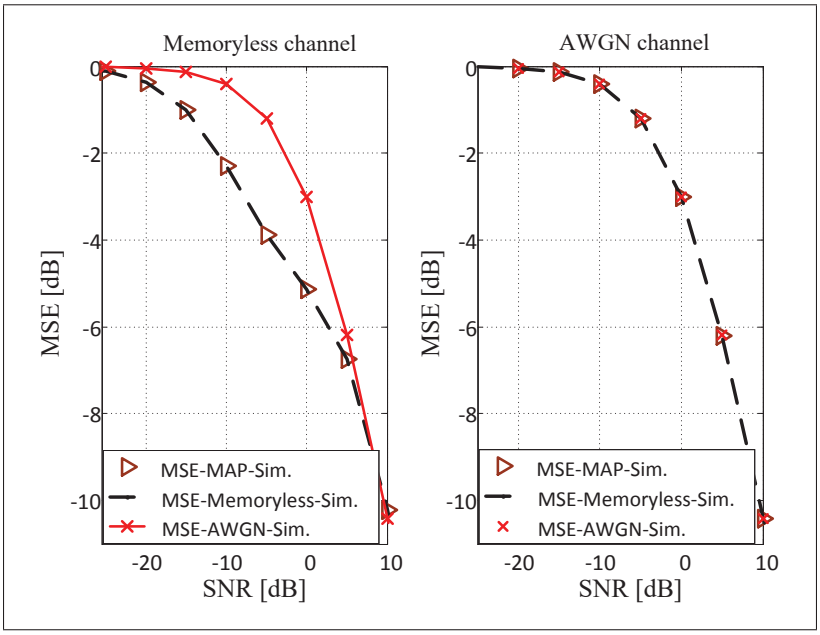

Figure 5.5 MSE performances of different estimation techniques against the SNR. It is assumed that $\pi_B = 0.1$ with $\gamma = 1$, $R = 100$ for the memoryless channel, and $\gamma = 1$, $R = 1$ in case of AWGN channel

Fig. 5.5 also shows the simulated MSE performances of different estimation techniques. The essence of plotting Fig. 5.5 is to visualize how the proposed MAP-based MMSE estimator behaves over the memoryless and AWGN channel. From Fig. 5.5, it can be inferred that both the MAP-based and sample-by-sample-based estimations show the same performance, when we consider $\gamma = 1$ in the noise process. These results confirm that the optimal MAP detector simplifies to the memoryless detector when the considered impulsive noise is memoryless. Again, the LMMSE estimator attains around 5 dB worse performance over them in these impulsive environments, in low SNR region. Finally, the three estimators obviously exhibit the same performance over AWGN channel.

5.8 Conclusion

In this letter, we have provided the necessary theoretical foundation for optimal Bayesian estimation of a scalar Gaussian source, in the presence of bursty impulsive noise. It is shown that

the presence of bursty impulsive noise makes the input-output characteristics of MMSE OBE non-linear. To combat the effect of non-linearity, we have proposed a novel estimation technique based on detecting the unobservable states of the noise process. The simulation results confirmed that the proposed MAP-based Bayesian MMSE estimator outperforms the various MMSE estimators employing memoryless estimation. Noteworthy, the proposed estimator can be easily adapted to any Gaussian source estimation in the presence of any Gaussian mixture noise with memory. Future extension of this work may include deriving the exact closed form expression for the MSE.

CHAPTER 6

PERFORMANCE ANALYSIS OF DISTRIBUTED WIRELESS SENSOR NETWORKS FOR GAUSSIAN SOURCE ESTIMATION IN THE PRESENCE OF IMPULSIVE NOISE

Md Sahabul Alam [1], Georges Kaddoum[1], Basile L. Agba [2]

[1] Département de Génie Electrique, École de Technologie Supérieure,
1100 Notre-Dame Ouest, Montréal, Québec, Canada H3C 1K3
[2] Hydro-Quebec Research Institute (IREQ), Varennes, QC, Canada, J3X 1S1

Article published in IEEE Signal Processing Letters, June, 2018.

6.1 Abstract

We address the distributed estimation of a scalar Gaussian source in wireless sensor networks (WSNs). The sensor nodes transmit their noisy observations, using the amplify-and-forward relaying strategy through coherent multiple access channel to the fusion center (FC) that reconstructs the source parameter. In this letter, we assume that the received signal at the FC is corrupted by impulsive noise and channel fading, as encountered for instance within power substations. Over Rayleigh fading channel and in presence of Middleton class-A impulsive noise, we derive the minimum mean square error (MMSE) optimal Bayesian estimator along with its mean square error (MSE) performance bounds. From the obtained results, we conclude that the proposed optimal MMSE estimator outperforms the linear MMSE estimator developed for Gaussian noise scenario.

6.2 Introduction

The difficulty of estimating a Gaussian source from its available noisy measurements is prevalent in numerous signal processing contexts. In this aspect, over the past few years, researches on the implementation of distributed WSN has been evolving very rapidly. For example, the authors in Xiao, J.-J., Cui, S., Luo, Z.-Q. & Goldsmith, A. J. (2008) considered the distributed

estimation of scalar source parameters using a collaborative WSN. It is shown that depending on the available information about the source statistics and the noise behaviour, different estimators can be used to achieve the MSE criterion. Similar performance analyses are carried out in Aysal, T. C. & Barner, K. E. (2008); Cui, S., Xiao, J.-J., Goldsmith, A. J., Luo, Z.-Q. & Poor, H. V. (2007); Wang, C.-H., Leong, A. S. & Dey, S. (2011a) to show the optimality of the maximum likelihood estimator (MLE) Aysal & Barner (2008), best linear unbiased estimator (BLUE) Cui *et al.* (2007), and the MMSE estimator Wang *et al.* (2011a) based on the available information about the source statistics.

However, all of the above performance analyses for distributed estimation schemes have been carried out over the Gaussian noise scenario. On the other hand, the noise characteristics, usually observed in many environments, such as the power transmission lines areas, the power substations, and in some mobile radio scenarios, are inherently impulsive in nature Middleton (1977). For example, in power substations, the noise emitted from various power equipment are impulsive Madi, G., Sacuto, F., Vrigneau, B., Agba, B. L., Pousset, Y., Vauzelle, R. & Gagnon, F. (2011). In this context, the impacts of impulsive noise have been widely investigated on the detection of finite alphabets in point-to-point and collaborative WSN communications Alam *et al.* (2016); Spaulding & Middleton (1977). However, the performance of estimation techniques in the presence of impulsive noise is not widely acknowledged.

Recently, the authors in Banelli (2013) considered the MMSE optimal Bayesian estimation (OBE) for a Gaussian source impaired by Middleton class-A impulsive noise. It is shown that the performance of the proposed MMSE OBE strictly depends on the statistical characteristics of the received signal. The authors in Flam *et al.* (2012) derived the MMSE OBE and its MSE performance bounds in closed form assuming that the noise and the source signals are Gaussian mixture (GM) distributed. The obtained results showed that the performance improvement of the optimal MMSE estimator over the linear MMSE (LMMSE) estimator under this condition is substantial. However, the analyses in Banelli (2013); Flam *et al.* (2012) are restricted to the point-to-point scenario and the effect of channel fading is not considered. To the best of authors knowledge, no result exists for the distributed estimation of Gaussian sources in

the presence of impulsive noise under Rayleigh fading. Here, we provide a mathematical framework for the performance analysis of distributed estimation of a scalar Gaussian source impaired by Middleton class-A noise. A Middleton class-A process is a simple and effective way to model an impulsive noise channel Banelli (2013); Middleton (1977). Our work is an extension of Banelli (2013) to the distributed WSN scenario. It is assumed that each sensor node transmits its observations to the FC through a coherent multiple access channel (MAC) using AF strategy. It is widely acknowledged that AF schemes significantly outperform the traditional source-channel coding for Gaussian signal estimation while preserving the sensor's radios low complexity Gastpar, M. & Vetterli, M. (2003). The FC uses the received signal to estimate the source parameter with minimum MSE.

The contributions of this work are as follows. First, we derive the MMSE OBE for a scalar Gaussian source estimation using distributed WSN in the presence of impulsive noise under Rayleigh fading. It is seen that the presence of impulsive noise makes the input-output characteristics of MMSE OBE non-linear especially when the environment is more impulsive, as indicated by the rare impulsive events. This leads to a non-linear MMSE estimator. Then, we provide upper and lower bounds for its MSE performance. Finally, the derived bounds are validated through the Monte Carlo simulation. Interestingly, from the obtained results, it is seen that the proposed optimal MMSE estimator attains the lower bound for highly impulsive noise environment and performs significantly better than the LMMSE estimator developed for AWGN scenario.

6.3 System model

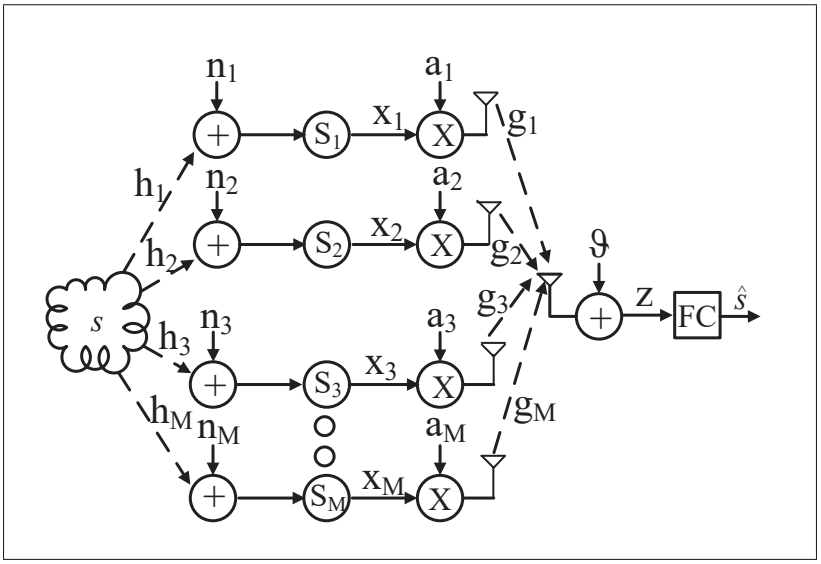

Figure 6.1 Distributed WSN for Gaussian source estimation

As shown in Fig. 6.1, we consider a WSN of M sensor nodes from S_1 to S_M and a FC. The sensor nodes observe a scalar parameter s, which is modeled by a Gaussian random variable (rv) with mean μ_s and variance σ_s^2. Let the signals measured by the ith sensor node, $i = 1,2,\ldots,M$, can be expressed as

$$x_i = h_i s + n_i, \tag{6.1}$$

where h_i and n_i denote the channel coefficient and the measurement noise at the ith sensor node, respectively. In this work, as usual, the measurement noise variables $\{n_i\}_{i=1}^{M}$ are assumed to be Gaussian with mean μ_n and variance σ_n^2. Now, the sensor nodes follow two-hop collaborative communications to send the data from the source to the destination using AF strategy. In the first hop, the sensor nodes measure the data of the source to be estimated and in the second hop, each sensor node amplifies its measured signal x_i by a factor of a_i and transmits it to the FC through a coherent MAC channel Xiao *et al.* (2008). The received signal, z, at the FC is then given by

$$z = \sum_{i=1}^{M} g_i a_i x_i + \vartheta, \tag{6.2}$$

where g_i is the channel coefficient between the ith sensor node and the FC, and ϑ is the communication noise. We assume that the channel coefficients follow the Rayleigh distribution and for each link, they are considered to be static for one symbol duration, while they vary from one symbol to another. Therefore, both h_i and g_i are modeled by a zero-mean independent, circularly symmetric complex Gaussian random variable with variances σ_h^2 and σ_g^2, respectively. It is assumed that the channel coefficients are known at both the transmitters and receiver side. Hence, the signals can be added coherently at the FC Xiao *et al.* (2008). It is also assumed that ϑ follows Middleton class-A distribution to account for impulsive communication disturbance. Hence, the probability density function (PDF) of ϑ is given by Middleton (1977)

$$f(\vartheta) = \sum_{m=0}^{\infty} \frac{p_m}{\sqrt{2\pi}\sigma_m} \exp\left(-\frac{\vartheta^2}{2\sigma_m^2}\right), \tag{6.3}$$

where $p_m = \frac{e^{-A}A^m}{m!}$ is the steady state probability of the m^{th} impulsive source and $\sigma_m^2 = \sigma_\vartheta^2 \frac{m/A+\Gamma}{1+\Gamma}$ is the variance of that impulsive source. For $m = 0$, the model generates the traditional AWGN component. Also, the parameters A, Γ, and σ_ϑ^2 are called the global parameters as they characterize the PDF Middleton (1977). The physical significance of these parameters are: A denotes the impulsive index, Γ indicates the Gaussian to impulsive noise power ratio, and σ_ϑ^2 represents the total power of the noise ϑ.

6.4 MMSE Optimal Bayesian Estimation

In this section, we consider the MMSE OBE of a scalar Gaussian source s impaired by Middleton class-A noise under Rayleigh fading. The MMSE OBE corresponds to the posteriori mean Kay (1993) and is given by

$$\hat{s} = \varepsilon(s|z) == \int s f(s|z)\, ds, \tag{6.4}$$

where $\hat{s}$ indicates the MMSE estimation of s and ε is the expectation operator. From equation (6.4), we can deduce that the posteriori probability $f(s|z)$ is required to derive the MMSE estimator. Although the distribution of $f(s|z)$ already exists for AWGN channel Xiao *et al.* (2008),

here, we derive the distribution for impulsive noise scenario. Now, (6.2) can be rearranged as

$$z = \mathbf{g}^T\mathbf{W}\mathbf{h}s + \mathbf{g}^T\mathbf{W}\mathbf{n} + \vartheta = \alpha s + \beta, \tag{6.5}$$

where $\mathbf{g} = [g_1,\ldots,g_M]^T$, $\mathbf{h} = [h_1,\ldots,h_M]^T$, $\mathbf{W} = \text{diag}(\mathbf{a})$ with $\mathbf{a} = [a_1,\ldots,a_M]^T$, and $\mathbf{n} = [n_1,\ldots,n_M]^T$. Here, the amplification factor for each node is $a_i = \sqrt{(P_T/M(\sigma_h^2\sigma_s^2 + \sigma_n^2))}$, where P_T is the total transmission power of all the sensor nodes. Also, $\alpha = \mathbf{g}^T\mathbf{W}\mathbf{h}$ and $\beta = \mathbf{g}^T\mathbf{W}\mathbf{n} + \vartheta$. It is assumed that $N = \mathbf{g}^T\mathbf{W}\mathbf{n}$ and ϑ are mutually independent with each other. Then, from the convolution property, the distribution of β is represented by

$$f(\beta) = \sum_{m=0}^{\infty} p_m \mathcal{N}(\beta, \mu_\beta, \sigma_{\beta,m}^2) \tag{6.6}$$

where $\mathcal{N}(\beta, \mu_\beta, \sigma_{\beta,m}^2)$ is a Gaussian random variable with mean $\mu_\beta = \mathbf{g}^T\mathbf{W}\mu_\mathbf{n}$ and variance $\sigma_{\beta,m}^2 = \mathbf{g}^T\mathbf{W}\sigma_\mathbf{N}\mathbf{W}^T\mathbf{g} + \sigma_m^2$, $\sigma_\mathbf{N} = \varepsilon\left\{\mathbf{n}\mathbf{n}^T\right\}$. Moreover, s and β are mutually independent. Then, the joint distribution of s and β is given by

$$f(s,\beta) = f(s) \times f(\beta) = \sum_{m=0}^{\infty} p_m \mathcal{N}(s, \beta, \mu_m, \sigma_m), \tag{6.7}$$

where $\mu_m = \begin{bmatrix}\mu_s & \mu_\beta\end{bmatrix}$ and $\sigma_m = \begin{bmatrix}\sigma_s^2 & 0;0 & \sigma_{\beta,m}^2\end{bmatrix}$. Now, from equation (6.5) we have,

$$\begin{bmatrix} z \\ s \end{bmatrix} = \begin{bmatrix} \alpha s + \beta \\ s \end{bmatrix} = \begin{bmatrix} \alpha & I \\ I & 0 \end{bmatrix} \begin{bmatrix} s \\ \beta \end{bmatrix} = \mathbf{C} \begin{bmatrix} s \\ \beta \end{bmatrix}, \tag{6.8}$$

It is well known that if s and β are jointly Gaussian, then z and s will also be jointly Gaussian, since the linear transformation of a Gaussian vector is Gaussian too (Kay, 1993, pg. 325). However, it holds for GM also and hence $[z,s]^T = \mathbf{C}[s,\beta]^T$ is also jointly GM with Flam *et al.* (2012)

$$f(z,s) = \sum_{m=0}^{\infty} p_m \mathcal{N}(z, s, \mathbf{C}\mu_\mathbf{m}, \mathbf{C}\sigma_\mathbf{m}\mathbf{C}^T), \tag{6.9}$$

where,

$$\mathbf{C}\mu_{\mathbf{m}} = \begin{bmatrix} \alpha & I \\ I & 0 \end{bmatrix} \begin{bmatrix} \mu_s \\ \mu_\beta \end{bmatrix} = \begin{bmatrix} \alpha\mu_s + \mu_\beta \\ \mu_s \end{bmatrix} = \begin{bmatrix} \mu_z^m \\ \mu_s \end{bmatrix}, \tag{6.10}$$

and

$$\mathbf{C}\sigma_{\mathbf{m}}\mathbf{C}^T = \begin{bmatrix} \alpha\sigma_s^2\alpha^T + \sigma_{\beta,m}^2 & \alpha\sigma_s^2 \\ \sigma_s^2\alpha^T & \sigma_s^2 \end{bmatrix} = \begin{bmatrix} \sigma_{z,m}^2 & \sigma_{zs}^2 \\ \sigma_{sz}^2 & \sigma_s^2 \end{bmatrix}. \tag{6.11}$$

Now, from the joint distribution of (6.9), the conditional PDF of s given z can be evaluated as

$$f(s|z) = \frac{f(s,z)}{f(z)} = \sum_{m=0}^{\infty} \chi_m(z)\mathcal{N}(s, \mu_{s|z}^m(z), \Sigma_{s|z}^m(z)). \tag{6.12}$$

Where the third equality comes from (Kay, 1993, Theorem 10.3) and considering

$$\chi_m(z) = \frac{p_m \mathcal{N}(z, \mu_z^m, \sigma_{z,m}^2)}{\sum_{m=0}^{\infty} p_m \mathcal{N}(z, \mu_z^m, \sigma_{z,m}^2)}. \tag{6.13}$$

Using (Kay, 1993, Theorem 10.3), we can write

$$\mu_{s|z}^m(z) = \mu_s + \frac{\sigma_s^2 \mathbf{h}^T \mathbf{W}^T \mathbf{g}}{\mathbf{g}^T \mathbf{W}\mathbf{h}\sigma_s^2 \mathbf{h}^T \mathbf{W}^T \mathbf{g} + \mathbf{g}^T \mathbf{W}\sigma_{\mathbf{N}}\mathbf{W}^T \mathbf{g} + \sigma_m^2} \left(z - \mu_z^m\right) \tag{6.14}$$

and,

$$\Sigma_{s|z}^m(z) = \sigma_s^2 - \frac{\sigma_s^2 \mathbf{h}^T \mathbf{W}^T \mathbf{g}\mathbf{g}^T \mathbf{W}\mathbf{h}\sigma_s^2}{\mathbf{g}^T \mathbf{W}\mathbf{h}\sigma_s^2 \mathbf{h}^T \mathbf{W}^T \mathbf{g} + \mathbf{g}^T \mathbf{W}\sigma_{\mathbf{N}}\mathbf{W}^T \mathbf{g} + \sigma_m^2}. \tag{6.15}$$

Hence, using equation (6.4) and (6.12), the MMSE estimation of s given z is obtained by

$$\begin{aligned} \hat{s} &= \int s \sum_{m=0}^{\infty} \chi_m(z)\mathcal{N}(s, \mu_{s|z}^m(z), \Sigma_{s|z}^m(z))ds, \\ &= \sum_{m=0}^{\infty} \chi_m(z)\mu_{s|z}^m(z). \end{aligned} \tag{6.16}$$

Where $\chi_m(z)$ and $\mu_{s|z}^m(z)$ are defined in (6.13) and (6.14), respectively. Equation (6.16) highlights how the MMSE OBE depends on the signal, noise, and channel parameters for the proposed scenario. In the special case of when both n_i and ϑ are Gaussian as in Xiao *et al.* (2008),

the corresponding MMSE estimation of s given z is given by

$$\hat{s} = \frac{\sigma_s^2 \mathbf{h}^T \mathbf{W}^T \mathbf{g}}{\mathbf{g}^T \mathbf{W} \mathbf{h} \sigma_s^2 \mathbf{h}^T \mathbf{W}^T \mathbf{g} + \mathbf{g}^T \mathbf{W} \sigma_{\mathbf{N}} \mathbf{W}^T \mathbf{g} + \sigma_\vartheta^2} z. \tag{6.17}$$

Which is equivalent to the expression in (Xiao *et al.*, 2008, pp. 760). It should also be noted that (6.16) is equivalent to the expression of the OBE in (Banelli, 2013, eqn. (8)) in the special case of when $\mu_s = 0$ and z is the measurement, for a point-to-point scenario.

6.4.1 Distortion Analysis

The distortion of this scheme is evaluated in terms of MSE and it can be obtained by

$$\begin{aligned} D &\equiv \varepsilon\left\{(s-\hat{s})^2\right\} = \int_s \int_z \left(s-\mu_{s|z}\right)^2 f(s,z)\,ds\,dz, && (6.18)\\ &= \int_s \int_z \left(s-\mu_{s|z}\right)^2 f(s|z) f(z)\,ds\,dz && (6.19)\\ &= \int_z \Sigma_{s|z} f(z)\,dz, \end{aligned}$$

where the posteriori covariance $\Sigma_{s|z}$ can be obtained as derived in Flam *et al.* (2012)

$$\Sigma_{s|z} = \sum_{m=0}^{\infty} \chi_m(z) \left(\Sigma_{s|z}^m + \left(\mu_{s|z}^m\right)^2\right) - \left(\mu_{s|z}\right)^2. \tag{6.20}$$

Hence, from equation (6.20) we have

$$\begin{aligned} D &= \int_z \sum_{m=0}^{\infty} \chi_m(z) \left(\Sigma_{s|z}^m + \left(\mu_{s|z}^m\right)^2 - \left(\mu_{s|z}\right)^2\right) f(z)\,dz,\\ &= \sum_{m=0}^{\infty} p_m \int_z \left(\Sigma_{s|z}^m + \left(\mu_{s|z}^m\right)^2 - \left(\mu_{s|z}\right)^2\right) f_m(z)\,dz, && (6.21) \end{aligned}$$

where $f_m(z) = \mathcal{N}(z, \mu_z^m, \sigma_{z,m}^2)$. However, equation (6.21) is similar to the expression in (Flam *et al.*, 2012, eqn. (21)) and can not be solved analytically. Hence, we may derive its bounds. In this vein, a lower bound (LB) is obtained under the hypothetical assumption that there is no uncertainty about the impulsive component m and the Rayleigh channel state information,

i.e., the genie condition. Following the same procedure as in Flam *et al.* (2012), the LB (D_{LB}) under this consideration can be obtained as

$$D_{LB} = \sum_{m=0}^{\infty} p_m \Sigma_{s|z}^{m}(z). \tag{6.22}$$

Where $\Sigma_{s|z}^{m}(z)$ is defined in (6.15). To derive the upper bound (D_{UB}), as in Flam *et al.* (2012), we invoke the LMMSE estimator since the LMMSE obtains the smallest MSE among all the estimators which are linear in the observations Flam *et al.* (2012). The MSE of the LMMSE estimator for this scheme is

$$D_{UB} = \sigma_s^2 - \frac{\sigma_s^2 \mathbf{h}^T \mathbf{W}^T \mathbf{g}\mathbf{g}^T \mathbf{W}\mathbf{h}\sigma_s^2}{\mathbf{g}^T \mathbf{W}\mathbf{h}\sigma_s^2 \mathbf{h}^T \mathbf{W}^T \mathbf{g} + \mathbf{g}^T \mathbf{W}\sigma_{\mathbf{N}} \mathbf{W}^T \mathbf{g} + \sigma_{\vartheta}^2}. \tag{6.23}$$

6.5 Numerical Results

In this section, the performance of MMSE optimal Bayesian estimator and distortion parameter bounds are evaluated under AWGN, and Middleton class-A noise over Rayleigh quasi-static flat fading channel with respect to the communication signal-to-noise ratio (SNR). Here, the communication SNR is defined as $\sigma_h^2\sigma_s^2+\sigma_n^2/\sigma_{\vartheta}^2$ and the measurement SNR as $\sigma_s^2/\sigma_n^2 = 0$ dB, where $\sigma_s^2 = 1$. In this model, a total number of 10 sensor nodes transmit with equal power their observations to the FC using AF strategy. The total transmission power of all the sensor nodes is $P_T = 1$ dB. Moreover, the channel fading have variances $\sigma_h^2 = \sigma_g^2 = 1$. The Middleton class-A model has the total number of impulsive sources which is equal to 30 and $\Gamma = 0.01$. As in Banelli (2013), it is assumed that the impulsive noise parameters are known at the receiver side.

Fig. 6.2 shows the input-output characteristics of MMSE OBE using equation (6.16) for different values of the impulsive index A. As observed in Fig. 6.2, when the value of A increases, the impulsive noise becomes closer to the Gaussian noise and the input-output characteristics of MMSE OBE tend to the well-known LMMSE estimation which is optimal in the case of Gaus-

sian noise. On the other hand, when the value of A decreases, the environment becomes more impulsive as indicated by rare impulsive events and the input-output characteristic becomes more non-linear. Thus, similar to point-to-point scenario, the presence of impulsive noise introduce non-linearity in the measurement z. Hence, the MMSE optimal Bayesian estimator becomes non-linear under that scenario.

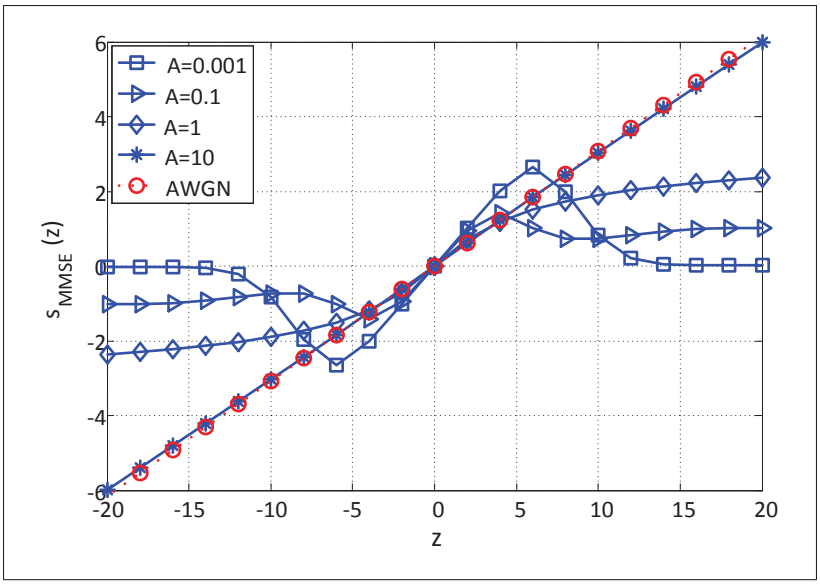

Figure 6.2 Impact of the impulsive index A on the input-output characteristics of MMSE optimal Bayesian estimation. It is assumed that both the measurement SNR and the communication SNR are equal to 0 dB

To visualize the effect of the non-linearity, we also have plotted the distortion performance for the proposed scenario. Fig. 6.3 shows the simulated MSE performances of the optimal MMSE estimation along with its derived analytical upper and lower bounds for different values of the impulsive index A. The simulated MSE performance is obtained by calculating the sample-mean of $(s-\mu_{s|z})^2$. From Fig. 6.3, it is seen that at both low and high SNR values the MMSE performs as the LMMSE (upper bound) estimator. However, at intermediate SNR levels, the MMSE estimator performs significantly better than the LMMSE estimator by using the impulsive noise characteristics in the estimation process and the amount of improvement

depends on the impulsive nature as indicated by different values of A. From Fig. 6.3, it is further confirmed that as the value of A increases, the nature of impulsive noise becomes more Gaussian and the MSE performance of MMSE estimator approaches to the LMMSE estimator for all SNR values. Under this situation, the performance gap between the lower and the upper bounds decreases and approaches to zero for sufficiently larger values of A. On the other hand, for small values of A, the impulses are less dominant (more impulsive) and the performance gap between the upper and lower bounds becomes larger. The MMSE estimator approaches the lower bound under this scenario. Interestingly, when the impulsive events are very rare, the MMSE converges to the lower bound. Hence, the derived lower bound is very tight for highly impulsive noise environments.

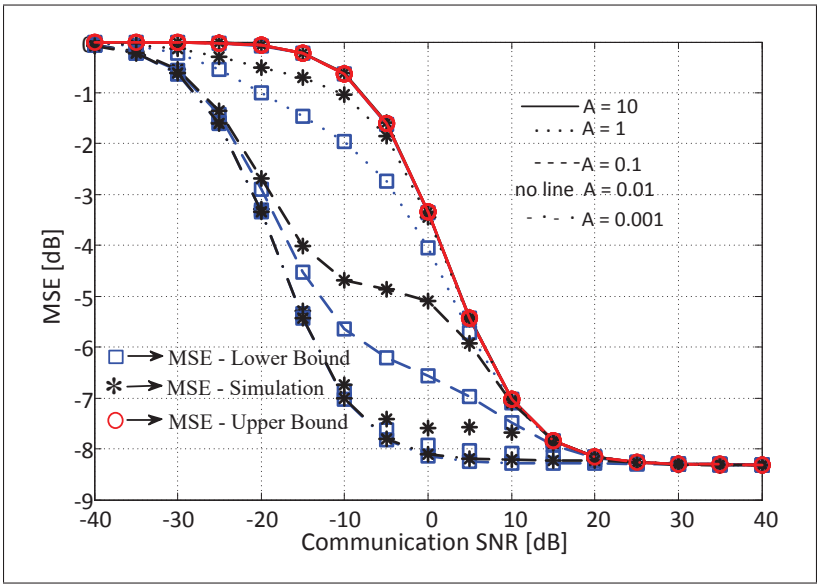

Figure 6.3 Impact of the impulsive index A on the distortion performance. It is assumed that the measurement SNR is equal to 0 dB

Lastly, Fig. 6.4 shows the simulated MSE performances of the proposed system as a function of the total number of sensor nodes under different values of the impulsive index A. From Fig. 6.4, it is seen that similar to Gaussian case, the distortion performance decreases exponentially as the value of M increases while keeping the total transmission power constant. Also, for

sufficiently large value of M the performance of the proposed non-linear MMSE estimator converges with the LMMSE estimator irrespective of the value of A.

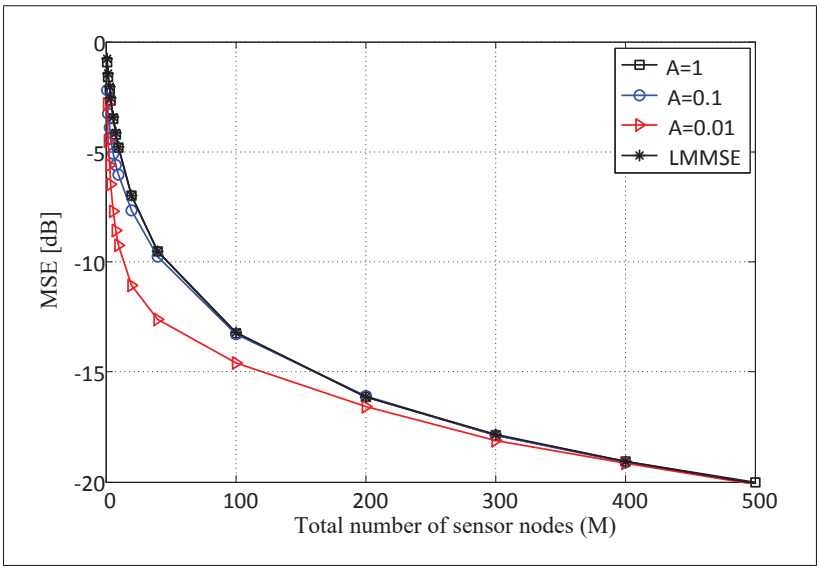

Figure 6.4 Plot of distortion versus the total number of sensor nodes under different values of impulsive index A. It is assumed that both the measurement SNR and the communication SNR are equal to 0 dB

6.6 Conclusion

WSN consists of spatially distributed sensors, identified as a promising technology for unknown parameters estimations. In this letter, the distributed estimation of a scalar Gaussian source in WSNs in the presence of Middleton class-A noise is considered. For this scheme, a closed-form expression for the MMSE optimal Bayesian estimation and the upper and lower bounds for the MSE are derived to show the effect of impulsive noise. It is shown that the performance improvement of the derived optimal MMSE estimator over the LMMSE estimator depends on the impulsive nature of the noise and on the operating SNR regions.

CHAPTER 7

CONCLUSION AND RECOMMENDATIONS

7.1 Conclusion

It is well-known that the most significant amount of GHG emissions (mostly carbon dioxide) all around the world in recent years came from the electricity sector. This is because there is an increase in electricity consumption due to the increasing rate of population and industrialization whereas power systems mainly use fossil fuels for electricity generation. To avert the severe impacts of climate change on human and natural systems, carbon dioxide (CO2) emissions from the electric power sector must rapidly decrease. One solution to reduce GHG emissions from electricity generation is to modernize the power grid, in which ICTs are playing a key role. Indeed, this novel concept has emerged to manage the increasing demand for energy resources while maintaining the CO2 emission at a certain level by enhancing the energy usage efficiency. The electric power research institute (EPRI) found that a full deployment of a smart grid and the new technologies that it enables can reduce GHG emissions by 13% - 25%. Other possible potential benefits of the smart grid applications include decreasing blackouts, ensuring safer and more secure delivery of electricity, lowering the power cost by giving more control over the power use, reducing expenses for energy production, increasing grid visibility, and more significantly making Canada's energy autonomous.

For a reliable smart grid, monitoring and control of power system parameters in the transmission and distribution segments as well as the substation devices is crucial. In order to allow such advanced functionalities and avoid possible disruptions in electric systems due to unexpected failures, a highly reliable, scalable, secure, cost-effective, and robust communication network must be operational within the power grid that conveys data from monitoring sensors in the field back to engineers in the control room. In this vein, the most promising method of smart grid communication explored in the literature is based on WSNs due to their inherent characteristics of being low-cost and flexible as well as their wider coverage, self-organization

and rapid deployment. Also, it circumvents the typical constraints associated with the installation of wired communication systems. Therefore, considerable efforts have been given to design a stable and efficient WSN for smart grid communications since the beginning of smart grid projects. However, harsh and complex electric power system environments pose great challenges on the reliability of wireless sensor nodes communications because of obstructions, strong RF interference, and noise. More specifically, the noise characteristics that are usually observed in smart grid scenarios are highly non-Gaussian and are inherently impulsive in nature. Impulsive noise degrades the system performance significantly because its spectrum is more powerful than the Gaussian noise. Also, the impulsive noise measurement campaigns in smart grid environments show that the impulses occur in bursts. Hence conventional WSNs explored in the literature for smart grid communication showed poor performance under such scenarios.

Therefore, the main research goal of this dissertation is to lay down the fundamental basis for the development of a robust and efficient WSN for smart grid communication to realize real-world smart grid applications. With this aim in mind, conclusively speaking, there are three main aspects of this dissertation: (i) investigation and performance analysis of impulsive noise mitigation techniques for point-to-point single-carrier communication systems impaired by bursty impulsive noise; (ii) design and performance analysis of a collaborative WSN for smart grid monitoring by considering the RF noise model in the design process, a particular intension is given to how the time-correlation among the noise samples can be taken into account; (iii) optimal MMSE estimation of physical parameters like the temperature, current, voltage, etc., typically modeled by a scalar Gaussian source in the presence of impulsive noise.To be specific, the aforementioned contributions are further detailed as follows:

- The first aspect of this dissertation (Chapter 2) evaluated some practical impulsive noise mitigation techniques for LDPC coded single-carrier point-to-point communication systems subject to bursty impulsive noise modelled by a Markov-Gaussian process. The provided simulation results showed that the LLR-based impulsive noise mitigation technique with the

MAP detection criterion outperforms the simple but more popular clipping, blanking, and combined clipping/blanking schemes at the expense of higher computational complexity.

- The second aspect of this dissertation contains two sub-contributions and are provided in Chapters 3 and 4, respectively. The performance analysis of a single relay DF collaborative WSN scheme over channels impaired by bursty impulsive noise has been conducted in Chapter 3. For this channel, the BER performances of DT and single relay collaborative WSN schemes using M-PSK modulation in the presence of Rayleigh fading with a MAP receiver are evaluated. From the obtained results, it is seen that the DF collaborative WSN in bursty impulsive noise channels still achieves the space diversity and performs significantly better than DT under the same power consumption. Moreover, the proposed MAP receiver attains the lower bound derived for the DF collaborative WSN scheme, and leads to large performance gains in terms of reliability compared to the conventional receiving criteria which were optimized for the AWGN channel and the memoryless impulsive noise channel.

- As a continuation of the single relay collaborative WSN scheme in Chapter 3, a novel relay selection protocol for a DF collaborative WSN taking into account the bursty impulsive noise was proposed in Chapter 4. The proposed protocol chooses the N'th best relay considering both the channel gains and the states of the impulsive noise of the source-relay and relay-destination links. For this scheme, to obtain the state of the impulsive noise, we propose a state detection algorithm using MAP detection. To analyze the performance of the proposed protocol, we first derive closed-form expressions for the PDF of the received SNR assuming all the relays know the state of impulsive noise perfectly. Then, these PDFs are used to derive closed-form expressions for the BER and the outage probability. Finally, we also derive the asymptotic BER and outage expressions to quantify the diversity benefits. We show that the proposed MAP-based N'th BRS protocol attains the derived genie-aided analytical results and outperforms the conventional relay selection protocol, optimized for the Gaussian case, and which does not take into account the impulsive noise memory.

- The aforementioned chapters talked about the reliable detection of finite alphabets in the presence of bursty impulsive noise. The performance of the optimal MMSE estimation for a

scalar Gaussian source impaired by impulsive noise has been conducted in Chapters 5 and 6, respectively. In Chapter 5, the MMSE OBE for a scalar Gaussian source, in the presence of bursty impulsive noise, as essentially encountered within power substations is considered. Clearly, it is observed that the presence of bursty impulsive noise makes the input-output characteristics of MMSE OBE non-linear. To handle the non-linearity, we propose a novel MMSE estimator, based on the detection of the unobservable states of the noise process, using the MAP detector. Resultantly, the proposed MAP-based MMSE estimator is shown to achieve the lower bound derived for the proposed scenario and outperform the various MMSE estimators that neglect the noise memory.

- On the other hand, in chapter 6, the distributed estimation of a scalar Gaussian source in WSNs in the presence of Middleton class-A noise is considered. For this scheme, a closed-form expression for the MMSE optimal Bayesian estimation and the upper and lower bounds for the MSE are derived to show the effect of impulsive noise. It is shown that the performance improvement of the derived optimal MMSE estimator over the LMMSE estimator depends on the impulsive nature of the noise and on the operating SNR regions.

The achievement of this project is expected to facilitate the industrial implementation of collaborative WSN based smart grid communication systems that will help in achieving the target of reducing Canada's 2005 greenhouse gas emission by 30% by 2030.

7.2 Future work

The contributions presented in this dissertation could be extended to the following future research directions:

7.2.1 Resource constraints of sensor nodes

In WSNs, all nodes are equipped with a battery and hence the sensor nodes applications are constrained by a limited battery life. Replacing or charging the batteries in WSNs may take time and be costly for a large number of sensors. This is particularly important for substation

and high voltage transmission line monitoring applications due to the relative inaccessibility of the regions for safety and regulatory purposes. To solve the issue of limited battery life of sensor nodes, many energy efficient protocols have been widely investigated in the literature where various energy-efficient medium access and routing protocols and duty-cycling have been considered. However, these techniques are able to provide only limited lifetime Erol-Kantarci & Mouftah (2012). On the other hand, energy harvesting methods play an important role in the lifetime of WSNs. By harvesting the energy from the ambient resources it is possible to extend the lifetime of the sensor nodes. In particular, RF signals can concurrently carry information and energy signals, also known as simultaneous wireless information and power transfer (SWIPT), which has attracted significant research interest recently Kaddoum, G., Tran, H.-V., Kong, L. & Atallah, M. (2016b); Tran, H.-V., Kaddoum, G. & Truong, K. T. (2018); Zhou, X., Zhang, R. & Ho, C. K. (2013). However, most existing works on this topic assume negligible background noise power. The performance of wireless energy harvesting systems with consideration of the practical impulsive noise environments is worthwhile to be examined and analyzed in the future research directions.

7.2.2 Effect of Network Geometry/Nodes' Locations Distributions

A typical WSN consists of a large number of sensor nodes deployed in an area of interest to collect specific information about the surrounding environment. In our previous works, it is assumed that the sensor nodes' locations are known. However, in most cases of WSNs applications, the sensor nodes are distributed randomly and it is hard to know the locations of the sensor nodes' due to harsh geographic conditions which is exactly the case in smart grid applications. In such cases, the nodes' locations distribution can be modeled by a two-dimensional Poisson point process (PPP) Haenggi, M. (2005); Sattar, Z., Evangelista, J. V. D. C., Kaddoum, G. & Batani, N. (2019). As a result, how the sensor nodes' locations distribution affects the performance will be a promising direction.

7.2.3 Security

The wireless nature of WSNs also makes WSN-based smart grid applications vulnerable to various external attacks, physical and cyber threats. Hence, security is an essential issue in the design of WSN-based smart grid communications in order to securely transmit the data from the end-users to the data collection centers. In addition to cyber security issues that have been widely investigated in the literature since the beginning of smart grid projects, one may also analyze the physical layer security aspects that have been hardly investigated in the smart grid scenario Atallah, M. & Kaddoum, G. (2019); Atallah, M., Alam, M. S. & Kaddoum, G. (2019); Jameel, F., Wyne, S., Kaddoum, G. & Duong, T. Q. (2018); Lee *et al.* (2012). How the performance of the later aspect can be improved by designing new advanced algorithms to satisfy smart grid scenarios needs further investigation.

7.2.4 Imperfect knowledge of noise parameters

As presented in the whole thesis, it is assumed that the availability of noise parameters are perfectly known at the receiver. Such an assumption is practically challenging in some scenarios. Towards this end, how to elaborate the influences led by the uncertainty of the noise parameters will be a promising direction.

APPENDIX I
PROOF FOR CHAPTER 4

Derivation of the Marginal PDF: Asymptotic case

In the high SNR regime, it is assumed that $1-e^{-x} \doteq x$. Then, from (4.27), we have

$$I_1 \doteq M\binom{M-1}{N-1}\frac{1}{\overline{\gamma}_{SR_m}\overline{\gamma}_{R_mD}}e^{-\frac{x}{\overline{\gamma}_{SR_m}}}\left(\frac{1}{\overline{\gamma}_a}\right)^{M-N}\int_{z=0}^{x} z^{M-N}e^{-\frac{z}{\overline{\gamma}_{R_mD}}}dz, \tag{A -1}$$

Assuming $\frac{z}{\overline{\gamma}_{R_mD}} = q$, (A -1) can be rearranged as

$$\begin{aligned} I_1 &= \frac{C_M}{\overline{\gamma}_{SR_m}\overline{\gamma}_{R_mD}}e^{-\frac{x}{\overline{\gamma}_{SR_m}}}\left(\frac{1}{\overline{\gamma}_a}\right)^{M-N}\int_{z=0}^{\frac{x}{\overline{\gamma}_{R_mD}}} q^{M-N}e^{-q}dq, \\ &= \frac{C_M}{\overline{\gamma}_{SR_m}}e^{-\frac{x}{\overline{\gamma}_{SR_m}}}\left(\frac{1}{\overline{\gamma}_a}\right)^{M-N}\gamma(M-N+1,\frac{x}{\overline{\gamma}_{R_mD}}), \end{aligned} \tag{A -2}$$

where $\gamma(a,b)$ is the lower incomplete gamma function. At high SNR scenario, $x \approx 0$ and I_1 can be neglected. Again,

$$\begin{aligned} I_2 &= \frac{C_M}{\overline{\gamma}_{SR_m}\overline{\gamma}_{R_mD}}\left(\frac{x}{\overline{\gamma}_a}\right)^{M-N}e^{-\frac{x}{\overline{\gamma}_{SR_m}}}\int_{z=x}^{\infty} e^{-\frac{z}{\overline{\gamma}_{R_mD}}}dz, \\ &= M\binom{M-1}{N-1}\frac{1}{\overline{\gamma}_{SR_m}}\left(\frac{x}{\overline{\gamma}_a}\right)^{M-N}e^{-\frac{x}{\overline{\gamma}_a}}, \qquad \text{(A -3)} \\ &\approx M\binom{M-1}{N-1}\frac{1}{\overline{\gamma}_{SR_m}}\left(\frac{1}{\overline{\gamma}_a}\right)^{M-N}x^{M-N}. \qquad \text{(A -4)} \end{aligned}$$

Substituting I_1 and I_2 in (4.27), yields (4.57).

REFERENCES

Agba, B. L., Sacuto, F., Au, M., Labeau, F. & Gagnon, F. (2019). Impulsive Noise Measurements. In *Wireless Communications for Power Substations: RF Characterization and Modeling* (pp. 35–68). Springer.

Ahmed, I., Nasri, A., Michalopoulos, D. S., Schober, R. & Mallik, R. K. (2012). Relay subset selection and fair power allocation for best and partial relay selection in generic noise and interference. *IEEE Trans. Wireless Commun.*, 11(5), 1828–1839.

Akyildiz, I. F., Su, W., Sankarasubramaniam, Y. & Cayirci, E. (2002). Wireless sensor networks: a survey. *Computer networks*, 38(4), 393–422.

Al-Badarneh, Y. H., Georghiades, C. N. & Alouini, M.-S. (2018). Asymptotic Performance Analysis of the k-th Best Link Selection Over Wireless Fading Channels: An Extreme Value Theory Approach. *IEEE Trans. Veh. Technol.*, 67(7), 6652–6657.

Al-Badarneh, Y. H., Georghiades, C. N. & Alouini, M.-S. (2019). On the Asymptotic Throughput of the k-th Best Secondary User Selection in Cognitive Radio Systems. *Proc. IEEE Veh. Technol. Conf.*, pp. 1–5.

Al-Dharrab, S. & Uysal, M. (2009a). Cooperative diversity in the presence of impulsive noise. *IEEE Trans. Wireless Commun.*, 8(9), 4730–4739.

Al-Dharrab, S. & Uysal, M. (2009b). Cooperative diversity over fading channels with impulsive noise. *Proc IEEE Wireless Commun. Networking Conf.*, pp. 1–6.

Al-Naffouri, T. Y., Quadeer, A. A. & Caire, G. (2014). Impulse noise estimation and removal for OFDM systems. *IEEE Trans. Commun.*, 62(3), 976–989.

Alam, M. S. & Labeau, F. (2015a). Performance analysis of DF cooperative relaying over bursty impulsive noise channel. *IEEE Sixth International Conference on Smart Grid Communications(SmartGridComm'2015)*, pp. Accepted for publication.

Alam, M. S. & Labeau, F. (2015b). Performance analysis of DF cooperative relaying over bursty impulsive noise channel. *Proc. IEEE Int. Conf. Smart Grid Commun.*, pp. 374–379.

Alam, M. S. & Labeau, F. (2016a). Effect of Bursty Impulsive Noise on the Performance of Multi-relay DF Cooperative Relaying Scheme. *Proc. IEEE Veh. Technol. Conf.*, pp. 1–5.

Alam, M. S. & Labeau, F. (2016b). On relay selection in bursty impulsive noise channel. *Proc. IEEE Wireless Commun. Networking Conf.*, pp. 1–6.

Alam, M. S., Labeau, F. & Kaddoum, G. (2016). Performance analysis of DF cooperative relaying over bursty impulsive noise channel. *IEEE Trans. Commun.*, 64(7), 2848–2859.

Alam, M. S., Kaddoum, G. & Agba, B. (2018a). Performance analysis of distributed wireless sensor networks for Gaussian source estimation in the presence of impulsive noise. *IEEE Sig. Proc. Letters*, 25(6), 803–807.

Alam, M. S., Kaddoum, G. & Agba, B. L. (2018b). Bayesian MMSE estimation of a Gaussian source in the presence of bursty impulsive noise. *IEEE Commun. Letters*, 22(9), 1846–1849.

Alamouti, S. M. (1998). A simple transmit diversity technique for wireless communications. *IEEE J. Sel. Areas Commun.*, 16(8), 1451–1458.

Ali, I. B. S., Au, M., Agba, B. L. & Gagnon, F. (2015). Mitigation of impulsive interference in power substation with multi-antenna systems. *Proc. Int. Conf. Ubiquitous Wireless Broadband*, pp. 1–5.

Arnold, D. M., Loeliger, H.-A., Vontobel, P. O., Kavčić, A. & Zeng, W. (2006). Simulation-based computation of information rates for channels with memory. *IEEE Trans. Inf. Theory*, 52(8), 3498–3508.

Asiyo, M. O. & Afullo, T. J. (2017). Analysis of bursty impulsive noise in low-voltage indoor power line communication channels: local scaling behaviour. *SAIEE Africa Res. J.*, 108(3), 98–107.

Atallah, M. & Kaddoum, G. (2019). Design and Performance Analysis of Secure Multicasting Cooperative Protocol for Wireless Sensor Network Applications. *arXiv preprint arXiv:1902.07345*.

Atallah, M., Alam, M. S. & Kaddoum, G. (2019). Secrecy Analysis of Wireless Sensor Network in Smart Grid with Destination Assisted Jamming. *IET Commun.*

Aysal, T. C. & Barner, K. E. (2008). Constrained decentralized estimation over noisy channels for sensor networks. *IEEE Trans. Signal Process.*, 56(4), 1398–1410.

Aziz, A. A., Iwanami, Y. & Okamoto, E. (2009). Efficient combining technique with a low-complexity detect-and-forward relay for cooperative diversity scheme. *Proc. IEEE Region 10 Conf.*, pp. 1–6.

Bahl, L., Cocke, J., Jelinek, F. & Raviv, J. (1974). Optimal decoding of linear codes for minimizing symbol error rate. *IEEE Trans. Inf. Theory*, 20(2), 284–287.

Bai, T., Zhang, H., Zhang, R., Yang, L.-L., Al Rawi, A. F., Zhang, J. & Hanzo, L. (2017). Discrete multi-tone digital subscriber loop performance in the face of impulsive noise.

IEEE Access, 5, 10478–10495.

Banelli, P. (2013). Bayesian estimation of a Gaussian source in Middleton's class-A impulsive noise. *IEEE Signal Process. Lett.*, 20(10), 956–959.

Berrou, C., Glavieux, A. & Thitimajshima, P. (1993). Near Shannon limit error-correcting coding and decoding: Turbo-codes. 1. *Proc. IEEE Int. Conf. Commun.*, 2, 1064–1070.

Blackard, K. L., Rappaport, T. S. & Bostian, C. W. (1993). Measurements and models of radio frequency impulsive noise for indoor wireless communications. *IEEE J. Sel. Areas Commun.*, 11(7), 991–1001.

Bletsas, A., Khisti, A., Reed, D. P. & Lippman, A. (2006). A simple cooperative diversity method based on network path selection. *IEEE J. Sel. Areas Commun.*, 24(3), 659–672.

Brak, M. E., Brak, S. E., Essaaidi, M. & Benhaddou, D. (2014). Wireless Sensor Network applications in smart grid. *Proc. Int. Renewable and Sustainable Energy Conf.*, pp. 587–592.

Changcai, H. & Weiling, W. (2008). Distributed generalized low-density codes for multiple relay cooperative communications. *EURASIP J. Wireless Commun. Net.*, 2008.

Cheffena, M. (2012). Industrial wireless sensor networks: channel modeling and performance evaluation. *EURASIP J. Wireless Commun. Net.*, 2012(1), 297.

Cheng, P., Wang, L., Zhen, B. & Wang, S. (2011). Feasibility study of applying LTE to Smart Grid. *Proc. First Int. Workshop Smart Grid Modeling and Simulation*, pp. 108–113.

Cover, T. & Gamal, A. E. (1979). Capacity theorems for the relay channel. *IEEE Trans. Inf. Theory*, 25(5), 572–584.

Cui, S., Xiao, J.-J., Goldsmith, A. J., Luo, Z.-Q. & Poor, H. V. (2007). Estimation Diversity and Energy Efficiency in Distributed Sensing. *IEEE Trans. Signal Process.*, 55(9), 4683–4695.

David, H. A. & Nagaraja, H. N. (2003). *Order Statistics*. Hoboken, NJ, USA: Wiley.

Erol-Kantarci, M. & Mouftah, H. T. (2011). Wireless sensor networks for smart grid applications. *Proc. Saudi Int. Electronics, Commun. Photonics Conf.*, pp. 1–6.

Erol-Kantarci, M. & Mouftah, H. T. (2012). Suresense: sustainable wireless rechargeable sensor networks for the smart grid. *IEEE Wireless Commun.*, 19(3), 30–36.

Fadel, E., Gungor, V., Nassef, L., Akkari, N., Maik, M. A., Almasri, S. & Akyildiz, I. F. (2015). A survey on wireless sensor networks for smart grid. *Computer Communications*, 71, 22–33.

Fang, X., Misra, S., Xue, G. & Yang, D. (2012). Smart grid−The new and improved power grid: A survey. *IEEE Commun. Surveys Tuts.*, 14(4), 944–980.

Fareed, M. M. & Uysal, M. (2009). On relay selection for decode-and-forward relaying. *IEEE Trans. Wireless Commun.*, 8(7), 3341–3346.

Farhangi, H. (2010). The path of the smart grid. *IEEE Power Energy Mag.*, 8(1), 18–28.

Ferreira, H., Lampe, L., Newbury, J. & Swart, T. (2010). *Power Line Communications: theory and Applications for Narrowband and Broadband Communications over Power Lines*. Wiley.

Fertonani, D. & Colavolpe, G. (2009). On reliable communications over channels impaired by bursty impulse noise. *IEEE Trans. Commun.*, 57(7), 2024–2030.

Fertonani, D., Barbieri, A. & Colavolpe, G. (2007). Reduced-complexity BCJR algorithm for turbo equalization. *IEEE Trans. Commun.*, 55(12), 2279–2287.

Flam, J. T., Chatterjee, S., Kansanen, K. & Ekman, T. (2011). Minimum mean square error estimation under gaussian mixture statistics. *arXiv e-print, 2011 [Oneline]. Available: arXiv:1108.3410*.

Flåm, J. T., Jaldén, J. & Chatterjee, S. (2011). Gaussian mixture modeling for source localization. *Proc. IEEE Int. Conf. Acoust., Speech Signal Process.*, pp. 2604–2607.

Flam, J. T., Chatterjee, S., Kansanen, K. & Ekman, T. (2012). On MMSE estimation: A linear model under Gaussian mixture statistics. *IEEE Trans. Signal Process.*, 60(7), 3840–3845.

Gastpar, M. & Vetterli, M. (2003). Source-channel communication in sensor networks. *Proc. Inf. Processing Sensor Net.*, pp. 162–177.

Ghosh, M. (1996). Analysis of the effect of impulse noise on multicarrier and single carrier QAM systems. *IEEE Trans. Commun.*, 44(2), 145–147.

Goldsmith, A. (2005). *Wireless communications*. Cambridge university press.

Gungor, V. C. & Lambert, F. C. (2006). A survey on communication networks for electric system automation. *Computer Networks*, 50(7), 877–897.

Gungor, V. C., Lu, B. & Hancke, G. P. (2010). Opportunities and challenges of wireless sensor networks in smart grid. *IEEE Trans. Ind. Electron.*, 57(10), 3557–3564.

Gungor, V. C., Sahin, D., Kocak, T., Ergut, S., Buccella, C., Cecati, C. & Hancke, G. P. (2011). Smart grid technologies: communication technologies and standards. *IEEE Trans. Ind. Informat.*, 7(4), 529–539.

Haas, Z. J., Halpern, J. Y. & Li, L. (2006). Gossip-based ad hoc routing. *IEEE/ACM Trans. Networking*, 14(3), 479–491.

Hadi, A., Rabie, K. M. & Alsusa, E. (2016). Polar codes based OFDM-PLC systems in the presence of Middleton class-A noise. *10th International Symposium on Communication Systems, Networks and Digital Signal Processing*, pp. 1–6.

Hadjtaieb, A., Chelli, A., Alouini, M.-S. & Boujemaa, H. (2014). Performance analysis of selective decode-and-forward multinode incremental relaying with maximal ratio combining. *Proc. Int. Conf. Commun. Networking*, pp. 1–6.

Haenggi, M. (2005). On distances in uniformly random networks. *IEEE Trans. Inf. Theory*, 51(10), 3584–3586.

Hikita, M., Yamashita, H., Hoshino, T., Kato, T., Hayakawa, N., Ueda, T. & Okubo, H. (1998). Electromagnetic noise spectrum caused by partial discharge in air at high voltage substations. *IEEE Trans. Power Del.*, 13(2), 434–439.

Hossain, E., Han, Z. & Poor, H. V. (2012). *Smart Grid Communications and Networking*. Cambridge University Press.

Hunter, T. E. & Nosratinia, A. (2006). Diversity through coded cooperation. *IEEE Trans. Wireless Commun.*, 5(2), 283–289.

Huynh, K. Q. & Aulin, T. (2012). Improved Iterative Decoders for Turbo-Coded Decode-and-Forward Relay Channels. *Proc. IEEE Int. Conf. Veh. Technol.*, pp. 1–5.

Ibrahim, A. S., Sadek, A. K., Su, W. & Liu, K. R. (2008). Cooperative communications with relay-selection: when to cooperate and whom to cooperate with? *IEEE Trans. Wireless Commun.*, 7(7), 2814–2827.

Ikki, S. S. & Ahmed, M. H. (2010). On the performance of cooperative-diversity networks with the Nth best-relay selection scheme. *IEEE Trans. Commun.*, 58(11), 3062–3069.

Jameel, F., Wyne, S., Kaddoum, G. & Duong, T. Q. (2018). A comprehensive survey on cooperative relaying and jamming strategies for physical layer security. *IEEE Communications Surveys & Tutorials*.

Jayakody, D. N. & Flanagan, M. F. (2015). A soft forwarding scheme for an arbitrary signal constellations in cooperative wireless networks. *IEEE Trans. Veh. Technol.*, 99.

Jayakody, D. N., Li, J. & Flanagan, M. F. (2015). A novel multilevel soft quantization based scheme for multiple access relay network in cooperative wireless networks. *IEEE Trans. Veh. Technol.*, 99.

J.Medhi. (2003). *Stochastic Models in Queuing Theory*. Orlando, USA: Academic Press.

Kaddoum, G., Tadayon, N. & Soujeri, E. (2016a). Performance of DCSK system with blanking circuit for power-line communications. *Circuits and Systems (ISCAS), 2016 IEEE International Symposium on*, pp. 1118–1121.

Kaddoum, G., Tran, H.-V., Kong, L. & Atallah, M. (2016b). Design of simultaneous wireless information and power transfer scheme for short reference DCSK communication systems. *IEEE Trans. Commun.*, 65(1), 431–443.

Kanemoto, H., Miyamoto, S. & Morinaga, N. (1998). Statistical model of microwave oven interference and optimum reception. *Proc. IEEE Int. Conf. Commun.*, 3, 1660–1664.

Kay, S. M. (1993). *Fundamentals of statistical signal processing, volume I: estimation theory*. Englewood Cliffs, NJ: Prentice Hall.

Khan, F., ur Rehman, A., Arif, M., Aftab, M. & Jadoon, B. K. (2016). A survey of communication technologies for smart grid connectivity. *Proc. Int. Conf. Comput., Electronic and Electrical Engineering*, pp. 256–261.

Kramer, G., Gastpar, M. & Gupta, P. (2005). Cooperative strategies and capacity theorems for relay networks. *IEEE Trans. Inf. Theory*, 51(9), 3037–3063.

Krikidis, I., Thompson, J., McLaughlin, S. & Goertz, N. (2008). Amplify-and-forward with partial relay selection. *IEEE Commun. Lett.*, 12(4), 235–237.

Krikidis, I., Thompson, J. S., McLaughlin, S. & Goertz, N. (2009). Max-min relay selection for legacy amplify-and-forward systems with interference. *IEEE Trans. Wireless Commun.*, 8(6), 3016–3027.

Kundu, A., Chatterjee, S., Murthy, A. S. & Sreenivas, T. (2008). GMM based Bayesian approach to speech enhancement in signal/transform domain. *Proc. IEEE Int. Conf. Acoust., Speech Signal Process.*, pp. 4893–4896.

Kwadjane, J.-M., Vrigneau, B., Langlais, C., Cocheril, Y. & Berbineau, M. (2013). Performance of the max-d min precoder in impulsive noise for railway communications in tunnels. *Proc. Int. Conf. Telecommun.*, pp. 390–395.

Lai, L., Liu, K. & El Gamal, H. (2006). The three-node wireless network: achievable rates and cooperation strategies. *IEEE Trans. Inf. Theory*, 52(3), 805–828.

Lampe, L. (2011). Bursty impulse noise detection by compressed sensing. *Proc. Int. Symposium Power Line Communications and Its Applications*, pp. 29–34.

Laneman, J. N. & Wornell, G. W. (2003). Distributed space-time-coded protocols for exploiting cooperative diversity in wireless networks. *IEEE Trans. Inf. Theory*, 49(10), 2415–2425.

Laneman, J. N., Tse, D. N. & Wornell, G. W. (2004). Cooperative diversity in wireless networks: efficient protocols and outage behavior. *IEEE Trans. Inf. Theory*, 50(12), 3062–3080.

Lee, E.-K., Gerla, M. & Oh, S. Y. (2012). Physical layer security in wireless smart grid. *IEEE Commun. Mag.*, 50(8), 46–52.

Lee, K. & Hanzo, L. (2009). Iterative detection and decoding for hard-decision forwarding aided cooperative spatial multiplexing. *Proc. IEEE Int. Conf. Commun.*, pp. 1–5.

Li, T., Mow, W. H. & Siu, M. (2008). Joint erasure marking and Viterbi decoding algorithm for unknown impulsive noise channels. *IEEE Trans. Wireless Commun.*, 7(9), 3407–3416.

Liang, D., Ng, S. X. & Hanzo, L. (2010). Relay-Induced Error Propagation Reduction for Decode-and-Forward Cooperative Communications. *Proc. IEEE Global Telecommun. Conf.*, pp. 1–5.

Lin, J., Nassar, M. & Evans, B. L. (2013). Impulsive noise mitigation in powerline communications using sparse Bayesian learning. *IEEE J. Sel. Areas Commun.*, 31(7), 1172–1183.

Lin, J., Zhu, B., Zeng, P., Liang, W., Yu, H. & Xiao, Y. (2015). Monitoring power transmission lines using a wireless sensor network. *Wirel. Commun. Mob. Comput.*, 15(14), 1799–1821.

Liu, K. R. (2009). *Cooperative communications and networking*. Cambridge University Press.

Liu, Y. (2012). Wireless sensor network applications in smart grid: recent trends and challenges. *Int. J. Distrib. Sensor Net.*, 2012, Article ID 492819.

Lo, C.-H. & Ansari, N. (2013). Decentralized controls and communications for autonomous distribution networks in smart grid. *IEEE Trans. Smart Grid*, 4(1), 66–77.

Mackay, D. J. C. (2009). Digital Video Broadcasting (DVB), Second generation framing structure, channel coding and modulation systems for Broadcasting, Interactive Services, News Gathering and other broadband satellite applications (DVB-S2). *ETSI Std. EN*, 302(307), V1.2.1.

Madi, G., Sacuto, F., Vrigneau, B., Agba, B. L., Pousset, Y., Vauzelle, R. & Gagnon, F. (2011). Impacts of impulsive noise from partial discharges on wireless systems performance: application to MIMO precoders. *EURASIP J. Wireless Commun. Netw.*, 186(1), 1–12.

Matta, N., Ranhim-Amoud, R., Merghem-Boulahia, L. & Jrad, A. (2012). A wireless sensor network for substation monitoring and control in the smart grid. *Proc. IEEE Int. Conf. Green Computing Commun.*, pp. 203–209.

Middleton, D. (1977). Statistical-physical models of electromagnetic interference. *IEEE Trans. Electromagn. Compat.*, EMC-19(3), 106–127.

Middleton, D. (1999). Non-Gaussian noise models in signal processing for telecommunications: new methods an results for class A and class B noise models. *IEEE Trans. Inf. Theory*, 45(4), 1129–1149.

Mitra, J. (2010). *Reliable Communication in Non-Gaussian Environments: receiver Design and Analytical Aspects*. (Ph.D. thesis, University of British Columbia).

Mitra, J. & Lampe, L. (2010). Convolutionally coded transmission over Markov-Gaussian channels: analysis and decoding metrics. *IEEE Trans. Commun.*, 58(7), 1939–1949.

Miyamoto, S. & Morinaga, N. (1997). Effect of microwave oven interference on the performance of digital radio communications systems. *Proc. IEEE Int. Conf. Commun.*, 1, 51–55.

Mushkin, M. & Bar-David, I. (1989). Capacity and coding for the Gilbert-Elliott channels. *IEEE Trans. Inf. Theory*, 35(6), 1277–1290.

Nakagawa, H., Umehara, D., Denno, S. & Morihiro, Y. (2005). A decoding for low density parity check codes over impulsive noise channels. *Proc. Int. Symposium Power Line Communications and Its Applications*, pp. 85–89.

Nasipuri, A., Cox, R., Conrad, J., Van der Zel, L., Rodriguez, B. & McKosky, R. (2010). Design considerations for a large-scale wireless sensor network for substation monitoring. *Proc. IEEE 35th Conf. Local Computer Networks*, pp. 866–873.

Nasri, A. & Schober, R. (2010). Performance of cooperative diversity systems in non-Gaussian environments. *Proc. IEEE Int. Conf. Commun.*, pp. 1–6.

Nassar, M., Lin, X. E. & Evans, B. L. (2011). Stochastic modeling of microwave oven interference in WLANs. *Proc. IEEE Int. Conf. Commun.*, pp. 1–6.

Ndo, G. (2010). *Optimization of impulsive noise countering strategies for high data rate communications over Indoor powerLines*. (Ph.D. thesis, Ph. D. dissertation, University of Rennes 1).

Ndo, G., Siohan, P. & Hamon, M.-H. (2010). Adaptive noise mitigation in impulsive environment: Application to power-line communications. *IEEE Trans. Power Delivery*, 25(2), 647–656.

Ndo, G., Labeau, F. & Kassouf, M. (2013). A Markov-Middleton Model for Bursty Impulsive Noise: modeling and Receiver Design. *IEEE Trans. Power Del.*, 28(4), 2317–2325.

Nosratinia, A., Hunter, T. E. & Hedayat, A. (2004). Cooperative communication in wireless networks. *IEEE Commun. Mag.*, 42(10), 74–80.

Oh, H. & Nam, H. (2017). Design and performance analysis of nonlinearity preprocessors in an impulsive noise environment. *IEEE Trans. Veh. Technol.*, 66(1), 364–376.

Onat, F. A., Adinoyi, A., Fan, Y., Yanikomeroglu, H., Thompson, J. S. & Marsland, I. D. (2008). Threshold selection for SNR-based selective digital relaying in cooperative wireless networks. *IEEE Trans. Wireless Commun.*, 7(11), 4226–4237.

Papoulis, A. & Pillai, S. U. (2002). Probability, random variables and stochastic processes. *New York, NY, McGraw-Hill Education*.

Portuguds, I., Moore, P. J. & Glover, I. (2003). Characterisation of radio frequency interference from high voltage electricity supply equipment. *Proc. 12th Int. Conf. Antennas Propag.*, 2, 820–823.

Proakis, J. G. (2001). *Digital Communications, 4th edition*. McGraw-Hill.

Qian, Y., Li, J., Zhang, Y. & Jayakody, D. N. K. (2018). Performance Analysis of an Opportunistic Relaying Power Line Communication Systems. *IEEE Systems J.*, 12(4), 3865–3868.

Report, U. S. (2012). Energy Information association, U.S. Department of Energy: Washington DC; Retrieved 22 June, 2012, from http: //www.eia.doe.gov.

Rožić, N., Banelli, P., Begušić, D. & Radić, J. (2018). Multiple-threshold estimators for impulsive noise suppression in multicarrier communications. *IEEE Trans. Sig. Process.*, 66(6), 1619–1633.

Sacuto, F., Agba, B. L., Gagnon, F. & Labeau, F. (2012). Evolution of the RF characteristics of the impulsive noise in high voltage environment. *Proc. IEEE 3rd Int. Conf. Smart Grid Commun.*, pp. 686–691.

Sacuto, F., Labeau, F. & Agba, B. L. (2013). Fuzzy C-means algorithm for parameter estimation of partitioned Markov chain impulsive noise model. *IEEE Int. Conf. Smart Grid Commun.*, pp. 348–353.

Sacuto, F., Labeau, F. & Agba, B. L. (2014). Wide band time-correlated model for wireless communications under impulsive noise within power substation. *IEEE Trans. Wireless Commun.*, 13(3), 1449–1461.

Sadek, A. K., Han, Z. & Liu, K. R. (2006). A distributed relay-assignment algorithm for cooperative communications in wireless networks. *IEEE Int. Conf. Commun.*, 4, 1592–1597.

Sadek, A. K., Su, W. & Liu, K. R. (2007). Multinode cooperative communications in wireless networks. *IEEE Trans. Signal Process.*, 55(1), 341–355.

Sattar, Z., Evangelista, J. V. D. C., Kaddoum, G. & Batani, N. (2019). Spectral Efficiency Analysis of the Decoupled Access for Downlink and Uplink in Two Tier Network. *IEEE Trans. Vehicular Technol.*

Savoia, R. & Verde, F. (2011). Performance analysis of decode-and-forward relaying in impulsive noise environments. *Proc. IEEE 8th Int. Symp. Wireless Commun. Syst.*, pp. 412–416.

Sendonaris, A., Erkip, E. & Aazhang, B. (2003a). User cooperation diversity. Part I. System description. *IEEE Trans. Commun.*, 51(11), 1927–1938.

Sendonaris, A., Erkip, E. & Aazhang, B. (2003b). User cooperation diversity. Part II. Implementation aspects and performance analysis. *IEEE Trans. Commun.*, 51(11), 1939–1948.

Shaikh, F. K. & Zeadally, S. (2016). Energy harvesting in wireless sensor networks: A comprehensive review. *Renewable and Sustainable Energy Reviews*, 55, 1041–1054.

Shan, Q., Glover, I. A. & et.al. (2011). Estimation of impulsive noise in an electricity substation. *IEEE Trans. Electromagn. Compat.*, 53(3), 653–663.

Shongwe, T., Han Vinck, A. & Ferreira, H. C. (2015). A study on impulse noise and its models. *SAIEE Africa Res. J.*, 106(3), 119–131.

Siamack, G., Jamil, H., Tarlochan, S. S. & Serguei, P. (2012). Effect of impulse noise on wireless relay channel. *Wireless Sensor Network*, 4(6), 167–172.

Simon, M. K. & Alouini, M.-S. (2005). *Digital communication over fading channels, 2nd edition*. John Wiley & Sons.

Sneessens, H. H., Louveaux, J. & Vandendorpe, L. (2008). Turbo-coded decode-and-forward strategy resilient to relay errors. *Proc. IEEE Int. Conf. Acoustics, Speech Signal Process.*, pp. 3213–3216.

Spaulding, A. & Middleton, D. (1977). Optimum reception in an impulsive interference environment-Part I: Coherent detection. *IEEE Trans. Commun.*, 25(9), 910–923.

Telatar, E. (1999). Capacity of Multi-antenna Gaussian Channels. *European Trans. Telecommun.*, 10(6), 585–595.

Tepedelenlioglu, C. & Gao, P. (2005). On diversity reception over fading channels with impulsive noise. *IEEE Trans. Veh. Technol.*, 54(6), 2037–2047.

Tisot, A. (2004). Rio grande electric monitors remote energy assets via satellite. *Utility Automation & Engineering T&D Magazine*.

Tosato, F. & Bisaglia, P. (2002). Simplified soft-output demapper for binary interleaved COFDM with application to HIPERLAN/2. *Proc. IEEE Int. Conf. Commun.*, 2, 664–668.

Tourki, K., Yang, H.-C. & Alouini, M.-S. (2011). Error-rate performance analysis of opportunistic regenerative relaying. *Proc. IEEE 22nd Int. Symposium Personal Indoor Mobile Radio Commun.*, pp. 1516–1520.

Tourki, K., Yang, H.-C., Alouini, M.-S. & Qaraqe, K. A. (2013). New results on performance analysis of opportunistic regenerative relaying. *Physical Communication*, 9, 97–111.

Tran, H.-V., Kaddoum, G. & Truong, K. T. (2018). Resource allocation in SWIPT networks under a nonlinear energy harvesting model: Power efficiency, user fairness, and channel nonreciprocity. *IEEE Trans. Vehicular Technol.*, 67(9), 8466–8480.

Tseng, D.-F., Han, Y. S., Mow, W. H., Chang, L.-C. & Vinck, A. H. (2012). Robust clipping for OFDM transmissions over memoryless impulsive noise channels. *IEEE Commun. Letters*, 16(7), 1110–1113.

Tuna, G., Gungor, V. C. & Gulez, K. (2013). Wireless sensor networks for smart grid applications: a case study on link reliability and node lifetime evaluations in power distribution systems. *Int. J. Distrib. Sensor Net.*, 2013, Article ID 796248, 1–11.

Umehara, D., Yamaguchi, H. & Morihiro, Y. (2004). Turbo decoding in impulsive noise environment. *Proc. IEEE Global Telecom. Conf.*, 1, 194–198.

Usman, A. & Shami, S. H. (2013). Evolution of communication technologies for smart grid applications. *Renewable and Sustainable Energy Reviews*, 19, 191–199.

Van Der Meulen, E. C. (1971). Three-terminal communication channels. *Advances in applied Probability*, 120–154.

Van Khuong, H. & Le-Ngoc, T. (2010). Performance of decode-and-forward cooperative relaying over Rayleigh fading channels with impulsive noise. *Proc. IEEE Int. Conf. Advanced Technol. for Commun.*, pp. 183–188.

Van Khuong, H. & Le-Ngoc, T. (2011). Effect of impulsive noise on decode-and-forward cooperative relaying over fading channel. *Proc. IEEE Wireless Commun. Networking Conf.*, pp. 1392–1397.

Vaseghi, S. V. (2008). *Advanced digital signal processing and noise reduction*. Wiley.

Wang, C.-H., Leong, A. S. & Dey, S. (2011a). Distortion outage minimization and diversity order analysis for coherent multiaccess. *IEEE Trans. Signal Process.*, 59(12), 6144–6159.

Wang, T., Cano, A., Giannakis, G. B. & Laneman, J. N. (2007). High-performance cooperative demodulation with decode-and-forward relays. *IEEE Trans. Commun.*, 55(7), 1427–1438.

Wang, W., Xu, Y. & Khanna, M. (2011b). A survey on the communication architectures in smart grid. *Computer Networks*, 55(15), 3604–3629.

Xiao, J.-J., Ribeiro, A., Luo, Z.-Q. & Giannakis, G. B. (2006). Distributed compression-estimation using wireless sensor networks. *IEEE Signal Process. Mag.*, 23(4), 27–41.

Xiao, J.-J., Cui, S., Luo, Z.-Q. & Goldsmith, A. J. (2008). Linear coherent decentralized estimation. *IEEE Trans. Signal Process.*, 56(2), 757–770.

Yan, Y., Qian, Y., Sharif, H. & Tipper, D. (2013). A survey on smart grid communication infrastructures: Motivations, requirements and challenges. *IEEE Commun. Surveys Tuts.*, 15(1), 5–20.

Zhang, J., Pan, G. & Xie, Y. (2018). Secrecy Analysis of Wireless-Powered Multi-Antenna Relaying System With Nonlinear Energy Harvesters and Imperfect CSI. *IEEE Trans. Green Commun. Net.*, 2(2), 460–470.

Zhang, X., Zhang, Y., Yan, Z., Xing, J. & Wang, W. (2015). Performance analysis of cognitive relay networks over Nakagami-*m* fading channels. *IEEE J. Sel. Areas Commun.*, 33(5), 865–877.

Zheng, L., Lu, N. & Cai, L. (2013). Reliable wireless communication networks for demand response control. *IEEE Trans. Smart Grid*, 4(1), 133–140.

Zhidkov, S. V. (2003). Impulsive noise suppression in OFDM-based communication systems. *IEEE Trans. Consumer Electronics*, 49(4), 944–948.

Zhidkov, S. V. (2006). Performance analysis and optimization of OFDM receiver with blanking nonlinearity in impulsive noise environment. *IEEE Trans. Veh. Technol.*, 55(1), 234–242.

Zhidkov, S. V. (2008). Analysis and comparison of several simple impulsive noise mitigation schemes for OFDM receivers. *IEEE Trans. Commun.*, 56(1).

Zhou, X., Zhang, R. & Ho, C. K. (2013). Wireless information and power transfer: Architecture design and rate-energy tradeoff. *IEEE Trans. Commun.*, 61(11), 4754–4767.

Zimmermann, M. & Dostert, K. (2002). Analysis and modeling of impulsive noise in broadband powerline communications. *IEEE Trans. Electromagn. Compat.*, 44(1), 249–258.